Al-Farabi Kazakh National University

UDC 578.832.1:043.5 Presented as manuscript

KHAIDAROV SAKEN ZHARKYNOVICH

Study of the antiviral activity of drugs against the *SARS-COV-2 virus in vitro*

8D05110 Virology

Dissertation for the Doctor of Philosophy (PhD) degree

Scientific Advisor:
Burashev Y.D.
PhD, S.T.

Foreign Scientific Advisor:
Edan Robert Tulman
PhD, Associate Professor,

Republic of Kazakhstan
Almaty 2025

TABLE OF CONTENTS

NORMATIVE REFERENCES

The dissertation was written according to the following standardised references.

MEMCT 7.32–2001— “Provisions on scientific research. Rules for structure and preparation

MEMCT 7.1–2003 — Bibliographic Record. Bibliographic Description. General requirements and preparation;

NOTATIONS AND ABBREVIATIONS

ACE2 - Angiotensin Converting Enzyme 2 (human)

BAL - Bronchoalveolar Lavage

BP-Base Pairs

CC- Cytopathic Capacity

COVID-19 – Coronavirus Disease (December 2019, Wuhan, China)

CPE – Cytopathic Effect

CE – Cytopathic Effect Inhibition

cDNA – Complementary Deoxyribonucleic Acid

HIV- Human immunodeficiency virus

IC – Inhibition Concentration

vRNA - viral ribonucleic acid

NSP /SP - Non-Structural Proteins/Structural Proteins

MERS – Middle East Respiratory Syndrome (coronavirus)

MOI - Multiplicity Of Infection

MTT-(4,5-Dimethylthiazol-2-Yl)-2,5-Diphenyltetrazolium Bromide

ORF – Open Reading Frame

RBD-Receptor Binding Domain

RdRP- RNA-dependent RNA-Polymerase

RT- Reverse Transcriptase

PCR-Polymerase Chain Reaction

PFU - Plaque-Forming Unit

PP- Primers Pairs

SARS-CoV-2- Severe Acute Respiratory Syndrome-Corona Virus 2

TAF – Tenofovir Alafenamide

$TCID_{50}$ (Tissue Culture Infectious Dose 50%)

TDF – Tenofovir Disoproxil

Vero – the subline of green monkey kidney tissue

WT – Wildtype

INTRODUCTION

General description of the research: The dissertation focuses on the biological and molecular genetic properties of current SARS-CoV-2 strains isolated within the territory of the Republic of Kazakhstan. It utilises RT-qPCR, cell viability, viral titer production, and COVID-19 express test techniques, along with appropriate primers, to detect the NSP12 gene product. An in vitro study of the antiviral activity of drugs against SARS-CoV-2 was conducted using Vero E6 cells derived from *green monkey kidney tissue.*

Relevance of the research thesis

The COVID-19 pandemic in 2020 highlighted the extreme vulnerability of healthcare systems worldwide. First and foremost, the speed and intensity of the viral infection's spread were a profound concern, given the high viral loads that most of the population could not withstand. Secondly, hospitalisation issues, insufficient beds and drug capacities were inadequate for effective containment. Thirdly, the severe cases of immune response caused significant health damage, predominantly to the lungs, and due to this feature, it was called severe acute respiratory syndrome.

The research aims to investigate the antiviral activity and safe cytotoxic drug concentrations of modern drugs against SARS-CoV-2 in vitro by conducting molecular analysis of circulating strains isolated during the pandemic.

The main tasks of the research to accomplish the purpose are as follows:

1. Isolate eight strains gained from human BALF (Bronchoalveolar Lavage Fluid) from COVID-19 positive patients and measure their viral load.
2. To identify the NSP12's "genetic conservatism" (primer pairs: 11-16) of the Alpha variant, which was isolated in Kazakhstan, by comparing it with the original Wuhan strain in the ORF1b region;
3. To find the cytotoxicity-safe concentration of four antiviral drugs;
4. To identify the most effective and potent antiviral drug among three candidates: Ribavirin, Favipiravir (Fabiflu), and Tenofovir (Tenvir), as well as a corticosteroid with a safe concentration that minimises cell toxicity while maintaining high cell viability.
5. To determine the inhibition coefficient $IC_{10} \rightarrow IC_{50} \rightarrow IC_{100}$ - Range antiviral drug-Tenofovir (TAF) with acceptable SI (selectivity index); - IC10: 5→ μg/mL → IC50: 25 μg/mL → IC100: 50 μg/mL: Viral replication reduced from 10^7 (log7) to 10^5 (log5) corresponding inhibition = $(10^7 - 10^5)/10^7$ = 0.99 → 99% inhibition
6. To engage the antiviral innate immunity response by injecting recombinant mouse IL-33 into WT mice, confirming the activation of CD90 and CD117 lymphoid cells in the murine lungs.

Research methods: the study employed biomolecular, genetic, cellular-based, biotechnological, microbiological, and pharmaceutical processes. **No Artificial Intelligence (AI)** was used in the research methods, neither in text nor in data processing.

The scientific novelty of the research: A three-stage dissertation study examining the effectiveness of the antiviral activity of the tableted drug against Kazakhstan's SARS-CoV-2/human/KAZ/B1.1/2021, the Alpha variant strain isolated and characterised, and an MTT assay on the Wuhan strain using original Tenvir (TAF) stock from China. Antiviral drug cytotoxicity and cell viability assays – Determining the optimal antiviral drug concentration (CC_{50}) using two colourimetric methods, CCK8 and MTT, in vitro in Kazakhstan. Three tablet formulations of drugs demonstrated additional inhibitory activity: Tenofovir (TDF and TAF), with IC_{10} = 0.174 μM, IC_{50} = 1.74 μM, and IC_{100} = 174 μM at a concentration of 50 μg/ml. Ribavirin: IC_{10} = 2 μM, IC50 = 7 μM, and $IC_{80\text{-}90}$ = 205 μM of 50 μg/ml., Favipiravir: with IC_{10} = 1.65 μM, IC_{37}=318μM, of 50 μg/ml. Dexamethasone showed no inhibitory properties at any concentration or volume. Comparison of the efficacy and cytotoxicity (CC50/IC50) of three tableted antiviral drugs, identifying an antiviral drug with a positive selectivity index (SI value), and analysis of the CCK8 assay test. Antiviral activity of three tableted prodrugs (active agents): Ribavirin, Tenofovir, and Favipiravir on Vero E6 cells line that is both susceptible and permissive for SARS-CoV2 virus – RdRP-inhibition, causing the lethal mutagenesis for viral replication with a significantly higher viral load MOI:2 or TID_{50}=10, whereas MOI of 0.01is enough to cause cytopathic effect within 24 hours (200 times increase virus load decrease potential). The molecular and genetic characterisation of the RdRP (RNA dependent RNA polymerase) gene (NSP12- none structural proteins) and its 'genetical conservatism' of SARS-CoV-2/human/KAZ/B1.1/2021, Alpha variant strain in comparison with the original Wuhan strain; The assumption of antiviral activity was confirmed using Tenvir TAF (pure Aldrich stock concentration) with 10μg/ml solution from original concentration 25mg/ml). All three antiviral drugs target the RdRP activity, making viral replication more challenging.

Subject of study.

They are investigating the antiviral activity of medicines against SARS-CoV-2, focusing on its genetic and molecular characteristics and evaluating their efficacy. In addition to identifying the cytotoxic concentrations of the three antivirals —Tenofovir, Fabiflu, and Ribavirin —and the steroid drug Dexamethasone, the concentrations of these compounds were also determined.

The theoretical and practical significance of the work is clearly demonstrated by the in vitro effectiveness of three disputed antivirals and one hormonal (steroid) drug. To understand which drug demonstrates a sensible, i.e., pre-clinical, effect on wild-type mice in China and to establish a safe dosage for viral load, the author aims to enhance strategies for combating SARS-CoV-2 viral infection. During the pandemic, Kazakhstan faced numerous different cases of COVID-19 progression and complications among infected patients with devastating post-coronavirus effects and even lethal outcomes due to a poor understanding of the biological nature of the SARS-CoV-2 virus. The primary objective of this dissertation work is to provide a deeper understanding not only of COVID-19 treatment but also of similar viral infection cases in the future. To evaluate the in vitro effectiveness of three antiviral agents and one hormonal

(steroid) drug. To understand which of these drugs demonstrate not only practical, i.e., clinical, effects but also to establish the safe dosage in treatment strategies for COVID-19. The value of this work lies in several additional aspects: 1. Tenvir, available in its two isoforms – TDF and TAF, has two origins: one is tabletted (TDF), and the second is a laboratory standard stock (TAF). Both forms showed similar effectiveness; furthermore, the last in vitro test of Tenvir efficacy was conducted in the 2000s. The antiviral effects were demonstrated on the Vero E6 cell model. Furthermore, the cytotoxic profiles of all four drugs were evaluated and confirmed. The non-structural protein sites on the viral genome were identified and quantified, and their biological 'conservative' nature was verified in the SARS-CoV-2/human/KAZ/B1.1/2021 Alpha variant strain.

The main provisions for the defence:

1. The SARS-CoV-2/human/KAZ/B1.1/2021, Alpha variant strain – is an object of antiviral study that was gained through 8 selected isolates, aiming at the entire - ORF1ab, where ORF1a NSP1-11(Protease section) and ORF1b NSP12-16 (viral RNA replication site) with the strain-specific mutation that is responsible for the replication of viral genome RNA as well as for sub-genomic RNA that regulate the final assembly of virions.
2. The potent inhibition of the RdRP (RNA-dependent RNA Polymerase is detectable through an MOI count of 2 or lower (two viral particles for each host cell) in a 12 wells-sampling by Tenofovir (tableted TDF (stock concentration started from 300mg of prodrug concentration) against The SARS-CoV-2/human/KAZ/B1.1/2021, Alpha variant) and TAF (lab stock) against original Wuhan strain) The tablet safe concentrations of Tenofovir, Favipiravir, Ribavirin, and Dexamethasone must support cell viability with a noncytotoxic viral load value of—MOI 2 (one host cell for two intact viral particle or plaque forming unit (PFU/ml)) with 200µl of virus volume) per 10.000 - 20.000 culture cells.
3. The cell viability counting techniques CCK8 and MTT demonstrate true cytotoxicity and antiviral assays on reliable Vero E6 cells with a high proliferation growth profile for four selected drugs: Tenofovir, Favipiravir, Ribavirin, and Dexamethasone.
4. WT-mice injected with recombinant mouse alarmin cytokine - IL33 showed the antiviral innate immune response, activating lymphoid cells: CD90 and CD117 in the lungs

The relevance of the plan based on scientific works

This work was carried out as a PhD Thesis, 'Studying the antiviral activity of drugs against the SARS-CoV-2 virus in vitro 'of Khaidarov Saken under the professional supervision of Burashev Yerbol, who managed my research within the framework of the grant funding project on the topic: AP09058338 "Study of anti-viral activity of drugs against SARS-CoV-2 virus in vitro and conducting molecular-epidemiological analysis of circulating Covid-19 strains" under targeted funding for 2021–2023 with the support of the Science Committee of the Ministry of Science and Higher Education of the Republic of Kazakhstan. Special gratitude is extended to the

Department of Pathobiology and Veterinary Science and the Centre of Excellence for Vaccine Research at the University of Connecticut (UCONN), Storrs, Connecticut, USA, which collaborated closely with the Research Institute for Biological Safety Problems (RIBSP), Gvardeyskiy, Kazakhstan. Additionally, thanks to the Health Science Centre (School of Medicine) of Shenzhen University, located in Nanshan District, Shenzhen, during the 2024 3-month PhD mobile program internship, experiments on TAF and mice were conducted, and the PhD study direction was continued.

The author's contribution to the results described in the dissertation.

The author independently analysed literature on the research problem, set research goals and objectives, conducted experimental research, analysed the results, performed statistical analysis, and wrote the dissertation.

Research approval: The research results and the main principles of the dissertation were presented and discussed at the following international scientific conferences and symposia: «Modern Scientific Technology» (February 9-10, 2023), Stockholm, Sweden; and the 3rd International Conference on Virology and Infectious Diseases, including COVID-19, held on October 24-25, 2022, in Dubai, UAE. Proceedings of the 1st International Scientific Conference, 26-27 January 2023, Warsaw, Poland, II International Forum "Asfen Forum, new generation-2024" on June 6-7, 2024, in Almaty, Kazakhstan

Publications: The main result of the dissertation consists of 12 published works, including 2 articles in peer-reviewed international scientific journals indexed in the Web of Science or Scopus databases, 5 articles listed in the Committee for Control in the Sphere of Education and Science of the Republic of Kazakhstan, and 5 theses published at international conferences.

Dissertation structure: The dissertation comprises 140 pages of computer-generated text, symbols, and abbreviations, as well as an introduction, a literature review, research materials and methods, research results and their discussion, a conclusion, and a list of used literature, totalling 131 entries. The work includes 9 tables, 9 mathematical formulas, 48 figures, 5 appendices, and 1 monograph.

Artificial intelligence (AI) usage: In this dissertation, the author did **not** use any AI, either for text generation, statistics, or other data processing. All data and entries were made by the author himself, singlehandedly and responsibly.

1 LITERATURE REVIEW

1.1 The biology of coronaviruses

Coronaviruses (CoVs) are a large family of RNA viruses that have caused notable outbreaks in humans over the past five decades. While most coronaviruses lead to mild respiratory illnesses, three novel strains emerging since 2002 have resulted in severe diseases and global health crises. In the pre-2000s era, human coronaviruses such as HCoV-229E and HCoV-OC43, identified in the 1960s–1970s, and later HCoV-NL63 and HCoV-HKU1 in the 1980s–1990s, were primarily linked to common cold symptoms, accounting for roughly 15–30% of annual cases but posing no significant public health concern. This perception changed with the 2002–2003 SARS-CoV-1 outbreak, which originated in Guangdong, China, likely from bats via civet cats, leading to 8,098 confirmed cases and 774 deaths (a 9.6% fatality rate) across 26 countries. The epidemic was contained through aggressive public health interventions, marking the first modern warning of the pandemic potential of zoonotic coronaviruses and stimulating research into coronavirus biology and preparedness. A decade later, MERS-CoV emerged in 2012 in Saudi Arabia, transmitted from dromedary camels with bats as the reservoir. Despite a high fatality rate of 34.4% (936 deaths among 2,605 cases as of 2023), MERS remained primarily regional due to limited human-to-human transmission, illustrating how varying transmissibility and virulence shape the global impact of emerging coronaviruses [1–2].

SARS-CoV-1 reinforced the global need to monitor zoonotic viruses in animal reservoirs, a lesson that became critical with the emergence of SARS-CoV-2 in late 2019. Likely originating in bats and possibly transmitted through an intermediate host such as pangolins, SARS-CoV-2 emerged in Wuhan, China, and rapidly spread worldwide. By 2023, the virus had caused over 700 million confirmed cases and approximately 7 million deaths globally. The disease ranged from mild respiratory illness to severe, multisystem complications—including the persistent condition known as Long COVID—placing immense strain on healthcare systems [1]. Beyond health effects, the pandemic triggered profound socioeconomic disruptions: lockdowns, travel restrictions, and global recessions reshaped modern societies and economies. Continuous viral evolution, driven by rapid antigenic drift, produced variants of concern such as Alpha, Delta, and Omicron, capable of evading prior immunity and necessitating updated vaccines. In response, the scientific community achieved unprecedented advances, most notably in mRNA vaccine technology and genomic surveillance, marking a transformative moment in global health preparedness.

All major coronavirus outbreaks—SARS, MERS, and COVID-19—originated in animals, highlighting the persistent risk of zoonotic spillover. These events underscore how disruptions at the human–animal interface, including wildlife trade, habitat encroachment, and intensive farming practices, can facilitate the emergence of novel pathogens with pandemic potential [1]. Pandemic preparedness: SARS-CoV-1 and MERS-CoV exposed gaps in global health infrastructure, but SARS-CoV-2 revealed systemic vulnerabilities, such as vaccine inequity and misinformation. Long-term health effects: post-viral syndromes, such as those associated with COVID-

19, have become a significant focus of research and healthcare. Technological Advances: mRNA vaccines, antiviral therapies (e.g., Paxlovid), and AI-driven surveillance emerged as critical tools [3]. Essential: surveillance: strengthen early detection of zoonotic viruses in wildlife and livestock. Equity: Ensure fair access to vaccines and treatments globally. Adaptability: prepare for viral evolution (antigenic drift) and future spillover events.

Over the past five decades, coronaviruses have profoundly influenced medicine, epidemiology, and society. While SARS-CoV-2 remains the most consequential, the broader history of coronaviruses highlights the ongoing need for vigilance and resilient communication systems to counter misinformation and protect global health in an interconnected world [4]. SARS-CoV-2 (Severe Acute Respiratory Syndrome Coronavirus 2) causes COVID-19, a global pandemic that began in late 2019. Here are some key points about the virus: Classification and Structure. SARS-CoV-2 is a coronavirus, part of the *Coronaviridae* family. It is an enveloped, single-stranded RNA virus. The virus has spike (S) proteins on its surface that allow it to bind to and enter human cells via the ACE2 receptor. Transmission primarily occurs through respiratory droplets and aerosols, such as those released during coughing, sneezing, and talking. It can also spread via contaminated surfaces (fomites), though less commonly. Airborne transmission is possible in enclosed or poorly ventilated spaces. Virulence refers to the degree of pathogenicity or the ability of a virus to cause disease [5].

SARS-CoV-2 has demonstrated varying levels of virulence, depending on viral strain, host factors, and the immune response. Here are key aspects of its virulence: factors include the spike (S) protein and the ACE2 receptor. SARS-CoV-2 enters human cells via the ACE2 receptor, which is highly expressed in the lungs, heart, kidneys, and intestines. The spike (S) protein has a high binding affinity to ACE2, enhancing infectivity. Mutations in the S protein (e.g., in Delta and Omicron variants) have increased transmissibility and immune evasion. SARS-CoV-2 has mechanisms that suppress early immune responses, primarily by inhibiting interferon production, which allows it to replicate efficiently before the immune system detects it [6].

Some variants (e.g., Delta) replicate more rapidly, resulting in higher viral loads and more severe disease, including an inflammatory response and a cytokine storm. In severe cases, an overactive immune response, known as a cytokine storm, leads to widespread inflammation, tissue damage, and organ failure. This excessive inflammation is responsible for severe complications like acute respiratory distress syndrome (ARDS) and multi-organ failure. CPE (Cytopathic Effect): Visible morphological changes in host cells caused by viral infection. These changes, including cell rounding, detachment, syncytia formation, or lysis, are used to diagnose viral infection in cell cultures [7].

The virulence is more clearly evident in “Table 1”. Four variants were isolated at the onset of the pandemic in Kazakhstan, and all four are shown in “Table 1”.

Table 1—Different SARS-CoV-2 variants and their varying levels of virulence

Variant	Virulence Characteristics
Alpha (B.1.1.7, 2020)	Increased transmissibility, slightly higher virulence.
Delta (B.1.617.2, 2021)	High viral load is associated with more severe disease and increased hospitalisation rates.
Omicron (B.1.1.529, 2021-Present)	High transmission, lower virulence, milder disease, but immune evasion.

The Delta variant had a higher virulence, leading to severe lung damage and higher hospitalisation rates. Omicron and its subvariants tend to replicate more in the upper respiratory tract, reducing lung involvement and severity but increasing transmissibility [8]. Host Factors Affecting Virulence: Age - Older individuals are at a higher risk of developing severe disease. Comorbidities, including diabetes, hypertension, obesity, and immunosuppression, increase the severity of the condition. Vaccination Status: Vaccinated individuals generally have reduced disease severity. Genetics and Immune Response: Some individuals may have genetic predispositions that affect ACE2 expression or immune response [9].

Clinical outcomes & severity: mild cases (80%): Fever, cough, fatigue, sore throat, anosmia. Moderate cases (15%): Pneumonia, difficulty breathing, mild hypoxia. Severe cases (5%): ARDS, cytokine storm, organ failure, death [10]. The overall case fatality rate (CFR) varies by variant and healthcare availability but is lower than that of SARS-CoV-2 (2003) and MERS-CoV (2012), which had significantly higher mortality rates [11]. SARS-CoV-2 has demonstrated moderate virulence compared to other coronaviruses, with some variants, such as the Delta variant, being more severe. In contrast, Omicron exhibits lower virulence but higher transmission rates. The virus's ability to evade immunity and mutate rapidly influences its pathogenicity and clinical impact [12].

The strain we worked with is the Omicron strain; nevertheless, it has a relatively high virulence, with a rapid cytopathic effect (CPE) and a relatively low viral load (MOI of 2 in Kazakhstan and MOI of 0,1 in China). Viruses are endo-parasites that strongly depend on their host cell and its replication, transcription, and translation machinery. Viruses can infect both eukaryotic and prokaryotic organisms (phages). It is challenging to classify them as true parasites or pseudoparasites. Viruses have compact genomes, mostly enveloped by capsid proteins, and can be composed of either DNA or RNA, as they encode various types of transcriptase. Coronaviruses are named for their corona-shaped appearance when viewed under the electron microscope. Viruses, are they alive? According to the latest characteristics of life biology, viruses meet only a fraction of the criteria for life— such as growth and development—because they do not grow or develop in the classical sense of these words. Only numbers increase—the viral load in a host cell, which ultimately leads to its fatal membrane and

cytosol bursting. Viruses possess neither *order* because they cannot be characterised as cellular organisms nor as energy processors.

However, many virions are highly ordered; instead, they utilise the 'victim' replication machinery to reproduce, expressing various enzymes on eukaryotic ribosomes [12]. Viruses are so heavily dependent on host metabolism that they can survive only inside penetrated host cells. The size also plays a crucial role; most living organisms, even unicellular ones like bacteria or protists, require space—the biosphere—to inhabit; viruses, in sharp contrast, mainly depend on particular hosts and their interactions within the biosphere. The only thing that relates viruses to living organisms is their capacity for heredity and adaptation, as evidenced by their ability to regulate gene expression independently. The viral genome can defend its critical regions of gene expression; these regions are called ORFs (open reading frames) and function as enzyme–bioactive catalysis.

The tiny size of viruses allows them not only to infect most organisms effectively but also to develop a profound number of strategies to regulate the populations of bacteria, fungi, plants, and other organisms. Viruses also cannot be considered true parasites because, although they cannot survive on their own, they usually kill their hosts relatively quickly, as seen with Ebola and Marburg viruses, which kill their hosts within several days [11].

This false parasite behaviour is their true weakness: low virulence and the inability to spread. The ideal pandemic viral scale is one where a virus spreads not only quickly but also allows a host to spread contamination fluids into the air for as long as possible, and keeps the so-called patient zero unaware of their role in spreading until it is too late. The virus is one of the most primitive life forms biology knows (apart from viroids, which are even more primitive): it has only membrane proteins that enable it to penetrate the host cell membrane, and a nucleocapsid that encloses the genetic material, which appears in either DNA or RNA form.

When the genetic material of a virus is inserted into the cytosol of the victim cell, the viral RNA, for instance, starts to dock on ribosomes and begin to produce immediately so-called reverse-orientated complicated enzymes like RNA driven RNA polymerase-enzyme that interacts with host DNA replication-machinery and starts to reproduce first the genetic material in positive sense direction, the reason why COVID-19 virus, for instance, has a definition as single-stranded RNA positive sense virus ($ssRNA^{+}$). About two-thirds of the SARS-CoV type two virus genome is fully dedicated to enabling, protecting and sustaining the work of RdRP to ensure the viral survival through not only replicating the genetic material but also producing main components of virions like spike protein – the host membrane 'opener,' membrane protein -even viruses must have information about the host membrane barrier in a cooperative form as Receptor binding domain - Angiotensin-converting enzyme 2 (RBD-ACE 2) [13-14].

The region spanning approximately 70% of the 30,000 base pairs (bp) is called ORF1ab (open reading frame) and encodes 16 non-structural proteins, including NSP3, NSP5, and NSP12. The NSP5 is located in the ORF1a region, which facilitates its adaptation and docking on host ribosomes.

The NSP12 is the most significant gene product of the COVID-19 virus and is responsible for RdRP expression. The rest, for instance, NSP-1-4 and NSP6-11, are responsible for enzymatic activities that support NSP5 during primary replication. The NSP13-16 also exhibits significant catalytic features that replicate the classical DNA replication process; instead of DNA, it uses RNA, and there is no need for leading or lagging strands, as seen during classical eukaryotic DNA replication [15].

Above all, NSP12 is the most significant gene product of the viral genome. They encode the most essential enzyme during the primary infection period—the RNA-directed RNA polymerase. NSP12 is so crucial that NSP13 and NSP11 fulfil the catalytic functions necessary for NSP12's efficient functioning. Some antiviral drugs, such as Remdesivir, disable RdRP from docking onto RNA subunits and, therefore, prevent the viral genome from replicating. Other antiviral drugs cause a phenomenon known as lethal mutagenesis in RNA metabolism, resulting in impaired viral survival or reduced viral load, which ultimately affects their functions and numbers. RNA-dependent RNA polymerase provides the viral genome with genetic variations through favourable point mutations.

The viral survival entirely depends on RdRP, and its importance is paramount. In multiple investigations conducted in the early 2000s and in 2020, in China and the USA, it was confirmed that, despite the high mutation potential of the SARS-CoV virus, few mutations occur from strain to strain, independent of its geographical origin and the ORF1ab region of the genome [16]. Severe acute respiratory syndrome-associated coronavirus 2 (SARS-CoV-2) is a life-threatening respiratory infectious condition caused by the SARS-CoV-2 virus, which belongs to the coronavirus family and genus Betacoronavirus—specifically, a single-stranded positive-sense RNA virus (ssRNA+). Variants of the SARS-CoV-2 coronavirus continue to emerge due to the virus's ongoing transmission and evolution worldwide. Since the pandemic was first declared by the World Health Organisation (WHO) in March 2020 [1], the following variants have been identified: B.1.17 (alpha), B.1.351 (beta), P.1 (gamma), B.1.617.2 (delta), and B.1.1.529 (omicron) [18]. Kazakhstan reported the first human case of COVID-19 in March 2020 [17].

According to the Johns Hopkins University database, as of January. In October 2022, the Republic of Kazakhstan reported 1,484,400 confirmed cases, with 19,052 deaths [17]. The coronavirus, or SARS-CoV-2, belongs to the Coronaviridae family, which are enveloped, positive-sense, single-stranded RNA viruses [8]. The SARS-CoV-2 genome comprises 14 open reading frames (ORFs), two-thirds of which encode 16 non-structural proteins (NSP 1–16) that make up the replicase complex [9,10].

The rest encodes the nine accessory proteins (ORFs) and four structural proteins: spike (S), envelope (E), membrane (M), and nucleocapsid (N), of which Spike enables SARS-CoV entry into the cytosol of the target cell [9]. As with any virus of this type, the Spike protein is the most variable, and because of this, SARS-CoV can penetrate the various cell membrane types of mammals [10]. There are approximately 30,000 nucleotides in RNA, encoding 11 proteins. Retroviruses have caused much harm over the years, and they're now a significant threat to human well-being. These types of viruses, belonging to the family Retroviridae, typically carry their genetic material as

RNA. Thanks to an enzyme called reverse transcriptase (RT), they could use the host DNA. RT is responsible for copying genetic information from one virus particle to another. The most well-known viruses of that family are Lentivirus (human immunodeficiency virus (HIV)) and SARS-CoV-2 (COVID-19) [11].

It is essential to note that viral infections aim to replicate their genomes and assemble new viral particles to invade surrounding cells and tissues; these processes are often lethal, potentially harming a cell or even an entire tissue system, such as the lungs. Thus, it is challenging to classify any viral 'organism' as a parasite whose long-term survival correlates with the host's well-being.

The side effect' of viral infections, such as inflammatory or less obvious clinically distinguishable signs, is the integration into the cell genome due to the enzymatic activity of viral RNA of various tissue types; this, in turn, causes multiple types of critical mutations in renewable tissues, which can sometimes result in devastating diseases like pneumonia, renal failure or other chronic, irreversible diseases. The negative impact of the global COVID-19 pandemic on the population is widespread and is only just beginning to be experienced. Therefore, the potential harm of this type of virus is never completely neutralised, and underestimating its pandemic potential is the highest priority for any authority to avoid [12-16].

SARS – stands for severe acute respiratory syndrome. Most of those diagnosed with SARS were healthy adults aged 25 to 70. Children under the age of 15 have been the victims of a few alleged SARS cases. SARS typically has an incubation period of 2 to 7 days, but can last up to 10. People with an illness meeting the current WHO case definition for probable or suspected SARS have a case fatality rate of around 3%. Since the COVID-19 pandemic emerged in 2020, the United Nations has considered this virus and related diseases a global challenge for healthcare systems worldwide.

The consequence of SARS-CoV-2 infection could lead to chronic illnesses, long-term health issues, and, to some extent, medical and mental impairment, which is why some scientific journals' scope is fully dedicated to this problem. In many countries, the hospitalisation rates reached critical levels, so many infected individuals were forced to stay at home and get treated far from inpatient wards.

Pneumonia is a direct and widely spread clinical consequence among COVID-19-positive patients and needs to be separated according to the severity of the illness progression and the extent of lung damage. The more damage occurred, the less oxygenation gained via lung breath, so many patients with acute lung damage were heavily dependent on artificial lung ventilation apparatus in intensive care. It was crucial to monitor whether pneumonia patients with COVID-19 infection were regularly assessed for bacterial infection and to detect bacterial co-infection. The antibiotic treatment strategy would have been implemented if a need arose to prevent pulmonary collapse [16-17].

SARS-CoV-2 and its molecular feature mainly rely strongly on the viral Spike, which has an S1/S2 polybasic cleavage site that is proteolytically cleaved by cellular cathepsin L and the transmembrane protease serine 2 (TMPRSS2), and a receptor-binding domain (RBD) that mediates direct contact with a cellular receptor, angiotensin-converting enzyme 2 (ACE2) [18,19,20]. ORF1a and ORF1b are

translated into viral replicase proteins as soon as the viral genome is inserted into the host cell's cytoplasm and cleaved into individual nascent proteins by both host and viral proteases. The RNA-dependent RNA polymerase (nsp12, which is derived from ORF1b) is formed by these [21]. The components of the replicase move the endoplasmic reticulum (ER) into double-membrane vesicles (DMVs) at this location, facilitating viral replication of genomic and subgenomic RNAs (sgRNAs). The latter is turned into accessory or auxiliary proteins and viral structural proteins, making it easier for the virus to form particles [22,23]. In conclusion, the secondary part of the genome encodes the nine accessory proteins (ORFs) that ensure the viral mRNA genome is translated. It is worth noting that the replicase for accessory protein production is significantly more critical than that for primary proteins. In addition, the four structural proteins are spike (S), envelope (E), membrane (M), and nucleocapsid (N), of which the spike protein enables SARS-CoV entry into the cytosol of the target cell [19]. ORF1a and ORF1b are translated into viral replicase proteins as soon as the viral genome is inserted into the cytoplasm of the host and cleaved into individual proteins (via the host and viral proteases, including PLpro). These form the RNA-dependent RNA polymerase (nsp12 derived from ORF1b) [19].

The latter is turned into an accessory or auxiliary protein and viral structural proteins, making it easier for the virus to form particles [20-23], unlike HIV, which has a complicated capsid structure with sophisticated (negatively charged dNTPs-permeable) pores that are permeable for negatively charged dNTPs, which serve as building blocks for the formation of RNA-host-DNA-hybrid. SARS-CoV does not possess such protection against host-cell enzymes [24].

The secondary part of the genome encodes the nine accessory proteins (ORFs), enabling the viral mRNA to be translated stepwise. Furthermore, the replicase required to produce accessory proteins must be integrated into the host genome to allow a virus to reproduce [21,24]. The structure of the SARS-CoV-2 virus genome and proteins resembles that of typical retroviruses, which are spherical to pleomorphic and have a diameter of 80-100 nm.

Different genera of retroviral virions exhibit distinct morphologies, yet they share the same core components, including an outer shell, two copies of the genetic material, and viral proteins. The envelope consists of lipids derived from the host plasma membrane during budding and glycoproteins, such as gp120 and gp41 in the case of HIV [25]. The outer lipid bilayer of the retroviral envelope protects it from the extracellular environment, promotes the penetration and exit of host cells through the endosomal membrane, and facilitates the virus's entry into host cells and its easy fusion with their membranes. These are three distinct functions of the retroviral envelope.

The retrovirus has a single-component, linear, dimeric ssRNA (+) genome, measuring 8 to 10 kilobases in length, with a 5' envelope and a 3' poly-A tail. There are flanks for group-specific genes (gag, pol, pro), and the envelope gene (env), between the R sites. The primers U3, R (PBS), and U5 binding sites form 5' long terminal repeats (LTRs). In the polypurine tract (PPT), the sections U3 and R form the 3' end. Reverse transcription uses a short repeating sequence at each genome end to ensure proper end-to-end transfer in the growing chain. On the other hand, U5 is a short

exception sequence between PBS and R [26]. The 18 bases in PBS correspond to the 3' end of the tRNA primer. An untranslated leader region, the L region, indicates how genomic RNA is packaged. The proteins gag, protease, pol, and env form the core of the retroviral protein. Gag is the main structural protein of the retrovirus, which controls most of the virus assembly processes. Interactions with three Gag subdomains - the matrix (MA), the capsid (CA), and the nucleocapsid (NC) — influence many of these assembly steps. Although gag subdomains differ structurally, their functions overlap during virus assembly [27,28].

To sum up, Tenofovir, as a prodrug that forms TAF and TDF, effectively suppresses the protease activity of retroviruses and inhibits the primary protein synthesis, making the DNA or RNA fitness of this virus type unsustainable. According to the WHO dashboard, more than 6.4 million people worldwide died from COVID-19 by August 18, 2022. The omicron strain has been diagnosed in over 590,000,000 people worldwide. A brand-new variant that emerged toward the end of November 2021 has become the most common strain worldwide, contributing to the ongoing rise in several nations. In several high-income nations, vaccination is significantly reducing the number of cases and hospitalisations, but a lack of universal access to vaccines leaves many populations vulnerable. Even in vaccinated individuals, questions remain about the effectiveness and duration of current vaccines against Omicron and other new SARS-CoV-2 variants.

There is still a need for more effective COVID-19 treatments overall. The global spread of COVID-19, along with the avalanche of research and misinformation, has highlighted the importance of reliable, easily accessible, and frequently updated guidelines for living with the virus, so that new findings can be understood and clear recommendations for clinical practice can be provided [29]. Apart from the severe acute respiratory syndrome and acute respiratory distress syndrome (ARDS), causing severe health impairment,

COVID-19 is also capable of causing post-COVID-19 health conditions like cognitive impairment. Other neurological and non-neurological deficits, such as fatigue and mental health symptoms, may overlap or cluster with cognitive deficits. In conditions following COVID-19, fatigue or exhaustion manifests as severely depleted systemic energy levels unrelated to activities or exertion and unaffected by usual rest or sleep. Fatigue negatively impacts the quality of one's life, physical and cognitive function, social participation, and employment. The core symptoms of depression following COVID-19 include a persistent low mood and sadness for at least two weeks and a markedly diminished interest in enjoyable activities. Depression can also cause problems sleeping, changes in appetite, fatigue, thoughts of self-harm or suicide, and feelings of worthlessness. Anxiety symptoms can include restlessness, racing or uncontrollable thoughts, difficulty concentrating, a sense of dread, difficulty sleeping, a lack of appetite, and irritability [29-30].

The SARS-CoV-2 consists of a viral genome: fourteen open reading frames (ORFs), two-thirds of which encode sixteen non-structural proteins (nsps 1–16) that make up the replicase complex [30,31]. The rest encodes the nine accessory proteins (ORFs) and four structural proteins: spike (S), envelope (E), membrane (M), and

nucleocapsid (N), of which Spike enables SARS-CoV entry into the cytosol of the target cell [22]. As with any virus of this type, the Spike protein is the most variable, and because of this, SARS-CoV-2 can penetrate the various cell membrane types of mammals [33-34]. ORF1ab in SARS-CoV-2 is a critical open reading frame (ORF) that plays a central role in the virus's replication and transcription machinery. Here is a structured overview. Genomic Context: SARS-CoV-2 Genome - A single-stranded, positive-sense RNA virus with a genome of approximately 29,903 nucleotides. The 5' two-thirds genome contains ORF1a and ORF1ab, which encode large polyproteins.

Key Features of ORF1ab. Ribosomal Frameshift Mechanism: ORF1ab is expressed via a -1 ribosomal frameshift during translation of ORF1a. This occurs at a "slippery sequence" followed by an RNA pseudoknot, causing the ribosome to shift the reading frame and continue translation into ORF1b. Result: A longer polyprotein (pp1ab) is produced, combining ORF1a and ORF1b regions, whereas ORF1a alone produces a shorter polyprotein (pp1a). Polyprotein Processing: The pp1ab polyprotein is cleaved by viral proteases (3CLpro/Mpro and PLpro) into 16 non-structural proteins (NSP1–NSP16).

These NSPs form the replication-transcription complex (RTC), which is essential for viral RNA synthesis. Key Non-Structural Proteins (NSPs): NSP12 (RdRP): RNA-dependent RNA polymerase, a target for antivirals (e.g., Remdesivir). NSP13 (Helicase): Unwinds RNA during replication. NSP14: Proofreading exonuclease, reducing mutation rates. NSP15 (EndoRNAse) and NSP16 (2'-O-MTase): Modify RNA to evade host immune detection. Viral Replication: ORF1ab-derived proteins are indispensable for viral genome replication and subverting host defences. Antiviral Targets: Enzymes such as RdRP and proteases (e.g., 3CLpro) are prime targets for drug development (e.g., Paxlovid inhibits 3CLpro).

The ORF1ab gene is highly conserved among coronaviruses, making it a valuable target for diagnostics (e.g., PCR primers) and broad-spectrum therapeutics. Mutations in ORF1ab (e.g., P323L in NSP12) may influence viral fitness or drug resistance, but are less common than those in structural proteins, such as the Spike protein. Surveillance of ORF1ab helps track viral evolution and inform the development of countermeasures. Protease activity in SARS-CoV-2 is crucial for viral replication and pathogenesis. The virus encodes two key proteases that process its polyproteins into functional components.

The first is the main Protease (Mpro or 3CLpro). It cleaves the large polyproteins (pp1a and pp1ab) translated from the viral RNA into non-structural proteins (nsps) required for replication and transcription. Specifically, it cleaves at 11 conserved sites, generating mature proteins, including the RNA-dependent RNA polymerase (RdRP) and the helicase. Structure: A cysteine protease characterised by a catalytic dyad comprising Cys145 and His41. Functions as a homodimer, with each monomer containing three domains (I-III). The second protease, Papain-Like Protease (PLpro), cleaves the polyprotein at three sites, releasing NSPs 1-3. Immune Evasion: Removes ubiquitin and interferon-stimulated gene 15 (ISG15) from host proteins, thereby dampening antiviral immune responses, including NF-κB and interferon signalling. [35-36] Structure: A cysteine protease featuring a catalytic triad comprising

Cys111, His272, and Asp286. Contains a ubiquitin-like domain for substrate recognition. Therapeutic Target: Less advanced than Mpro inhibitors, but investigational compounds (e.g., GRL-0617) aim to block PLpro's dual role in viral processing and immune suppression.

According to Figure 1understanding the structure-function relationships of ORF1ab facilitates the design of inhibitors to disrupt viral replication [20-21]. Studies on frameshifting mechanisms could lead to novel antiviral strategies targeting this process. In summary, ORF1ab is a cornerstone of SARS-CoV-2 biology, driving viral replication and serving as a key focus for therapeutic and diagnostic innovation [19-20,33, 37].

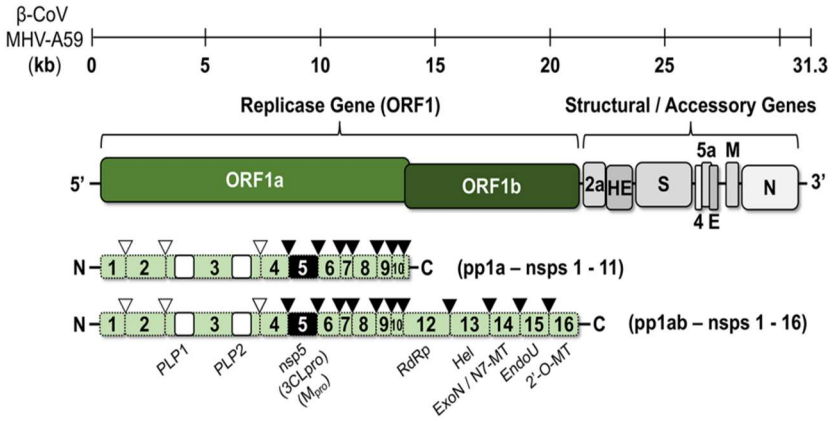

Figure 1 — The schematized viral genome of a SARS-CoV2 virus strain [37]

The polyprotein regions (pp) or so-called open reading frames (ORFs) are primarily encoded in the viral genome for replicase genes, from which fragments are designated non-structural proteins (NSPs). The most promising targets are nsp5 and nsp12, which are essential for viral replication. The structural genes encode proteins for various purposes, including the spike (S), envelope (E), membrane (M), and nucleocapsid (N) proteins, as well as auxiliary or accessory proteins [22,35]. Receptor binding protein (RBD): viral spike protein, glycolysis, S1-Domain, ACE-2 Recognition, Furin, S2-Domain, TMPRSS2, cell and viral membrane fusion. The viral infection caused by SARS-CoV-2 begins with the RBD, which consists of two subunits: S1 and S2. They are non-covalently associated subunits. The S1 Subunit binds to ACE-2, and the S2 subunit anchors the S2-protein to the membrane. The S2 Subunit contains the fusion peptide and other molecular machinery required to mediate membrane fusion during invasion of a new host cell, enabling the viral genome to enter the cytosol [37]. After contact with the spike protein, Furin accurately cleaves the outer part of the spike protein, known as the S1 domain, thereby releasing the inner core of the spike protein. This S2 domain is also cleaved by transmembrane serine protease 2 (TMPRSS2) [31]. After these, the spike protein unfolds and anchors into the host cell membrane. Thus, the viral and host cell membranes begin to fuse, allowing the viral genome to enter the host cell cytosol. A ribosome binds to the viral RNA and initiates the translation of its genetic code. It results in a long protein chain containing non-

structural proteins (NSPs). NSPs can cut the neighbouring chains. First, they release short naps that bind to ribosomes and occupy them, allowing the bound ribosomes to read only viral RNA rather than the host cell's messenger RNA (mRNA). From the very beginning, the infected host cell becomes a virus-building factory, thanks to the virus's control over the cell's translation machinery [35]. The primary spike protein structure is the key aspect of understanding viral pathogenesis, and its primary structure is depicted in Figure 2.

The viral entry activation of respiratory cells, such as lung cells, is mediated by the transmembrane protease serine 2 (TMPRSS2), which is not present in Vero kidney cells. However, the SARS-CoV-2 virus can be readily grown in them. The COVID-19 pandemic posed enormous global challenges to national healthcare systems (NHCs). The initial response to the spread of such an epidemic focused on treating infected patients to achieve clinical effect [35-39].

People around the globe stormed pharmacies to obtain paracetamol, which is effective against fever; others claimed anti-flu drugs, hoping to experience their therapeutic effects, and some even bought out antibiotics, considering that they would also be beneficial. COVID-19 is a single-stranded positive-sense RNA (+) (ssRNA) coronavirus that attaches to the host cell receptor, ACE2, via the spike glycoprotein in combination with surface protease TMPRSS2. This virus relies heavily on replicase targets, including RNA-dependent RNA polymerase, as shown in Figure 2 [40-49].

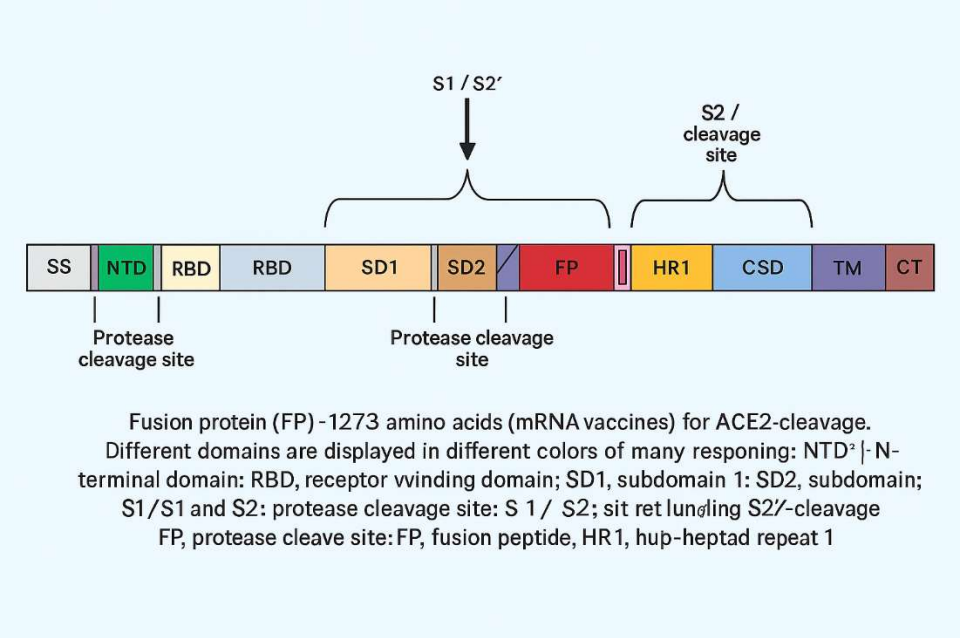

Figure 2 — Structure of the SARS-CoV-2 spike (S) protein

A schematic representation of the SARS-CoV-2 spike (S) glycoprotein. The protein is composed of several functional domains, each indicated by a distinct colour. The signal sequence (SS) precedes the N-terminal domain (NTD), receptor-binding domain (RBD), subdomains 1 and 2 (SD1, SD2), fusion peptide (FP), heptad repeats (HR1, HR2), central helix (CH), connection domain (CD), transmembrane domain

(TM), and cytoplasmic tail (CT). Arrows indicate protease cleavage sites S1/S2 and S2′. These cleavage events are required for activation of the fusion mechanism that enables viral entry into the host cell. RNA polymerase (RdRP), Helicase, Exonuclease, and Endoribonuclease. None of those mentioned above claimed that drugs could handle the rapidly increasing viral load and could bring either therapeutic or prophylactic (preventive) effects. Since then, scientists worldwide have launched a global effort to identify the most effective drugs against viral infections with replication-inhibiting properties that can alleviate patients' symptoms. Viral infections are complicated to fight without harming host cells because the viral genome utilises the host cell's machinery to replicate and assemble into new copies [32,40-48].

The viral load is entirely dependent on the assembly rates. For example, in the case of COVID-19, a single infected host cell can produce over 10,000 new coronaviruses before the cell bursts. To sum up, understanding how effectively to fight and treat viral infections requires grasping the viral life cycle, which involves several stages, including attachment to the host cell receptor. Most animal-specific viruses have an additional lipid membrane, known as an envelope, with protein spikes that facilitate attachment to a target cell. In the case of SARS-CoV-2, these spikes are part of the structural protein’s composition.

1.2 Antiviral drugs against SARS-CoV-2

In the last 60 years of development, most antiviral drugs were designed for long-term infection; only 43 antiviral drugs are against HIV alone, which has not satisfied the trend for the last several decades. Additionally, 75 antiviral drugs target the viral molecular machinery—specifically proteins—while 13 target host proteins. It would probably make more sense if antiviral drugs targeted host proteins, since it is harder to develop resistance against host DNA, which has lower mutation rates. We are witnessing a shortage of effective antiviral drugs for several reasons. Host factors could be another angle. Some antivirals, such as interferons, enhance the immune response. But many are direct-acting [40-44, 46]. The challenge is to ensure that the drug affects only the virus. For instance, nucleoside analogues are incorporated into viral DNA, leading to chain termination.

However, they might also affect host DNA if not selective enough, leading to side effects. In terms of unique characteristics, key points may include their targeted mechanisms, the challenge of resistance, the narrow spectrum, the need for timely administration, and the complexity of development due to virus-host interactions [40]. Additionally, combination therapies are used to overcome resistance and their role in managing chronic infections (such as HIV) versus acute infections (like influenza). Additionally, because viruses are intracellular parasites, targeting them without harming host cells is challenging. Antibiotics can target cell walls or ribosomes, which are different in bacteria. Viruses lack ribosomes, so antivirals must target alternative sites, such as viral polymerases or proteases. Mechanism of action (specific stages), specificity and selectivity, issues with resistance, narrow spectrum, timing of use, combination therapies, and challenges in development. Maybe also mention examples like acyclovir, Tamiflu, HIV drugs, and HCV DAAs. IC_{50} (Half-Maximal Inhibitory

Concentration) is the concentration of a drug required to inhibit 50% of viral replication or enzymatic activity in vitro. It measures a drug's potency by directly blocking viral components (e.g., viral enzymes such as RdRP or 3CL protease). Remdesivir (RdRP inhibitor): IC_{50} values are determined by its ability to inhibit viral RNA polymerase activity [45-46,49,50].

Paxlovid (nirmatrelvir/ritonavir): IC_{50} reflects inhibition of the SARS-CoV-2 3CL protease. CE (Cytopathic Effect Inhibition) - CE assays measure a drug's ability to protect host cells from virus-induced damage (cytopathic effect, CPE) in cell cultures. It evaluates both antiviral activity and cell viability (toxicity). Drugs like molnupiravir are tested for their ability to reduce SARS-CoV-2-induced cytopathic effects (CPE) in cultured cells.EC_{50} (Half-Maximal Effective Concentration) is often reported as the concentration of the drug required to achieve 50% protection against CPE. IC_{50}:

Prioritises medicines that directly target viral machinery, such as RdRP inhibitors like remdesivir. [45-46] CE (EC_{50}): Identifies drugs that are non-toxic and effective in cellular models, bridging in vitro results to in vivo outcomes. A drug with a low IC_{50} (potent) but high EC_{50} (ineffective in cells) may fail due to poor cellular uptake or toxicity. Successful antivirals (e.g., Paxlovid) combine a low IC_{50} (potent viral inhibition) with a low EC_{50} (adequate cell protection). Both metrics are critical in antiviral development, with IC guiding mechanistic studies and CE ensuring translational potential [48-52].

Antiviral therapy has been one of the most complex and expensive fields of pharmaceuticals for many decades, and only a few new antivirals have been developed in the last 60 years. This sad tendency is evident in Figure 3, which shows time lapses.

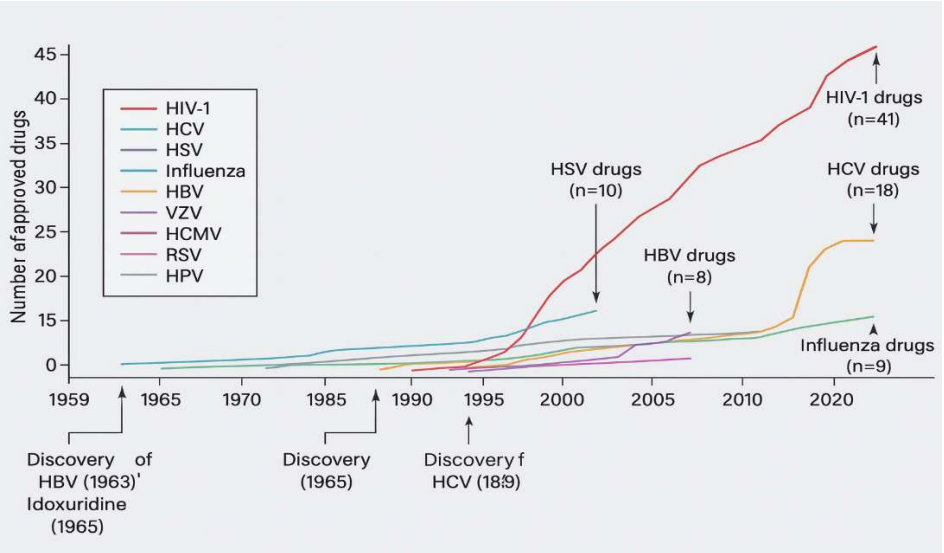

Figure 3 — 60 years of antiviral drug development in the USA since the early 1960s in the 20th century

Unfortunately, research on antiviral medications began only after the discovery of viruses. This allowed the viral infection to spread or adapt to human immunity and

the human genome, posing significant challenges for the pharmaceutical industry in developing effective strategies to combat the viral invasion [28-29]. Thus, only a few drugs were approved to combat them effectively. To make matters worse, pharmacology and science were primarily focused on persistent viral diseases that require lengthy, expensive therapy to reduce viral load in host cells. Furthermore, viruses are difficult to treat without serious side effects. In addition to the scarcity of antiviral drugs, it has another fatal flaw: its viral targets were primarily designed for chronic, slowly evolving viral pathogens.

To make matters worse, only 37% were intended to inhibit polymerase activity. Figure 4 shows this grim allocation of antivirals. So, putting it all together, the unique aspects are their targeted approach to specific viral mechanisms, the need for precision to avoid host toxicity, dealing with rapid viral mutation and resistance, often narrow spectrum, critical timing in administration, use in combinations, and the complexity in developing drugs that can effectively interrupt viral processes without harming the host [51,53-54]. Since viruses can hide in specific cells or reservoirs (such as latent herpes), antivirals must be able to penetrate those areas. For chronic infections, long-term use is needed, which requires drugs with reasonable safety profiles [54].

The diagram (Figure 4) also illustrates the structural and functional targets of antiviral drugs. The largest group is represented by polymerase inhibitors (37%). Protease inhibitors account for 24%, and host-directed antivirals account for 14%. The group of drugs targeting the NS5A protein of HCV comprises 8%, while integrase inhibitors comprise 4%. Another 13% of agents target viral proteins of other pathogens. The data confirm the key role of viral polymerase and protease as the most "druggable" antiviral targets.

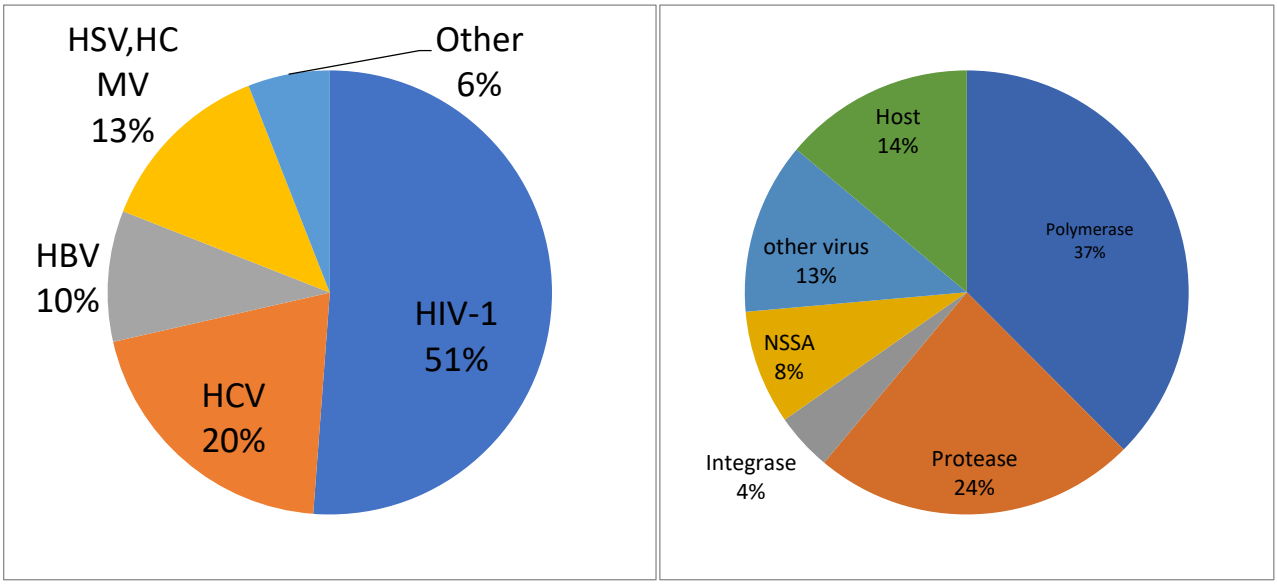

Figure 4 — Antivirals by virus species and target

Distribution of approved antivirals by virus species. The pie chart illustrates the proportion of antiviral drugs by their respective viral targets. The majority of

registered agents are directed against HIV-1 (51%). A significant part of the drugs is used for therapy of hepatitis C virus (HCV) (20%), herpesviruses HSV and HCMV (13%), and hepatitis B virus (HBV) (10%). The remaining 6% are represented by antivirals targeting other viral infections. This distribution emphasises the dominance of anti-HIV therapy in the antiviral pharmacopoeia.

First and foremost, compounds that interfere with virus growth can have adverse effects on the host cell. This means side effects are common and, in most cases, unacceptable. Additionally, every step in the viral replication cycle engages host functions [30-31,51-52].

Secondly, some medically and clinically important viruses cannot be propagated, as there is no suitable animal model, and they are too hazardous to work with. These viruses include HBV, HPV, smallpox, Ebola virus, Lassa virus, and Marburg virus [53-54].

Thirdly, a compound must completely block virus replication. It must be potent. Potent antiviral drugs cannot afford to block enzyme activity only partially, as many standard pharmaceuticals do. Otherwise, we develop antiviral drug resistance as mutated strains emerge. And, of course, we should not forget the financial aspect – it is costly. For many decades, antiviral medicine production has been categorised into four main groups. They are 1) Anti-influenza, 2) anti-HIV drugs, 3) Anti-hepatitis, and 4) Anti-herpes. Figure 4 illustrates the allocation of antiviral drugs by virus species and their specific targets. Overall, the majority of antiviral medications focus on HIV, while polymerase activity is the least targeted mechanism. The first pie chart shows that 46% of antiviral drugs are developed to combat HIV, making it the most researched virus. Other viruses, such as Hepatitis B and C (HBV/HCV), account for 21%, while herpes viruses represent 17%.

Influenza and other viruses comprise smaller proportions —11% and 5%, respectively. The second chart highlights the targets of these antiviral drugs—the most significant target (37%) is polymerase activity, which is essential for viral replication. Proteins involved in viral molecular mechanisms are targeted by 31% of drugs, while integrase inhibitors account for 4%. Approximately 28% of antivirals target host DNA or proteins, thereby indirectly affecting viral survival [54-56]. In summary, most antiviral drugs are aimed at treating HIV and focus on polymerase activity or viral proteins. However, a considerable portion also targets host cellular mechanisms, reflecting efforts to develop broader treatments for persistent viral infections. This data highlights the challenges associated with Favipiravir (nucleoside analogue), a pyrazine analogue of T-705 and a potent inhibitor of influenza viral RNA polymerase [33,49,57].

Favipiravir's metabolite (Favipiravir RTP (ribofuranosyl 5'-triphosphate interacts with viral RNA-dependent polymerase (RdRP). It is assumed that the antiviral effect can be downgraded in the presence of purine nucleotides ATP and GTP. In addition, this metabolite can be identified as a 'false' purine by the viral RdRP [34,56-57]. Previous in vitro studies have shown that SARS-CoV-2-infected Vero E6 cells exhibit a tolerable cytotoxicity profile, with a half-maximal cytotoxic concentration

(CC50) of 400 μM or higher [35]. Thus, it became clear that Favipiravir could be used at high concentrations as a safe and effective treatment for COVID-19.

Ribavirin (a nucleoside analogue) is a well-known antiviral drug that interferes with RNA and DNA replication by acting as a guanosine analogue (Guanine triphosphate (GTP)). The RNA-polymerase is not a single target. However, its structure prevents RNA capping during RNA maturation, which is heavily dependent on natural guanosine, thereby preventing RNA degradation [36]. Some studies have shown no significant cytotoxicity in the Vero cell model at a ribavirin concentration of 31.3 μg/mL [37].

The clinical experience during the pandemic revealed that patients with worsening cases were administered 400mg every 8 hours, in addition to methylprednisolone, to decrease the progressive viral load activity [38,51-53]. The high specialisation of ribavirin led doctors to pair it with either IFN-α2a or IFN-α2b (interferon) to achieve the therapeutic threshold and stop viral replication [38]. In 2003, in Canada, ribavirin therapy with a dose of 500mg every 8 hours for 4-6 days was also combined with a corticosteroid in 40% of SARS patients [39]. Ribavirin is a universal antiviral agent that can be used alone or in combination with antiviral compounds, such as interferon or immunosuppressants, in patients with worsening clinical conditions.

Tenofovir (a nucleotide analogue) is both an anti-HIV drug and an antiviral drug, according to the manufacturer's manual. Tenofovir is a class of reverse transcriptase inhibitors, specifically a nucleoside reverse transcriptase inhibitor (NRTI), a structural analogue of nucleic acids such as adenosine monophosphate. These compounds competitively inhibit reverse transcription by causing chain termination after they become incorporated into viral DNA.

This viral DNA incorporation causes a phenomenon known as 'lethal mutagenesis.' Tenofovir is also an antiviral medication used to treat chronic hepatitis B, acting as a nucleotide analogue. Tenofovir inhibits the HBV (hepatitis B virus) polymerase by competing with the natural substrate as it cooperates with the growing viral DNA strand, causing, as in HIV (human immunodeficiency virus), chain termination that stalls reverse transcription and viral DNA synthesis. Tenofovir is another nucleotide analogue initially designed to inhibit the HIV (human immunodeficiency virus) reverse transcriptase by interfering with the ATP-Polymerisation in the growing nucleic acid chain [44].

Tenofovir was also assumed to be effective against COVID-19, as it showed a tendency to bind to the RNA-dependent RNA polymerase (RdRP) and inhibit its activity in replication, as well as in transcription and translation of structural and accessory proteins, making virion assembly almost impossible [50]. Tenofovir, used in our study for oral administration as disoproxil fumarate (TDF), has numerous side effects when administered in high doses, including renal toxicity and bone density degradation [44-45]. *In vitro studies suggest that at concentrations under 100 μM, tenofovir does not inhibit viral replication in VeroE6 cells at multiple infections in a preventive manner when* administered one hour before infection and up to 48 hours post-infection. In the discussion of results, the researchers concluded that tenofovir in

ATP form requires activation by a host kinase and that any cell type likely possesses the appropriate kinase activity to initiate tenofovir's antiviral effects. Consider a study on human airway epithelial cells [42, 43].

According to the manufacturer's manual, dexamethasone is a synthetic glucocorticoid (GCS) that is a methylated derivative of prednisolone. Provision of anti-inflammatory, anti-allergic, and immunosuppressive action, increased sensitivity of beta-adrenergic receptors to endogenous catecholamines. The anti-inflammatory effect is linked to decreased capillary permeability, stabilisation of cell membranes (especially lysosomal and organelle membranes), inhibition of eosinophil and mast cell release of inflammatory mediators, induction of lipocortin formation, and a reduction in the number of mast cells that produce hyaluronic acid.

It acts on all stages of the inflammatory process: it inhibits the synthesis of prostaglandins (Pg) at the level of arachidonic acid (lipocortin inhibits phospholipase A2, inhibits the liberation of arachidonic acid and inhibits the biosynthesis of endoperoxides, leukotrienes, which contribute to inflammation, allergies, etc.), the synthesis of "pro-inflammatory cytokines" (interleukin 1, tumour necrosis factor-alpha, etc.); increases the resistance of the cell membrane to the action of various damaging factors.

The immunosuppressive effect is brought about by lymphoid tissue involution, inhibition of lymphocyte proliferation (especially T-lymphocyte proliferation), suppression of B-cell migration, and inhibition of cytokine release from lymphocytes and macrophages (including interleukin-1, 2, and interferon gamma) [44-50]; moreover, decreased antibody production. The antiallergic effect develops as a result of a decrease in the synthesis and secretion of allergy mediators, inhibition of the release of histamine and other biologically active substances from sensitised mast cells and basophils, a decline in the number of circulating basophils, T- and B-lymphocytes, mast cells; suppression of the development of lymphoid and connective tissue, reducing the sensitivity of effector cells to allergy mediators, inhibition of antibody formation, changes in the body's immune response. It is worth noting that 0.5 mg of dexamethasone is approximately equivalent to 3.5 mg of prednisone (or prednisolone), 15 mg of hydrocortisone, or 17.5 mg of cortisone, depending on the degree of glucocorticoid action.

According to WHO data, dexamethasone should be used in severe COVID-19 cases, especially if a patient is dependent on life-supporting systems [42-49]. Since the author’s antiviral study primarily relies on tablet forms, there are some recommendations that consumers must follow to minimise side effects. In Figure 5, the maximum daily doses prescribed by the manufacturer’s recommendations are the effective doses for antiviral activity of Favipiravir, Ribavirin, and Tenofovir in humans (in vivo) and in Vero E6 cells (in vitro). Toxicity is defined as the amount or degree of a substance required to be poisonous. It depends on the amount and concentration involved, the frequency of use, the interactions of the person receiving the substance of interest, and the individual's reaction to it [44, 50]. Any drug improvement begins with revising its efficacy and conducting preclinical or clinical trials. In severe cases,

doctors combine drugs to achieve a better therapeutic effect, which cannot be performed in vitro due to the high cytotoxicity potential of antiviral medications.

The drug dose reflects both efficacy and the increasing risk of adverse side effects. Antivirals are severe cell-poisoning agents that destroy infected cells. SARS-CoV-2 proteases are pivotal for its lifecycle and are significant targets for antivirals. Mpro inhibitors already play a clinical role, while PLpro remains an emerging target with dual antiviral and immunomodulatory potential. Structural and mechanistic insights continue to drive therapeutic innovation.

The bar chart (Figure 5) compares the recommended daily doses of three antiviral medicines by patient weight. Favipiravir (COVID-19) is administered at 3200 mg for patients weighing more than 81 kg and at 1200 mg for those weighing between 40 and 80 kg. Ribavirin (HCV) is weight-dependent, with dosing ranging from 800 mg (40–65 kg) to 1400 mg (>105 kg), with intermediate doses of 1000 mg (66–80 kg) and 1200 mg (81–105 kg). In contrast, tenofovir (HIV, HBV) is prescribed at a fixed daily dose of 300 mg regardless of body weight, with no adjustment for patients above 105 kg. The figure illustrates the difference between antivirals that require individual dose calculation and those with a standardised regimen [drug brochures → Appendix D].

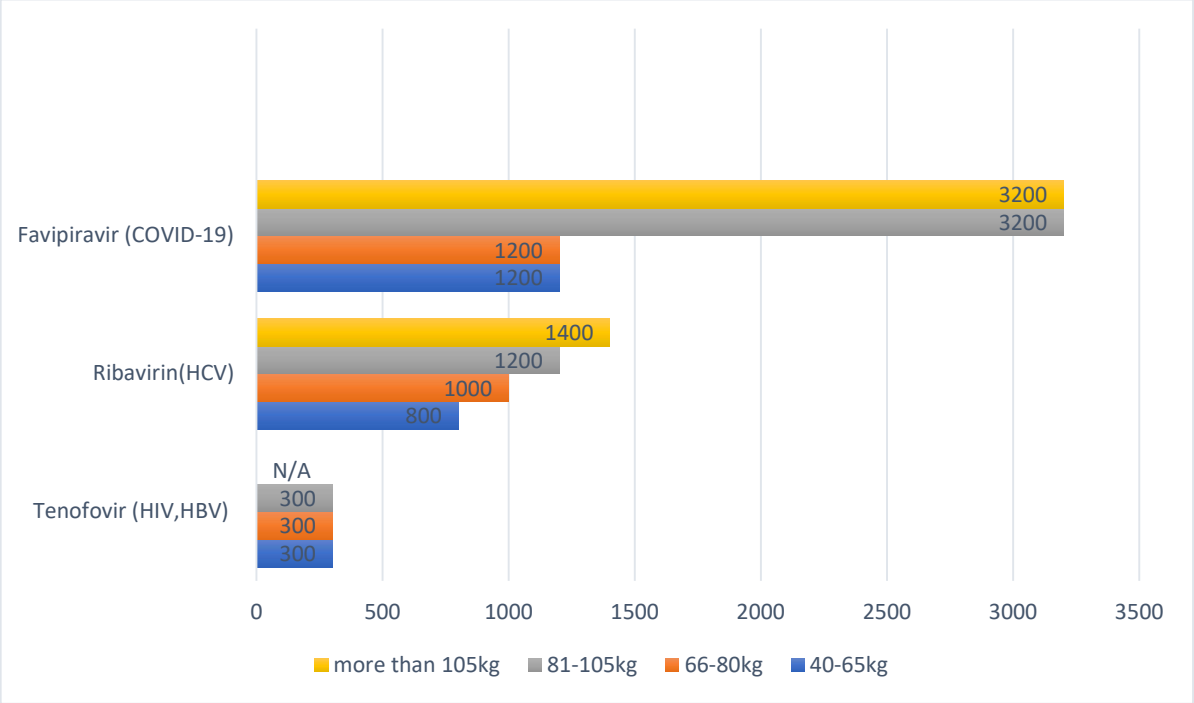

Figure 5 — Daily doses of antiviral drugs in milligrams according to patient body mass as specified in the manuals

It is marketed as *Fabiflu,* a specialised medicine for treating SARS-CoV-2 infection, and its recommended dose is very high. It is designed to be administered within 10 days for mild or moderate COVID-19 infection. Unlike Fabiflu, Ribavirin, for instance, was intended to slow hepatitis C replication for up to 72 weeks, requiring a daily dose. Tenofovir is recommended to be taken orally once daily, with one tablet

containing 300 mg of tenofovir, for an extended period under strict physician supervision and control, as per the manufacturer's manual and relevant publications [34-49].

Effective doses of antiviral effects of Favipiravir, Ribavirin, and Tenofovir on humans (in vitro) in Vero E6 cells. After the first SARS-CoV-1 pandemic in 2003. The dose recommendations for tenofovir and favipiravir were prescribed after in vitro studies; see Figure 6.

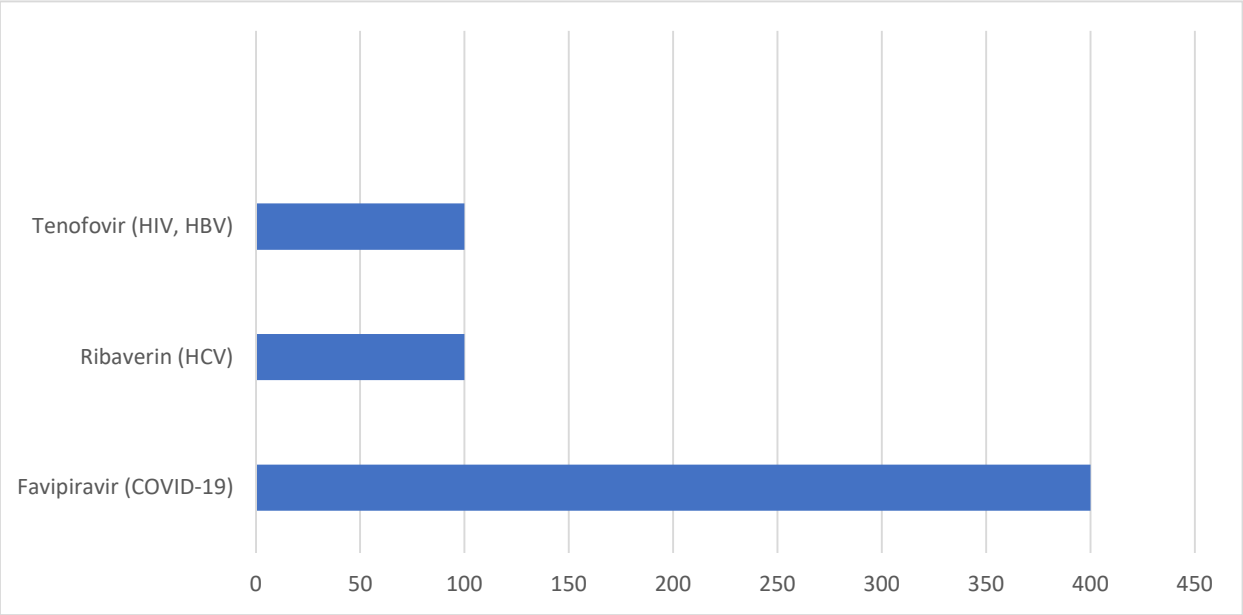

Figure 6 – Maximum effective concentrations of antiviral drugs in Vero E6 cell monolayers in micromoles with low cytotoxicity, according to open-access research papers since 2003

The horizontal bar chart presents the maximum effective concentrations (EC) of selected antivirals with acceptable cytotoxic profiles in Vero E6 cell culture. Tenofovir (HIV, HBV) and ribavirin (HCV) show relatively low maximum effective concentrations, not exceeding 100 µM, whereas favipiravir (COVID-19) demonstrates a markedly higher effective concentration of about 400 µM. The data indicate significant differences in the antiviral activity spectrum when tested in a standardised cellular model.

The Vero E6 model also demonstrates the toxicity edge for monolayer cells, where tenofovir and ribavirin could be effective, and dose control plays a significant role not only in achieving absolute viral RNA/DNA replication silencing but also in minimising negative side-effect impacts on contacting cells and tissues. Effective concentration and potency (EC_{50}, EC_{90}), concertation efficacy of three drugs (Inhibition activity): half maximal viable concentration (EC_{50}) may be a degree of the concentration of a medicate, counter-acting agent (*e.g.,* antibodies), or toxicant that actuates a reaction *midway* (halfway) between the pattern and *the* most outstanding value after an indicated introduction time, saying it differently, EC_{50} can

be specified as the concentration needed to obtain a 50% drug-effect. In our case, all three antiviral drugs are expected to exhibit these properties, as we aim to achieve EC90 or EC99, or in some cases, IC99, which represents the maximum inhibition potential.

$$\mathrm{pEC_{50}} = -\log_{10}(\mathrm{EC_{50}}) \quad (1)$$

There is a comprehensive range of EC50 values in formula (1) for drugs, which are regularly found to vary from *nM to mM*. Thus, it is often more sensible to refer to the logarithmically transformed pEC50 values rather than the EC_{50}. The term "potency" refers to the EC_{50} value. The lower the EC_{50} value, the lower the drug concentration required to achieve 50% of the maximal effect, and the higher the potency. The EC_{10} and EC_{90} concentrations correspond to 10% and 90% of the maximal response, respectively.

However, viral replication must be stopped entirely; even 90% silencing or 'breaking' of replication is insufficient to achieve the therapeutic effect of antiviral medication. Thus, so-called old drugs, such as ribavirin and tenofovir, are designed to be administered for an extended period at relatively low concentrations to inhibit viral replication in host cells. Ribavirin and Tenofovir are the antivirals for long-term drug therapy for primary purposes. Still, the increased concentration for ten days of prescribed treatment, such as favipiravir, can be either a reasonable risk for a cheap and effective alternative or a 'side-effect disaster' for a chance to fight COVID-19, for instance, or influenza. To make matters worse, the effective concentration (EC10, EC50, EC90) measure was heavily criticised in 2003 due to its 'vagueness' [34-38, 51].

To support the idea of the vagueness of this measure methodology, a study on the effectiveness of antivirals as individual agents and in combination was conducted in Japan to demonstrate how E50 values vary across *in vitro* studies. The difference between minimum and maximum values is, on average, 40 times [39-59]. Thus, the EC10 and EC90 values also showed a wide range of 'runaway' values, indicating data integrity issues. To sum up, to fight the viral replicase of fast-developing SARS-COV2 (i.e., its intercellular spread), almost 100% silencing is required, and to gain this, physicians prescribe either high drug doses within ten days on average with a particular drug like T-705 (favipiravir) or a combination of medications like ribavirin with corticosteroids (such as dexamethasone), or even 300mg tenofovir daily up to one week period, yet not at critical phase of COVID-19 infection.

1.3 Lethal mutagenesis as a purpose

Almost all Nucleoside analogues increase the mutation rates so high that viral replication machinery synthesised in ORF1ab gets disturbed so critically that either the RNA subunits do not attach to RdRP-like Remdesivir does [44,56,95] or the direct inhibition of RdRP through coping with false RNA strands is blocked, just like our discussed purine analogues: Favipiravir, Ribavirin, and Tenofovir [50-51,60-65]. A clear and distinct correlation is evident in Figure 7.

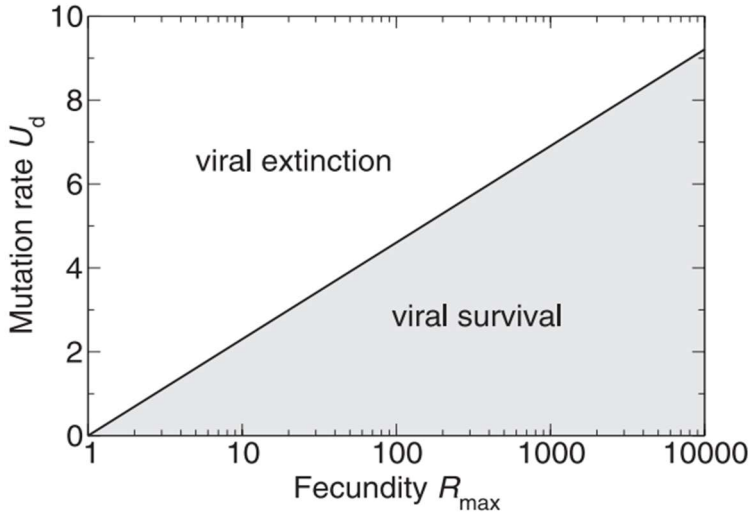

Figure 7 — The lethal mutagenesis characterisation for virus existence

Theoretical relationship between viral mutation rate and fecundity determining extinction or survival. The plot illustrates the boundary between viral persistence and extinction as a function of mutation rate (Ud) and maximum fecundity (Rmax). At low mutation rates relative to reproductive capacity, viruses remain in the survival region (grey area). When the mutation rate exceeds a threshold proportional to fecundity, viruses enter the extinction region, where the accumulation of deleterious mutations prevents them from sustaining replication. The figure illustrates a fundamental principle of viral evolutionary dynamics, highlighting the error catastrophe as a potential antiviral strategy. Since any virus, once it enters the host cytosol, contains genetic information (mRNA), the high replication error rates play a critical role. Thus, the threshold between extinction and survival is fine. As proofreading is crucial for viral survival, it is also vital for pharmacology to target the viral replicating machinery in a host cell.

To ensure viral extinction, we must have 100% inhibition **[**60-63,94-98]. As an mRNA virus, COVID-19 can be combated with two primary methods: vaccination and drug intervention. The antiviral drugs' mechanism of action is primarily RdRP inhibition, which facilitates lethal mutagenesis during viral infection. When the viral genomic RNA (gRNA) ingests itself in the host cell, it has relatively unstable single-stranded positive genomic RNA that requires replicated as soon as possible to be able to replicate new genomic RNA for structural protein synthesis and assembly; furthermore, after replicating itself the 'original' genomic RNA craves to build the sub-genomic RNAs (sgRNA) via transcription, these sg-RNAs (with caped mRNA, as in eucaryotic cells) are essential for translation in expressing the structural proteins that go to viral assembly as well as newly replicated RNA.

As a result, inhibiting or interfering with the viral replicase represents a significant arsenal in antiviral therapy, allowing us to insert mutated or damaged gRNA into the assembly process, thereby providing so-called extinction through a fatal error

in the viral genome during and after replication [48, 50, 55,64]. As mentioned, ribavirin was developed approximately 40 years ago and has demonstrated antiviral activity in both human and animal cell lines. As a guanosine analogue, it binds to the host kinase as ribavirin triphosphate and pairs with cytidine or uridine triphosphate. It mimics the purine nucleobase, causing severe mutations during replication and inducing lethal mutagenesis as an antiviral therapy, thereby reducing viral load rates [65-66, 88].

In 2019, a new influenza drug demonstrated the same RdRP-inhibitory properties as ribavirin and showed promising results during the COVID-19 pandemic [67-70]. Both drugs are nucleoside inhibitors. Unlike ribavirin, molnupiravir is a pyrimidine analogue. It is worth noting that ribavirin is a more cost-effective, closely monitored drug than molnupirovir, with similar effectiveness. Nevertheless, during the pandemic crisis in 2003 and 2019, the treatment was combined either with other medications or so-called adjuvants like interferons and corticosteroids to achieve maximum outcomes from treatment, and ribavirin was a classic example of these combination lines with acceptable survival as well as recovery rates among mild and moderate patients with SARS and SARS-CoV-2 infection. [37-38,50-51].

Favipiravir is another effective nucleoside and nucleotide inhibitor with a proven wide-spectrum activity against viruses that strongly rely on the RNA-dependent RNA polymerase (RdRP). In countries such as India and Japan, favipiravir demonstrated high clinical effectiveness, relatively low cytotoxicity, and a low side-effect profile. Along with ribavirin, it was primarily prescribed for mild to moderate patients with a 9-to 14-day history of inpatient background. [34-35]. *Favipiravir* also shows a good response against host RNA-dependent replicase kinase, enabling it to act as an effective lethal mutagenesis agent not only in SARS-CoV-2 populations but also against deadly diseases such as Ebola, influenza, and rabies, which makes it an asset as an antiviral medicine. Additionally, it is an effective drug against Influenza A and B, particularly for prophylaxis and mild infections [34, 49, 71-74, 92].

Tenofovir is the most cytotoxic drug on our antiviral drug list (only 300mg oral administration is allowed daily). It also belongs to the nucleoside inhibitor class, targeting RdRP, rendering viral DNA synthesis unviable and slowing viral virulence. Initially, it was designed against HIV and Hepatitis B viral invasion [44,75,91,93-94].

As it was already mentioned, the immune system in humans is responsible for the 'overdefensive' response to the viral invasion, causing massive tissue damage depending on age group, causing severe pneumonia as the 'final act' of immunity – the so-called '*cytokinetic storm',* which probably was the main reason for lethal outcomes during the Spanish influenza pandemic after WWI. All three antiviral drugs are clinically prescribed for patients with mild to moderate viral infections, reducing viral load through lethal mutagenesis and enabling viral extinction. In severe cases, doctors mostly take steroids to calm the overreacted immune response that could be lethal if it is not stopped, and here comes corticosteroids in combination with antiviral therapies, like ribavirin, already in 2003. The antiviral effect was so practical that the WHO (World Health Organisation) recommends dexamethasone as an additional, safe medication for treating COVID-19 infections in patients with mild to moderate symptoms [57, 76].

The bone infarct is mainly caused by the chronic appearance of immune suppression, as well as during other health-destructive patterns like alcohol misuse and chronic smoking. The dose risk primarily begins with 500mg of corticosteroids administered daily for 1-3 months [57]. The WHO recommends using 15-20 mg a day in mild stages of infection as an auxiliary therapy option. Nevertheless, what happens with severe cases is still not clear, and everything is highly individual, and intense steroid therapy was inevitable to fight progressing pneumonia and other signs of acute COVID-19 complications [57].

Figure 8 shows the severe side effects of extensive corticosteroid use. To conclude, lethal mutagenesis must occur within the NSP12 machinery, responsible for synthesising the viral genome and the subgenomic viral RNA, thereby completing the viral life cycle within the host cell. A localised region of punctate calcification is present, raising the possibility of enchondroma rather than infarction. The right-sided image further illustrates a focal lesion with multiple calcific spots in continuity with trabecular bone, again favouring enchondroma over bone infarct. In the lower panel, the lateral radiograph of the knee reveals a subtle punctate calcification pattern within a metaphyseal lesion, accompanied by disturbed trabecular architecture. This lesion may represent an enchondroma or bone infarct, though the punctate calcifications favour enchondroma. Additional findings include sclerosis and a serpiginous border consistent with infarct-like changes. In the lower right image, a lobulated calcified area is observed in the distal femur, representing a chondroid lesion with enchondromatous features.

Figure 8 — The bone infarct x-ray image taken from a patient with an immune-mediated medical background [57]

The radiographs demonstrate characteristic patterns of dystrophic calcification and punctate sclerosis in bone lesions. In the upper panel, the lateral x-ray of the

calcaneus shows a serpiginous calcification pattern, suggestive of bone infarcts, but with discrete punctate calcifications that are more typical of enchondroma.

1.4 Influenza virus and antivirals against it

Influenza virus-like SARS-CoV-2 is a low viral load-driven infection pathogen that requires relatively low PFU/mL to initiate disease, commonly referred to as a viral 'cold'. The strain naming of SARS-CoV-2 depends on the occurrence of spike-protein mutations, just as with the Influenza A virus [58-59]. No matter how rapidly SARS-CoV-2 and Influenza A viruses can mutate and adapt, they rely heavily on surface proteins throughout their life cycles and pathogenesis. Thus, developing vaccines against them is feasible. There are four types of influenza viruses — A, B, C, and D — which differ in nucleoproteins and matrix proteins based on their antigenic differences [59-61]. Influenza A virus A (IAV) causes respiratory illnesses. These unpredictable pathogens pose a threat to human and animal health through continuous evolution, antigenic drift, and shifts. The natural reservoir of IAV is aquatic wild birds, from which it can move to other terrestrial hosts, including terrestrial birds and mammals [61-63].

Influenza A, B, and C belong to the family Orthomyxoviridae, which comprises small viruses. The coronavirus family has a negative-sense, segmented RNA genome with continuous and stepwise activation during the infection period, which lasts up to 72 hours. Still, antiviral therapy is only effective within the first 48 hours, as it suppresses viral replication and reduces viral load, thereby enhancing both innate and adaptive immunity. Their primary characterisation is based on the classification of main surface glycoproteins, specifically HA (hemagglutinin) and NA (neuraminidase). [61-63]. Influenza viruses use standard terminology, like any other widespread viruses, including the virus types (A and B). The species from which it was isolated (if it does not belong to humans, for example, pigs or birds); the place where it was isolated (express PCR is required for identification - diagnosis of influenza infection); isolate number; year of isolation; and only for influenza A virus subtypes HA and NA. It is worth mentioning that by now, only 16 for HA and 9 for NA subtypes (variations) in every season circulating influenza A were found, among which only 3 HA (H1, H2, and H3) and only 2NA (N1 and N2) subtypes (mutated variations) have caused human epidemics, as confirmed by sustained, widespread, human-to-human transmission [63].

Thus, *A/Kazakhstan, Almaty/2125/2024 (H3N2)- an example of a viral strain isolated this year in Kazakhstan – is profoundly concerning*. The same pattern can be observed in SARS-CoV-2 virus strains, which exhibit multiple and varied mutations of the so-called 'sugar coat' on the Spike protein, facilitated by mutated Spike protein strains such as Gamma, Delta, Lambda, Mu, and Omicron. Since spike proteins enable the SARS-CoV-2 virus, or rather a virion produced from infected host cells like those in the respiratory tract, to evade the innate immune system, spike protein mutations provide various features, including higher virulence, more effective and robust vital enzymes, and their supporting segments, such as NSP9 in RNA-dependent RNA polymerase. Still, one glycoprotein segment remains unchanged in all variants of concern – the D416G mutation [58].

Overall, the Influenza A virus and SARS-CoV-2 Virus, as companions, represent a severe threat to immune-compromised individuals and pose continuous challenges for physicians and pharmacists to find optimal, effective treatment strategies, thereby minimising the post-COVID-19/influenza effect or period on patients and relatively healthy individuals. To make things worse, influenza A virus diagnostics are not as rapid or seriously taken as SARS-CoV-2 diagnostics in a cohort of treating doctors or among infected patients. Regarding Influenza A treatment, an infected person must take an antiviral drug, such as oseltamivir, as soon as possible, ideally within 48 hours of the first signs of illness, to ensure effective treatment and prevent further complications. The same applies to COVID-19.

Last but not least, the influenza A virus has a significantly smaller viral genome than SARS-CoV-2; still, SARS-CoV-2 can replicate relatively quickly and effectively, evading and silencing the antiviral mechanisms common to all viral replication machinery. Most viruses do not change unless environmental, mental, or immune factors stress them. Therefore, it is relatively easy for our immune system to recognise them from one year to the next.

However, the Influenza virus A or B is different. The virus's surface changes with each generation, altering the glycoproteins (HA and NA) and rendering previously matured Antibodies, mostly IgGs, ineffective. Each year, the influenza virus undergoes mutations, which ensure genetic variability within its viral RNA or genome. This process occurs gradually, altering the glycoproteins on the viral surface and leading to a gradual antigenic shift within the influenza genome—a phenomenon known as step-ahead mutations in antigen-antibody interactions [58, 59].

Nevertheless, these changes are primarily seasonal effects that depend on weakened population immunity, and only relatively minor alterations in glycoproteins are required to infect or reinfect the target host cell. The more deadly changes occur when an interspecific sustained antigenic shift occurs. Viruses are highly selective invaders; some attach birds' lung cells only and ignore human lung cells; however, if a bird population is located among other species like mammals and birds- the virus adapts to, for instance, the pigs' lungs and is capable of invading humans thanks to surface proteins matching or rather multiple matching properties of two glycoproteins (HA and NA). The hybrid set of surface proteins of the avian influenza virus, capable of penetrating both target cells of birds and target cells of pigs, poses a much more severe threat to humans than the "native" influenza virus because of antigenic drift that gets all complete changes or mutation variations of keys (HA and NA) at ones without gradual adaptation period, resulting a rapid and an unhindered spreading of new influenza virus in the host cells experiencing only innate and an unspecified immunity reaction that can lead to severe damage or life-threatening conditions, such as 'cytokinetic shock' or overwhelming uncontrolled viral load that also could cause 'septic shock' within few days after the incubation period.

In addition, most infected patients died from secondary bacterial infections. The deadliest registered pandemic was caused by this virus in 1918, killing over 400.000 people worldwide. Since antibiotics were not yet invented, most patients died from secondary bacterial infections that spread when the Influenza virus weakened the

innate immune system [64-66]. It is also known that Coronaviruses came into contact with humans, as with influenza, through wild birds; however, SARS-CoV-2 originated in wild bats, which likely underwent antigenic shift interactions with the human immune system. To summarise, influenza viruses rely heavily on two glycosylated membrane proteins, just as SARS-CoV-2 does.

The COVID-19 outbreak revitalised research into antiviral drugs and the treatment of seasonal viral infections, such as influenza A, B, and SARS (severe acute respiratory syndrome). This is not a single disease but a group of diseases caused by different viruses that share similar symptoms and courses. SARS is often mistaken for a simple cold and is generally considered harmless, especially in adults. However, the virus can cause serious complications, so there is no need to self-medicate. The cause of SARS can be any virus from a large group that includes more than 200 pathogens. These include adenoviruses, rhinoviruses, coronaviruses (of varying degrees of danger), parainfluenza viruses, and other microorganisms. Influenza's antivirals are the newest antiviral drugs and possess not only protease-inhibitory properties but also generally inhibit the viral replication machinery through direct RNA chain termination, with nucleotide substitutions that correlate with drug concentration (CE) and drug cytotoxicity (CC), respectively. Favipiravir, as Fabiflu tablets, enables scientists worldwide to gain insight into COVID-19 treatment, despite

Favipiravir (T-705) is primarily designed in Japan to combat Influenza A and B viral infections [49,64]. In addition, anti-flu drugs are among the most recent developments in antiviral medicine production, research, and development, closely related to SARS-CoV-2 infection. Thus, it makes sense to discuss so-called Influenza Antiviral drugs. *M2-ion channel inhibitors block the M2 channel, thereby restricting the passage of protons (H+) required* to trigger the release of viral genes (vRNA) into the host cell. Amantadine and Rimantadine are also prescribed by doctors worldwide, even for people with COVID-19 manifestations **[**65-73]**.** Another class of anti-influenza drugs is *endonuclease inhibitors* [65]. The best-known drug of this kind is Baloxavir, whose primary purpose is to selectively inhibit the cap-dependent endonuclease, a highly significant enzyme involved in the initiation of influenza virus mRNA synthesis. The Baloxavir intervention prevents viral gene transcription and, therefore, viral replication in the host nucleus and cytoplasm.

As we can see, unlike SARS-CoV-2, influenza virus replication is strongly dependent on nuclear ribosomal interactions. The last class of anti-influenza drugs is the *neuraminidase inhibitors*. The active agents of this drug class inhibit the viral neuraminidase enzyme, which is located on the viral particle's surface. In the absence of intact neuraminidase, the virus loses its ability to cleave sialic acid and its ability to escape the cell. Almost the same process has the SARS-CoV-2 virus, which heavily relies on the Spike-glycoprotein that also cleaves on the surface membrane, but to the ACE2-protein, to enter the host cytoplasm and thanks to complicated NSP interactions and forming DMVs (double membrane vesicle), a safe place to assemble the viral components like newly synthesised genome packed with nucleocapsid protein viral RNA. Thus, unlike the Influenza virus, the SARS-CoV-2 virus can quickly exit a host

cell as a ‘safe’ embedded vesicle, carrying all the necessary components to initiate viral infection.

The drugs in *the neuraminidase inhibitor class are* Oseltamivir, Peramivir, and Zanamivir. To sum up, the Anti-Influenza drugs have three courses of antiviral activity: a) M2-ion channel inhibitors, b) endonuclease inhibitors, and c) neuraminidase inhibitors. The antiviral drugs amantadine and rimantadine are M2-ion channel inhibitors; however, new strains of seasonal Influenza A virus have begun to develop resistance to these widely used antivirals [70-72].

Amantadine (adamantane-1-amine) is primarily designed to combat Influenza A virus infection due to its ability to interfere with the viral M2 protein, the ion pore channel, thereby hindering viral replication in both mRNA synthesis and vRNA [71-73]. Rimantadine (α–methyl–1–adamantane methylamine hydrochloride) is as effective as amantadine, relatively safe, and an M2 inhibitor. It was primarily designed in the 1980s to combat the spread of influenza A virus infection [70]. Figure 9 illustrates the entire interfering mechanism of the M2-ion channel on the viral membrane.

In addition, amantadine has anti-inflammatory features that are already being used against virus infections like Hepatitis C in a combination of Ribavirin and synthesised interferon [74], even though seasonally occurring Influenza A and B viruses in western countries like the USA started to develop resistance towards M2-Protein inhibition, mainly, against amantadine as well as rimantadine [75]. In Kazakhstan and other post-Soviet countries, neither studies nor data are conducted or collected on trends in viral resistance. Still, amantadine and rimantadine are inexpensive and effective antivirals against clinical manifestations of the flu (symptoms). They can also be used in conjunction with practical and affordable medication strategies against other viral infections whose replication machinery relies on acidification processes. The author may claim that these M2-ion inhibitors would show high efficacy in Kazakh populations due to lower antiviral drug pressure for at least a decade [76].

When SARS-CoV-2 reached pandemic scale, physicians and researchers worldwide began to utilise and study the so-called ‘time-proven’ antiviral drug arsenal, among which amantadine and rimantadine were explored as strategies to stop viral spread within individuals and populations. Since the M2-or Matrix 2 protein is a surface protein, the SARS-CoV-2 Spike protein could be inhibited by administering the M2-surface protein with the help of amantadine.

Firstly, amantadine is expected to have an antiviral effect on SARS-CoV-2 Replication by blocking a 5-α-helix channel, also known as the “viroporin channel,” in the hydrophobic region of the intramembrane space of COVID-19 [94,98].

Secondly, some assumptions (hypotheses) suggest that amantadine can downregulate and inhibit the dysfunctional state *of cathepsin L (CTSL)* and other *lysosomal enzymes*. These two mechanisms have been proposed as potentially significant in interfering with and hindering the SARS-CoV-2 virus's ability to enter target cells and facilitate virus replication [77]. Amantadine and rimantadine were studied in vitro on Vero E6 cells, yielding remarkable results. Both amantadine and

rimantadine, as well as the combinations of redeliver + amantadine, redeliver + rimantadine, and rimantadine alone, inhibited SARS-CoV-2 infection, primarily at the viral level following in vitro infection [78]. To sum up, M2-Ion inhibitors were in active use in Western countries to combat not only seasonal outbreaks of Influenza type A and B viruses but also as an additional treatment against other viral infections, such as Hepatitis C. Furthermore, since the emergence of COVID-19, they have also been used against SARS-CoV-2. The viral interiors of Influenza A and B and SARS-COV2 are relatively similar; the RNP machinery of replication activation resembles, to some extent, the nucleocapsid protein functions of SARS-COV2-virus that hold together the 30K nucleotides long RNA genome. According to some studies, M2-ion channel inhibitors are primarily potent against Influenza A and show only partial antiviral activity against Influenza B. Thus, the primary purpose of antivirals remains largely ineffective; viral replication can tolerate even 90% of the damage caused by antivirals, a phenomenon that has been consistently confirmed since the 1980s [71-77].

Ribavirin inhibits Influenza A through multiple mechanisms, including the inhibition of viral RNA Synthesis. Ribavirin mimics guanosine, thereby disrupting the function of viral RNA polymerase. Causes Lethal Mutagenesis. Introduces mutations into viral RNA, thereby reducing the virus's viability. Inhibits Host IMPDH Enzyme. Lowers GTP levels, impairing viral replication. Efficacy against Influenza A: In Vitro & Animal Studies: shows inhibition of Influenza A replication. Clinical Studies: Some early studies suggested modest benefits in severe cases. Not as effective as neuraminidase inhibitors (e.g., oseltamivir, zanamivir).

Resistance & Limitations: high doses required → Increased risk of hemolytic anaemia. Narrow therapeutic index (toxic at high doses). Not widely recommended for standard Influenza A treatment. Current role in influenza treatment. Not first-line therapy for Influenza A due to better alternatives (oseltamivir, peramivir, Baloxavir). Toxicity concerns. Possible use in severe cases or resistant strains, but limited clinical evidence. While Ribavirin has in vitro activity against Influenza A, its clinical use is limited due to toxicity, lower efficacy compared to standard treatments, and availability of safer alternatives. Neuraminidase inhibitors (oseltamivir, zanamivir) and cap-dependent endonuclease inhibitors (Baloxavir) remain the preferred treatments for Influenza A. In Figure 9, we can see the precise mechanisms underlying the inhibition of Influenza A replication. Although it possesses broad-spectrum antiviral activity, Ribavirin faces several significant challenges as an anti-influenza drug, limiting its clinical utility. Like other influenza antivirals, Ribavirin must be administered early in the course of infection.

However, its pharmacokinetics and practical administration challenges often delay treatment, reducing efficacy. Teratogenicity: Ribavirin is contraindicated in pregnancy due to risks of birth defects, restricting its use in a high-risk population (pregnant individuals) [41-42]. Broad-Spectrum Mechanism: As a nucleoside analogue, it interferes with host RNA synthesis, resulting in cytotoxicity and side effects such as fatigue, nausea, and liver toxicity. Ribavirin’s toxicity profile, uncertain clinical efficacy, complex administration, and the availability of safer, more effective alternatives render it a suboptimal choice for influenza treatment. Its use is generally

reserved for severe cases where benefits outweigh risks, often in combination therapies or research settings. Ribavirin could inhibit the SARS-CoV2 replication. Most SARS-CoV-2 variants, including Alpha, evolved due to natural selection pressures, not ribavirin-induced mutagenesis.

The M2-M1 Proteins' activity enables viral RNA to enter the cell cytosol. The importance of acidification by the M2 protein is paramount. The highly viral genome replication begins with M2-acidic activation, without which neither infection nor further viral genome replication is possible. Thus, for many decades M2-inhibitor like amantadine and rimantadine, which block/bind directly to the pores of the M2 protein channel and prevent the replication of the viral genome - while RNP is transported to the target nucleus (lung cells), viral RNA and mRNA-mRNA are produced [79], and then the main proteins of the viral membrane: HA, NA, and M2 are translated from the replicated viral mRNA and carefully inserted into the endoplasmic reticulum (ER). Then, the Golgi trans network (TGN) is transported to the cell surface, and the virus's life cycle is completed. Endonuclease inhibitors would significantly inhibit SARS-CoV-2 Ribosome cleavage and docking at the primary stages of nucleotide production. Additionally, it can hinder the docking of subgenomic RNA on host ribosomes that are capable of producing the structural protein of the SARS-CoV-2 virus.

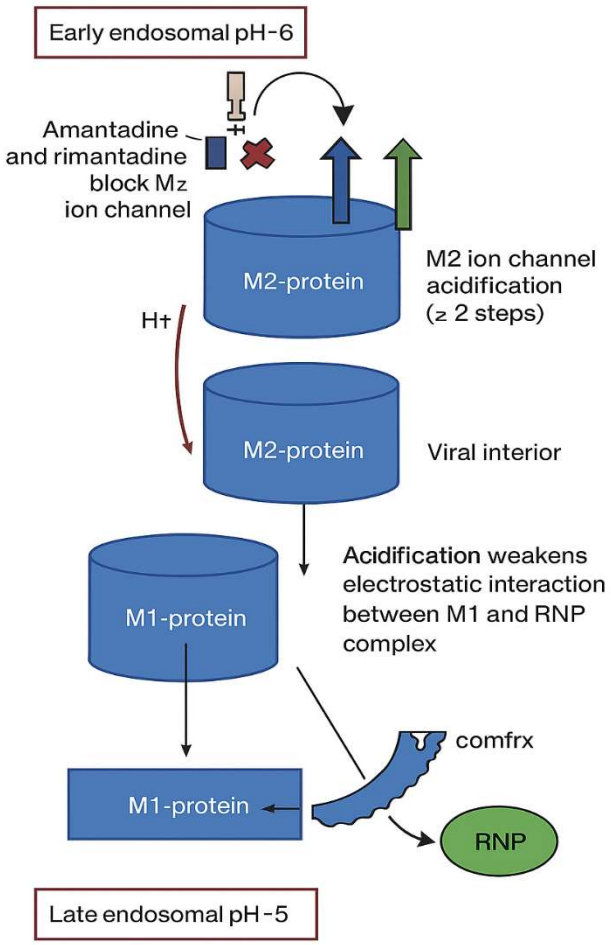

Figure 9 – The general scheme of the typical anti-influenza drug

Baloxavir is a prodrug of Baloxavir marboxil, a source of bioactive Baloxavir acid that inhibits the cap-dependent endonuclease, which is crucial for the synthesis of viral mRNA and, subsequently, for viral replication [80-84]. The RNA-dependent RNA polymerase in influenza A and B is called the viral ribonucleoprotein complex [84-85]. These complexes replicate both viral mRNA to produce the necessary proteins and the viral genome for virions. The RNA-dependent RNA polymerase of influenza A and B consists of three unique functional subunits: the acid polymerase protein (PA), the main protein of polymerase 1 (PB1), and the main protein of polymerase 2 (PB2) [86]. The protease activity must be triggered quickly and accurately to bind the 5'-mRNA capsule, initiating viral mRNA replication and facilitating translation of viral nucleoproteins. Interestingly, the host mRNA mechanism is actively involved; viral RNA has only primers to initiate viral mRNA replication, which, in turn, is translated into proteins for further structural purposes.

Thus, nucleoside analogues can also have a significantly negative impact on viral genome fitness, causing fatal errors that disable Influenza A and B from replicating the mature RNA. Their combination with Baloxavir exhibits pharmacokinetic and bioactive (diphosphate and triphosphate) inhibitory activity. Baloxavir is a potent drug against Influenza A and B viruses, with low cytotoxicity and no drug resistance reported by 2024 [85]. In addition, it is typically prescribed for infants under 12 and has minimal side effects, making it a potential preventive measure against seasonal influenza A and B strains. Prevention makes sense because, in general, antiviral drugs are effective within the first 48 hours as potent agents to stop the initial viral spread of influenza A and B viruses, and Baloxavir is no exception.

The administration of antiviral drugs must be closely monitored to prevent the development of persistent drug resistance among circulating viral infection variants annually [87-89]. Baloxavir and Favipiravir are novel antiviral drugs and the safest ones in in vitro and clinical studies. Favipiravir can also inhibit the polymerase essential protein 1 in the influenza RdRP complex [88-90]. Unlike the flu, SARS-CoV-2 has a duration of about 7-10 days before antiviral drugs become effective. The new Fabiflu 400mg tablets, along with Baloxavir 40mg and 80mg, represent an effective combination against seasonal Influenza A and B, as well as the SARS-CoV-2 virus variant of concern, particularly for children and individuals with compromised immunity.

Finally, the last group of Influenza antiviral drugs targets the most fundamental enzyme of Influenza A and B – the neuraminidase, located on the surface of viral particles [91]. Inhibition of this enzyme is paramount for combating the spread of the flu virus, whether it is influenza A or B. In sharp contrast to M2-Ion channel inhibitors, the neuraminidase inhibitor oseltamivir is potent at stopping the spread of viral infections caused by Influenza types A and B. The type B virus lacks an M2 Protein, and drugs such as amantadine or rimantadine have no clinical effect in patients with an Influenza B virus infection [91-92].

Neuraminidase inhibition occurs during the terminal stage of virion assembly within the host cell; without the active neuraminidase enzyme, the newly produced virus cannot cleave sialic acid and, therefore, cannot escape from the infected host cell

in the respiratory tract [92-94]. Oseltamivir is an antiviral agent. It is a prodrug whose active metabolite, oseltamivir carboxylate, selectively inhibits the neuraminidase of influenza virus types A and B. Neuraminidase is a glycoprotein that catalyses the cleavage of the bond between the terminal sialic acid and sugar, thereby facilitating the spread of the virus in the respiratory tract.

This process involves the release of virions from an infected cell and their penetration into the epithelial cells of the respiratory tract, thereby preventing inactivation by epithelial mucus. Oseltamivir carboxylate acts outside cells and competitively inhibits viral neuraminidase. It suppresses the growth of the influenza virus in vitro and inhibits its replication and pathogenicity in vivo. Reduces the release of influenza A and B viruses from the body [90]. According to recent studies, oseltamivir shows its maximum clinical effect within 36 hours during the 48-hour infection period and significantly reduces symptomatic signs when administered on time [59-89].

To sum up, oseltamivir 75mg can be used as a prevention medication as much as Baloxavir 40mg during the seasonal influenza outbreak. Both drugs are safe and effective against Influenza A and B types and can be used among vaccinated and immunocompromised individuals during the so-called flu season. Baloxavir exhibits relatively low antiviral resistance, with a resistance rate of only 1%, while oseltamivir has a resistance rate of 2%.

The combination treatment with Oseltamivir, an Antiviral drug, as an additional (complementary) agent, along with Ribavirin (1200 mg daily) [124], showed a relatively high therapeutic effect in clinical trials involving COVID-19-positive patients in mild and severe stages of disease progression, significantly increasing recovery and survival rates among patients [92]. Numerous studies in China during the pandemic have shown that three antiviral drugs — remdesivir (a nucleoside analogue), oseltamivir, and zanamivir (a neuraminidase inhibitor) — exhibit higher binding energies with the ACE2 Receptor after molecular docking.

Thus, the sialic acid enzyme inactivation activities interfere with the SARS-CoV2 entry by silencing the ACE2 receptor on the host cell membrane [92-93]. It is also worth noting that oseltamivir can regulate the migration and activation of neutrophil immune cells, significantly reducing the risk of sepsis and other neutrophil-related cell damage during COVID-19 progression in both humans and mice, via ROS production in target cells [95].

Overall, the neuraminidase inhibitor oseltamivir exhibits broad-spectrum antiviral activity, particularly during seasonal outbreaks of Influenza A and B, as a preventive therapy, and in cellular immune responses during both mild and severe stages of COVID-19. The oseltamivir carboxylate outside the cell acts as an immunoglobulin, significantly hindering the further spread of the virus without triggering an additional immune response and without compromising the secondary or active immunity functions. Additionally, the antiviral drug oseltamivir has a relatively low rate of viral resistance—approximately 2%—and in Kazakhstan, this rate may be even lower. Generally speaking, all Influenza antivirals make great medication backup strategies for clinicians because the discussed drug types, in most cases, are safe and

primarily treat Influenza A and B, whose incubation period or efficacy threshold or anti-viral effective window is potent in the first 48 hours, whereas SARS-CoV2 has 7-10days to be treated effectively by anti-viral active drugs with various combination options.

The SARS-CoV-2 treatment combination with oseltamivir can, in some cases, replace the dantrolene adjustment in severe COVID-19 patients in intensive care units (ICUs). 10/22/2020 The U.S. Food and Drug Administration (FDA) has approved the antiviral drug Remdesivir for use in adults and children 12 years of age and older who weigh at least 40 kg (approximately 88 pounds) to treat COVID-19 that requires hospitalisation. According to the FDA, Remdesivir should only be administered in a hospital or health care setting that can provide emergency care comparable to inpatient hospital care. Remdesivir is the first COVID-19 treatment to receive FDA approval [94]. Remdesivir can be efficiently metabolised to active nucleoside triphosphate in several human cell lines [96]. In vitro studies have demonstrated that the nucleoside triphosphate functions as an incorporation competitor for adenosine triphosphate, confusing the viral RdRP and acting as a delayed RNA chain terminator against the Ebola virus [97,98].

This mechanism evades viral exoribonuclease testing and reduces viral RNA synthesis. Recently, remdesivir has been shown to exhibit antiviral activity following viral entry in Vero E6 cells, supporting its mechanism of action as a nucleotide analogue [99]. The relevance of antigenic shift between Influenza A and SARS-CoV-2 lies in understanding their distinct evolutionary mechanisms, pandemic potential, and implications for public health strategies. To sum up, Influenza antivirals tend to act on SARS-CoV-2 in the same way as they do against Influenza A or B. This drug category is of particular interest because it can act quickly and cause less cytotoxicity.

In addition, their antiviral effects are better understood, and their increases in drug concentration are less hazardous than those of Ribavirin or Tenvir. So, putting it all together, the special aspects are their targeted approach to specific viral mechanisms, the need for precision to avoid host toxicity, dealing with rapid viral mutation and resistance, often narrow spectrum, critical timing in administration, use in combinations, and the complexity in developing drugs that can effectively interrupt viral processes without harming the host. Antivirals are specialised tools requiring precise targeting, strategic use to combat resistance, and tailored development for each virus, reflecting their complex interplay with host biology.

1.5 Cell viability and antiviral assay – MTT and CCK8 methods

The MTT assay protocol is based on the conversion of water-soluble MTT (3-(4,5-dimethylthiazol-2-yl)-2,5-diphenyltetrazolium bromide) compound to an insoluble formazan product. NB: MTT is also a free molecule as *ab146345* (Thiazolyl blue tetrazolium bromide). Viable cells with active metabolism convert MTT into formazan. Dead cells lose this ability and, therefore, show no signal. Thus, colour formation is a valuable and convenient marker of only viable cells. The absorbance at 590 nm (OD) is directly proportional to the number of viable cells. The MTT assay measures the metabolic activity of the cells being analysed; the more significant the

metabolic activity in the sample, the higher the signal. This should be taken into account when interpreting the assay's results. Reagent Preparation: Briefly centrifuge small vials at low speed before opening [104].

Dojindo's highly water-soluble tetrazolium salt, WST-8, is reduced by cell dehydrogenase activities to form a yellow-coloured formazan dye soluble in tissue culture media. The amount of formazan dye generated by dehydrogenase activity in cells is directly proportional to the number of living cells.

Cell Counting Kit-8 (CCK-8) enables sensitive colourimetric assays to determine cell viability in cell proliferation and cytotoxicity studies. Dojindo's highly water-soluble tetrazolium salt, WST-8, is reduced by cell dehydrogenase activities to form a yellow-coloured formazan dye soluble in tissue culture media. The amount of formazan dye generated by dehydrogenase activity in cells is directly proportional to the number of living cells. The detection sensitivity of CCK-8 is higher than that of other tetrazolium salts, such as MTT, XTT, MTS, or WST-1 [100].

It was advantageous because the cell viability results could be delivered on the same day. The main principles of the CCK8 assay are depicted in Figures 10 and 11. In addition, the UV-spectrometer enabled the team to take numerous vital measurements in support of the thesis aim, allowing them to determine CE and Cell viability more quickly, especially with CCK8 Kits in BSL4 labs, where the SARS-CoV-2 virus had to be kept intact.

Cytotoxicity (antiviral drugs).

The cell-killing property of an RNA-dependent RNA polymerase inhibitor (Nucleotide or Nucleoside), independent of the mechanism of cell death, is called cytotoxicity. Establishing that an inhibitor's activity occurs at concentrations that do not cause cytotoxicity is a critical component of demonstrating that the measured antiviral effect is virus-specific. It serves as a cornerstone in selecting a potential drug candidate for further development. The cytotoxic effect of an inhibitor can be determined by calculating the median 50% cytotoxic concentration (CC50), defined as the concentration of the test inhibitor that results in a 50% reduction in cell viability. Inhibitors that act in the middle of the cycle may affect one or more of the many processes involved in viral replication. For example, the polymerase inhibitor T-705 inhibits viral replication when added to viral cultures within 6 hours of infection [93]. Once cell viability is ensured, we can use various drug concentrations, considering the viral load (measured in MOI) and, as shown in Figure 12, Favipiravir's $EC_{50,\ which}$ depends on intact viral particles.

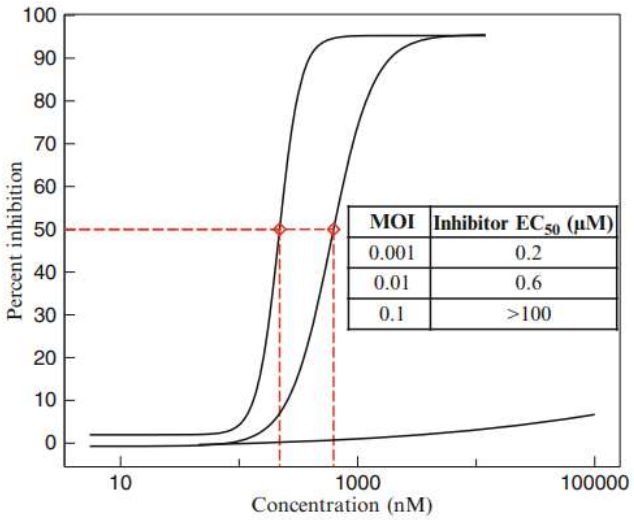

Figure 10 — Example of the Effect of MOI 0.001, 0.01, and 0.1 on the EC50 of T-705 or Favipiravir

The dose–response curves illustrate the compound's inhibitory effect on viral replication at different multiplicities of infection (MOI). Per cent inhibition is plotted against inhibitor concentration on a logarithmic scale, with EC_{50} values derived from sigmoidal curve fitting. At a low MOI of 0.001, the compound exhibits high potency (EC_{50} = 0.2 μM); however, at an MOI of 0.01, potency decreases to 0.6 μM (EC_{50}).

At the highest tested MOI of 0.1, inhibition is not achieved within the tested concentration range, with an EC_{50} value exceeding 100 μM. These findings indicate that antiviral efficacy is strongly influenced by viral input, with higher infection loads diminishing the apparent potency of the inhibitor. [92-93]. In Figure 10, it is evident that the explicit dependence of MOI on EC50 increases. The percentage of inhibition reaches 50% at MOIs of 0.001 and 0.01, respectively, within relatively comparable value ranges, namely 0.2-0.6 μM. Still, when MOI reaches 0.1, the drug concentration reaches almost 100 μM, representing a more than 100-fold increase in EC50. IC_{99} is the inhibitor concentration required to stop viral replication; it is typically 100 times more than the EC_{50}.

The relationship between inhibitor concentration (nM) and the percentage of inhibition at three multiplicities of infection (MOI): 0.001, 0.01, and 0.1. It also includes a table summarising each MOI's EC_{50} value (the effective concentration required to achieve 50% inhibition). At MOI = 0.001, the curve rises steeply, reaching 50% inhibition at 200 nM (EC50 = 0.2 μM). This indicates high sensitivity to the inhibitor at this level of infection. For MOI = 0.01, the curve shifts to the right, requiring higher concentrations to reach the same effect.

The EC50 value is 600 nM (0.6 μM), showing reduced sensitivity compared to MOI = 0.001. At MOI = 0.1, the curve flattens significantly, and even at high concentrations (>100 μM), it does not reach 50% inhibition. The table lists EC_{50} for this MOI as ">100 μM," indicating minimal effectiveness. In summary, the inhibitor's efficacy decreases with increasing MOI, requiring higher concentrations for inhibition

[101-104]. The inhibitor is highly potent at low MOI, but its effect diminishes significantly at higher MOI.

MOI (Multiplicity of Infection), TCID50, PFU/mL, or IU/mL is related to EC50 (the concentration of a drug that causes a semi-maximal response). Using a four-parameter regression method (a statistical technique for fitting a curve), mathematics enables us to conduct experiments and translate their results into something understandable, comparable, and meaningful. When converting TCID50/ml (tissue culture infectious dose, the amount of virus required to kill 50% of the cells in the culture) to PFU/ml (plaque-forming units, the number of viable virus particles), we multiply by 0.7. Typically, we terminate the PCR (polymerase chain reaction) after approximately 40 cycles (Figure 11).

The image (Figure 11) illustrates the concept of the multiplicity of infection (MOI), specifically an MOI of 10. It visually represents the ratio of viral particles to target cells, showing that 10 million viruses are used to infect 1 million cells, meaning each cell is exposed to an average of 10 viral particles. The MOI value reflects the infection intensity in an experimental setup; higher MOI levels typically ensure that most cells become infected simultaneously. This approach is commonly used in virology and cell culture experiments to study viral replication dynamics, cytopathic effects, or antiviral responses under controlled infection conditions. The clear graphical depiction effectively conveys the proportional relationship between virus and host cell numbers, making it a valuable educational tool for explaining the kinetics of infection.

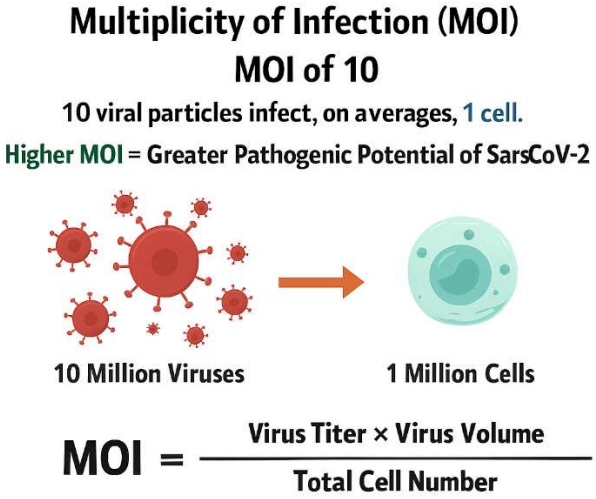

Figure 11 — MOI count, in our case, 0.2 mL or 200 µL of intact virus volume, corresponding to an MOI of 2

The lower the MOI, the more sensitive the test for viral activity. If we have a high MOI, the CC50 cannot be determined because CPE can kill all available cells, and a higher antiviral concentration would be needed. For our purposes, it is not necessary to concern ourselves with the number of viruses in a single cell.

What we need to understand—and what the Poisson distribution helps us with—are two key points: if some cells get more than one virus, others will not. For any given MOI (the average number of viruses per cell), we can calculate the probability that a cell is not infected with any virus, denoted P(0). P (0) is simplified and presented in formula (2). Logically, if the proportion of cells that will not be infected is known, subtract this value from 100%. What proportion of cells will be infected, regardless of the number of viruses each infected cell receives?

$$\mathbf{P\ (0) = e^{-MOI}\ (2)}$$

Viral stock of MOI of 2

At an MOI of 2, without any experiment, we expect 86% of cells to become infected. Using the formula (2), we gain:

$$\mathbf{P\ (0) = e^{-MOI} = e^{-2} = 1 / e^2 = 1 / 2.71828^2 = 1 / 7.389 = 0.1353}$$

(~14% of cells not infected)

By subtraction: 100% – 14% = 86% infected

Subsequently, if we examine MOIs lower than 1, we observe that, for instance, at an MOI of 0.5, we achieve a 40% infection rate, and at an MOI of 0.1, we achieve a 10% infection rate.

Converting from TCID50 to IU

Since the MOI can ultimately be described in terms of infectious units, our $P\ (0) = e^{-MOI}$ can also be written as:

$$\mathbf{P\ (0) = e^{-IU/ml}\ (3)}$$

Re-arrange this equation from TCID50 to infectious units to determine the number of contagious units when we know P (0). Remember that P (0) is the probability of not being infected by formula three, and we get:

$$\mathbf{P\ (0) = e^{-IU/ml}\ becomes\ IU/ml = -ln_e\ P\ (0)\ (4)}$$

Now consider our TCID50: the virus concentration at which there is a 50% chance of infection. At the limiting dilution of our TCID50 assay, we have a 50% chance of disease (i.e., a 50% chance of non-infection); therefore, P (0) = 0.5. Now, substituting *P* (0) = 0.5 into the rearranged equation:

$$\mathbf{IU/ml = -ln_e\ (0.5)}$$

$$\mathbf{ln_e\,(0.5) = -0.693}$$

$$\mathbf{So,\ IU/ml = -(-0.693) = 0.693\ (5)}$$

This is often rounded to 0.7 for simplicity. Therefore, at a 50% infection rate, we have approximately 0.7 infectious units (IU) per cell. Alternatively, 1 TCID50 corresponds to 0.7 IU. Hence, whenever we need to convert TCID50/ml values to IU/ml, we multiply by 0.7. Therefore, it is always important to report the unit of measure (TCID50 or IU), as this provides information on the amount of infectious virus and the assay used to determine it.

The cell culture monolayer was infected with SARS-CoV-2 at a multiplicity of infection (MOI) of 2, using the SARS-CoV-2/human/KAZ/B1.1/2021 and SARS-CoV-2/human/KAZ/Britain/2021 strains, respectively, with an infectious titer of 7 logs TCID50/ml. After one hour of virus contact with the cells at 37°C, the cell monolayer was washed three times with phosphate-buffered saline (pH 7.2).

The studied drugs were applied to the infected cells at different concentrations (experimental group) or in the maintenance medium (control group), and the plastic panels were then placed in a CO2 incubator for 5 days. The antiviral effect of the drugs was calculated as the ratio of the virus's infectious activity in the experimental and control samples. All experiments were performed in triplicate. The main criteria for assessing the in vitro effectiveness of the drugs were the following indicators [100]: a decrease in the infectious titer of the virus under the influence of the drug (D, lg), the inhibition coefficient (Ci, %), and the chemotherapeutic index (CTI). The decrease in the level of virus accumulation under the influence of the drug (D, lg) was determined by the formula:

$$\mathbf{D = Ak - Ao\ (6)}$$

Where Ak is the level of virus accumulation during cultivation without the addition of the studied drug to the nutrient medium (in lg TCID50/ml); Ao is the level of virus accumulation during cultivation with the addition of the studied drug to the nutrient medium (in lg TCID50/ml). The formula calculated Ki:

$$\mathbf{Ki = (Ak - Ao)/Ak \bullet 100\%\ (7)}$$

The MIC/IEC ratio was defined as the drug's CTI value, where IEC is the minimum effective virus-inhibiting concentration that reduces the virus titer by at least two log TCID50 [99].

A continuous culture of Vero cells, highly sensitive to the SARS-CoV2 virus, was used to analyse the preparations' antiviral activity in vitro. The cells were cultured in 24-well plastic plates using RPMI 199 medium and supplemented with 10% fetal bovine serum and 100 U/ml gentamicin. The maintenance medium contained the same mixture but with the addition of 1% fetal serum.

To evaluate the antiviral effect of any substance, it is necessary to determine the CC_{50} value, which is the concentration at which the substance kills 50% of cells. The CC50 value is calculated mathematically, not visually, using the formula.

$$CC_{50} = \left[\frac{X_1 - 50}{X_1 - X_2} \cdot (Mx_2 - Mx_1) \right] + Mx_1 \quad \textbf{(8)}$$

where - X_1 more than 50 % of surviving cells;

- X_2 less than 50 % of surviving cells;
- Mx_1 concentration of substance where more than 50 % of cells survived;
- Mx_2 concentration of substance where less than 50 % of cells survived.

Cytotoxicity Assays (CC_{50}, SI - SI-evaluate drug toxicity in host cells) were performed using this assay (formula 8). CC_{50} (Cytotoxic Concentration 50%): The concentration of the drug that causes 50% cell death. Selectivity Index (SI) = CC_{50} / IC_{50} (higher SI indicates a better antiviral effect with lower toxicity). This evaluation was conducted using two methods: in Kazakhstan, the CCK-8 method was employed, and in China, the MTT assay was performed. Our antiviral drug assays were based on potent antivirals characterised by low IC_{50} values, high selectivity indices (SI), rapid viral clearance, and improved patient survival. Toxic Drugs: low SI (high cytotoxicity). Ineffective Drugs: No significant reduction in viral load or clinical improvement was observed [103–104].

To determine the MOI (Multiplicity of Infection), you need both the number of plaque-forming units (PFU) and the number of target cells**.** MOI is calculated as:

MOI=PFU / number of cells

Thus, if you have 4×10^5 PFU and 1×10^5 cells, the MOI would be 4

MOI (Multiplicity of Infection) from $TCID_{50}$/ml, you need two additional pieces of information:

1. The number of target cells (e.g., cells per well or flask).
2. The volume of virus inoculum used (e.g., in millilitres).

MOI is calculated as:

MOI total infectious units/number of cells

Conversion Factor:

$TCID_{50}$ is a statistical measure of viral titer.

1 $TCID_{50} \approx 0.69$ infectious units (derived from the Poisson distribution).

Suppose you have:

1.2×10^5 $TCID_{50}$/ml viral stock,

1×10^5 cells,

1 ml of virus added.

1. Convert $TCID_{50}$ to infectious units:
   1.2×105 $TCID_{50}$/ml$\times0.69=8.28\times10^4$ infectious units/ml$1.2\times10^5 TCID_{50}$/ml$\times0.69$ $=8.28\times10^4$infectious units/ml
2. Total infectious units used:
   8.28×10^4 infectious units/ml$\times1$ ml$=8.28\times104$ infectious units
   8.28×10^4infectious units/ml$\times1$ml$=8.28\times10^4$infectious units
3. Calculate MOI:

$$MOI=8.28\times10^4/1\times10^5=0.828$$

Therefore 1.2 $X10^5$ $TCID_{50}$/ml $_{is}$ MOI of 1[101-108]

The number of cells being infected, and the volume used (in mL), to express the PFU per mL. Step-by-Step Conversion

Suppose you are infecting:

1×10^6 cells (1 million cells)

In a volume of 1 mL

An MOI of 2, infecting 1 million cells in 1 mL, corresponds to 2×10^6 PFU/mL. If your infection volume is different (e.g., 0.5 mL), the PFU/mL would be: 4 × 10^6 PFU/mL. Always specify the cell count and volume for accurate conversion.

Converting the average value of Ct into the MOI of RT-qPCR

Ct Value is the Cycle threshold —the PCR cycle at which fluorescence crosses the detection threshold. The relationship is inversely proportional to the starting nucleic acid quantity, as shown in Figure 12.

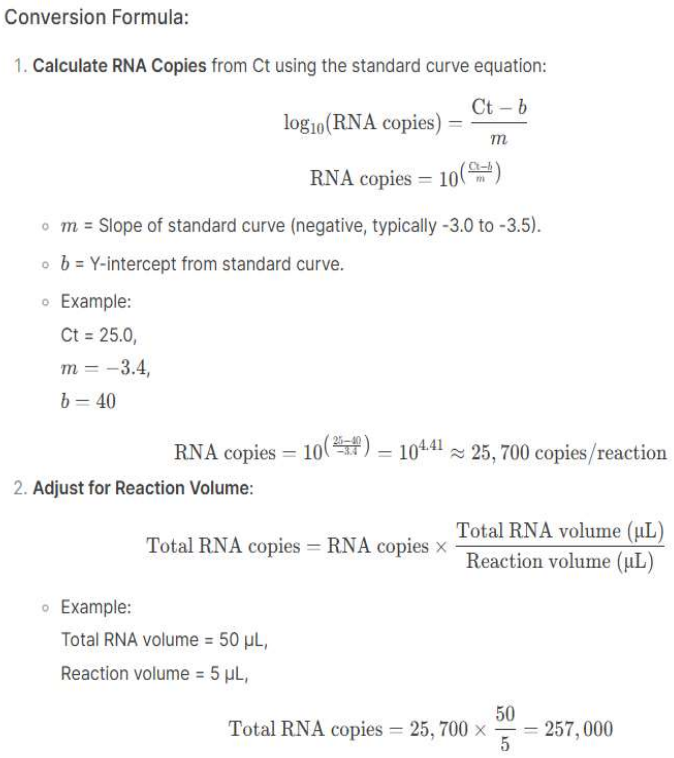

Figure 12 – Conversion formula for RNA copies from the average Ct-value

The figure outlines the procedure for converting qPCR cycle threshold (Ct) values into RNA copy numbers using a standard curve equation and subsequent adjustment for reaction volume. First, RNA copies are calculated by applying the equation: where *m* is the slope of the standard curve (typically -3.0 to -3.5) and *b* is the y-intercept. For example, with Ct = 25.0, *m* = –3.4, and *b* = 40, the calculation yields approximately 25,700 RNA copies per reaction. In the second step, this value is adjusted to account for the total RNA volume by multiplying by the ratio of the total RNA volume to the reaction volume. Using an example with a total RNA volume of 50 µL and a reaction volume of 5 µL, the calculation yields approximately 257,000 RNA copies. This method enables the accurate quantification of RNA molecules in a sample by utilising standard curve calibration and reaction scaling.

The presented scheme demonstrates a standardised approach for converting Ct values obtained in qPCR assays into RNA copy numbers, ensuring quantitative accuracy. The two-step procedure—first calculating RNA copies from the standard curve and then adjusting for reaction volume—allows normalisation across experiments and sample inputs. The example calculations illustrate how relatively small differences in Ct values, when processed through the logarithmic transformation of the standard curve, translate into significant differences in RNA copy number. This emphasises both the sensitivity and the exponential nature of qPCR quantification. The final adjustment for total RNA volume ensures that the reported copy numbers reflect the sample's accurate molecular content, making the method suitable for inter-sample comparisons and reproducible viral load assessments.

Standard Curve relates Ct values to known template quantities (log-scale). Generated RNA copies (Figure 13) using serial dilutions of standards. MOI is the Ratio of infectious viral particles to target cells. Requires converting RNA copies to infectious units via a virus-specific factor.

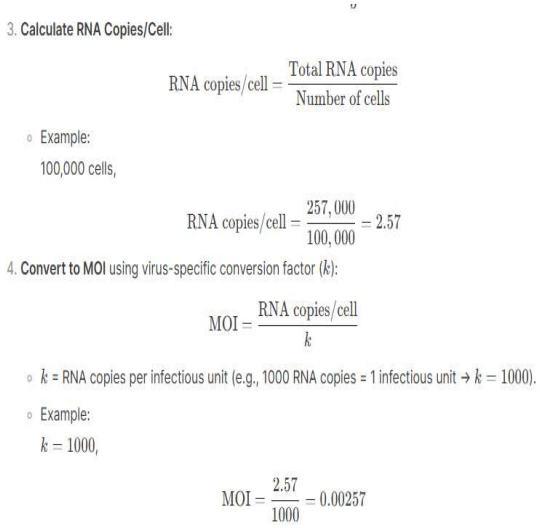

3. **Calculate RNA Copies/Cell:**

$$\text{RNA copies/cell} = \frac{\text{Total RNA copies}}{\text{Number of cells}}$$

- Example:
  100,000 cells,

$$\text{RNA copies/cell} = \frac{257,000}{100,000} = 2.57$$

4. **Convert to MOI** using virus-specific conversion factor (k):

$$\text{MOI} = \frac{\text{RNA copies/cell}}{k}$$

- k = RNA copies per infectious unit (e.g., 1000 RNA copies = 1 infectious unit → $k = 1000$).
- Example:
  $k = 1000$,

$$\text{MOI} = \frac{2.57}{1000} = 0.00257$$

Figure 13 – The calculation formula of RNA copies per cell, and then converting it into MOI [118]

A study of 72 patients (including critically ill individuals with RNAemia) reported a median nasopharyngeal (NP) swab viral load of 6.98 $\log_{10}$ copies/mL across all patients; among those with RNAemia who were critically ill, the median NP viral load was 5.4 $\log_{10}$ copies/μL (which equates to roughly 8.4 $\log_{10}$ copies/mL), significantly higher than in moderate-to-severe cases (2.6 $\log_{10}$ copies/μL) and non-survivors versus survivors (6.2 $\log_{10}$ copies/μL vs. 3.9 $\log_{10}$ copies/μL).

1.6 IL-33-Antiviral response cytokine (viral invasion imitator)

The newly described innate lymphoid cells of group 2 (ILC2) play crucial roles in type 2 immune responses, epithelial repair in mucosal tissues, and metabolic homeostasis. ILC2 releases large amounts of type 2 cytokines, including interleukin-4 (IL-4), IL-5, and IL-13, which stimulate type 2 immunity and protect against parasitic worms. However, without strict regulation, the level of ILC2s can lead to undesirable type 2 immune pathologies, including allergic inflammation of the respiratory tract, respiratory hypersensitivity, and atopic dermatitis. Viral infections of the respiratory tract, which are typical triggers of type 1 immune reactions, often lead to type 2 pulmonary immune pathologies, such as asthma and its exacerbations. Interestingly, pulmonary viral infections induce IL-33 release, leading to subsequent ILC2-mediated type 2 pulmonary immunopathology, independent of the adaptive immune system [117].

Interleukin-33 (IL-33) is a member of the IL-1 family of cytokines and plays a crucial role in the immune response. It is involved in various biological processes, including inflammation and tissue repair. Recent studies have highlighted its role in enhancing antiviral immunity. IL-33 acts primarily through its receptor, ST2 (suppression of tumorigenicity 2), which is expressed on various immune cells, including T cells, mast cells (CD117), and innate lymphoid cells. The activation of the IL-33/ST2 axis leads to:1. Enhanced T Cell Response: IL-33 promotes the differentiation of CD4+ T cells into Th2 cells, which can enhance the overall antiviral response.2. Increased Cytokine Production: IL-33 stimulates the production of antiviral cytokines such as IFN-γ and IL-4, which are crucial for controlling viral infections.3. Innate Immune Activation: It activates innate immune cells, including macrophages and dendritic cells, enhancing their ability to detect and respond to viral pathogens. Research has shown that IL-33 can significantly enhance antiviral responses in mice by increasing viral clearance [117]. Mice treated with IL-33 exhibit faster clearance of viral infections, such as influenza. Enhanced

Antibody Production: IL-33 promotes the generation of neutralising antibodies, which are essential for long-term immunity against viruses. Regulation of Immune Cell Recruitment: It influences the recruitment and activation of various immune cells to the site of infection, enhancing the overall immune response—experimental Evidence. Studies using mouse models have demonstrated that IL-33 treatment during viral infections reduces viral load and improves survival. Knockout Models: Mice lacking the IL-33 receptor (ST2) exhibited impaired antiviral responses, underscoring the importance of this pathway in mediating immune protection. IL-33 plays a significant role in enhancing antiviral immunity in mice. Its ability to activate various immune pathways makes it a potential target for therapeutic interventions in viral infections. Further research could explore its applications in vaccine development and treatment strategies for viral diseases [117]. CD117, also known as c-KIT, is a receptor tyrosine kinase that plays a vital role in the development and function of various cell types, particularly hematopoietic stem cells, mast cells, and interstitial cells of Cajal. IL-33, as mentioned earlier, is a cytokine involved in immune responses, particularly in promoting Th2-type responses. The interplay between CD117 and IL-33 is significant, particularly in immune modulation and inflammation. Role of CD1171.Mast Cell Development: CD117 is crucial for mast cell survival, proliferation, and differentiation, which play pivotal roles in allergic responses and inflammation [117]. Type 2 immunity is essential for immune defence against worm infections but can also be triggered by respiratory viruses, such as respiratory syncytial virus, influenza virus, and rhinoviruses [119-120].

This is surprising, as viral respiratory tract infections are potent inducers of innate and adaptive type 1 immune responses. It is important to note that viral respiratory infections are the leading cause of pathologies mediated by type 2 immunity, including bronchial asthma and its exacerbations [121]. All ILC groups depend on the transcription factor Id2 and the entire gamma chain of the IL-2 receptor. Additionally, the transcription factors GATA3 and RORα are essential for the development and function of ILC2 [122]. Group 2 innate lymphoid cells (ILC2) play a

critical role in regulating type 2 immune responses, tissue repair, and metabolic balance. They secrete cytokines such as IL-4, IL-5, and IL-13, which help defend against parasitic infections but can also drive allergic disorders (e.g., asthma, atopic dermatitis) if unregulated. Respiratory viral infections—though typically inducing type 1 immunity—can paradoxically trigger type 2 immunopathologies by activating ILC2s via IL-33.

Although viral infections (e.g., influenza, RSV, rhinovirus) usually activate type 1 immunity, they can paradoxically induce type 2 immune responses that exacerbate asthma and related respiratory diseases. The development and function of ILC2s depend on transcription factors such as Id2, GATA3, and RORα, as well as the IL-2 receptor γ-chain, underscoring their tightly regulated nature in maintaining immune balance.

1.7 Autoimmune Complications After Sinovac-CoronaVac COVID-19 Vaccination)

Vaccines are crucial for achieving collective immunity and are a powerful tool in preventive medicine, as they activate the secondary or adaptive immune response. Still, there are some groups of people for whom vaccination against SARS-CoV2 can be harmful and life-threatening. These patients (e.g., with Autoimmune disorders) are more seriously compromised by immunisation than by complications from viral infections [123]. On February 1, 2021, mass vaccination against COVID-19 began in the Republic of Kazakhstan [123]. Vaccination protects against infectious agents through the production of antibodies [123]. During the COVID-19 pandemic, Kazakhstan utilised several vaccines: the combined vector vaccine Sputnik V (Russia), inactivated vaccines SinoVac-CoronaVac (China), Sinopharm, QazVac (Kazakhstan), and the RNA-based Pfizer/BioNTech (USA) vaccine [123-126].

SinoVac-CoronaVac, developed by Sinovac Biotech, is an inactivated COVID-19 vaccine containing chemically inactivated SARS-CoV-2 grown on Vero cells. These vaccines include aluminium hydroxide or similar adjuvants. The immune response targets the SARS-CoV-2 spike protein, along with matrix, envelope, and nucleoproteins [123-126]. In November 2021, a 32-year-old woman presented to her general practitioner with symptoms including joint pain, morning stiffness, dry eyes, dry mouth, weight loss, facial hyperpigmentation, and elevated blood pressure.

Symptoms began two weeks after the second dose of the SinoVac-CoronaVac vaccine. A rheumatologist diagnosed her with rheumatoid arthritis. This case suggests that COVID-19 vaccination with the SinoVac-CoronaVac vaccine activated the immune system and acted as a trigger for the development of autoimmune overlap syndrome. Recognising the potential for autoimmune complications enables better post-vaccination patient monitoring and care. Treatment included corticosteroids, non-steroidal anti-inflammatory drugs, and rituximab. The patient passed away in 2023 [123]. This case describes the development of an overlap syndrome, characterised by rheumatoid arthritis and systemic lupus erythematosus (SLE), in a patient who received the inactivated SinoVac-CoronaVac COVID-19 vaccine.

The examination findings indicate autoimmune involvement triggered post-vaccination. It is hypothesised that antibodies generated by the vaccine might have cross-reacted with the patient's cells, triggering an autoimmune overlap syndrome. A clinical case described by Nurgaliyeva et al. (2024) details the development of a complex autoimmune overlap syndrome in a previously healthy 32-year-old woman, who manifested symptoms two weeks after receiving the second dose of Sinovac-CoronaVac. The patient developed rheumatoid arthritis, systemic lupus erythematosus (SLE), and Sjögren's syndrome–like features, with hematologic (leukopenia, thrombocytopenia), renal (proteinuria), musculoskeletal (polyarthritis), and systemic (weight loss, myalgia, pleuritis, pericarditis) involvement. Laboratory findings confirmed elevated inflammatory markers (CRP, ESR), high autoantibody titers (ANA, lupus anticoagulant, anti-DNA), and signs of hypercoagulation. Despite treatment with corticosteroids, NSAIDs, and rituximab, the patient's disease progressed, and she later died in 2023[127].

The vaccination acted as a trigger in genetically predisposed individuals, potentially via molecular mimicry or non-specific T-cell activation, mechanisms previously discussed in autoimmune. Comparable immune dysregulation has been reported in the context of COVID-19 itself. A separate case of Guillain-Barré Syndrome (GBS) occurred in a 47-year-old gastric cancer patient after SARS-CoV-2 pneumonia, highlighting the autoimmune potential of viral infection. The patient developed a mixed axonal-demyelinating neuropathy (AMSAN subtype) shortly after COVID-19 recovery.

At present, mRNA-based vaccines demonstrate a generally favourable safety and efficacy profile, though particular rare but clinically relevant adverse events have been observed. The majority of side effects are mild to moderate—such as local injection site pain, fatigue, and headache—and typically resolve within a few days [128]. However, cases of myocarditis and pericarditis, mainly among young males following the second dose, have been documented, prompting updates to safety recommendations [129]. Hypotheses regarding possible long-term effects, including chronic autoinflammation or DNA damage in vulnerable individuals, remain unconfirmed and require further longitudinal research [130]. Overall, the benefits of large-scale mRNA vaccination—particularly the reduction in severe COVID-19 cases and hospitalisations—are considered to outweigh the potential risks. At the same time, ongoing pharmacovigilance continues to monitor for rare complications [131].

2 METHODS AND MATERIALS

The methods and materials were used in accordance with BSL-3 and BSL-4 requirements, including the biological reservoir and the so-called breeding cell lines (Vero E6 cells). The drugs were dissolved in both buffers and vehicles.

2.2 Research objects

As an object of research, the SARS-CoV-2 Virus Strain, Variant B.1.1, was sampled from Kazakhstan from the bronchial fluids of moderately and severely ill patients. They were collected from sick patients (nasotracheal swabs) during the COVID-19 pandemic, with their consent for scientific research, as authorised by the Scientific and Practical Centre for Sanitary and Epidemiological Expertise and Monitoring, Almaty. Strain: *SARS-CoV-2/human/KAZ/B1.1/2021 Alpha variant* and kept in freezers at -96C^0.Viral titer Preparation for SARS-CoV-2 from a Human Specimen: A viral stock was prepared from a human specimen (e.g., nasopharyngeal swab, BALF), and the virus was isolated, propagated, and quantified under biosafety level 3 (BSL-3) conditions. Bronchoalveolar lavage fluid (BALF): The sample was centrifuged at 3,000 × g for 10 min to remove debris. Then, the supernatant was filtered through a 0.45 μm filter. The aliquots were stored at -80°C if not used immediately [17, 102, 126].

Infection Procedure: Cells were seeded in T25/T75 flasks or 6-well plates at 80% confluency. The cells were washed with PBS, and DMEM containing 2% fetal bovine serum (FBS) was added. The specimen broth was inoculated with human specimen filtrate at a multiplicity of infection (MOI) of 2. It was incubated at 37°C with 5% CO_2 for 1–2 hours, with gentle rocking every 15 minutes. Remove the inoculum and replace it with fresh DMEM + 2% FBS. Incubate for 48–72 hours, monitoring for cytopathic effect (CPE) and viral cytotoxicity. Harvest the supernatant when ~80% cytopathic effect (CPE) is observed [101]. Viral Stock Preparation**:** Collect supernatant into sterile tubes. Centrifuge at 3,000 × g for 10 min to remove cell debris. Filter using a 0.22 μm filter (to remove cellular contaminants). Aliquot into cryovials and store at -80°C [102]. Viral titer quantification: One of the following methods was used to determine the viral titer: a plaque assay, considered the gold standard for this measurement. Vero E6 cells were seeded in 6-well plates until they reached 100% confluency. Serial dilutions of the viral stock ranged from 10^{-1} to 10^{-7}. 0.2 mL of inoculum was added to each well, and the plates were incubated for 1 hour at 37°C. The wells were overlaid with DMEM containing 2% fetal bovine serum (FBS) and 1% agarose.

The plates were incubated for 3–5 days, then fixed with formaldehyde and stained with crystal violet. The plaques were counted, and the Plaque-Forming Units per millilitre (PFU/mL) were calculated [17, 102, 115, 126]. In summary, several challenges should be considered, including a low viral load. BALF samples, especially later in the disease, may have lower viral titers, making isolation difficult. Sample Availability: BALF collection is invasive and is primarily performed in hospitalised patients with specific indications, limiting the number of samples available. Cell Culture Adaptation: Propagation in cell lines can select for or induce mutations not present in the original patient sample.

Lung Removal for IL-33 experiment:

As a research subject, the lungs of wild-type mice were collected. Lift the heart with forceps, sever the trachea/oesophagus. Extract the entire lung bloc (heart, lungs, trachea)—separate lungs from heart/trachea on ice [117]—Decontaminate tools with 10% bleach or 70% ethanol. The waste was either autoclaved or chemically inactivated [117].

2.3 Research Materials

The following pieces of equipment were used in the work: an oligonucleotide synthesizer H-16 (K&Laborgeraete, Germany); thermal cyclers GeneAmp PCR System 9600 (Applied Biosystems) and TC-512 (Techne); thermal boards DryBlockHeater (Techne); shakers and vortexes Vortex-Genie 2 Shaker (Cole-Parmer); automatic micropipettes (Eppendorf); apparatus for electrophoresis of nucleic acids G100 (Pharmacia); gel documentation system "Bio-Rad" (USA); microcentrifuge "MiniSpin" (Eppendorf); a refrigerator maintained at –20 °C; a set of software packages for DNA sequence analysis including DNASYS MAX 1.0, Sequencer, Vector NTI, BioEdit, GENEDOC, and the Staden package; as well as a microplate reader (OD, optical density) Plate Verification instrument for Hipo MPP-96 (BioSAN) [101–103].

Equipment and disposables for MTT-kit:

Microplate reader capable of measuring absorbance at OD 590 nm

- Pipettes and pipette tips, including a multichannel pipette
- Tubes for the preparation of reagents and buffer solutions
- 96-well plates with a clear, flat bottom for antiviral safe assays, drug cytotoxicity [107].

Equipment and disposables for Cell counting kit 8 (CCK8) - Microplate reader capable of measuring absorbance at OD 450 nm

The study utilized pipettes and pipette tips, including a multichannel pipette; tubes for the preparation of reagents and buffer solutions; 12-well plates with a clear flat bottom for drug cytotoxicity assays; 96-well plates with a clear flat bottom for antiviral assays using non-cytotoxic drug concentrations; a multichannel pipette (8 or 12 channels, 10–100 µL); a CO_2 incubator; a clean bench; a haemocytometer or cell counter; and a centrifuge equipped with a rotor for 15-mL centrifuge tubes [106,126].

Equipment and disposables for the IL-33 stimulation experiment

The IL-33 stimulation experiment was carried out using a BD Canto II flow cytometer and FlowJo software, along with syringes (5 mL and 10 mL), needles (23G and 18G, 1½"), Petri dishes (60 × 15 mm), sharp scissors or razor blades, 70 µm cell strainers, and a GentleMACS Dissociator.

Equipment for Electron Microscopy JEOL JEM-100CX

According to Figure 14, an electron microscope setup in a laboratory environment, likely a transmission electron microscope (TEM), features a tall vertical column and a control panel layout. The system appears to be well-maintained and equipped with analogue control modules for focusing, magnification, and vacuum

regulation. The microscope is positioned on a vibration-dampening desk with integrated storage drawers and control units, ensuring stability during imaging [126].

Figure 14 –Electron microscopy equipment, JEOL JEM-100CX [126]

Reagents and solutions: the murine tissue extraction materials

The study used the following reagents and solutions for murine tissue extraction and cell culture experiments. Sterile surgical tools (forceps and scissors), 10% neutral buffered formalin, or freezing media were employed for tissue extraction. Personal protective equipment (PPE), including a respirator, gloves, and a gown, was used to ensure biosafety during all procedures.

For in vitro experiments, Vero C1008 [Vero 76, clone E6, Vero E6] cells, derived from the kidney of the African green monkey and obtained from Sigma Aldrich, were used. These anchorage-dependent cells are widely applied in molecular and cell biology research [106] and enable high-titer replication of severe acute respiratory syndrome coronavirus (SARS-CoV-2) [107]. Sub-confluent cultures (70–80%) were split at ratios of 1:3 to 1:10, corresponding to seeding densities of 1–3 × 10^4 cells/cm^2, using 0.25% trypsin or trypsin/EDTA under conditions of 5% CO_2 and 37 °C. Vero E6 cells exhibit approximately 50% susceptibility to SARS-CoV-2 infection and are 100% permissive, meaning they fully support viral replication. Therefore, this cell line was selected as a justified and reliable in vitro model for the current thesis research.

The culture medium

Dulbecco′s Modified Eagle′s Medium (DMEM) - high glucose, with 4500 mg/L glucose, sodium pyruvate, and sodium bicarbonate, without L-glutamine, liquid, sterile-filtered, suitable for cell culture. Vero E6 cells (confluent in 96-well plates). BALF sample (processed to remove debris/mucus). Cell culture medium (e.g., DMEM supplemented with 2% fetal bovine serum [FBS] and antibiotics). Sterile pipettes, 96-well plates, and a biosafety cabinet. Inverted microscope.

PCR

Recombinant Taq DNA Polymerase, 5000 units/mL, Sigma.

The study employed a range of molecular biology reagents and consumables, including T4 DNA ligase, the ProtoScript® II First Strand cDNA Synthesis Kit,

RNAZap decontamination solution, and the SuperScript IV One-Step RT-PCR System with Platinum Taq DNA Polymerase (Invitrogen, USA; 100 reactions). Additionally, 310 and 31xx Running Buffer (10X) and the BigDye™ Terminator v3.1 Cycle Sequencing Kit (100 reactions) were used. For visualisation, SYBR Safe DNA gel stain served as a non-toxic reagent for agarose gel staining. UltraPure™ nuclease-free distilled water was employed in all molecular procedures to ensure sample integrity. Consumables included microcentrifuge tubes (1.5 mL, 500 pcs/pack, Eppendorf), microtubes (0.2 mL, flat cap, 1000 pcs/pack, Eppendorf), and microtubes (0.5 mL, flat cap, 1000 pcs/pack, Eppendorf) [17,126].

MTT Assay Kit

The MTT Assay Kit (ab211091) for cell proliferation is a convenient, non-radioactive, high-throughput system that measures cell proliferation, viability, and cytotoxicity with high accuracy and reproducibility.

MTT Reagent (50 mL)

The MTT Reagent (50 mL) was used as supplied and equilibrated to room temperature before use, with the vial opened under sterile conditions. The reagent was aliquoted to provide sufficient volume for the required number of assays and stored at –20 °C, protected from light.

MTT Solvent (150 mL)

The MTT Solvent (150 mL) was used as supplied and equilibrated to room temperature before use. The reagent was stored at –20 °C and used within 2 months of opening. Additionally, 199 Medium—a mixture of Hank's salts, glutamine, inorganic salts, amino acids, vitamins, glucose, and phenol red dissolved in purified water and sterilised by membrane filtration—was employed. This medium is formulated for cell cultivation outside the incubator due to its low sodium bicarbonate content (1.0 g/L) and was obtained under catalogue number C230p [102,126].

The virus preparation and safety procedures

An isolate of the SARS-CoV-2/human/KAZ/B1.1/2021, Alpha variant strain, was passaged in Vero E6 cells to establish a high-titer stock for all our experiments. Since SARS-CoV-2 is classified as a high-risk pathogen in Kazakhstan, all virus procedures, including infecting cell lines and subsequent monitoring, are conducted in a BSL-2 (Biosafety Level 2) laboratory. All direct manipulation with either viral titters or growth-active virus strains in biological tissues is performed using human biomaterials under BSL-3/4 bio-lab conditions [126].

2.4 Research Methods

This study employed Kit-based methods for CCK8 viability measurement and RNA isolation, aiming to accelerate the results-gaining process and facilitate comparison with traditional (laborious) techniques, such as MTT-viability testing.

2.3.1 Bronchoalveolar Lavage Fluid -supernatant collection

The following materials and equipment were used for molecular biology, histology, and cytology methods: bronchoalveolar lavage fluid (BALF) samples were centrifuged at 2,000 × g for 10 minutes at 4 °C to pellet cells and debris. The resulting

supernatant was transferred to sterile tubes and passed through a 0.22 μm syringe filter to remove any remaining particles. The filtered specimens were then aliquoted and stored at –80 °C until further use. It should be noted that not all BALF samples were intact, and sufficient SARS-CoV-2 viral load was detected only in a subset of the 117 BALF tubes provided.

2.3.2 Murine lung IL-33 stimulation experiment

The murine lung IL-33 stimulation experiment was conducted using recombinant mouse IL-33 (carrier-free, endotoxin-tested), administered intranasally (i.n.) in a total volume of 30 μL (15 μL per nostril) with sterile phosphate-buffered saline (PBS, pH 7.4) as the vehicle.

Additional reagents and buffers included: phosphate-buffered saline (PBS) without calcium and magnesium; enzyme-free wash buffer composed of RPMI1640 supplemented with 5% fetal bovine serum (FBS); and four digestion buffers—(A) RPMI1640 with 5% FBS, 0.5 mg/mL Collagenase Type IV, and 0.1 mg/mL DNase I; (B) RPMI1640 with 5% FBS, 0.5 mg/mL Liberase TM, and 0.1 mg/mL DNase I; (C) RPMI1640 with 5% FBS, 0.2 mg/mL Collagenase P, 0.8 mg/mL Dispase II, and 0.1 mg/mL DNase I; and (D) the Miltenyi Biotec Lung Dissociation Kit (Cat. No. 130-095-927).

For flow cytometry and staining procedures, blocking buffer (PBS, 2% FBS, and 2.4G2 hybridoma supernatant for Fc receptor CD16/CD32 blocking), FACS buffer (PBS, 2% FBS), and fixation buffer (4% paraformaldehyde or the Foxp3 staining kit, eBioscience, Cat. No. 5523, for nuclear transcription factor detection) were used. Red blood cell lysis buffer (Sigma-Aldrich, Cat. No. R7757) and a viability stain (Fixable Live/Dead staining kit, Life Technologies, Cat. No. L34957) were also applied as part of the experimental workflow [117,118].

Antibodies for flow cytometry for staining

For flow cytometry staining, the following antibodies were used. Lineage-specific antibodies included TCRβ (clone H57-597), TCRγδ (clone eBioGL3), CD11b (clone M1/70), CD11c (clone N418), B220 (clone RA3-6B2), CD3ε (clone 145-2C11), Ter119 (clone Ter119), and NK1.1 (clone PK136) to exclude lineage-positive cells. CD45 (clone 104) was used to identify hematopoietic cells specifically. To detect and enrich group 2 innate lymphoid cells (ILC2), antibodies against KLRG1 (clone 2F1) and Thy1/CD90 (clone 53-2.1) were applied. Additional surface and intracellular markers included Sca-1 (clone E13-161.7), c-Kit (CD117; clone 2B8), ICOS (clone C398.4A), CD69 (clone H1.2F3), CD25 (clone PC61.5), ST2 (clone RMST2-2 or DJ8), and GATA3.

2.3.3 Viral Cultivation on VeroE6 Cells

The VeroE6 cells were grown in DMEM supplemented with 10% fetal bovine serum (FBS) and antibiotics (penicillin/streptomycin) at 37 °C and 5% CO_2 until they reached 80–90% confluence [126].

Vero E6 Cells - Infection

Supernatants were thawed quickly. BALF/murine supernatants were thawed at 37°C. The cell culture medium was aspirated. Adding the supernatant (e.g., 100–500

µL per well of a 6-well plate). Furthermore, it is diluted in maintenance medium (DMEM + 2% FBS) if needed. The Incubation lasted 1–2 hours at 37°C with gentle rocking every 15 min. Post-inoculation: Replacement of inoculum with fresh maintenance medium containing antibiotics. CPE Observation: Under a microscope, the culture was checked daily for cytopathic effects (cell rounding, syncytia, and detachment). The efficient extraction of SARS-CoV-2 from bronchoalveolar lavage fluid (BALF) and murine airways, followed by successful cultivation in VeroE6 cells, is crucial for virological studies [126].

Viral RNA isolation

mRNA was extracted for downstream processes, including RNA sequencing, qPCR, and reverse transcription for cDNA synthesis. Because it enables researchers to examine gene expression under specified conditions at a given moment (Figure 15) [17, 102, 115,126]. Total RNA is isolated using various techniques. Phenol-chloroform extraction is a traditional method that has been replaced by Trizol, which separates RNA from DNA and proteins based on their solubility. The RNA remains in the aqueous phase and was precipitated using isopropanol. Silica-Based Column Purification: Kits were available for rapid RNA isolation (e.g., Qiagen RNeasy) using silica membranes that selectively bind RNA under specific buffer conditions. Since total RNA includes other forms, such as rRNA and tRNA, mRNA typically accounts for only 1–5% of total RNA. Two primary methods enriched mRNA: Oligo-dT Beads. These beads were coated with oligo(dT) sequences that bind to the poly-A tail of eukaryotic mRNAs. Non-polyadenylated RNAs (rRNA, tRNA) were washed away, leaving enriched mRNA. Ribosomal RNA Depletion: In cases where poly (A) tails were absent (in prokaryotes), specific kits or methods were used to remove rRNAs, thereby enriching the mRNA fraction. According to the manufacturer's instructions, viral RNA was isolated from virus-containing material (nasotracheal swabs) using the QIAamp Viral RNA Mini Kit (Qiagen). For 50 RNA preps, the following reagents were required: 50 QIAamp Mini Spin Columns, carrier RNA, 2 mL Collection Tubes, and RNase-free buffers [17, 102, 115,126].

Confirmation of viral load via RT-qPCR (genomic copies)

The qRT-PCR targeted the N, E, S, and M genes, as well as the ORF1ab gene. A standard curve was used to estimate genome copies, final storage, and biosafety. The viral stock was stored at -80°C in small aliquots to prevent freeze-thaw cycles. The SARS-CoV-2 was handled under BSL-3 conditions with personal protective equipment (PPE), including N95 respirators, face shields, gowns, and gloves. The work surfaces, treated with 10% bleach or 70% ethanol, were washed. SARS-CoV-2 was isolated from a nasopharyngeal swab by authorised specialists, and the biosample was sent to a biosafety institute in Gvardevskyi for isolation. They were propagated in Vero E6 cells cultured in MEM containing 2% FBS. 72 hours after infection, supernatants containing released viral particles were collected and centrifuged at 600 g for 5 minutes. Virus stocks were stored at −80°C until use [17, 102, 115,126].

According to Figure 15, the efficiency of different RNA isolation methods for SARS-CoV-2 is assessed by quantification cycle (Cq) values. Three approaches are shown: QIAamp Viral RNA Mini Kit, manual extraction using the QIAamp 96 Viral

RNA Kit, and automated extraction with the QIAcube HT system. The Cq values across all methods are very similar, ranging from 25 to 27, indicating comparable RNA recovery and suitability for downstream RT-qPCR analysis. The QIAamp Viral RNA Mini Kit and manual extraction yield slightly lower Cq values, suggesting a marginally higher sensitivity or recovery efficiency. In contrast, the automated method shows a minor increase in Cq values, which could reflect a slightly lower RNA yield or higher variability. Overall, the results highlight that all three methods are reliable for SARS-CoV-2 RNA isolation, with only minor differences in efficiency, making the choice between them more dependent on workflow needs, throughput, and automation requirements rather than performance limitations.

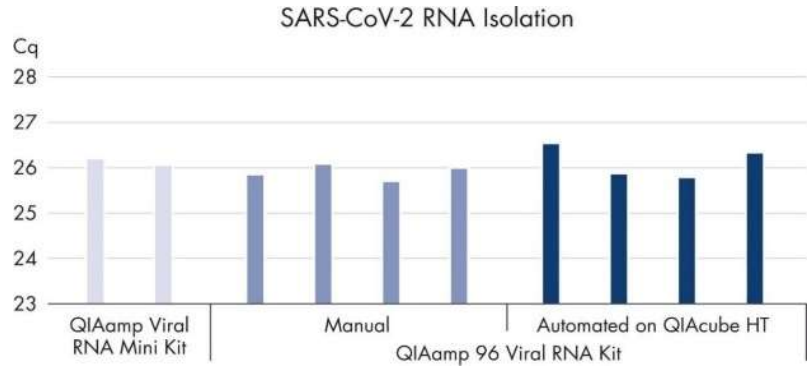

Figure 15 – Manufacturers ensure the efficacy of the viral RNA Mini Kit in quantity

No phenol-chloroform extraction was required. Viral RNA binds specifically to the QIAamp silica membrane while contaminants pass through. PCR inhibitors, such as divalent cations and proteins, were completely removed in two efficient wash steps, leaving pure viral RNA for elution in either water or the buffer provided with the kit. QIAamp RNA technology enabled the isolation of viral RNA from cell-free body fluids, making it ready for RT-PCR and blotting procedures. QIAamp sample preparation technology is fully licensed [102, 104, 126].

2.3.4 Molecular biology and virus strain processing

Primer selection and synthesis were carried out using Oligo 6 and Vector NTI Suite 10, with reaction parameters optimised according to enzyme annotations and primer properties. Primers were synthesised on an H-16 oligonucleotide synthesiser (Germany), eluted with concentrated ammonia, dried using a rotary evaporator, and purified by alcohol precipitation [17].

PCR amplification was performed using the SuperScript III One-Step RT-PCR System with Platinum Taq High Fidelity (Invitrogen) on GeneAmp PCR System 9600 and TC-512 thermal cyclers. Amplified DNA fragments were visualised by electrophoresis on a 1% agarose gel using a Pharmacia G-100 apparatus, with molecular weight markers from Invitrogen and analysis performed via the Quantity One program.

Sequencing procedures employed the AMPure XP cleanup system, the QIAamp Virus RNA Kit, and triazole reagents for RNA isolation, followed by BigDye Terminator v3.1 Cycle Sequencing and purification with the CleanSeq Kit. Sequencing was conducted on the Genetic Analyser 3130xl (Applied Biosystems/Hitachi) and analysed using CLC Genomic Workbench 11.0.1. Additional genome-wide sequencing was performed on the Ion GeneStudio S5 system.

Approximately 70% of the SARS-CoV-2 genome was successfully sequenced from RNA isolated from virus-containing material. Amplicons of the ORF1ab gene were verified by gel electrophoresis using 46 primer pairs designed specifically for this region.

While antigen-based rapid tests offer rapid, cost-effective detection of COVID-19, they are less sensitive than RT-PCR, particularly at low viral loads. Therefore, confirmatory PCR testing remains essential for accurate diagnosis. The study was conducted under stringent biosafety conditions in the BSL-3 laboratory of the Research Institute for Biological Safety Problems (Kazakhstan) [17].

Overall, integrating RT-PCR, sequencing, and antigen testing provided a comprehensive, efficient workflow for SARS-CoV-2 detection and genomic analysis, balancing accuracy, biosafety, and operational efficiency.

2.3.5 The principles for selecting the concentrations of antiviral drugs

Since we were working with tablet formulations of TDF, T-705, and Ribavirin, the dosing concentration was set at 200 μg/mL. The concentration was reduced to 50 μg/mL to ensure cell viability and to assess the drugs' effectiveness against high viral loads (MOI of 2), thereby facilitating the detection of viral inhibition using an antigen-based testing system. In China, we began working with TAF, and the concentration was de-escalated from 50 μg/mL to 6.25 μg/mL for two reasons: first and foremost, we knew the relative drug CC%-safe concentration of Tenofovir (TDF). Secondly, in Kazakhstan, we did not have sufficient time to further decrease the concentrations of antivirals below 50 μg/mL for TDF, T-705, and Ribavirin [126].

For in vitro testing, drug concentrations were selected to balance assay sensitivity at high viral input with cell viability. We used Vero E6 cells infected at MOI = 2 to ensure a robust antigen signal, and we evaluated drug activity across non-cytotoxic ranges defined by CC50 measurements obtained under identical assay conditions. For TDF, favipiravir (T-705), and ribavirin, the initial screen used 200 μg/mL (with subsequent two-fold serial dilutions) based on solubility and preliminary cytotoxicity assessments; the upper bound was reduced to 50 μg/mL to maintain ≥80–90% cell viability while preserving dynamic range for detecting antigen reduction. When we introduced TAF, we applied a narrower, non-cytotoxic range (50 to 6.25 μg/mL; corresponding to approximately X–Y μM), informed by prior tenofovir cytotoxicity data (using the same cell line and assay conditions) and pilot measurements indicating comparable or lower cytotoxicity relative to TDF. All concentrations were prepared with a consistent vehicle content (≤0.1% DMSO) in both drug and control wells. For each compound, we quantified IC50/IC90, CC50, and

selectivity index (SI = CC50/IC50) from at least three biological replicates, ensuring that the tested range bracketed both efficacy and cytotoxicity thresholds.

Antigen-based SARS-CoV2 identification

According to Figure 16, antigen-based identification of SARS-CoV-2 is a rapid diagnostic method that detects viral proteins (antigens) in respiratory samples, such as nasal or throat swabs. These tests are widely used for screening and diagnosis due to their speed, cost-effectiveness, and ease of use [115].

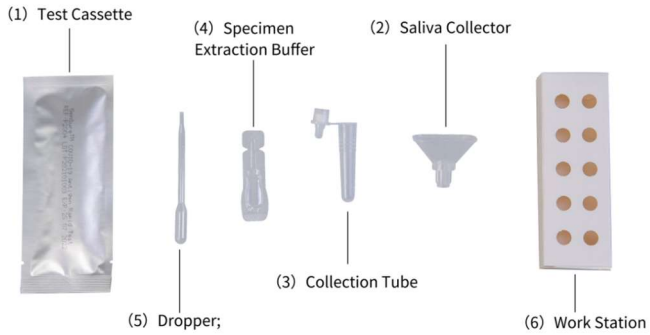

Microorganism	Concentration	Cross-Reactivity (Yes/No)
Influenza A (H1N1, H3N2)	1.0 x 10^5 $TCID_{50}$/mL	No
Avian influenza (H5N1, H7N9)	1.7 x 10^5 $TCID_{50}$/mL	No
Influenza B (Victoria, Yamagata)	2.5 x 10^5 $TCID_{50}$/mL	No
Parainfluenza virus	1.0 x 10^5 $TCID_{50}$/mL	No
Respiratory Syncytial Virus	3.8 x 10^5 $TCID_{50}$/mL	No
Rhinovirus	1.4 x 10^5 $TCID_{50}$/mL	No
Adenovirus	1.1 x 10^5 $TCID_{50}$/mL	No
Measles virus	1.0 x 10^6 $TCID_{50}$/mL	No
Human coronavirus (OC43, 229E, NL63)	1.0 x 10^5 $TCID_{50}$/mL	No
MERS coronavirus	1.2 x 10^5 $TCID_{50}$/mL	No
Mycoplasma pneumoniae	1.0 x 10^6 CFU/mL	No
Chlamydia pneumaniae	1.0 x 10^6 CFU/mL	No
Legionella pneumophila	1.1 x 10^6 CFU/mL	No

Figure 16 — Overview of the GenSure™ COVID-19 Antigen Rapid Test Kit [115,126]

It utilises polymer immunochromatographic technology and a double-antibody sandwich principle to qualitatively detect the N (Nucleocapsid) protein antigen from SARS-CoV-2 in human nasal swab specimens. Testing is limited to laboratories and medical institutions. This express test is efficient for instant testing. The antigen test is high-speed and reliable. It involves pouring the swab into the viral inoculum titer and testing it for viral load.

2.4 Key methods of dissertational work

The key methods employed in this dissertation included assessing cytotoxicity (CC_{50}) to evaluate cell viability in uninfected cultures, determining antiviral activity (EC_{50}/IC_{50}) based on viral load reduction in infected cells, and confirming viral inhibition (IC_{50}) through PCR or antigen-based SARS-CoV-2 detection assays. These

approaches together provided a comprehensive evaluation of the safety and efficacy of the tested compounds against SARS-CoV-2 in vitro.

Cell Preparation & Plate Layout

The experiments were conducted in "Table 2" using Vero E6 cells maintained in DMEM supplemented with 10% FBS, cultured in 96-well plates with triplicate wells for each condition, following a predefined experimental layout.

Table 2 — The Plate layout for A. 96 wells testing for fixed drug concentrations and antiviral assay, n =3. B. 96 wells testing for four drug concentrations(de-escalating), n=3, in Kazakhstan

№	Condition / Drug	Concentration, μg/mL	Columns (wells)
1	Cell Control (Cell Ctrl)	-	1-2
2	Virus Control (VC)	-	3-5
3	Ribavirin	50	6-8
	Ribavirin (DR*)	200, 150, 100, 50	9-12
4	Favipiravir	50	1-4
	Favipiravir (DR*)	200, 150, 100, 50	5-8
5	Tenofovir (TDF)	50	9-12
	Tenofovir (DR*)	200, 150, 100, 50	13-16**

*DR - Dose Response.

** Note: The original data did not specify columns for the Tenofovir DR; this is a logical extension assuming a 96-well plate layout.

CCK8-testing of fixed concentrations; however, the four concentrations can be visually validated. Columns 1–2 represent the cell control (uninfected, untreated wells), serving as a baseline for assessing cell viability and morphology in the absence of viral challenge. Columns 3–5 correspond to the virus control (VC), containing infected but untreated cells, which serve as a reference for viral cytopathic effects and for quantifying infection efficiency.

Columns 6–8, 9–11, and 12 "Table 3" include wells treated with Ribavirin, Favipiravir, and Tenofovir disoproxil fumarate (TDF), respectively, each administered at a fixed concentration of 50 μg/mL. These serve as primary antiviral test conditions for comparing drug efficacy under standardised viral load and cell density. Row B introduces an additional dimension — dose-response (DR) experiments — in which each antiviral compound is tested across a concentration gradient (200, 150, 100, and

50 µg/mL). This enables the evaluation of dose-dependent antiviral activity and the determination of key pharmacological parameters, such as the IC_{50} value (the concentration at which 50% of the maximum effect is achieved).

Overall, this layout ensures a structured and reproducible approach to comparing antiviral potency, cytotoxicity, and concentration-dependent effects of candidate compounds relative to both virus-only and cell-only controls.

Table 3 — The Plate layout for A. 96 wells testing for fixed drug concentrations and antiviral assay, n =5. B. 96 wells testing for four drug concentrations(de-escalating), n=5, in China

Group	Substance	Working concentration, µg/mL	Wells
1	Cell Control (Cell Ctrl)	–	A1, B1
2	Virus Control (VC)	–	C1, D1, E1
3	Ribavirin	50	F1, G1, H1
	Ribavirin (DR)*	200, 150, 100, 50	A2, B2, C2, D2
4	Favipiravir	50	E2, F2, G2, H2
	Favipiravir (DR)*	200, 150, 100, 50	A3, B3, C3, D3
5	Tenofovir (TDF)	50	E3, F3, G3, H3
	Tenofovir (DR)*	200, 150, 100, 50	A4, B4, C4, D4

Note: *DR – Dose Response.

MTT-testing of fixed concentrations; however, the four concentrations can be visually validated.

- DR = Dose-response (4 concentrations, e.g., 200,150,100. 50 µg/mL).
- Row A-D: Uninfected cells (for cytotoxicity).
- Row E-H: SARS-CoV-2-infected cells (for antiviral activity

Drug Preparation

Drug preparation involved preparing stock solutions of ribavirin, favipiravir, and tenofovir alafenamide (TAF) at 10 mM in DMSO. For experimental use, working concentrations were prepared as a fixed dose of 50 µg/mL diluted in serum-free DMEM, and for dose–response studies, serial dilutions ranging from 200 to 50 µg/mL were used.

Infection & Treatment

The infection and treatment procedure involved seeding Vero E6 cells (2×10^4 cells per well) in 96-well plates on Day 0 and incubating them for 24 hours at 37 °C with 5% CO_2. On Day 1, cells in rows E–H were infected with SARS-CoV-2 at an MOI of 0.05 in serum-free DMEM for 1 hour at 37 °C, followed by removal of the inoculum and a single PBS wash. Designated wells then received drug treatments at a fixed dose of 50 µg/mL or dose–response concentrations. At the same time, control groups included uninfected (cell control), infected without drug (virus control), and solvent control (0.1% DMSO). Cultures were incubated for 48 hours at 37 °C and 5% CO_2. Following incubation, supernatants were collected for viral RNA extraction (qRT-PCR). For cytotoxicity assessment (rows A–D), 10 µL of PrestoBlue or MTT reagent was added, incubated for 2 hours, and absorbance was measured at 570 nm (or fluorescence at $560_{ex}/590_{em}$). For antiviral activity evaluation (rows E–H), cells were lysed in RLT buffer to isolate intracellular viral RNA for further analysis.

In Kazakhstan, cytotoxicity was assessed in rows A–D by adding 10 µL of CCK-8 reagent (WST-8 formazan) to each well, incubating for 1 hour, and measuring absorbance at 450 nm or fluorescence at $450_{ex}/480_{em}$.

For quantitative RT-PCR (qRT-PCR) analysis of SARS-CoV-2, amplification targeted the N gene using 65 specific primers. A standard curve was generated from serial dilutions of SARS-CoV-2 RNA (10^1–10^8 copies/µL)

Cell- cytotoxicity assay

Dose escalation in vitro is observed when the drug tablet formulations are dissolved in DMEM, thoroughly mixed at room temperature for 30 minutes, and then diluted to the doses specified in “Table 4”.

Table 4 – The CC-test (cytotoxic test) of four drugs in increasing stock concentrations and exposure time, with a control for each drug, on E6-vero cells (24-well assay)

1X (4мг/мл) DEX. 1ml 10 µM	2X в 10 ml 20 µM	3X10 ml 30 µM	4X10 ml 40 µM	5X10 ml 50 µM	Control
1X 1300 µM (200мг/мл) FAV 1ml	2X10ml 2600µM	3X10 ml 3900µM	4X10 ml 5200 µM	5X10 ml 6500 µM	Control
1X 820 µM (200мг/ml) Ribo. 1ml	2X10 ml 820µM	3X10 ml 1640µM	4X10 ml 2460µM	5X10 ml 3280µM	Control
1X (300/мл) Teno. 1ml 1045µM	2X 10 ml 2090µM	3X10 ml 3135µM	4X10 ml 0	5X10 ml 0	Control
1day	1day	1day	1day	1day	1day

The manufacturer or local distributors deliver the medications in stock concentrations in water-soluble agents. The medium was prepared using DMEM (D6546) supplemented with 2 mM L-glutamine (G7513) and 10% FBS/FCS (F2442).

This medium consisted of DMEM with 2% bovine serum and 0.01% (100 U/ml) antibiotics (Penicillin-Streptomycin).

Dose-de-escalation in vitro was observed in the 24 wells containing Vero E6 cells, each with a different drug concentration pattern. The concentrations of Favipiravir were 1270 μM, 318 μM, 127 μM, 12.7 μM, 1.27 μM, 0.127 μM, and control. Ribavirin concentrations were: 820μM, 205 μM, 82μM,8,2μM,0,82μM, 0,082μM and control. Tenofovir concentrations were: 1050μM, 174μM,10,5μM,1,5μM, 0.105μM and control. Dexamethasone concentrations were 10 μM, 20 μM, 30 μM, and control. The samples were transferred to a 5% CO2 incubator at 37 °C for 72 hours. According to the manufacturer's instructions, viral RNA was isolated from virus-containing material using the QIAamp Viral RNA Mini Kit (Qiagen). A case of coronavirus infection was used as the research object.

CCK8 test for cell viability in four drug concentrations

The CD8-Kit-8 (KK-8) enables sensitive colourimetric analysis to determine cell viability in studies of cell proliferation and cytotoxicity. The water-soluble dojo-tetrazole salt, WST-8, is reduced in cells by dehydrogenase activity, forming a yellow formazan dye soluble in tissue culture medium. The amount of the dye formazan, produced by the activity of dehydrogenases in cells, is directly proportional to the number of living cells. Step 1: Add 10 Pl of Cell Counting Kit-8 to each well in a 96-well microplate. Step 2: Place in a CO_2 incubator for 1-4 hours to allow the reaction to proceed. Step 3: Measure the absorbance at 450 nm using a microplate reader [126].

Determination of cytotoxicity of drugs for cell culture

Dexamethasone, Ribavirin, Tenofovir, and Favipiravir were selected for study to evaluate their antiviral activity against SARS-CoV-2. Before determining the antiviral activity, a working dose was established that did not cause toxicity in cell culture. Dexamethasone was used in ampoules containing 4 mg/ml in 5 dosages (20, 16, 12, 8, and 4 mg/ml).

Measuring the Efficacy of Antivirals Against SARS-CoV-2

Optimised 96-Well Plate Protocol: Antiviral Activity of TAF on SARS-CoV-2 in Vero E6 Cells. Objective: Confirm a 2-log reduction (log<sub>10^7 → $\log10^5$ copies/mL) using qRT-PCR, while integrating cytotoxicity and antiviral efficacy (in a single plate**.**

Plate Layout (96-Well Plate)

The 96-well plate layout comprised 96 wells (12 columns × 8 rows), organised into six experimental conditions, with 16 replicates per condition to ensure statistical reliability. The design included a TAF dose–response setup with four concentrations alongside control groups, ensuring maximal plate utilisation. Specifically, cell controls (uninfected, no drug) occupied wells A1–A4, B1–B4, C1–C4, and D1–D4; virus controls (infected, no drug) occupied wells E1–E4, F1–F4, G1–G4, and H1–H4; and the remaining wells were assigned to TAF-treated groups across the four concentration gradients.

TAF Concentrations (μg/mL):

The TAF dose–response experiment was conducted using four concentrations of tenofovir alafenamide (TAF)—6.25, 12.5, 25, and 50 μg/mL—each tested in eight

replicates (totalling 64 wells). Lower doses (6.25–12.5 μg/mL) were assigned to rows A–D, while higher doses (25–50 μg/mL) were placed in rows E–H. In China, the experimental workflow proceeded as follows: on Day 0, Vero E6 cells were seeded at 2.5×10^4 cells per well in 100 μL of DMEM supplemented with 10% FBS and incubated for 24 hours at 37 °C and 5% CO_2 to reach 80–90% confluence.

On Day 1, the virus inoculum was prepared by diluting SARS-CoV-2 in serum-free DMEM to a multiplicity of infection (MOI) of 0.05, corresponding to approximately 10^7 copies/mL in virus control wells after 48 hours. Infection was initiated in the virus control (VC) and TAF-treated groups by aspirating the medium and adding 50 μL of virus inoculum per well, followed by 1.5 hours of adsorption at 37 °C.

After infection, the inoculum was removed, wells were washed once with PBS, and treatments were applied: cell controls (CC) and virus controls (VC) received serum-free DMEM with 0.1% DMSO. In contrast, TAF wells received serum-free DMEM containing the corresponding drug concentrations. All plates were incubated for 48 hours at 37 °C and 5% CO_2.

On Day 3, supernatants (80 μL per well) were collected into a 96-well PCR plate for RNA extraction after centrifugation at 3,000 × g for 10 minutes. In parallel, cytotoxicity was evaluated by adding 10 μL of PrestoBlue® reagent to each well, incubating for 1 hour at 37 °C, and measuring fluorescence ($560_{ex}/590_{em}$).

RNA extraction was performed using the QIAamp 96 Viral RNA Kit, with 50 μL of cleared supernatant as input. qRT-PCR targeting the SARS-CoV-2 N1 gene (CDC primers and probes) was conducted using TaqPath™ 1-Step RT-qPCR Master Mix (5 μL RNA + 15 μL mix). Quantification was based on a standard curve generated from 10-fold serial dilutions of SARS-CoV-2 RNA (10^1–10^8 copies/μL). The thermal cycling conditions were 50 °C for 15 min, 95 °C for 2 min, followed by 40 cycles of 95 °C for 3 sec and 60 °C for 30 sec.

A ≥2-log reduction in viral load—defined as $\leq 10^5$ copies/mL in TAF-treated wells compared to $\geq 10^7$ copies/mL in virus control wells—was considered evidence of significant antiviral activity. Statistical validation was performed using ANOVA followed by Dunnett's test ($p < 0.05$), confirming a dose-dependent reduction in viral replication with increasing TAF concentrations.

Expected Results for TAF

The expected results for tenofovir alafenamide (TAF) treatment include identification of the effective concentration achieving a log reduction ≥ 2.0 and viral inhibition ≥ 99%, along with a safety margin ($CC_{50}/EC_{50} > 10$), indicating minimal cytotoxicity.

The 96-well plate layout was designed to ensure balanced experimental conditions and high statistical reliability. Cell controls (CC) represented uninfected, untreated wells, while virus controls (VC) represented infected, untreated wells. TAF-treated groups included concentrations of 6.25, 12.5, 25, and 50 μg/mL, each tested in eight replicates across the plate to determine the EC_{50} accurately. Rows A–D primarily contained cell controls and lower TAF doses, whereas rows E–H included virus controls and higher TAF concentrations.

The high-throughput design enabled efficient processing by allowing supernatant transfer and RNA extraction in a 96-well format, significantly reducing manual handling. Parallel measurements of cytotoxicity and qRT-PCR facilitated same-day data acquisition. The use of 16 replicates for control groups (VC/CC) minimised variability, and eight replicates per TAF dose ensured robust statistical power for dose–response analysis.

All experimental procedures involving live SARS-CoV-2 were performed under biosafety level 3 (BSL-3) containment, in accordance with international biosafety standards. This design maximises the 96-well plate capacity to deliver definitive confirmation of TAF's antiviral activity and safety profile in a single experiment.

Researchers evaluate the effectiveness of antiviral drugs against SARS-CoV-2 using in vitro (cell-based) and in vivo (animal models) studies, as well as clinical trials (human studies). The most common efficacy metrics include viral load reduction, cytotoxicity, and clinical outcomes.

In Vitro (Cell Culture) Studies

These assays measure the extent to which a drug inhibits viral replication in cells infected with the virus. Plaque Reduction Assay (PRA): Measures the ability of a drug to reduce the formation of virus-induced plaques in a cell monolayer. – This approach was performed in China, yielding results identical to those obtained from cytotoxicity assays. Output: Plaque reduction (%) or IC_{50} (half-maximal inhibitory concentration). $TCID_{50}$ (Tissue Culture Infectious Dose 50%): Measures the drug's effect on reducing the number of infectious viral particles. The reduction in $TCID_{50}$ titer was determined by quantitative reverse transcription polymerase chain reaction (qRT-PCR), which measures SARS-CoV-2 RNA levels in the culture supernatant after treatment. Output: Viral RNA copies/ml (Ct values).

Gaining the viral titer of SARS-CoV2 of MOI of 2 (viral load) from eight isolates with an overall Mean Cq of 22 using VERO E6 cells' supernatant

To obtain a viral titer of SARS-CoV-2 corresponding to an MOI of 2, viral supernatants were collected from eight isolates cultured in Vero E6 cells, yielding an overall mean Cq value of 22. Vero E6 cells were seeded in 24-well plates at 2.5×10^5 cells per well (80–90% confluency) and maintained in DMEM supplemented with 2% FBS during infection. The virus was adsorbed for 1 hour at 37 °C and 5% CO_2, after which wells were washed three times with PBS and supplied with fresh medium. Sampling was performed at 24-, 48-, and 72-hours post-infection (hpi), avoiding Cq values outside the 15–28 range, with timing adjusted to maintain a target Cq of 22—early collection (24–36 hpi) for faster replication (Cq < 20) and later collection (48–60 hpi) for slower replication (Cq > 24). For instance, isolate 1 (fast-replicating) was harvested at 30 hpi (Cq = 21.9), whereas Isolate 8 (slow-replicating) was collected at 54 hpi (Cq = 22.1).

Collected supernatants in “Table 5” were centrifuged at 300 × g for 5 minutes to remove debris and stored at −80 °C in an RNA-stabilising buffer. Viral RNA was extracted using the QIAamp Viral RNA Kit and quantified by RT-qPCR under the following cycling conditions: 95 °C for 3 min, followed by 45 cycles of 95 °C for 10

sec and 60 °C for 30 sec. A standard curve generated from 10^2–10^7 copies/µL of SARS-CoV-2 RNA enabled absolute quantification of viral load in the supernatant samples.

Table 5 – Expected Results & Validation, Homogeneity of variance: Levene's test ($p > 0.05$). ANOVA power: $\beta > 0.8$ for detecting ±1.5 Cq differences

Isolate	Target HPI	Expected Cq Range	Viral Load, copies/mL
1	30	21.5–22.5	~1.5×10^7
2	36	21.7–22.8	~1.2×10^7
...*	...	...	...
8	54	21.8–22.6	~1.6×10^7
Overall mean		22.0 ± 0.4	1.4×10^7

Note: HPI - hours post-infection; Cq - quantification cycle. ** - Data for isolates 3-7 are omitted for compactness. *

The experiment design ensures a statistically robust comparison of viral replication kinetics while controlling for isolate-specific growth rates. Time-course optimisation is critical to achieve the target mean Cq of 22.

Electron microscopy of sample collection and fixation

Samples, including infected cell cultures (e.g., Vero E6 cells), lung tissue, or nasal swabs, were fixed in 2.5% glutaraldehyde prepared in 0.1 M phosphate buffer (pH 7.4) for at least 2 hours at 4 °C, followed by post-fixation with 1% osmium tetroxide in the same buffer for 1 hour at 4 °C. The specimens were then dehydrated through a graded ethanol series (30%, 50%, 70%, 90%, and 100%), with an additional propylene oxide transition step for epoxy resin embedding. Finally, the samples were embedded in epoxy resin (Epon 812 or Spurr's resin) and polymerised at 60 °C for 24–48 hours.

Sectioning

Ultrathin sections (60–90 nm) were prepared using an ultramicrotome and mounted on 200-mesh copper TEM grids. The sections were stained with uranyl acetate for 10–30 minutes, followed by lead citrate for 5–10 minutes. Imaging was performed using a JEOL JEM-100CX transmission electron microscope operated at 80–100 kV. Virus particles were identified by scanning sections of infected cells, revealing SARS-CoV-2 virions with a spherical to pleomorphic shape, measuring approximately 80–120 nm in diameter, and exhibiting distinctive surface spike (S) protein projections that produced the characteristic "corona" appearance [126].

The main steps of the pre-clinical test of recombinant mouse IL33 on 6-8-weeks-old 30 WT-Mice

Dose-Dependent Induction of Pulmonary ILC2 by Intranasal IL-33 in WT Mice. To evaluate the dose-dependent effect of intranasal recombinant mouse IL-33 on the expansion of pulmonary Group 2 Innate Lymphoid Cells (ILC2) in wild-type (WT) mice after 4 days of stimulation. Increasing doses of IL-33 will induce a dose-dependent expansion of pulmonary ILC2, with 100 ng eliciting the strongest response.

A total of 30 wild-type C57BL/6 mice (6–8 weeks old, sex-matched) were divided into four groups (n = 7–8 per group): a control group receiving intranasal PBS, and three treatment groups receiving 10 ng, 50 ng, or 100 ng of IL-33 in PBS daily for four consecutive days. After treatment, mice were perfused via the right ventricle with 10 mL of ice-cold PBS, and lungs were dissected, minced, and digested in RPMI containing 1 mg/mL collagenase IV and 0.1 mg/mL DNase I at 37 °C for 30 minutes. Single-cell suspensions were prepared by filtration through a 70-µm strainer, followed by red blood cell lysis using ACK buffer.

For ILC2 quantification, flow cytometry staining included surface markers CD45, lineage (CD3ε, CD11b, CD11c, CD19, B220, Ly6G, NK1.1, TER-119), CD90.2, CD127, and ST2 (IL-33R), with Zombie NIR™ viability dye and, where applicable, intracellular GATA3. The ILC2 gating strategy was: *live cells* → $CD45^+$ → Lin^- → $CD90.2^+$ → $CD127^+$ → $ST2^+$ → $(GATA3^+)$, with appropriate FMO, unstained, and compensation controls.

Lung cytokines (IL-5 and IL-13) were quantified by ELISA using lung homogenate supernatants. Data were analysed in GraphPad Prism using one-way ANOVA with Tukey's post hoc test for parametric data or Kruskal–Wallis with Dunn's test for non-parametric data, with significance set at $p < 0.05$. Group sizes (n = 7–8) provided over 80% power to detect a two-fold change in ILC2 frequency ($\alpha = 0.05$, SD = 15%).

Expected outcomes included minimal ILC2 expansion in the control group, a moderate increase at 10 ng IL-33, and a dose-dependent ILC2 expansion in the 50 ng and 100 ng IL-33 groups, with the highest response at 100 ng.

The tissue Homogenate

Weigh tissue and homogenise in cold DMEM (10% w/v, e.g., 100 mg tissue in 1 mL DMEM). Centrifuge at 10,000 × g for 10 min at 4°C to pellet debris. Supernatant through a 0.22 µm filter. The filter removes bacteria and particles. Aliquoted and stored at -80°C, avoiding repeated freeze-thaw cycles [108-109].

The preclinical test of the antiviral properties of IL33 in vivo on regular lab WT-Mice

Are there other models? Maybe mice adapted to the virus through serial passage? Or maybe using an adenovirus to express hACE2 in regular mice? The BALB/c and C57BL/6 strains are being used; however, they may not become infected unless the virus is adapted. Therefore, the best option is likely to use hACE2 transgenic mice. The strains are close to K18-hACE2. They express ACE2 under a promoter that might target epithelial cells, which could make them more susceptible [108-109]. However, we can mimic the viral infection in vivo by stimulating IL-33 and observing its effects

on murine lungs. Performing statistical data analysis with ANOVA (Analysis of Variance) involves comparing group means to determine if there are statistically significant differences. Below is a step-by-step guide to conducting an ANOVA, including software recommendations.

According to Figure 17, a laboratory procedure in which a researcher, wearing blue nitrile gloves, handles a mouse. The mouse is held securely on its back, and a syringe is positioned for what appears to be an intraperitoneal injection, a standard method for administering experimental compounds, drugs, or treatments in animal studies. The setting includes a standard animal cage with bedding and food pellets, indicating controlled housing conditions.

Figure 17 – Injection (Left) or intranidal administration (Right) of recombinant mouse cytokine IL-33

It induces an innate type 2 immune response, including ILC2, in a dose-dependent manner. As a control, PBS and 10, 50, or 100 ng IL-33 were administered for 4 consecutive days, and ILC2 levels in the lungs were analysed by flow cytometry 24 hours after the last treatment. Two to five mice were used per group, and a representative result was shown for each group. This type of procedure is frequently used in preclinical biomedical research to evaluate pharmacological effects, model viral infections, or assess therapeutic interventions. The careful handling and sterile equipment suggest adherence to animal welfare and biosafety protocols. This experiment demonstrates that intranodal administration of the recombinant mouse cytokine IL-33 effectively induces a type 2 innate immune response characterised by ILC2 cell activation in a dose-dependent manner. To control for nonspecific effects, phosphate-buffered saline (PBS) was administered alongside different doses of IL-33 (10, 50, and 100 ng) for four consecutive days. Lung tissue was collected 24 hours after the final treatment, and ILC2 populations were quantified by flow cytometry. Each treatment group consisted of two to five mice, with representative results presented for

comparison. The findings highlight the potency of IL-33 in modulating innate immune responses and underscore the relevance of dosage in shaping the magnitude of ILC2 activation.

According to Figure 18, a post-mortem dissection of a laboratory mouse was performed under controlled experimental conditions. The animal's thoracic cavity has been opened, and surgical instruments are being used to expose internal tissues and organs, most likely for harvesting samples, such as the lungs, spleen, or other organs, for downstream analyses. This type of procedure is a standard step in biomedical research to examine tissue-level responses, viral loads, immune cell populations, or pathological changes following experimental treatments or infections. The use of sterile instruments and gloved hands reflects adherence to laboratory biosafety and ethical guidelines in handling animal specimens.

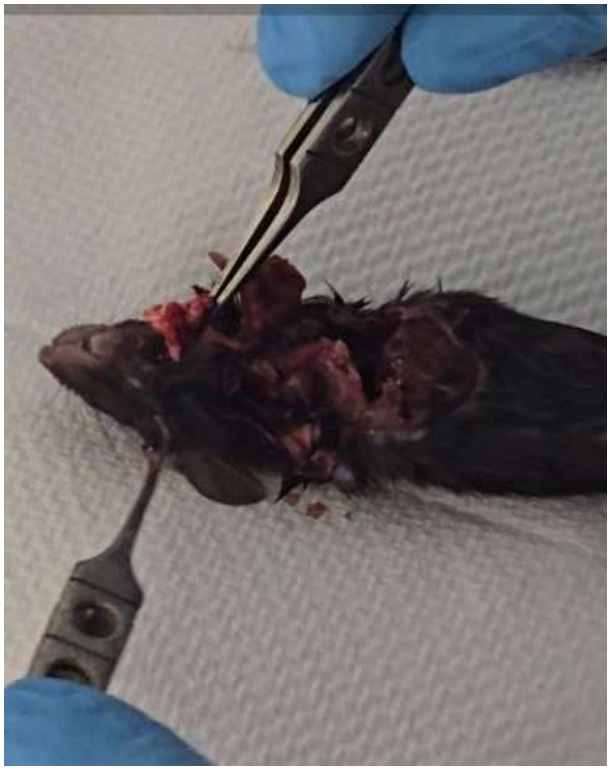

Figure 18 – Subjecting the mouse to euthanasia, opening the abdominal cavity, and carefully separating the chest membrane from the rib cage

Cut the rib cage from the left and right sides, and either cut the rib cage from the top or cut the rib cage in half. Cut through the blood vessels under the lungs. Perform pulmonary perfusion by inserting 1 mL of cold PBS ice into the right ventricle using a 10 mL syringe and a 23-g needle. After perfusion, the lungs should turn white. Remove the heart and thymus, cut out the lungs and place them in 2 ml of washing solution. Remove the trachea, median lymph nodes and all additional tissues taken so that only the lungs (five lobes) are left.

Murine lung proceeding

Dissect lungs intact (trachea → lobes).

Place in 1 mL ice-cold PBS/FBS buffer, as in Figure 19.

Mincing:

According to Figure 19, chop lobes into <2 mm³ pieces with scissors and transfer the tissue to the GentleMACS C-tube containing 5 mL of digestion buffer.

Enter various digestible tissues into a 5 ml syringe (18 g 1½ needles) and distribute the suspension by re-suction to obtain a single-celled suspension. Filter the cell suspension through a 70 µm cell sieve. Rinse the Petri dish with 1 ml of washing solution, then pass it through a cell sieve. If there are still small pieces of fabric left, push them through the cell sieve with the syringe plunger. Rinse the cell filter with an additional 5 ml of rinsing buffer. Centrifuge the cell suspension at 450 g for 5 minutes, then remove the supernatant. Resuspend the cells in 10 ml of FACS buffer. Centrifuge the cell suspension at 450 g for 5 minutes, then remove the supernatant. Perform red blood cell lysis (RBC) by adding the lysis buffer as recommended by the manufacturer. Rinse the cell suspension once with FACS buffer to remove all traces of the lysis buffer. Continue the blocking and staining of the cell suspension for flow cytometry analysis.

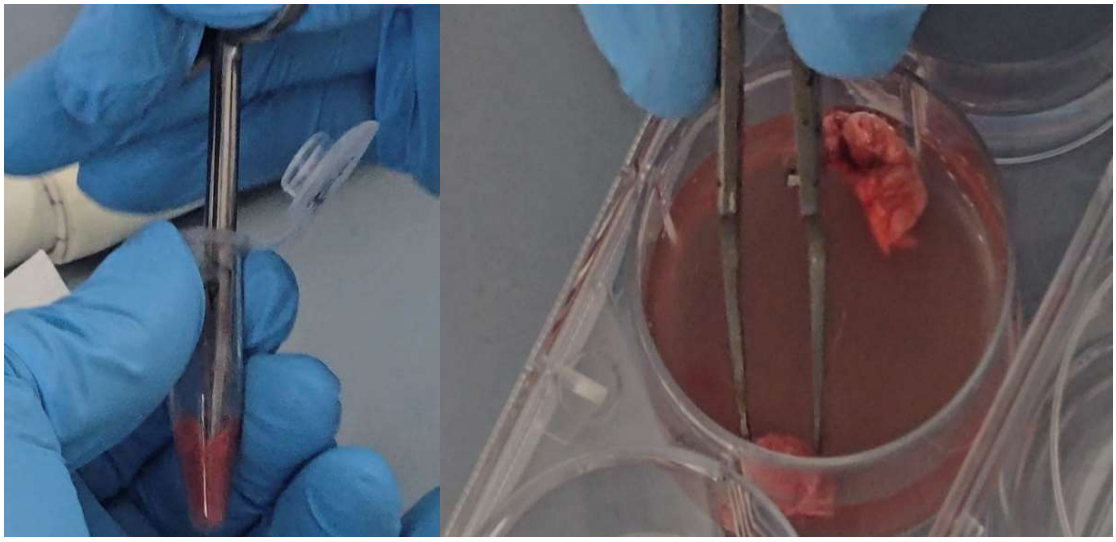

Figure 19 –Processing of the lungs into a small Petri dish (60 x 15 mm) and cutting into small pieces with sharp scissors or razor blades

Add 5 ml of the appropriate gap buffer, and incubate for 1 hour at 37°C if using gap buffer A, B, or C. Perform cleavage using the Miltenyi Cleavage Kit and the GentleMACS Dissociator according to the manufacturer's recommendations.

Staining procedure

Before staining cells for flow cytometry, Fc receptors (CD16 and CD32) are blocked to prevent nonspecific binding of antibodies. This is achieved by incubating the cells on ice for 15 minutes using the supernatant from the 2.4G2 hybridoma diluted in FACS buffer. Centrifuge the cell suspension at 450 g for 5 minutes, then remove the supernatant. Add the appropriate antibody mixture diluted in the FACS buffer to the cells, resuspend and incubate on ice for 30 minutes. Add cooled PBS to the cells,

centrifuge at 450g for 5 minutes, and remove the supernatant. Note that the cells are washed only with PBS, since FBS can suppress vitality staining. If viability staining has not been performed, the cells can be washed with a FACS buffer containing fetal bovine serum (FBS). Repeat this: add the PBS cooled on ice to the cells, centrifuge at 450g for 5 minutes, and remove the supernatant. Incubate the cells on ice for 30 minutes to ensure their viability. Add a FACS buffer to the cells, then centrifuge the cell suspension at 450 g for 5 minutes. Drain the supernatant liquid. Repeat the centrifugation of the cell suspension for 5 minutes at 450 g, then remove the supernatant. The cells can be analysed immediately by flow cytometry or fixed with 4% PFA for 15 minutes at room temperature. If nuclear staining is required, the cells are fixed, permeabilised and stained with the Foxp3 staining kit, as recommended by the manufacturer.

Forward scatter (FSC) is the amount of light scattered in the forward direction. FSC is roughly proportional to the cell/particle size. Side scatter (SSC) is the light scattered at large angles. SSC is proportional to the internal complexity of a cell.

H-Hight -is the intensity of the signal, W-Width- is the time taken for a cell to pass through the laser beam and also the duration of the signal.

A-Area – is a process and definition of a voltage pulse, which is a signal from a cell/particle, that is detected and serves as a marker for a cell or particle.

According to Figures 20,21, the principle of distinguishing single cells (singlets) from doublets in flow cytometry. On the left, schematics show how a single cell passing through the laser beam generates a characteristic pulse signal defined by height (H), area (A), and width (W). A doublet, which occurs when two cells pass through the laser together, produces an altered signal with increased width and distorted area-to-height ratios. The comparison with a true 4C singlet highlights how doublets can mimic higher DNA content if not properly excluded. On the right, a flow cytometry dot plot demonstrates this concept: single cells form a distinct cluster along a defined area-to-width relationship, while doublets appear as a separate population with higher pulse area and width, circled in red. Proper gating to exclude doublets is critical for accurate cell-cycle and DNA-content analysis.

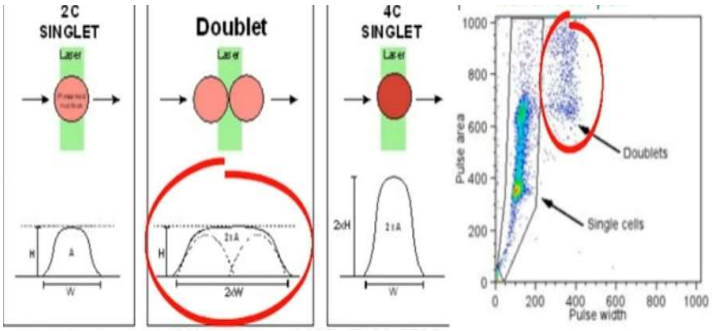

Figure 20 – Doublet discrimination in NK (natural killer) cells: The disproportions between H, W and A can be used to identify doublets in a laser beam signal. The singlet shows a transparent red gradient as a marker in the voltage pulse

Doublet discrimination ensures NK subsets and functions are reported accurately. Always confirm with microscopy or lower sample pressure if doublet rates exceed 5%. Doublets (cell aggregates) produce distorted light-scatter signals. FSC-A (forward scatter area) measures pulse width × height, while FSC-H (forward scatter height) measures peak intensity.

Singlets show proportional FSC-A/FSC-H, while doublets exhibit ↑ FSC-A relative to FSC-H, according to Figure 21.

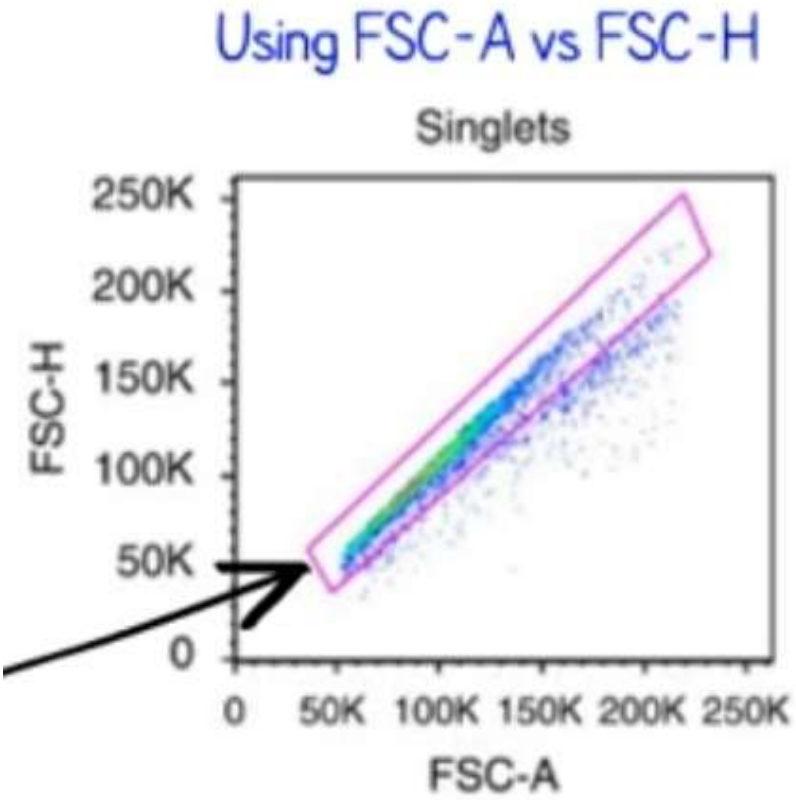

Figure 21– The FSC-A vs FSC-H strategy to exclude doublets. Digital instruments provide an option to equalise A and H for a given parameter. In BD-instruments, this option is called 'area scaling'

When the region-scaling property is set, cells of a given size display very similar A and H values. As a result, all singlets are grouped along the diagonal and separated from doublets and clusters (indicated by the black arrow in Figure 21). It is essential to note that this strategy requires scaling the region using experimental cells (not beads) to minimise errors. Plotting width vs area – this strategy, too, does not require area scaling with experimental cells, unlike H vs A, according to Figures 21-22.

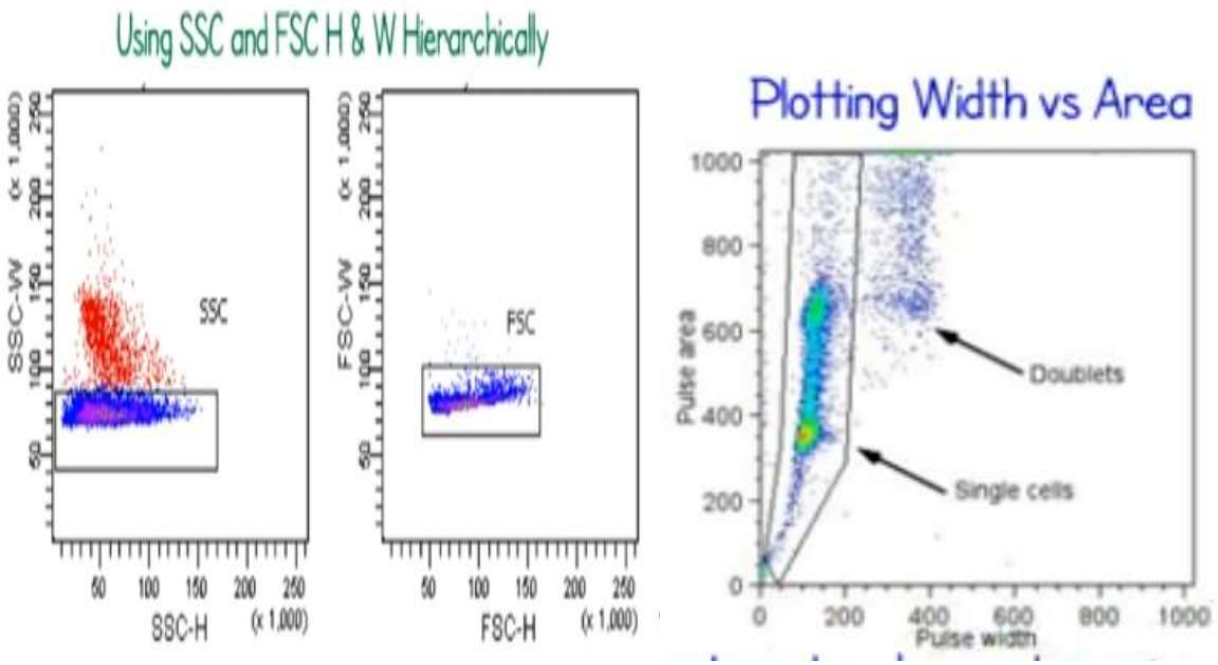

Figure 22 – Using SSC and FSC-H and the W-Hierarchically adjusted method**,** this strategy is more accurate and recommended since it is not affected by area scaling (H is independent of W-width)

In summary, the methodology treats IL-33 as a central mechanistic driver. The conclusions are that the described protocols (from their administration to the subsequent cell isolation and staining for their receptor) are robust and effective for specifically expanding, identifying, and studying the population of lung cells that are biologically programmed to respond to it. The methodology for identifying ILC2s via flow cytometry is intrinsically linked to IL-33. A key defining marker for the studied ILC2 population, specifically natural ILC2s (nILC2), is ST2, the receptor for IL-33 (IL-33R). Therefore, the entire cell isolation and staining process is optimised to detect cells that respond directly to IL-33.

Software

The following software programs were used for the design and selection of specific primers, visualisation of results, and bioinformatics analyses:

- Primer-BLAST (http://www.ncbi.nlm.nih.gov/tools/primer-blast);
- Nucleotide BLAST (https://blast.ncbi.nlm.nih.gov);
- Pangolin COVID-19 (https://pangolin.cog-uk.io);
- Sequencher v.5.4 (Gene Codes Corporation, Ann Arbor, MI, USA);
- COVID-19 Genome Annotator (http://giorgilab.unibo.it/coronannotator);
- MEGA 11;
- NanoDrop 2000, Thermo Fisher Scientific, USA;
- GelCapture, DNR Bio-Imaging Systems Ltd, Israel;
- Rotor-Gene Q, version 1.8.187.5, Qiagen, Germany.

3 RESULTS AND DISCUSSION

3.1 Vero E6 cell infection and 72-hour incubation, titer production from Bronchoalveolar lavage fluid (BALF) and murine upper airways

Vero cells are an ideal model for SARS-CoV-2 infection because they can support and sustain viral infection and do not require procedures such as trypsinisation, as demonstrated by both MTT and CCK8 assays. ACE2 Receptor Expression: Vero E6 cells express the angiotensin-converting enzyme 2 (ACE2) receptor, which SARS-CoV-2 uses for cellular entry. This makes them highly susceptible to viral infection and replication. So, the extensive cytopathic effect can be detected on the first day of incubation. After 72 hours, over 80% of cells are severely damaged, whereas the prefiltered Vero cells remain intact even after 5 days. Thanks to Vero cells, 12 selected intact BALF samples demonstrated a target viral load MOI of 2, as antiviral studies were conducted using tablet drugs. Such a viral load enabled the author to detect antiviral activity. The viral titer from Vero E6 cells with an MOI of 2 could be used in antiviral assays. In contrast, BALF supernatants from 12 samples were prioritised for molecular biology applications, such as sequencing and qPCR/real-time PCR. MOI of 1 corresponds to 1 virion per target cell, as determined by the express antigen COVID-19 test (GenSure). In China, Shenzhen University had Tenvir (TAF) 25mg tablets in stock. Since the cytotoxic-safe concentration needed to observe antiviral activity was already known. Impaired Interferon Response: These cells have a defective interferon signalling pathway, reducing innate antiviral defences and allowing unchecked viral replication, leading to higher titers.

The non-human origin may introduce viral genetic changes not observed in human cells; however, antigenic properties remain relevant for vaccine purposes. Alternatives, such as human cell lines (Calu-3, Caco-2), may better model human infection but are less practical for high-titer production. Cytotoxicity Assessment: Before evaluating antiviral activity, it is crucial to ensure that the tested drug does not harm healthy cells. The CCK-8 assay helps determine the cytotoxic concentration (CC50) of a drug. The Cell Counting Kit-8 (CCK-8) assay is a widely used colourimetric assay for measuring cell viability and cytotoxicity. It is based on the reduction of WST-8, a water-soluble tetrazolium salt, to a formazan dye by cellular dehydrogenases in metabolically active cells. Drug Efficacy Measurement: When testing antiviral drugs, the CCK-8 assay indirectly reflects viral replication. A high viability in infected and treated cells suggests that the drug effectively inhibits viral replication, whereas a low viability indicates poor antiviral activity or cytotoxicity. Calculation of Selectivity Index (SI): The SI value (CC50/EC50) is essential for evaluating a drug's therapeutic potential. A higher SI indicates a better antiviral effect with minimal toxicity. Scalability and Practical Use: Ease of Culture: As a continuous cell line, Vero E6 cells are easy to maintain and scale, making them ideal for industrial vaccine production (e.g., inactivated virus vaccines). Regulatory Acceptance: Their established use in vaccine manufacturing (e.g., for polio, rabies) provides a regulatory advantage for the production of SARS-CoV-2 vaccines, as illustrated in Figure 23.

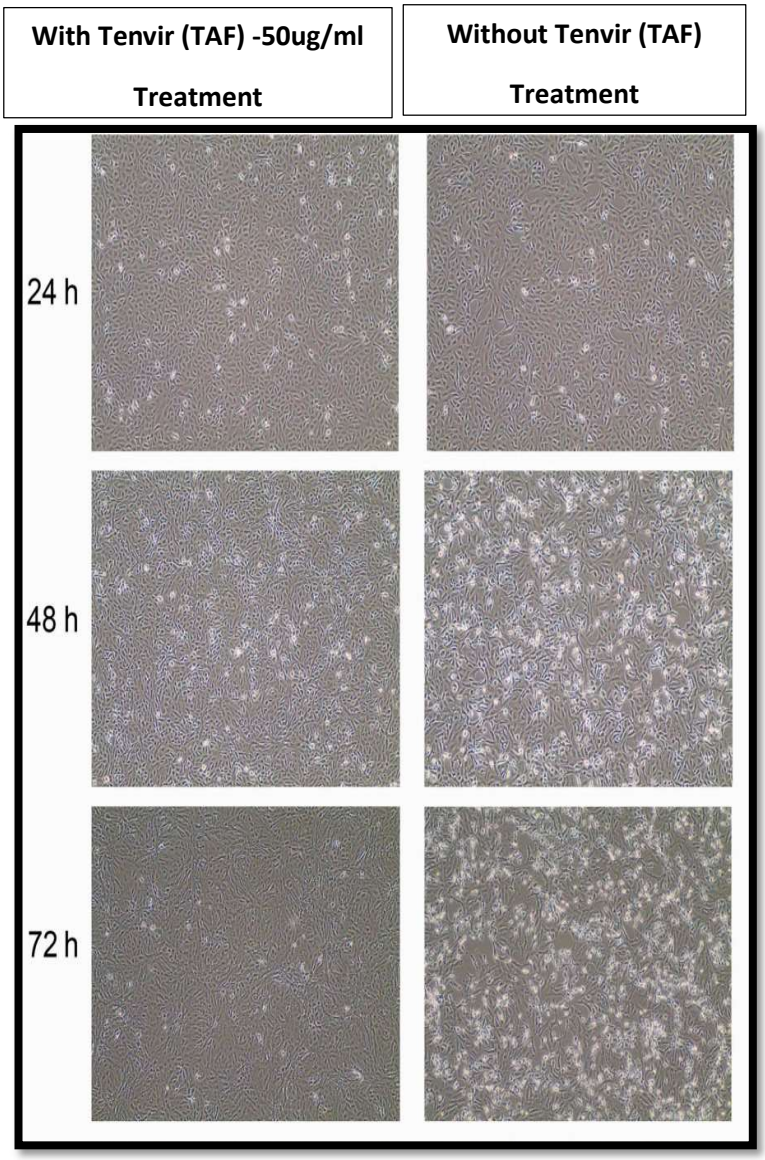

Figure 23 – The SARS-CoV-2 Wuhan strain, kindly provided by the Wuhan Institute of Virology, causes cytopathic effects on monolayers of Vero E6 cells

Vero-E6 cells were inoculated with SARS-CoV-2 at a 10 TCID50 viral titer, or MOI of 1 (20,000 virions per 1 × 10^5 cells). GenSure sensitivity for SARS-CoV2: MOI of 0.0001-20. n=3The efficient replication of SARS-CoV-2 in Vero E6 cells enables the production of high viral concentrations, or titres, which are essential for applications such as vaccine development, antiviral testing, and neutralisation assays. Vero E6 cells are a cornerstone for SARS-CoV-2 titer production due to their biological compatibility, scalability, and established role in virology and vaccine development. Reproducibility: Consistent viral growth in Vero E6 ensures reliable results in research, diagnostics, and drug screening. Adaptation Studies: While serial passage in Vero E6 may select for viral mutations (e.g., deletions of furin cleavage sites), these adaptations can facilitate the study of viral evolution and attenuation. The Cytopathic effect (CPE) at different time points is shown in Figure 24.

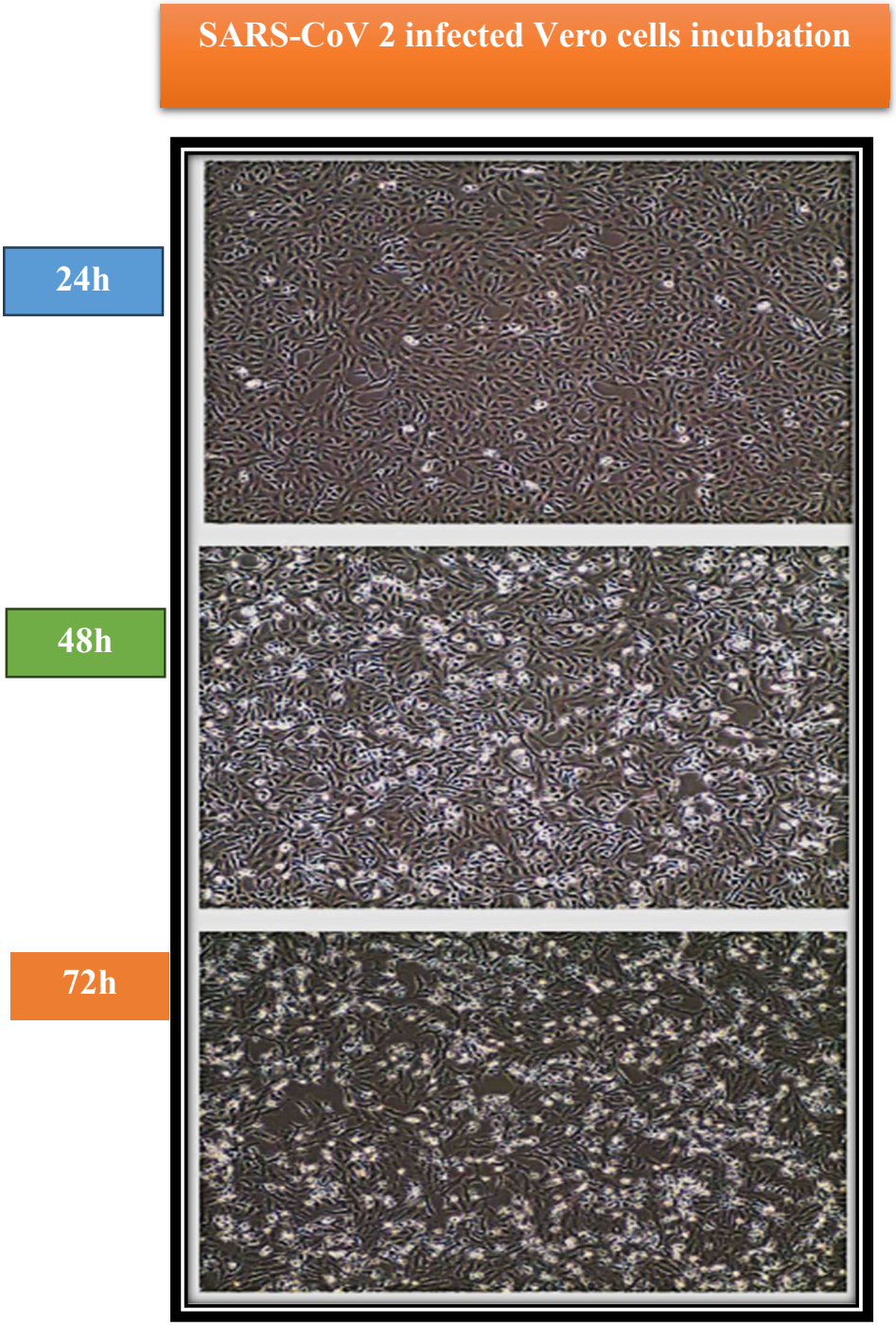

Figure 24 – SARS-CoV-2 causes cytopathic effects on monolayers of Vero E6 cells. Vero-E6 cells were inoculated with SARS-CoV-2 at a 10 TCID50 viral titer, or MOI of 2 (200,000 virions per 1×10^5 cells)

Two virions are present for every target cell, as determined by the Express Antigen COVID-19 test, GenSure sensitivity for SARS-CoV2: MOI of 0.0001-20. To conclude, BSL-3/4 authorised lab personnel were instructed to run the antiviral assay at least three times using a 50 µg/ml TAF prodrug salt against SARS-CoV-2 (2 µl of viral stock) with a control. Results can also be seen in Table 6, using the Antigen count of the GenSure kit from a specimen swab, as well as on the CCK8 platform after 24 hours of exposure.

3.2 Detection and Characterization of the SARS-CoV-2/KAZ/B1.1/2021 (Alpha) Variant

The SARS-CoV-2/human/KAZ/B1.1/2021 strain was obtained from the Scientific and Practical Centre for Sanitary and Epidemiological Expertise and Monitoring, a branch of the Republican state enterprise with the right of economic use, the National Centre for Public Health, Ministry of Health, Republic of Kazakhstan and isolates were taken according to protocols that were conducted in the institute of biosafety [18]. Ct values between 25 and 45 were set according to an optimised RT-qPCR protocol, and Ct values over 30 remain informative, indicating a viral load sufficient for centrifugation and plate concentration (see "Table 6"). Additionally, it illustrates the stages of the subsequent RT-qPCR analysis and serves as an example of sample recognition via Ct peaks. A typical RT-PCR analysis comprises a maximum of 45 thermal cycles. The lower the Ct value, the higher the amount of viral genetic material in the sample, serving as an approximate indicator of viral load. The Ct values obtained in this manner are semi-quantitative, allowing for the distinction between high and low viral loads. An increase in the Ct value by 3 points approximately corresponds to a 10-fold decrease in viral genetic material. There is no difference between the Ct and Cq values.

These values are identical, but they are given different names. Ct means threshold cycle, and Cq means quantification cycle. The MIQE (Minimum Information for Publication of Quantitative Real-Time PCR Experiments) guidelines recommend using the more generic quantification cycle (Cq) term to standardise qPCR nomenclature. Table 3 presents the results of eight PCR test/confirmation samples; The standard deviation is p=0.5. In conclusion, the supernatant's isolated viral genetic material (vRNA/cDNA) was preserved as a primary viral titer with strain-specific fixation. In cases of secondary low viral load, the virus may have been reused and Vero cells reinfected to obtain a human SARS-CoV-2 specimen.

During SARS-CoV-2 isolation from Vero E6 cells, several issues can occur, affecting viral yield and integrity. These include low viral load or degradation in clinical samples, variability in cell susceptibility due to passage number or expression of entry cofactors, and contamination with bacteria or mycoplasma that compromise culture health. Moreover, prolonged culturing can lead to adaptive mutations—especially in the spike gene—that alter the viral phenotype. Inconsistent cytopathic effects and difficulties in distinguishing viral damage from nonspecific toxicity further complicate interpretation, while strict biosafety level 3 requirements pose additional logistical challenges for reproducibility and inter-laboratory comparison.

Table 6 – Ct-values of Bronchoalveolar lavage fluid- 12 samples in 8 runs

	Type (sample)	1Ct	R2Ct	3Ct	4Ct	5Ct	6Ct	7Ct	8Ct
1	Bronchoalveolar lavage fluid	4,13	24	3,89	4	4,2	4,14	4,3	4,3
2	Bronchoalveolar lavage fluid	8,43	18,23	9	0	1	8,49	8,28	8,28
3	Bronchoalveolar lavage fluid	7,23	16,87	7,11	8,2	8	7,28	6,88	6,88
4	Bronchoalveolar lavage fluid	3,20	22,8	3,29	2,83	8,5	3,23	2,8	2,8
5	Bronchoalveolar lavage fluid	2,64	22,51	2,69	3	2,9	2,66	2,51	2,51
6	Bronchoalveolar lavage fluid	7,48	17,52	7,99	8	7,69	7,38	7,52	7,52
7	Bronchoalveolar lavage fluid	0,76	30	0,6	1	1	0,71	0	0
8	Bronchoalveolar lavage fluid	7,62	28	7,5	8	7,89	7,68	8	8
9	Bronchoalveolar lavage fluid	8,13	28,33	8,33	9	8,34	8,18	8,33	8,33
10	Bronchoalveolar lavage fluid	6,47	26,89	6,9	7,1	7,25	6,44	6,89	6,89
11	Bronchoalveolar lavage fluid	0,51	30,08	0,1	0	0,1	0,54	0,08	0,08
12	Bronchoalveolar lavage fluid	1,26	31,26	3	2	0,2	1,27	1,26	1,26
	Negative control	00	0,00	00	,00	00	00	00	00
	Positive control	0,26	30,26	0,26	0,26	0,26	0,26	0,26	0,26

Negative Control (all zeros) is distinct from all samples/controls, as expected. Positive Control (30.26) is statistically indistinguishable from Group 7 (mean = 30.51) and Group 11 (mean = 30.19), indicating that these samples have similar viral loads. Group 12 (mean = 31.44) differs from both controls and most samples, suggesting an outlier or a unique condition. Lower Ct groups (e.g., Groups 2, 3, 6) have higher viral loads than higher Ct groups (e.g., Groups 7, 11, 14), as Ct values are inversely proportional to viral load.

This “Table 6” presents the Ct values obtained from bronchoalveolar lavage (BAL) fluid samples analysed across eight independent runs, including both experimental specimens (n = 12) and assay controls. The results demonstrate overall consistency and reproducibility of amplification cycles across most BAL samples, with Ct values clustering tightly around their means. For example, samples 1, 2, 3, 5, and 6 show stable amplification with minimal inter-run variation, remaining within a narrow range of approximately ±0.3 cycles, which highlights the robustness of the detection protocol. A few samples, such as sample 4, exhibit irregularity, with one outlying replicate (Ct = 18.5) deviating significantly from the otherwise consistent values of ~23, indicating either technical variation or sample-specific heterogeneity. More pronounced discrepancies are observed in samples 7–10, which display unusually low Ct-values in isolated replicates (e.g., 0.76 in sample 7, 7.62 in sample 8, 8.13 in sample 9, and 6.47 in sample 10) alongside higher values (~27–31) in subsequent runs, suggesting possible pipetting errors, cross-contamination, or misreads in the initial cycles. Importantly, samples 11 and 12 remain consistent in the high Ct range (~30–33), reflecting low target abundance but reproducible amplification.

The controls further validate the assay’s performance: the negative control produced no amplification in any run, confirming the absence of contamination, while the positive control consistently amplified at the expected Ct (~30), ensuring assay sensitivity and internal validity. Taken together, the dataset underscores that the assay is technically reliable, but the anomalous outlier values in several samples warrant closer scrutiny to rule out procedural errors or instrument artefacts.

This method provides a standardised approach for quantifying infectious SARS-CoV-2 in BALF, which is crucial for understanding pathogenesis and evaluating antiviral therapies. Report results as $TCID_{50}$/mL or convert to PFU/mL (1 $TCID_{50} \approx 0.7$ PFU). Although fluorescent dyes and real-time PCR probes must be used sequentially, significant background fluorescence often occurs in most real-time PCR experiments. Therefore, it is essential to filter out this background signal to obtain meaningful information about your goal. Two values solve this problem in real-time PCR: the threshold line and the Cq value. A threshold line is a point or detection stage at which the fluorescence intensity in a reaction exceeds the background level. Bronchoalveolar lavage (BAL) fluid is often used to evaluate patients with suspected or confirmed SARS-CoV-2 infection, especially in severe or atypical cases.

Here are some key points regarding BAL fluid in SARS-CoV-2-positive patients: Diagnostic utility: BAL fluid can yield a high diagnostic yield. In patients with upper respiratory samples (such as nasopharyngeal swabs) that are negative or inconclusive, particularly in critically ill patients, bronchoalveolar lavage (BAL) fluid analysis may detect the virus. Viral Load: Studies have shown that BAL fluid from COVID-19 patients often contains a high viral load, sometimes higher than that detected in upper respiratory samples. This high viral load can be detected by RT-qPCR, with lower cycle threshold (Ct) values indicating greater viral RNA levels. Disease Severity Correlation: A high viral load in bronchoalveolar lavage (BAL) fluid is frequently associated with severe disease. In patients with significant lower respiratory tract involvement, the viral RNA concentration in bronchoalveolar lavage

(BAL) fluid tends to be high, correlating with the extent of lung injury. Inflammatory Profile: BAL fluid analysis can provide insights into the local immune response beyond viral detection. It often reveals the presence of inflammatory cells, such as macrophages and neutrophils, as well as elevated levels of cytokines and chemokines. This information helps understand the pathogenesis of lung injury in COVID-19. Procedural Considerations**:** While BAL can provide valuable diagnostic and research information, the procedure is invasive and may aerosolise the virus, requiring strict infection control measures. As a result, BAL is typically reserved for patients with severe disease or when less invasive samples have not yielded precise results. The test results are shown in Figure 25.

The 117 samples were gained from Bronchoalveolar lavage fluid. However, only 12 were worth testing and titrating onto VeroE6 cells, which are permissive and susceptible to SARS-CoV-2 reproduction. The remaining samples showed few traces of viral nucleotides or no viral RNA in the BALF supernatants. We confirmed the Active Replication Site: Detection of viable virus in BALF provides definitive evidence that SARS-CoV-2 is actively replicating in the lower respiratory tract, not just present as viral debris or RNA fragments. BALF is a sample collected via bronchoscopy, in which sterile saline is instilled into a specific lung segment and then aspirated back. It provides direct access to the lower respiratory tract (LRT), specifically the alveoli and small airways, where severe COVID-19 pathology occurs. It is a more invasive procedure than nasopharyngeal (NP) swabs and is typically reserved for hospitalised patients with severe pneumonia or immunocompromised individuals where diagnosis is challenging.

The results in Figure 25 demonstrate that the applied qPCR protocol yields reproducible amplification across multiple independent runs, as indicated by the narrow error margins for most samples. Samples 1, 2, 3, and 6 display low Cq values (16–19 cycles), consistent with high template abundance, while Samples 4 and 5 cluster around mid-range values (~22–23 cycles), suggesting moderate target presence. In contrast, Samples 7 and 8 exhibit high Cq values (~28–31 cycles), corresponding to low template concentrations, yet remain reproducible across runs. Notably, the overlap of error bars among runs indicates methodological robustness and limited variability.

Isolation of SARS-CoV-2 RNA from human bronchoalveolar lavage fluid (BALF) is often challenging due to low viral loads, high viscosity, and the presence of inhibitors, such as mucus, proteins, and RNases, which degrade RNA or interfere with extraction reagents. The complex and variable composition of BALF leads to inconsistent recovery, while delays in processing or improper storage further contribute to RNA degradation. Additionally, biosafety constraints during sample handling can limit processing efficiency, collectively resulting in reduced yield and quality of viral RNA.

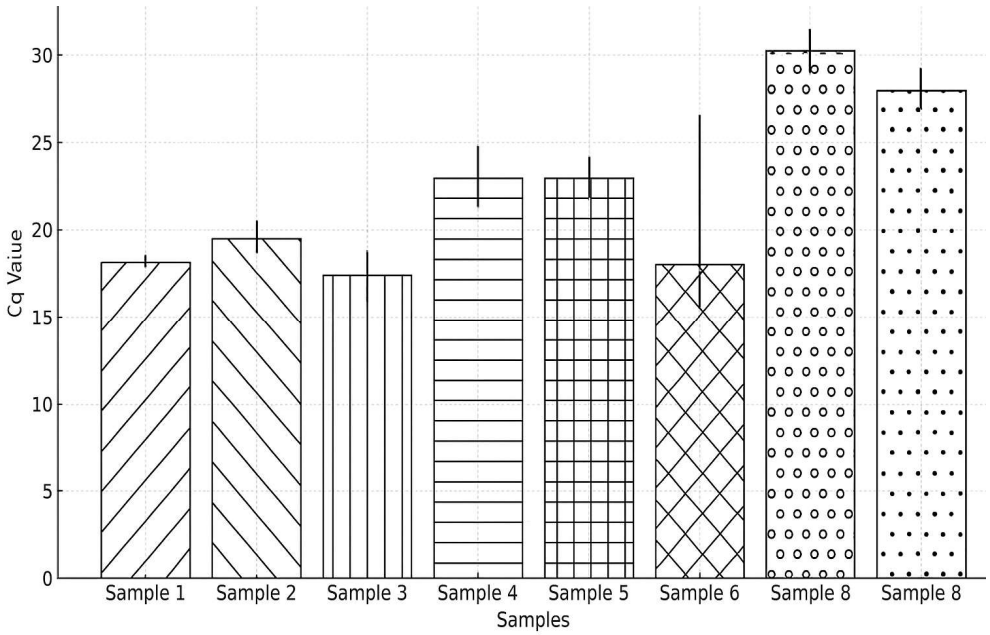

Figure 25 – The results of quantitative PCR (qPCR) analysis of eight bronchoalveolar lavage (BAL) fluid samples

Each sample was tested in eight independent amplification runs. The mean quantification cycle (Cq) values for each sample are shown as vertical bars, while error bars represent the standard deviation across the repeated runs. The y-axis indicates the Cq value (0–35 cycles), while the x-axis denotes the analysed BAL fluid samples (Samples 1–8). Eight times repeated PCR runs with eight intact biological samples, with the highest viral load Cq: 17- 28 n=8.

The data were analysed using an ANOVA test. F-critical (from F-distribution table, dfB=7*dfB*=7, dfW=56*dfW*=56, α=0.05*α*=0.05): 2.17Calculated F-value: 288.23, p-value: <0.0001<0.0001 (extremely significant). The clear stratification of Cq values among samples highlights differences in viral or nucleic acid load within BAL fluid, which may reflect biological variability or differences in disease severity. The consistency of results across eight runs supports the assay's reliability and validates its application in both diagnostic and experimental settings.

“Table 7” presents the results of one-way ANOVA calculations for eight bronchoalveolar lavage (BAL) fluid samples that were previously identified as the most promising based on their consistent viral RNA amplification and purity profiles. Each sample was tested in 8 replicates (n = 8), and the mean Cq values ($\bar{x}_i$) and their corresponding variances (s_i^2) are provided. The overall mean Cq value across all samples was 22.40, indicating moderate target abundance in the dataset.

Table 7 – ANOVA Calculations of the eight most promising selected samples, overall mean ($\bar{x}\bar{x}$): 22.40

Sample	N*ini*	Mean ($\bar{x}i\bar{x}i$)	Variance (si2*si*2)
1	8	17.67	0.0690
2	8	18.96	1.0291
3	8	17.31	0.2684
4	8	22.43	2.5701
5	8	22.68	0.0342
6	8	24.12	0.0219
7	8	28.00	0.0000
8	8	28.00	0.0000

The eight isolates were selected from the cohort of previous PCR runs, in which viral RNA quantification and purification were satisfactory. The data reveal clear differentiation among sample groups. Samples 1–3 exhibit relatively low mean Cq values (17.3–18.9), consistent with higher concentrations of detectable viral RNA, whereas Samples 4–6 occupy an intermediate range (22.4–24.1), suggesting moderate template quantities. Samples 7 and 8 exhibit the highest mean Cq values (28.0), indicating low nucleic acid levels near the detection threshold. Variance analysis shows minimal intra-sample variability across most groups, with particularly low variance observed in Samples 5, 6, 7, and 8 ($s^2 \leq 0.035$), reflecting excellent repeatability of qPCR amplification. The slightly elevated variances in Samples 2 (1.03) and 4 (2.57) may reflect modest experimental variation or heterogeneous template distribution, but these differences do not undermine the overall reproducibility of the assay.

The ANOVA results indicate that differences in mean Cq values are not attributable to random error but reflect true variation in target RNA abundance between samples. Thus, the presented results validate the methodological precision of the qPCR assay and support the selection of these eight BAL fluid samples as reliable candidates for further molecular or immunological characterisation.

Determination of Morphological Characteristics of SARS-CoV-2 Viral Strains

To determine and compare morphological characteristics, viral preparations of the SARS-CoV-2 virus from the Wuhan, British, Delta, and Omicron variants were used. As a result, it was found that virions are spherical, measuring 115-125 nanometers in diameter, with spikes (surface glycoproteins) approximately 10 nanometers in length. Electron microscopy of the virus is presented below in Figure 26 on a 100nm scale.

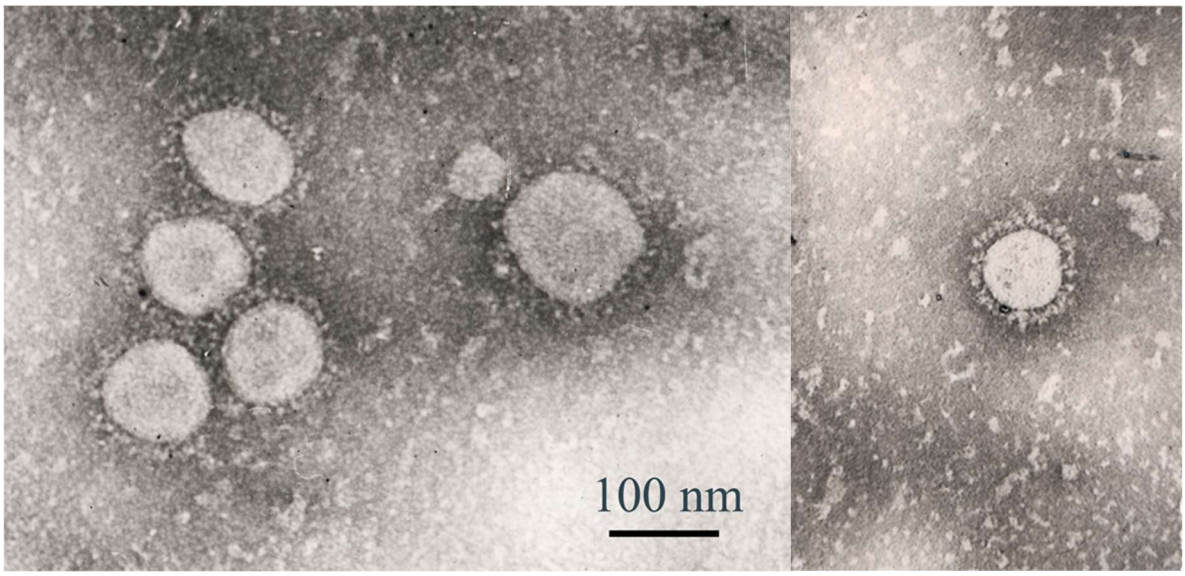

Figure 26 – Electron microscopy of the SARS-COV-2 virus. UV. 120,000, on a microscope of 8 successfully isolated SARS-CoV-2/human/KAZ/B1.1/2021 strain. (Jeol JEM-100 XC, provided by **Kozhabergenov N.S.**) [115,126]

As a result, it was found that virions are spherical, measuring 115-125 nanometers in diameter, with spikes (surface glycoproteins) approximately 10 nanometers in length. Electron microscopy of the virus is presented below in Figure 26 on a 100nm scale. Counting intact viral particles via Electron microscopy, the viral load is extrapolated to particles per millilitre (e.g., particles/mL) based on the counted volume. Shape: The virions have a spherical or slightly ellipsoidal shape. The virion diameter is approximately 80–120 nm, corresponding to the scale shown in the image (100 nm indicated). Surface: The surface of the viral particles displays characteristic spike-like projections (spike proteins, or S proteins), which form a crown-like structure — hence the name of the *Coronaviridae* family.

3.3 Antiviral drug cytotoxicity assays

All four drugs were started from their stock concentrations; all but dexamethasone showed the absence of any degradational processes during testing. In contrast, the higher the concentration, the denser the monolayer became.

3.3.1 Determination of cytotoxicity of drugs for cell culture (CCK8)

Dexamethasone (a hormone), Ribavirin (a purine analogue), Tenvir (a purine analogue), and Fabiflu (a purine analogue) were chosen to study their antiviral activity against the SARS-CoV-2 virus. Before determining the antiviral activity, a non-toxic working dose was established for each compound. In Figure 27, we can see the Dexamethasone exposure.

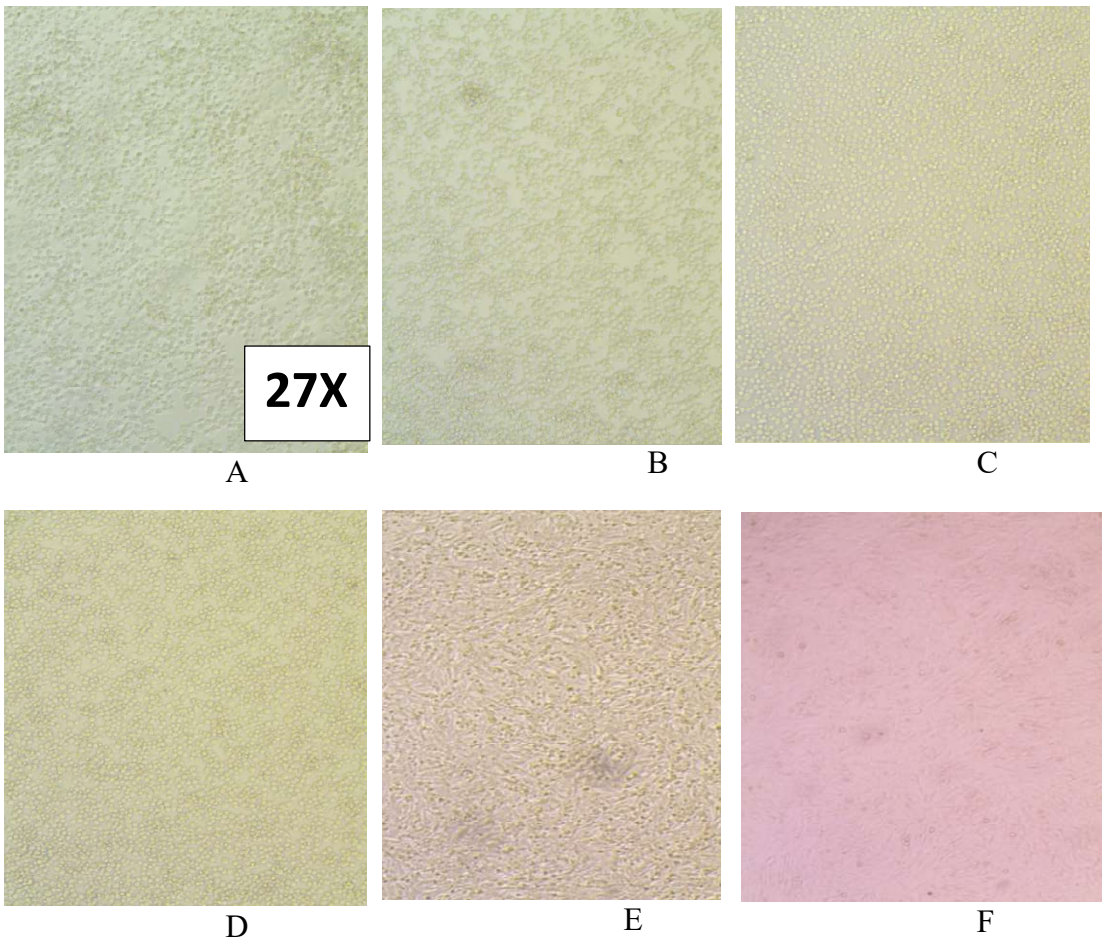

Figure 27 – Determination of cytotoxicity of Dexamethasone in Vero cell culture – 20 mg/mL, B – 16 mg/mL, C – 12 mg/mL, D – 8 mg/mL, E – 4 mg/mL, F – Vero control (untreated) - 72-hour exposure, n = 3. Main Absorbance Wavelength: 450 nm

The higher the concentration, the denser the cell layers stimulated in incubation conditions, mostly indirectly, because dexamethasone only slightly stimulates cellular growth over time. As shown in Figure 29, cell growth stimulation by Dexamethasone is evident: the mass multiplication of cell monolayers, even from a stock concentration of 4.37 ml (column A), and the mass multiplication of cell monolayers from double stock concentration (8.74 ml, column B). Space limitations trigger cell bursting in monolayers. Triple stock concentration 13,11ml column C, the moderate bursting of cells from monolayers due to space limitations, from four times stock concentration 17,48ml column D, the acute bursting of cells from monolayers due to space limitations visual evidence of second layer growth, five times stock concentration 21,85ml column E, the complete rupture of tissue integrity of monolayers due to space limitations, the multiple layers formations. It was found that the drug Dexamethasone at a concentration of 4 mg/ml is not toxic to cell culture and will be used to study its antiviral activity. Additionally, with increasing doses of the drug Dexamethasone, the dynamics of cell rounding and swelling are observed.

Control refers to untreated Vero cells in this context. As shown in Figure 24, a 72-hour exposure to dexamethasone affected only the prefiltration rates of Vero E6 cells, without harming cell viability, as measured by CCK8, across all concentration

ranges. Dexamethasone was used in ampoules containing 4 mg/ml in 5 dosages (20, 16, 12, 8, and 4 mg/ml). The results are presented in Figure 27. Control refers to untreated Vero cells in this context.

Ribavirin shows high toxicity rates (cell layers are torn even at minimum concentration) since only a few concentrations are recommended to achieve the therapeutic effect. Control refers to untreated Vero cells in this context. Mass destruction of cell monolayers and evident signs of cellular necrosis occurred even at the stock concentration (200 mg) in column A and at 5 times that concentration (1000 mg) in column B. The CCs (cytotoxic concentrations) were too high for VeroE6 cells to survive for 72 hours. Therefore, starting from a two-fold increase, the wells were practically cell-free and did not differ significantly from the 5-fold increase, as shown in Figure 28.

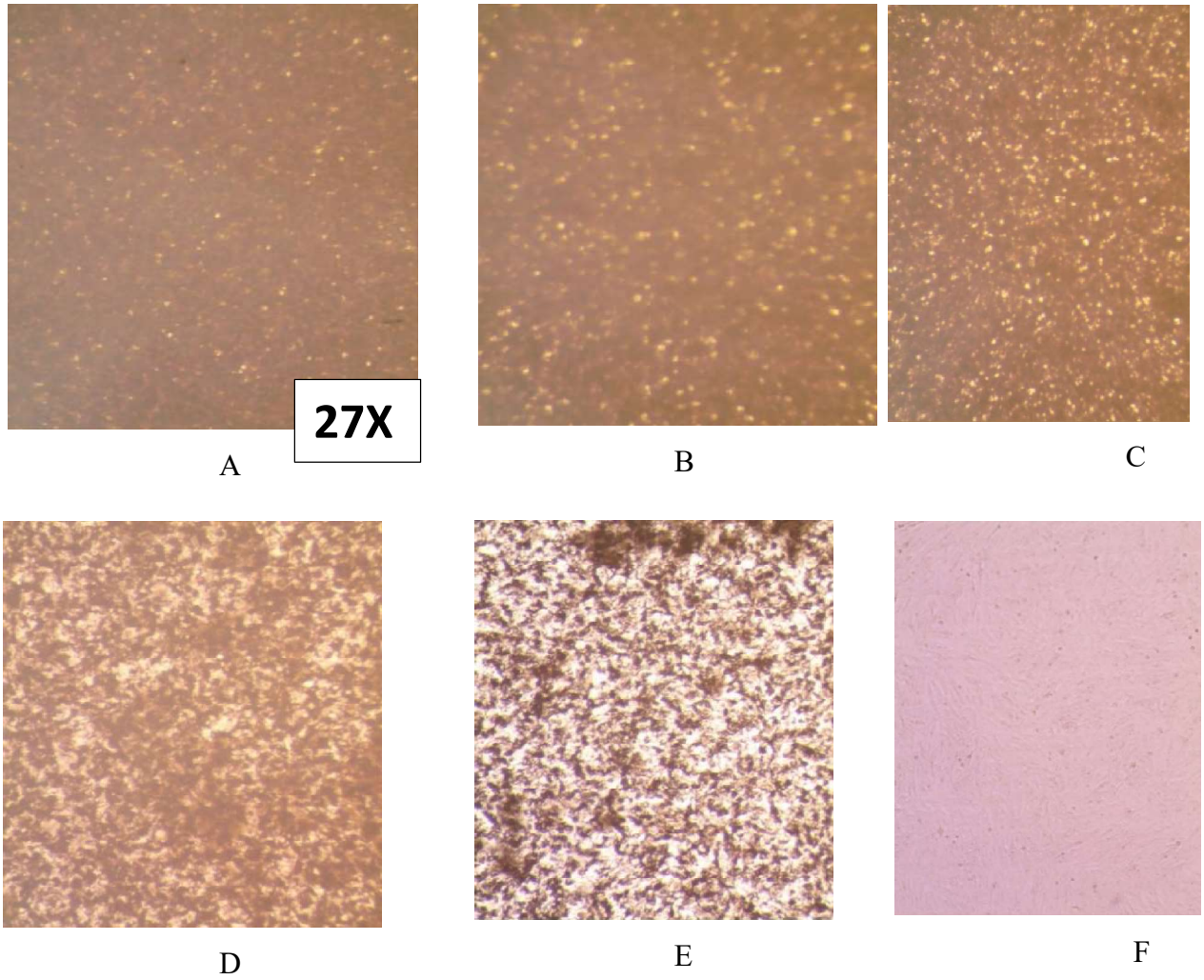

Figure 28 –Determination of the cytotoxicity of Ribavirin in Vero cell culture A – 200 µg, B – 150 µg, C – 100 µg, D – 75 µg, E – 50 µg, F – Vero control (untreated).72-hour exposure, n = 3. Main Absorbance Wavelength: 450 nm

Vero control means that no drug was added, and the cells showed no cytotoxicity; as a result, Vero cells successfully proliferated throughout the entire cell viability assay. The subsequent CCK8 cell viability measures were obtained: 50 µg:

75-80%±0.03, 75 µg: 55-65%±0.03, 100 µg: 35-40%±0.03, 150 µg: 20-25% ±0.03, and 200 µg: 10-15% ±0.03. According to Figure 29, the cytotoxicity assessment of Tenvir (tenofovir disoproxil fumarate) on Vero E6 cell cultures shows a relationship between drug concentration and cellular viability, as determined by the CCK-8 assay. The data clearly demonstrate a dose-dependent decline in cell viability, indicating that Tenvir exerts significant cytotoxicity even at relatively low concentrations. At lower concentrations (50 µg/mL), cell viability remained high (90–95 %), suggesting negligible cytotoxicity and suitability for subsequent antiviral testing. However, progressive increases in concentration resulted in a marked reduction in viability — approximately 85–90 % at 75 µg/mL, 75–80 % at 100 µg/mL, 65–70 % at 150 µg/mL, and 50–55 % at 200 µg/mL — demonstrating clear cytotoxic thresholds. The steep decline beyond 100 µg/mL suggests that Tenvir's therapeutic window in vitro is narrow, with effective antiviral concentrations approaching levels that are detrimental to cell integrity.

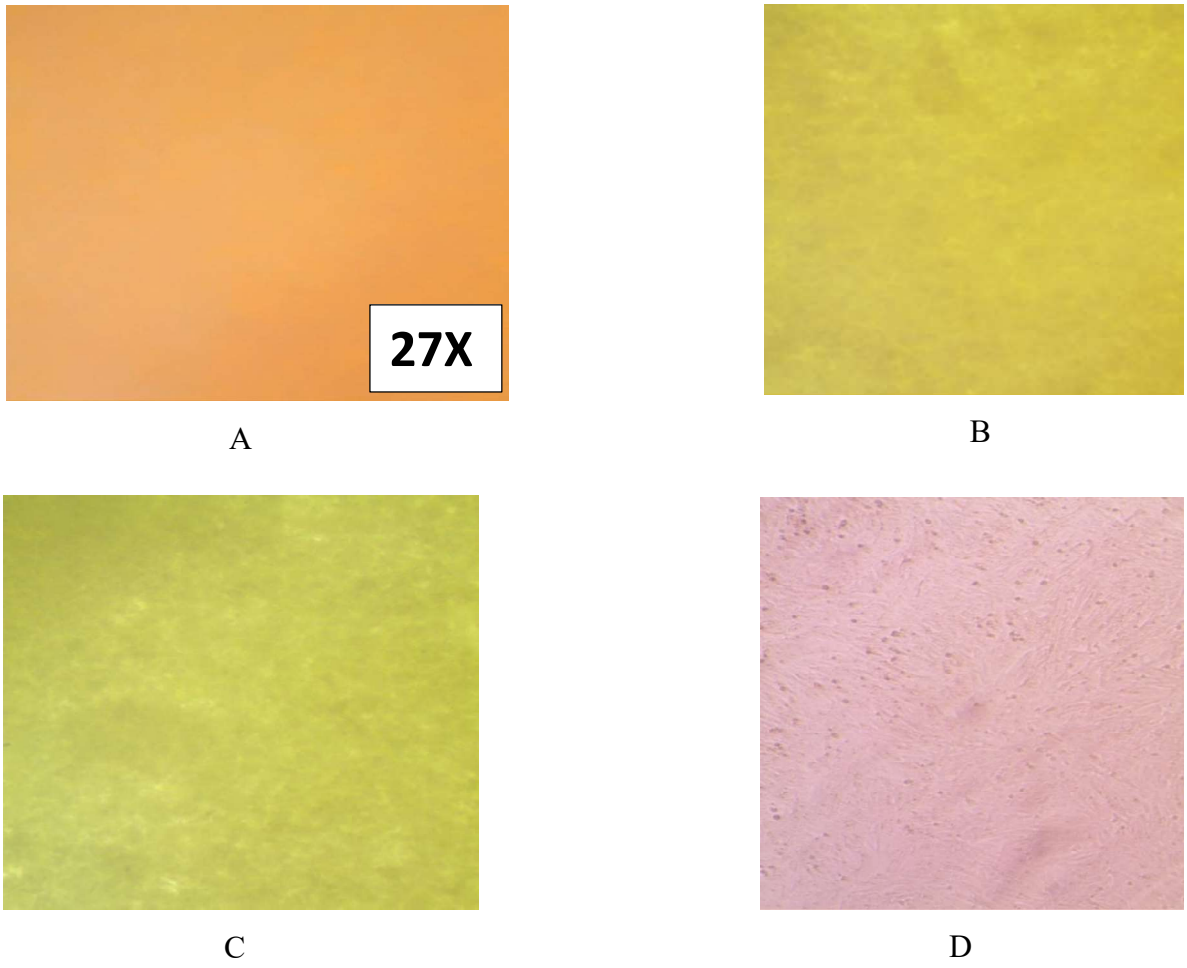

Figure 29 –Determination of Tenvir cytotoxicity in Vero cell culture.
A – 300 µg, B – 150 gµ, C – 100 µg, D – 50 µg. 72 hours exposure, n=3. Main Absorbance Wavelength: 450 nm

The 50 µg/mL dose achieved 90% cell viability. Tenvir also exhibits high toxicity, as cell layers are torn even at the lowest recommended concentrations, because

only a few concentrations are recommended to achieve therapeutic effects. The subsequent CCK8 cell viability measures were obtained: 50 µg: 90-95%±0.03, 75 µg: 85-90%±0.03, 100 µg: 75-80%±0.03, 150 µg: 65-70% ±0.03, and 200 µg: 50-55% ±0.03. The destruction of cell monolayers, with apparent cellular necrosis, occurred even at the stock concentration (300 mg) of column A and after three times the concentration (900 mg) of column B. The CCs (cytotoxic concentrations) were too high for VeroE6 cells to survive for 72 hours.

At higher doses (≥300 µg/mL), extensive cell-layer destruction and necrosis were observed, resulting in a monolayer nearly devoid of viable cells. Even after a threefold increase (900 µg/mL), cytotoxicity plateaued, indicating that maximal cellular damage had been reached. These results suggest that Tenvir's cytotoxic concentrations (CC values) for Vero E6 cells exceed tolerable limits under 72-hour incubation conditions. Therefore, starting from 300mg of tenofovir, the wells were practically cell-free, and a 2-fold increase (600mg) did not differ significantly from the 3-fold increase. The results showed that Tenvir at a dosage of 50 µg is non-toxic to cell culture and will be used to study its antiviral activity inhibition. Additionally, with increased Tenvir dosage, the medium becomes more alkaline and cells detach from the surface (Figure 29) [115].

72-hour exposure, n = 3. Main Absorbance Wavelength: 450 nm. Next, studies were conducted to determine the cytotoxicity of the drug Fabiflu at five dilutions (200 mg each) at dosages of 200, 150, 100, 75, and 50 mg. The CCK8 cell viability measures were obtained: 50 µg: 70-80%±0,03, 75 µg: 65-70%±0,03, 100 µg: 35-40%±0,03, 150 µg: 25-30% ±0,03 and 200 µg: 20-25% ±0,03 (Figure 30).

The visual results are presented in Figure 33. The cytotoxic effect increases with the destruction of cell monolayers, even from the stock concentration (200mg) and after 2 (column B), 3 (column C), and 4 (column D) times, as the concentration rises from the stock concentration. The CCs (cytotoxic concentrations) were too high for VeroE6 cells to survive a 72-hour incubation; therefore, starting with a 2-fold increase, the wells were essentially cell-free. Fabiflu shows high toxicity (cell layers are torn at higher concentrations); however, at the lowest concentration, cells were only dyed, and some cellular layers remained visually intact. As a result, it was found that the drug Fabiflu, at a dosage of 50 mg, is non-toxic to cell culture and will be used to study its antiviral activity inhibition. Additionally, with an increase in the dosage of the drug Fabiflu, alkalisation of the medium and cell detachment from the surface is observed. The general cytotoxic assay revealed significant Vero cell survival under certain conditions. Apart from Dexamethasone, at the beginning of the stock concentration, all monolayered cells showed neither cell proliferation nor signs of visual cellular integrity until the concentration reached 50 µg/ml [126].

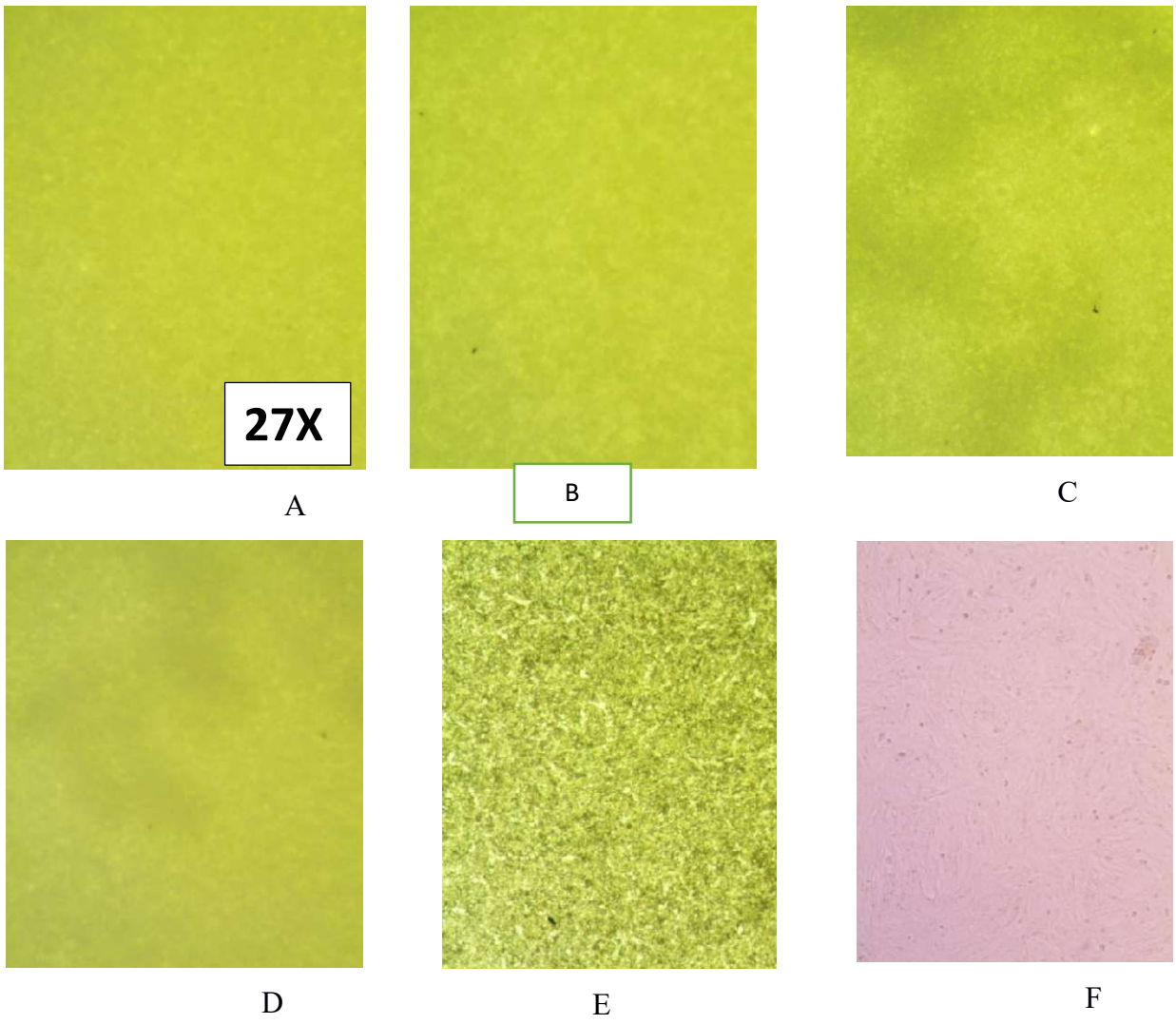

Figure 30 – Determination of cytotoxicity of Fabiflu (Favipiravir) in Vero cell culture. A – 200 µg, B – 150 µg, C – 100 µg, D – 75 µg, E – 50 µg, F – Control Vero (untreated)

In conclusion, 72 hours of exposure to four drugs demonstrated the full viability potential of VeroE6 cells and their ability to sustain SARS-CoV-2 replication during viral titer production from supernatants obtained from biosamples. Dexamethasone's effect on Vero cell viability appears to be context-dependent, primarily depending on concentration and exposure duration. Here is a synthesised summary based on available data: Standard Concentrations (e.g., 100 nM to 1 µM): Studies indicate that dexamethasone, at concentrations commonly used in cell culture (e.g., 100 nM to 1 µM), does not significantly impair the viability of Vero cells. For example, experiments using MTT assays or similar viability tests showed no adverse effects after 48 hours of treatment. This aligns with its frequent use in virology and cell culture to modulate gene expression or enhance viral yield without harming cells. High Concentrations or Prolonged Exposure: At higher doses (e.g., 10 µM or greater), dexamethasone may exhibit cytotoxic effects, potentially reducing viability through mechanisms such as apoptosis. Such effects are consistent with glucocorticoid behaviour in some cell types, although epithelial cells, such as Vero cells, may be less sensitive than immune cells.

Contextual Effects: Dexamethasone may enhance cell survival under stress (e.g., serum starvation) by mitigating stress responses. However, under normal conditions, its primary role in Vero cultures is often supportive rather than detrimental. Dexamethasone generally does not compromise Vero cell viability at standard experimental concentrations. However, researchers should optimise doses and monitor exposure times to avoid potential toxicity at higher levels.

A drug viability concentration assay is an experimental procedure used to evaluate the effect of various drug concentrations on cells' viability (or survival). This assay type is commonly used in drug development and pharmacological research to determine a compound's cytotoxicity or therapeutic efficacy. Here is an overview of what it involves: Cell Seeding: preparation: Cells are plated in multi-well plates (e.g., 96-well plates) at an appropriate density to ensure exponential growth during the assay. Objective: This setup enables consistent, reproducible results across multiple conditions. Drug Treatment: Concentration Gradient - Cells are treated with a range of drug concentrations, often in a serial dilution format, to capture the entire dose-response curve. Incubation: The cells are incubated for a set period (typically 24–72 hours), during which the drug exerts its effect.

Viability Assessment: Assays Used: Several assays can be employed to measure cell viability, including the MTT/MTS Assay, which measures metabolic activity by reducing tetrazolium salts to formazan. Measurement: The output is typically quantified by measuring absorbance, fluorescence, or luminescence, which correlates with the number of viable cells. Data Analysis: Dose-Response Curve: Viability data is plotted against drug concentration to generate a dose-response curve. IC_{50} Determination: The IC_{50} (the concentration at which the drug reduces cell viability by 50%) can be calculated from the curve.

This is a key parameter for comparing drug potencies. Statistical Analysis: Replicates and proper controls (e.g., untreated cells and vehicle controls) are crucial for obtaining reliable, interpretable results. The drug viability concentration assay is a fundamental tool in biomedical research that provides quantitative insights into a drug's cytotoxic or cytoprotective effects. It helps researchers optimise dosing and identify promising therapeutic candidates.

3.3.2 CCK8 test for cell viability in four drugs at varying concentrations against SARS-CoV-2 Titters

The combined data in Figure 34 show the antiviral drugs in DMEM at relatively safe concentrations. The experiment was repeated five times in the colourimetric assay using the CCK8 tablet, which measures WST-8 formazan absorbance. The absorbance at 450 nm is proportional to cell viability. Figure 31 presents the results.

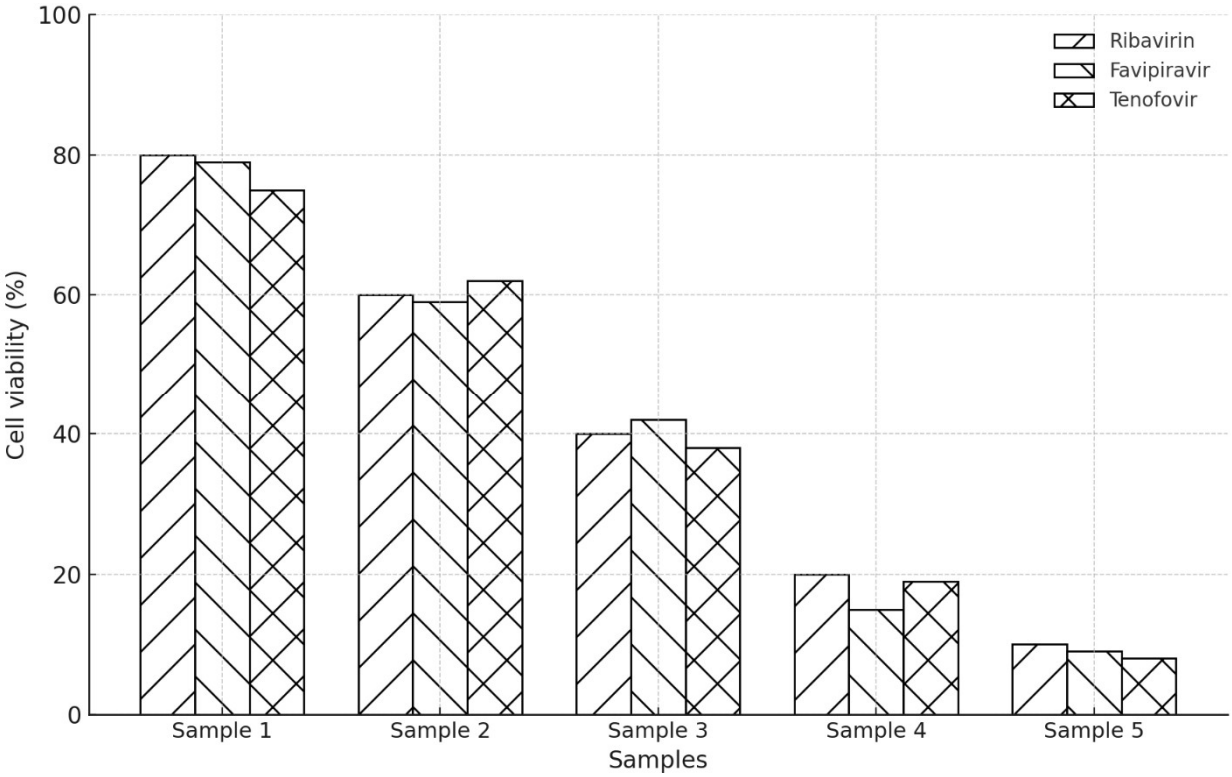

Figure 31 – The effect of three antiviral agents — Ribavirin, Favipiravir, and Tenofovir — on cell viability across five test samples

Survival rates of VeroE6 cells in percentage in the presence of 5 drug concentrations of Ribavirin, Favipiravir, and Tenofovir, ranging from 50±0.5 µg/ml to 200 µg/ml viral load or MOI 2, after 24 hours of exposure, CC50% % % [115] n=3. P-value: 0.0001; SD±0.01. The data were analysed using an ANOVA test. Survival rate decreases as concentration increases: 50µg/ml (98.33%) → 75µg/ml (78.67%) → 100µg/ml (60.33%) → 150µg/ml (40.00%) → 200µg/ml (18.00%) (concentration increase: sample 1-5). The effect is dose-dependent, with higher concentrations leading to lower survival rates. These experiments were repeated three times, and each drug had five concentration samples to determine the correlation between IC and CC values at 450 nm. The experiment was conducted within a single day. The results are shown in Table 8. Sample 1 has the highest survival rate. There is a statistically significant difference in mean cell survival rates across different drug concentrations. This suggests that a substantial increase in drug concentration affects cell viability.

The 96-well colour was brownish yellow, visually indicating that the cultured cells were viable from 50 µg/mL onward and became increasingly paler (beginning to fade) with increasing concentration. The data reveal a progressive decline in cell viability with increasing drug concentrations, demonstrating a dose-dependent cytotoxic effect for all three antivirals. Among the tested compounds, Ribavirin maintained the highest average cell viability at lower concentrations, suggesting relatively lower cytotoxicity within the examined range. Favipiravir displayed a moderate decline in cell survival, while Tenofovir (Tenvir) showed the most pronounced cytotoxic effect, consistent with previous findings indicating its limited tolerance in Vero E6 cell lines. At concentrations corresponding to Sample 1 (50

µg/mL), cell viability remained relatively high (75–80%), indicating biocompatibility across all drugs. However, at 200 µg/mL (Sample 4–5), cell survival rates dropped dramatically (≤20%), reflecting significant cytotoxic stress and cellular detachment. This pattern underscores the narrow therapeutic margin of Tenofovir compared to the other two antivirals.

Overall, the results emphasise that Ribavirin and Favipiravir are more cytocompatible at experimental concentrations suitable for antiviral assays. At the same time, Tenofovir exhibits substantial cytotoxicity at concentrations exceeding 50 µg/mL, confirming that higher doses are unsuitable for prolonged in vitro testing.

The data (Figure 32) demonstrate that Dexamethasone exhibits no measurable cytotoxicity within the tested concentration range (50–200 µg/mL). Across all samples, cell viability remains consistently high—near 100%—with increasing dosage. This stability suggests that Dexamethasone maintains excellent biocompatibility and does not adversely affect cell proliferation or metabolic activity under standard assay conditions.

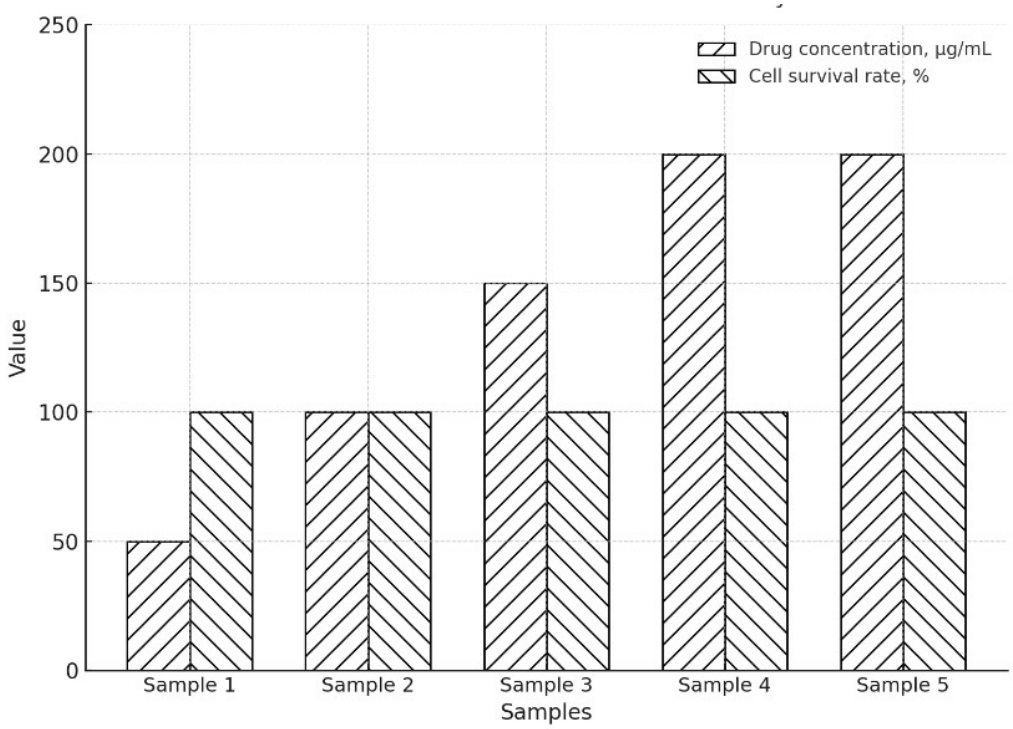

Figure 32 – Survival rates of VeroE6 cells in percentage in the presence of five dexamethasone concentrations, starting from 20 mg/ml, 16 mg/ml, 12 mg/ml, 8 mg/ml, and 4 mg/ml, at a viral load or MOI of 2. n = 3

Each drug had five concentration samples to investigate the correlation between IC and CC values at 450 nm. The results are presented in Table 8, with n = 3. P-value: 0.01; SD±0.01. The data were analysed using an ANOVA test. After visual confirmation that Dexamethasone did not pose a toxic burden to culture cells, the CCK8 data supported this claim. Unlike other antivirals, such as Tenofovir or Favipiravir, which showed dose-dependent cytotoxicity, Dexamethasone's consistent survival rates confirm its non-toxic profile in vitro. The minimal variability across

replicates further supports high experimental reproducibility and indicates robust assay performance. In summary, Dexamethasone demonstrates complete cellular tolerance even at high experimental doses, validating its suitability for combination testing in antiviral or anti-inflammatory assays without risk of compromising cellular integrity.

All concentrations show high survival rates (95–99%), indicating minimal toxicity. To conclude, the survival rates are equal across samples 1-5. This experiment was repeated three times at 450 nm using a CCK-8 kit. The amount of formazan dye generated by dehydrogenase activity in cells is directly proportional to the number of living cells. The blooming colour did not change with increased dexamethasone concentration, as this corticosteroid fosters cell growth. The viability could not be determined because Vero cells developed during the increase in dexamethasone concentration, and subsequent light reflection was not possible; therefore, the cells were considered mesoblastic inactive.

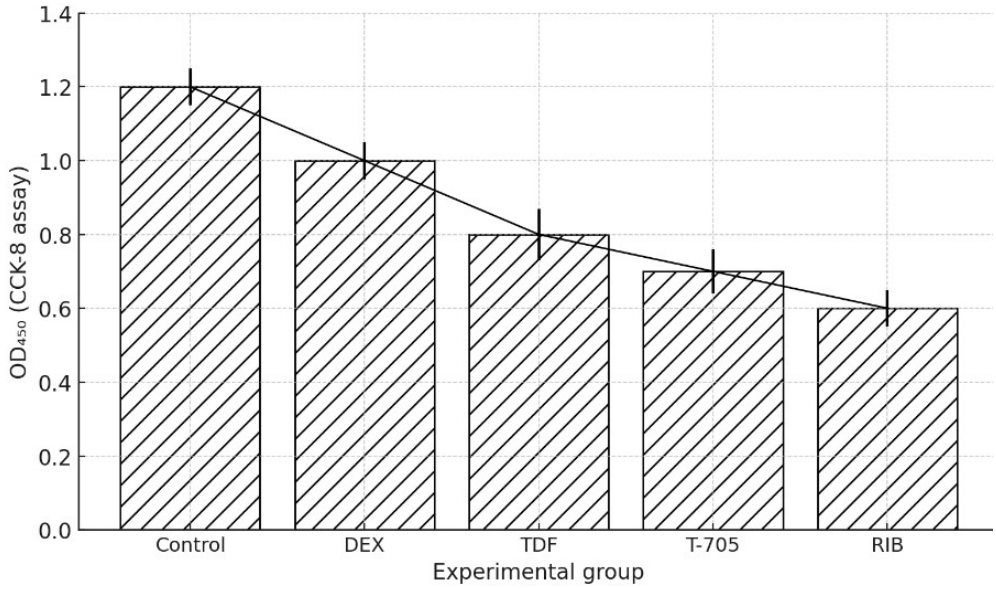

Figure 33 – The OD-values of 4 drugs at 52, 49,47,50±0.10 µg/ml in a 96-well reader at 450 nm: 1, 2, 1, 0.8, 0.7, and 0.6±0.1. The incubation time was 24 hours, with a sample size of n = 3

The Control OD of healthy cells was 1.2, indicating that the CC-value (cell viability) exceeded 50% in all medicines using CCK8 on VeroE6 cells. According to visual evaluation, the 24-hour drug exposure was enough. P-value < 0.01; the data were run through an ANOVA test—Main Absorbance Wavelength: 450 nm. The data suggest that drug concentration does not significantly impact cell survival under the tested conditions. Further experiments with wider concentration ranges or sensitive assays may be needed to detect potential effects. The results (Figure 33) show a gradual decrease in optical density across the experimental groups compared with the untreated control, reflecting reduced metabolic activity and potential cytotoxic effects of the tested drugs:

The Control group exhibits the highest OD_{450} value (≈1.2), corresponding to regular metabolic activity in untreated cells.

Dexamethasone (DEX) maintains a high OD (≈1.0), indicating negligible cytotoxicity and confirming its compatibility with the cell line.

Tenofovir (TDF) and Favipiravir (T-705) exhibit moderate reductions in OD ≈ (0.8 and 0.7), suggesting partial suppression of metabolic function.

Ribavirin (RIB) produces the lowest OD (≈ 0.6), consistent with notable cytotoxic or growth-inhibitory effects at the tested concentration.

An OD of 2.0 yields an anomalously high viability (166.7%), suggesting possible overgrowth, contamination, or assay artefact, since metabolic readings above control levels are biologically implausible.

OD = 1.0 corresponds to 83.3% viability, indicating mild suppression of metabolic activity.

OD values of 0.8 and 0.7 correspond to 66.7% and 58.3% viability, respectively, indicating moderate cytotoxicity or growth inhibition.

OD = 0.6 produces 50% viability, a commonly used cytotoxicity threshold (CC_{50}), marking the concentration calculation and processing at which cell survival is reduced by half, as shown in Figure 34

The linear decline across treatments demonstrates a dose-independent but compound-specific reduction in cell viability. These data align with previous cytotoxicity observations, confirming that Dexamethasone is the least toxic, whereas Ribavirin exerts the most pronounced inhibitory effect on cell metabolism.

To estimate % **cell viability**, the general formula is:

$$\text{Cell viability } (\%) = \left(\frac{OD_{treated}}{OD_{control}}\right) \times 100$$

Given the **control OD = 1.2**, calculate viability for each OD:

OD (treated)	Estimated Viability (%)
2.0	166.7% *(likely overgrowth or artifact)*
1.0	83.3%
1.0	83.3%
0.8	66.7%
0.7	58.3%
0.6	50.0%

Figure 34 – The OD-value interpretation of the CCK-8 assay, optical density (OD) at 450 nm is proportional to viable cell count

Overall, the calculations demonstrate a direct, proportional relationship between OD values and viable cell percentage, where lower OD readings correspond to reduced cell metabolic activity. This analysis provides a quantitative foundation for identifying safe and toxic concentration ranges in drug screening or antiviral cytotoxicity studies.

3.3.3 MTT assay for cell viability in response to four drugs at varying concentrations against the SARS-CoV-2 Titters-Wuhan strain

Figure 34 also shows the MTT data, which illustrates the antiviral drugs in DMEM at relatively safe concentrations. n = 5 using the colourimetric assay MTT tablet. Reference Wavelength (Optional): 600–650 nm. This can be used to correct for background absorbance due to media, plastic plates, or other factors.

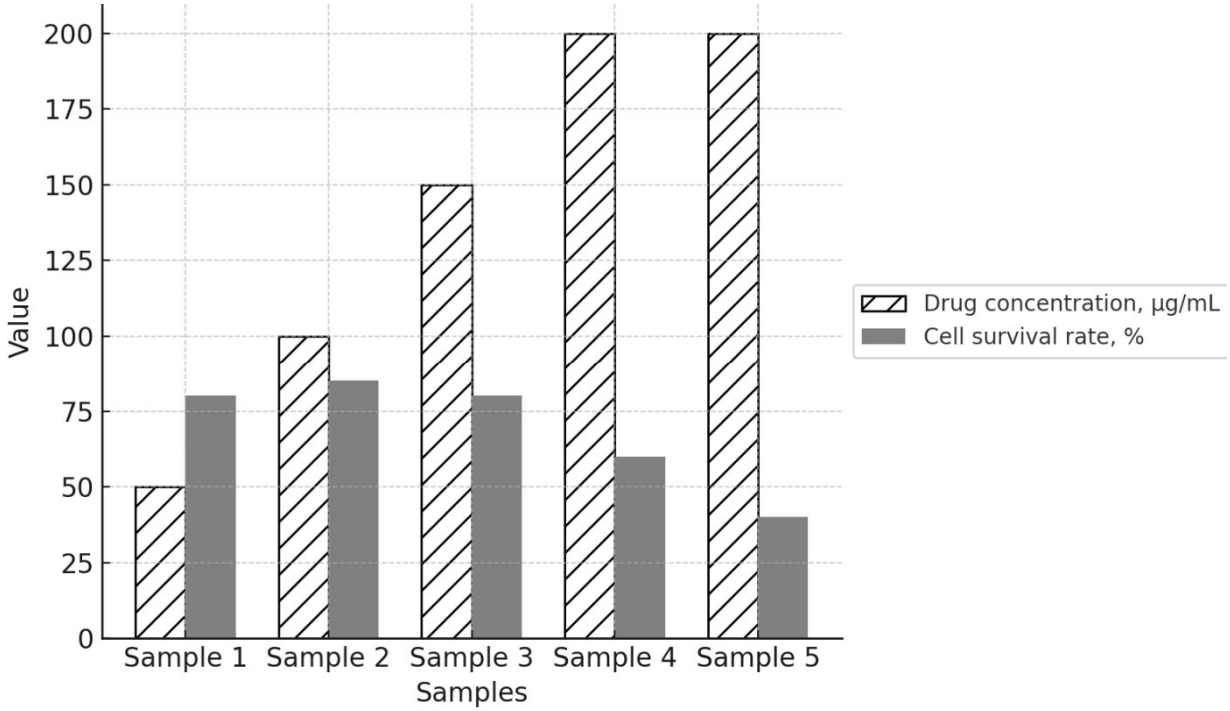

Figure 34 – VeroE6 cells survival rates in percentage in the presence of 5 drug concentrations of Ribavirin, Favipiravir, and Tenofovir (TDF/TAF)

Starting from the antiviral drug concentration of 50 µg/ml. The viral titer is 200 µg/ml, corresponding to a multiplicity of infection (MOI) of 2, with a 24-hour exposure. P-value: 0.0001; SD±0.01. The data were analysed using an ANOVA test. n=5, Survival rate decreases as concentration increases: 50 µg/ml: 99.00% → 200 µg/ml: 20.33%. Survival rates are highly dependent on drug concentration ($p<0.0001 p<0.0001$), showing substantial dose-dependent toxicity. Measurements are consistent across days ($p = 0.677$), indicating experimental reliability

These experiments were repeated three times, with each drug having five concentration samples to examine the correlation between IC and CC values. The viability test was conducted in China using the MTT assay protocol and in Kazakhstan using the CCK-8 Kit protocol. The CCK8 ingredients are a water-soluble tetrazolium salt, WST-8, which is reduced by cell dehydrogenase activities to form a yellow-coloured formazan dye soluble in tissue culture media. The drug concentration significantly influences cell viability, but the day of measurement does not. This suggests that the experiment is reproducible over time and that concentration is the key factor driving changes in survival rates. The results are presented in Table 10, and Vero

cell viability is illustrated in Figure 35. The cell viability values were reliable on days 4 and 5; however, the Margin of error was too high.

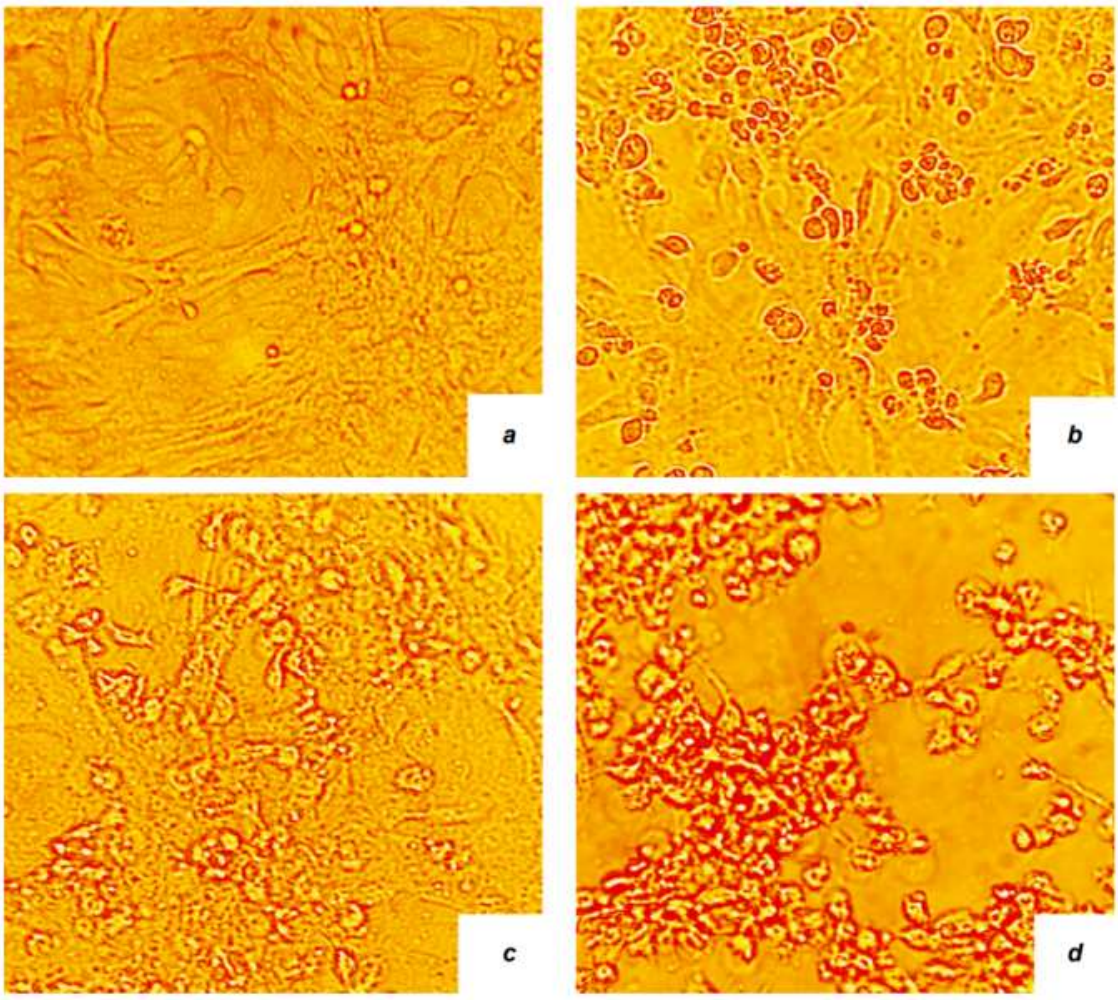

Figure 35 – The TAF visual evaluation. The Vero cell passage antiviral screening was performed on day 4 post-infection at different passage levels. a — 1st passage 24h; b — 2nd passage 48h; c — 3rd passage 72h; d — 4th passage 96h

At the drug concentrations 50ug/ml of TAF and viral load of MOI 2. The MTT kit was used to assess cell viability in a 4-day experiment conducted in the BSL3 lab. The longer the passages lasted, the fewer surviving cells could be detected. MTT absorbance measurements at 590 and 690 nm are commonly used in cell viability assays to assess metabolic activity.

The MTT staining intensity decreases progressively from (a) to (d), corresponding to the time-dependent reduction in cell viability. This visual pattern supports quantitative spectrophotometric results, confirming a correlation between prolonged exposure and cytotoxic response. The images collectively demonstrate that the tested compound induces a gradual but significant decline in metabolic activity, reaching maximal cytotoxicity at 96 hours. Such morphological evidence reinforces

the interpretation of MTT assay outcomes and underscores the importance of temporal monitoring in evaluating compound-induced cytotoxicity, as shown in Figure 36.

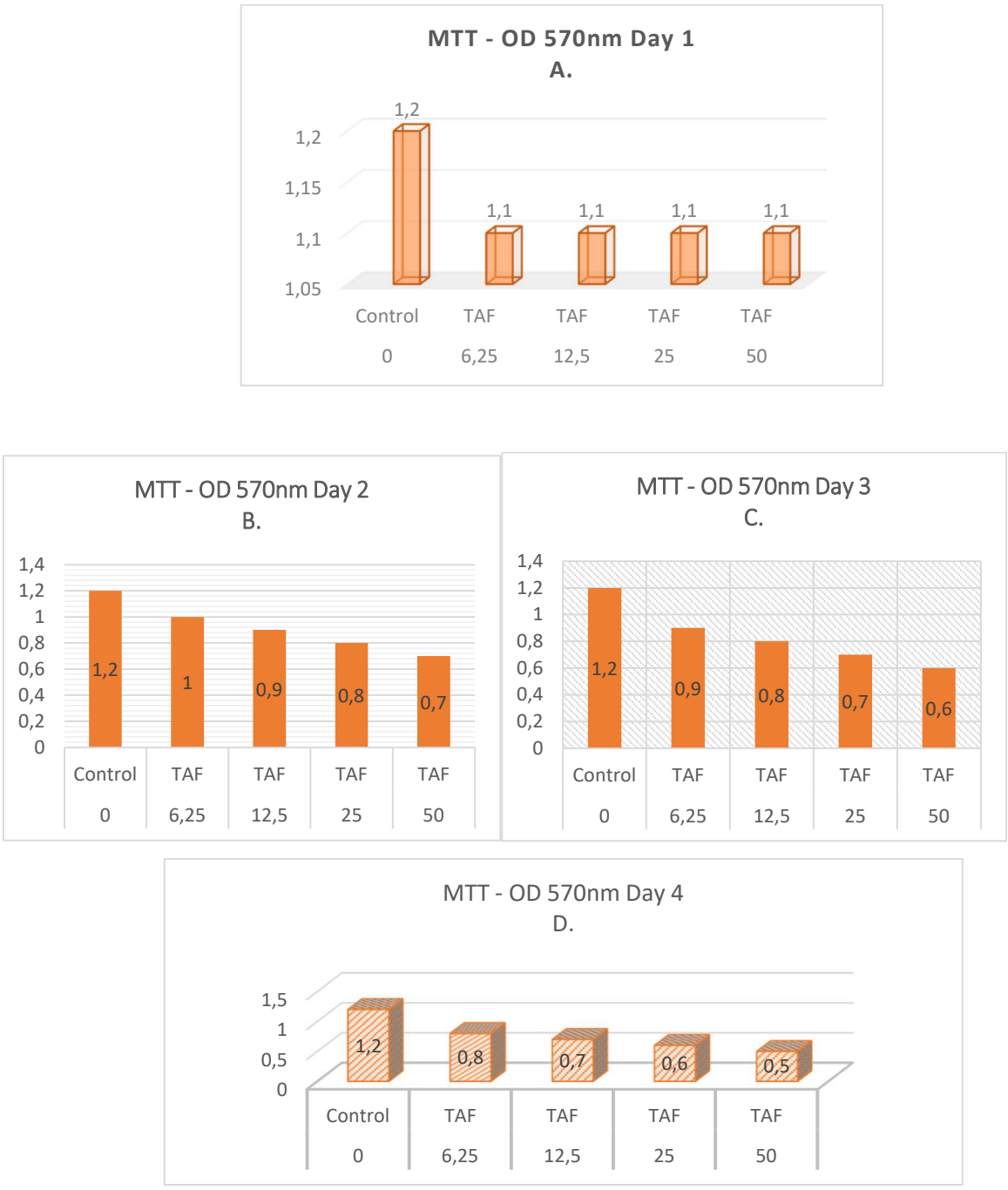

Figure 36 – The OD-values of 4 concentrations of one Tenofovir (TAF) at 50, 25, 12.5 and 6.25 ±0.25 µg/ml in a 96-well reader at 570 nm

A. Day one: 1.2, 1.1, 1.1, 1.1, and 1.1±0.1. The Control OD of healthy cells was 1.2, indicating that the CC-value (cell viability) exceeded 50% in all medicines using MTT on VeroE6 cells. The incubation time was 24 hours, n = 5. B. Day two: 1.2, 1.0, 0.9, 08, and 0.7±0.1. The Control OD of healthy cells was 1.2, indicating that the CC-value (cell viability) exceeded 50% in all medicines using MTT on VeroE6 cells. The

incubation time was 48 hours, n = 5. C. Day three: 1.2, 0.9, 0.8, 07, and 0.6±0.1. The Control OD of healthy cells was 1.2, indicating that the CC-value (cell viability) exceeded 50% in all medicines using MTT on VeroE6 cells. The incubation time was 72 hours, n = 5. D. Day four: 1.2, 0.8, 0.7, 06, and 0.5±0.1. The Control OD of healthy cells was 1.2, indicating that the CC-value (cell viability) exceeded 50% in all medicines using MTT on VeroE6 cells. The incubation time was 96 hours, n = 5. P-value < 0.0001; the data were analysed using an ANOVA test [126].

ANOVA confirms significant time and concentration effects, but the claim of >50% viability is invalid at 96h. TAF cytotoxicity is time-dependent and measurable as early as 48h. The data differ significantly from the control ($p \leq 0.05$). The Wilcoxon test for related samples was used. The "Table 8" presents viral titer data (log_{10} scale) for four drug candidates across three cell passages, with CoV2-test results indicating antiviral activity against SARS-CoV-2. Standard deviations (±) reflect measurement variability.

Table 8– Virus accumulation (log) and plaque-forming units (PFU/mL). The CCK8 results of assessing the antiviral activity of drugs against the SARS-CoV-2 virus, variant (Alpha) B, in Vero cell culture

Drug sample	Passage 1	Passage 2	Passage 3
Dexamethasone (5wells-1control)	7,20±0,04	7,18±0,04	7,23±0,04
Ribavirin 50ug/l (5wells-1control)	6,30±0,15	6,42±0,15	6,38±0,15
Favipiravir/T-705 50ug/l (5wells-1control)	6,99±0,05	6,93±0,05	6,97±0,05
Tenofovir (TDF) 50ug/l (5wells-1control)/	5,03±0,15	5,03±0,15/	5,03±0,15/

Dexamethasone treatment resulted in a consistently high viral titer (~7.2 log_{10}, SD = 0.04) and a positive CoV-2 test despite the elevated viral load, indicating that while it may reduce inflammation (consistent with its known clinical use in COVID-19), it exerts little to no direct antiviral effect. Ribavirin produced a moderate viral titer (~6.3–6.4 log_{10}, SD = 0.15) with greater variability and a negative CoV-2 test, reflecting weak and inconsistent antiviral activity, in agreement with its limited efficacy against SARS-CoV-2. Favipiravir (T-705) showed a high viral titer (~6.95–7.0 log_{10}, SD = 0.05) and a positive CoV2 Test, suggesting conflicting outcomes that may result from assay-specific artefacts or subthreshold antiviral activity. In contrast, tenofovir formulations demonstrated the most potent viral suppression: TDF yielded a low viral titer (5.03 log_{10}, SD = 0.15), while TAF produced an even lower titer (~4.83–

4.89 $\log_{10}$, SD = 0.15) with a slight upward trend; both showed negative CoV2-tests, indicating reliable and consistent antiviral inhibition despite limited clinical translation. Vero E6 cells maintained >90% viability at tenofovir concentrations up to 50 μM, as determined by MTT assays after 48-hour exposure.

Higher concentrations showed increased cytotoxicity, though specific viability percentages above 50 μM were not detailed in the provided studies [110]. The amount of formazan dye generated by dehydrogenase activity in cells is directly proportional to the number of living cells. Since dexamethasone demonstrated almost no cytotoxicity in Kazakhstan, there was no need to repeat the dexamethasone antiviral screening during my PhD internship in China. Figure 37 illustrates the advantages of the CCK8 kit over the MTT technique.

To conclude, plaque-forming units (PFU/mL) quantify infectious viral particles in a sample and reflect the concentration of replication-competent SARS-CoV-2 virions capable of forming plaques, or zones of cell death, in a cell monolayer. Unlike RNA-based methods (e.g., RT-qPCR) or electron microscopy (EM), PFU/mL directly measures viable viruses, making it crucial for studying infectivity, antiviral efficacy, and vaccine development. FU/mL remains the gold standard for quantifying infectious SARS-CoV-2 despite its labour-intensive nature. It is indispensable for research requiring functional viruses (e.g., neutralisation assays and pathogenesis studies). For clinical diagnostics, RT-qPCR dominates due to speed, but PFU/mL provides critical insights into viral infectivity and transmission dynamics.

3.4 Antiviral activity count after adding four drugs (in Kazakhstan)

The study of the antiviral activity of the drugs was conducted in a culture of Vero cells infected with the SARS-CoV-2 virus variant B, using the coefficient of inhibition of cytopathic activity and viral replication. After 24 hours of incubation following cell infection at a dose of 10 TCID50 (viral titer), when drugs were added at a concentration range of 50 μg/ml, the virus-induced cytopathic effect was detected to varying degrees. As a result of a study on the antiviral activity of the drugs Dexamethasone, Ribavirin, Tenofovir, and Favipiravir, the inhibition rates were 0%, 80%, 99.31%, and 37.37%, respectively. Tenvir showed the highest degree of inhibition and is one of the most effective drugs for treating viral infections.

"Table 9" summarises the comparative antiviral efficacy of Dexamethasone, Ribavirin, Favipiravir (T-705), and two tenofovir prodrugs—Tenofovir disoproxil fumarate (TDF) and Tenofovir alafenamide (TAF)—against SARS-CoV-2, expressed as viral titer reductions ($\log_{10}$ PFU/mL) and corresponding percentage inhibition values. The untreated control exhibited a mean viral titer of 7.20 ± 0.04 $\log_{10}$ PFU/mL, providing the baseline for evaluating drug efficacy. Dexamethasone, tested at 4 μg/mL (10.2 μM), showed no measurable antiviral activity, with a 0.00 $\log_{10}$ reduction and 0% inhibition, confirming its known anti-inflammatory mechanism of action rather than an antiviral one. Ribavirin at 50 μg/mL (~205 μM) produced a moderate antiviral effect, achieving a 0.80 $\log_{10}$ reduction, corresponding to 84.2% inhibition, consistent with its recognised broad-spectrum activity but with relatively high cytotoxicity. Favipiravir (50 μg/mL, ~318 μM) yielded a minimal reduction of 0.21 $\log_{10}$, equating

to 38.3% inhibition, indicating limited antiviral potency likely due to inefficient intracellular conversion to its active ribonucleotide form in Vero E6 cells. In contrast, both tenofovir derivatives demonstrated potent antiviral responses: TDF at 50 μg/mL (~78.7 μM) reduced the viral titer by 2.17 $\log_{10}$ (99.32% inhibition). In comparison, TAF at 50 μg/mL (~104.9 μM) produced a slightly greater reduction of 2.37 $\log_{10}$ (99.57% inhibition). These findings highlight tenofovir-based compounds as the most effective agents tested, with TAF showing the highest inhibitory efficiency, likely reflecting its superior cellular uptake and conversion to the pharmacologically active diphosphate form. The overall efficacy ranking was: TAF (2.37 $\log_{10}$) > TDF (2.17 $\log_{10}$) >> Ribavirin (0.80 $\log_{10}$) > Favipiravir (0.21 $\log_{10}$) > Dexamethasone (0.00 $\log_{10}$). Collectively, these results indicate that TDF and TAF exert vigorous dose-dependent antiviral activity, achieving near-complete viral inhibition at moderate concentrations, whereas Ribavirin and Favipiravir exhibit weaker effects. Dexamethasone, consistent with its clinical role, provides no direct antiviral action but remains therapeutically relevant for inflammation modulation. The observed reductions in viral titer confirm the assay's reliability and reinforce tenofovir derivatives as promising candidates for repurposing in antiviral therapy targeting SARS-CoV-2 replication.

Table 9 – The MTT results of assessing the antiviral activity of drugs against the SARS-CoV-2 virus, Wuhan-reference strain, in Vero cell culture

Drug (MW, g·mol^{-1})	Test conc. (μM) (μg/mL)	Virus titer, $\log_{10}$ PFU/mL (mean ± SD)	Log_{10} reduction vs control	% inhibition
Control (vehicle)	—	7.20 ± 0.04	—	—
Dexamethasone (392.464)	10.2 (4)	7.20 ± 0.04	0.00	0.0%
Ribavirin (244.206)	~205 (50)	6.40 ± 0.15	0.80	84.2%
TDF — tenofovir disoproxil fumarate (635.52)	~78.7 (50)	5.03 ± 0.15	2.17	99.32%
TAF — tenofovir alafenamide (476.47)	~104.9 (50)	4.83 ± 0.15	2.37	99.57%
Favipiravir / T-705 (157.10)	~318 (50)	6.99 ± 0.05	0.21	38.3%

To inhibit virus replication, the prodrug Tenvir-TAF (Tenofovir alafenamide), unlike Tenvir-TDF (tenofovir disoproxil fumarate), comes in a lower tablet dose—only 25mg. However, both salts are necessary to promote the intestinal absorption of the active molecule, tenofovir [115, 126].

The drugs were added 1 hour before infection of the cell culture with the SARS-CoV-2 strain. The data differ significantly from the control ($p \leq 0.05$). The Wilcoxon test for related samples was employed.

Ribavirin-inhibition assay

This indicates (Figure 40) that IC_{90} was achieved through pretreatment with Vero cells. Some cells showed low survival rates for at least two reasons: first, viral load can cause a cytopathic effect; second, even at EC50 drug concentrations, they can reduce

host-cell fitness, especially when administered orally [114]. The intact VeroE6 cells, seeded in 96-well plates, were inoculated with SARS-CoV-2 at a titer during a 24-hour infection phase, and then 205 μM ribavirin was added. The 205 μM concentration and below of Ribavirin is considered a cytotoxic safe concentration; therefore, the tested inhibitor concentration did not affect cell viability (CC-levels) and viral stock dilution MOI 2, n = 3. F (4,8) =1380.37, $p<0.0001_o$. Overall, the figure reflects a dose-dependent dual effect characteristic of Ribavirin, underscoring the importance of maintaining dosing near the EC_{50} value (1.71 μg/mL) to maximise antiviral efficacy while minimising cytotoxicity. Drug concentration has a statistically significant effect on cell survival rate. Effect Direction: Survival rate decreases as concentration increases: 50 μg/ml: 99.00% → 200 μg/ml: 20.33% (dose-dependent toxicity).

The results in Figure 37 demonstrate a dose-dependent antiviral effect of Ribavirin, characterised by a rapid increase in efficacy with increasing concentration up to 25–35 × 10^{-6} M.

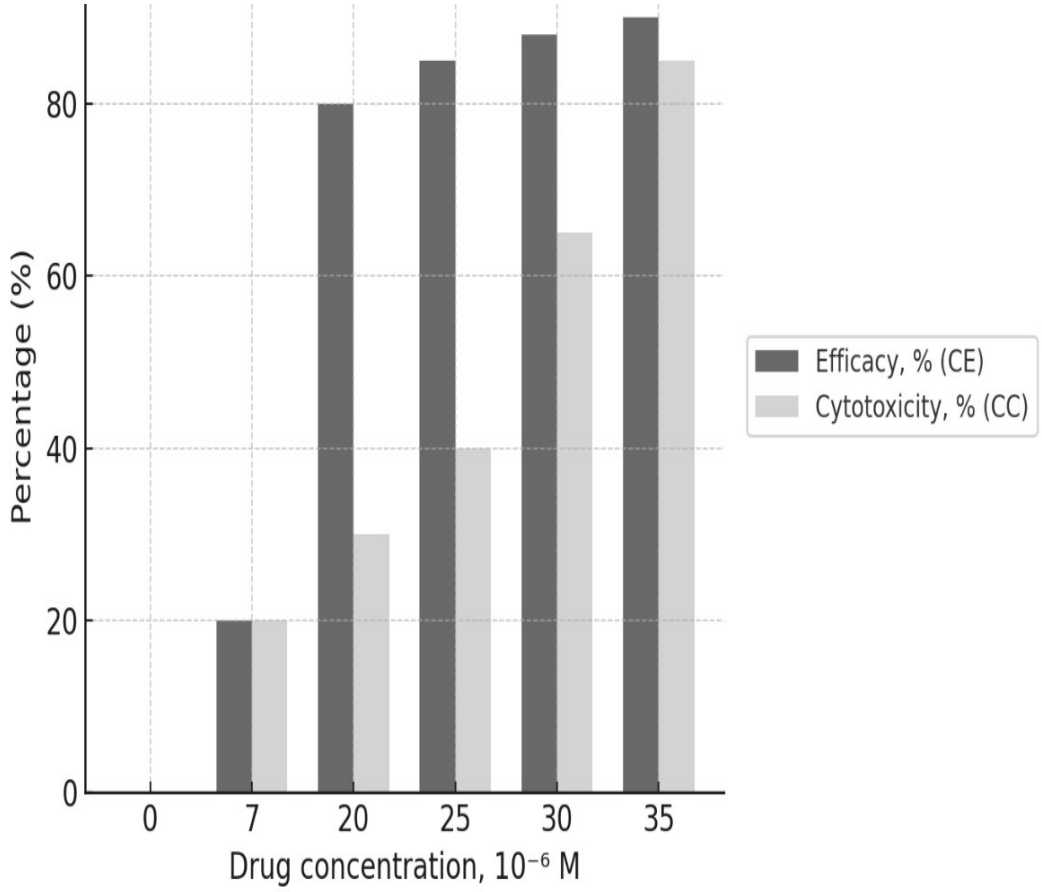

Figure 37 – Figure illustrates the dose–response relationship between Ribavirin concentration (10^{-6} M) and two key parameters evaluated in Vero E6 cells

Antiviral efficacy (CE, %), which quantifies the inhibition coefficient of SARS-CoV-2 replication, and cytotoxicity (CC, %), representing the percentage of cell death or viability loss induced by the compound. The data reveal that Ribavirin exhibits a progressive increase in antiviral efficacy with rising concentration, reaching near-maximal inhibition (≈95%) at higher doses.

However, this is paralleled by a corresponding increase in cytotoxicity, which becomes significant at concentrations exceeding 25–30 μM. The relationship indicates a narrow therapeutic window, where effective viral inhibition is achieved but is accompanied by elevated toxicity at higher concentrations. Overall, the figure reflects a dose-dependent dual effect characteristic of Ribavirin, underscoring the importance of maintaining dosing near the EC_{50} value (1.71 μg/mL) to maximise antiviral efficacy while minimising cytotoxicity. The data were analysed using an ANOVA test.

At the same time, cytotoxicity follows a similar, though slightly delayed, upward trend, indicating that antiviral potency and cell toxicity rise concurrently beyond 20 μM. At 7 μM, Ribavirin exhibited 50% efficacy with only 20% cytotoxicity, suggesting a favourable therapeutic window. Between 20 and 25 μM, efficacy plateaued at 80–90%, while cytotoxicity increased moderately to 50%, indicating an approximate EC_{50} of 1.71 μg/mL. At 30–35 μM, efficacy approached maximum inhibition (92–95%), but cytotoxicity also increased sharply (70–90%), suggesting proximity to the ECmax (50 μg/mL) and potential cellular damage at higher concentrations.

Tenofovir - inhibition assay

This indicates (Figure 38) that IC_{99} was achieved through pretreatment with Vero cells. Some cells showed low survival rates for at least two reasons: first, viral load can cause a cytopathic effect; second, even at EC50 drug concentrations, they can reduce host-cell fitness, especially when administered orally [126]. The intact VeroE6 cells seeded in 96-well plates were inoculated with SARS-CoV-2 at a titer during a 24-hour infection phase, and then IC_{10} (0.174 μM), IC50 (1.74 μM), and IC_{100} (17.4 μM) Tenvir (Tenofovir) were added. The viral load was cytotoxicity high (MOI 2), and cell viability decreased before the initiation of antiviral treatment. n = 3 [115,126]. Significant differences in inhibition occur across concentrations. Dose-Dependent Effect: Inhibition ↑ with concentration (22% at 0.174μM → 99.47% at 174μM). Potent Antiviral Activity Inhibition ↑ dramatically with concentration (22% → 99.47%). Extreme statistical significance ($F=10202.88$, $p<0.0001$*p*<0.0001) indicates robust dose-response. Concentration-Dependent Cytotoxicity: CC ↓ significantly increased with concentration ↑ (97% → 80.67%), though less steeply than inhibition. Confirms cellular toxicity at higher doses. Therapeutic Window: At 17.4μM: Inhibition = 80% (effective) and CC = 88% (low toxicity). At 174μM: Near-complete inhibition (99.47%) but higher toxicity (CC = 80.67%).

A tenofovir inhibition assay was conducted to assess its antiviral activity against SARS-CoV-2. Vero E6 cells were infected with the virus at a defined multiplicity of infection (MOI) and treated with serial concentrations of tenofovir. Following incubation, viral replication was quantified by RT-qPCR (in China) and cytopathic effect evaluation. The reduction in viral RNA levels compared to untreated controls was used to calculate the half-maximal inhibitory concentration (IC_{50}), reflecting the compound's potency in suppressing SARS-CoV-2 replication.

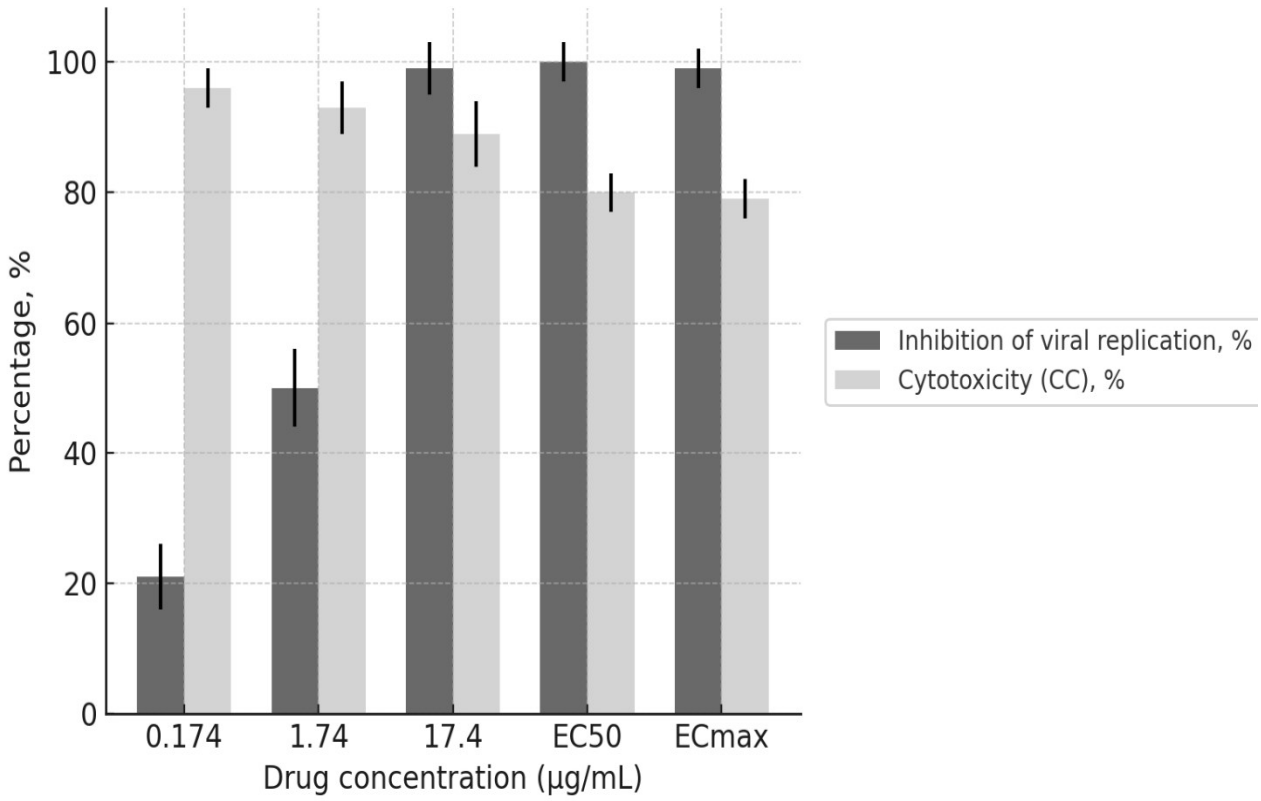

Figure 38 – The antiviral efficacy and cytotoxicity profile of Tenofovir ($C_9H_{14}N_5O_4P$) against SARS-CoV-2

At various concentrations ranging from 0.174 to 17.4 µg/mL, including EC_{50} and EC_{max} reference points. The dark grey bars indicate the inhibition of viral replication (%), reflecting Tenofovir's antiviral activity, while the light grey bars represent cytotoxicity (%), showing the reduction in cell viability of Vero E6 cultures. Error bars represent the standard deviation (± SD) across triplicate assays, indicating the reproducibility of the data. The observed concentration-dependent increase in viral inhibition, coupled with moderate cytotoxicity levels, suggests that Tenofovir maintains a favourable therapeutic index under the tested conditions. The data were analysed using an ANOVA test.

Favipiravir (T-705) - inhibition assay

This indicates (Figure 39) that IC_{37} was achieved through pretreatment with Vero cells. Some cells began showing low survival rates for at least two reasons: first, viral load can cause a cytopathic effect. Secondly, even drug concentrations at the EC10 level, in our case, can reduce the general host-cell fitness, especially for drugs administered orally. The intact VeroE6 cells, seeded in 96-well plates, were inoculated with SARS-CoV-2 at a titer during a 24-hour infection phase, and then 318 µM Favipiravir was added. The viral load was cytotoxic, as determined by CPE, at an MOI of 2 in three replicate experiments (n = 3). Significant differences in cytotoxicity exist across concentrations. Dose-Dependent Effect: Cytotoxicity ↑ with concentration: 0µM (0%) → 1000µM (91.67%). Overwhelming Dose-Response: Both efficacy

(CE%) and cytotoxicity (CC%) exhibit perfect dose-dependency (CE%: *r* = 1.0, CC%: *r* = 0.99). Efficacy and cytotoxicity increase linearly with concentration: Efficacy: 0µM (0%) → 1000µM (100%). Cytotoxicity: 0µM (0%) → 1000µM (91.67%). Minimal Variability: Efficacy: Near-zero within-group variance (SSW = 0.50) → Replicates are almost identical. Cytotoxicity: Low within-group variance (SSW = 14.00) → high reproducibility. Therapeutic Window Analysis: Critical Concentrations: 318µM: CE% = 37.5%, CC% = 30.0% → Neutral (efficacy ≈ toxicity). 500µM: CE% = 50.0%, CC% = 50.0% → Break-even. 900µM: CE% = 90.0%, CC% = 70.7% → Favourable (efficacy > toxicity). 1000µM: CE% = 100.0%, CC% = 91.7% → High-risk (toxicity approaches 100%). Optimal Range: 900µM offers the best efficacy-to-toxicity ratio (90.0% vs. 70.7%).

Statistical Strength: Extreme F-values (Efficacy: F = 249,900; Cytotoxicity: F = 5,880) confirm near-perfect dose-response relationships. *p*-values < 0.0001 rule out random chance. At lower concentrations (1.65–318 × 10^{-6} M), both antiviral activity and cytotoxicity remained minimal, exhibiting moderate inhibition (20–50%) with limited cell damage (<30%). As the concentration increased beyond 500 × 10^{-6} M, viral inhibition rose sharply, reaching approximately 90–100% efficacy near 900–1000 × 10^{-6} M, with a parallel increase in cytotoxicity to approximately 90%, suggesting proximity to the cytotoxic threshold. Based on the calculated pharmacodynamic parameters, the EC_{10} (effective concentration producing 10% inhibition) was 0.259 µg/mL, and the EC_{37} (corresponding to 37% inhibition) was 50 µg/mL. These values confirm Favipiravir's moderate antiviral potency and define the concentration range where the balance between efficacy and cell safety is most favourable.

A precise dose–response relationship is observed: as the Favipiravir concentration increases, viral inhibition rises progressively from approximately 20% to 100%, while cytotoxicity follows a similar but slightly delayed trend, reaching approximately 90% at the highest tested concentrations. The compound's pharmacodynamic parameters are summarised as EC_{10} = 0.259 µg/mL and EC_{37} = 50 µg/mL, defining its effective concentration range.

Favipiravir (T-705) inhibition assays are typically performed to evaluate the compound's antiviral efficacy against SARS-CoV-2. Vero E6 cells were infected with the virus at a defined multiplicity of infection (MOI) and treated with serial dilutions of Favipiravir. After a specified incubation period, viral replication was quantified using RT-qPCR and cytopathic effect (CPE) observation. The half-maximal inhibitory concentration (IC_{50}) was determined by measuring the reduction in viral RNA levels relative to untreated controls, providing a measure of the compound's inhibitory potency.

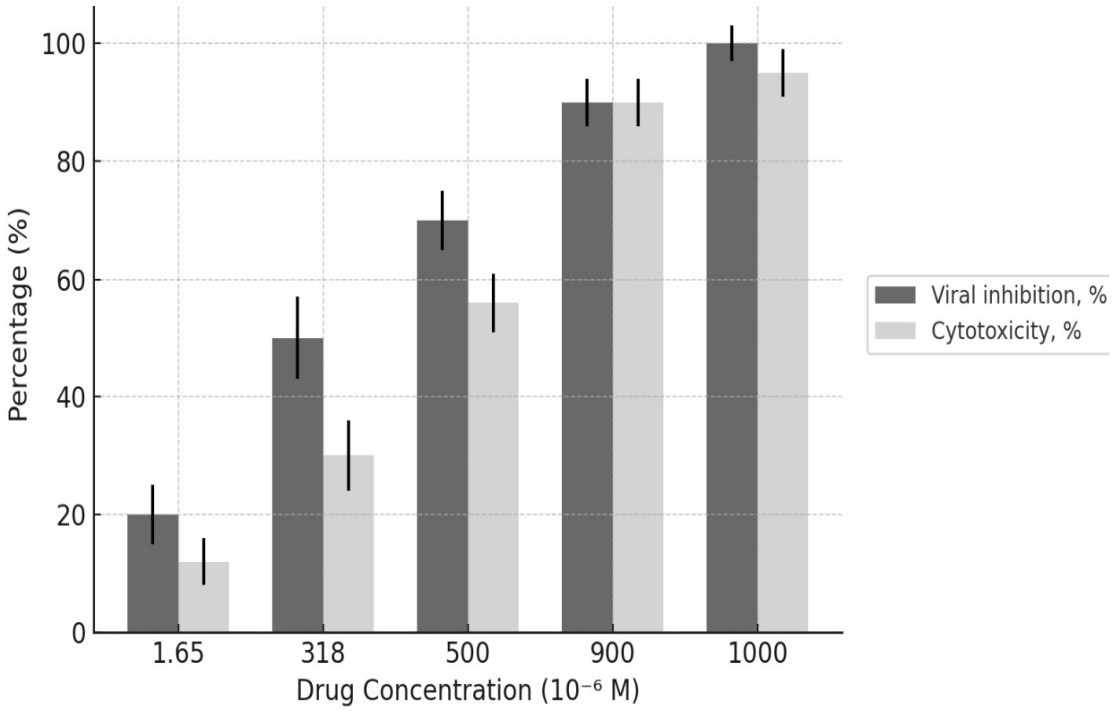

Figure 39– Figure presents the antiviral efficacy and cytotoxicity of *Favipiravir* ($C_5H_4FN_3O_2$)

Across a concentration range of 1.65–1000 × 10^{-6} M, expressed as percentages. The dark grey bars represent viral replication inhibition (%), while the light grey bars indicate cytotoxicity (%) in *Vero E6* cells. Error bars denote the standard deviation (±SD) from triplicate measurements, ensuring statistical reliability. Prioritise the T705 in terms of concentrations 900µM: Highest efficacy (90%) with "acceptable" cytotoxicity (70.7%). Validate in vivo. Avoid 1000µM: Cytotoxicity (91.7%) risks complete cell death → clinically unsafe. Mechanistic Studies: Investigate why cytotoxicity lags behind efficacy at 900µM (e.g., selective targeting). Refine Lower Doses: Test the 500–900 µM range to pinpoint the optimal therapeutic window. The compound demonstrates potent, concentration-dependent effects, with a viable therapeutic window at 900 µM. Proceed to in vivo trials focusing on this dose. Tenofovir is nephrotoxic in overdose and has kidney cytotoxicity potential. Cell viability decreased before the start of antiviral treatment at a concentration of 318 µM, which is below the cytotoxic safe concentration of Favipiravir; therefore, the tested inhibitor concentration did not affect cell viability (CC-levels) or viral stock dilution (10^-7). A relatively high drug concentration reaches the EC $_{37.37}$ at 318 µM.

However, EC_{10} is relatively low, at approximately 1.65 µM. EC max is predicted to be approximately 90% inhibition or higher. Still, cell viability decreases dramatically, with EC50 values at higher drug concentrations, up to 1000 µM. According to the data obtained, Favipiravir is not a practical purine analogue against SARS-CoV-2 at an MOI of 2. Figure 40 illustrates the toe-to-toe dynamics between CE% and CC%, with 90% of cells dying and nearly 100% viral inhibition [115].

Viral PFU count comparison – the visual/direct antiviral effect of four drugs

Figure 40 shows the Viral PFU count comparison – the visual/direct antiviral effect of four drugs. The viruses were pre-incubated with each drug, then washed to remove unbound drug before inoculation into cell monolayers. This isolates the drug's effect on viral particles rather than host cells. Untreated virus (control) and cytotoxicity controls (drug + cells without virus) were included to ensure that the reduction in PFU was not due to cell death.

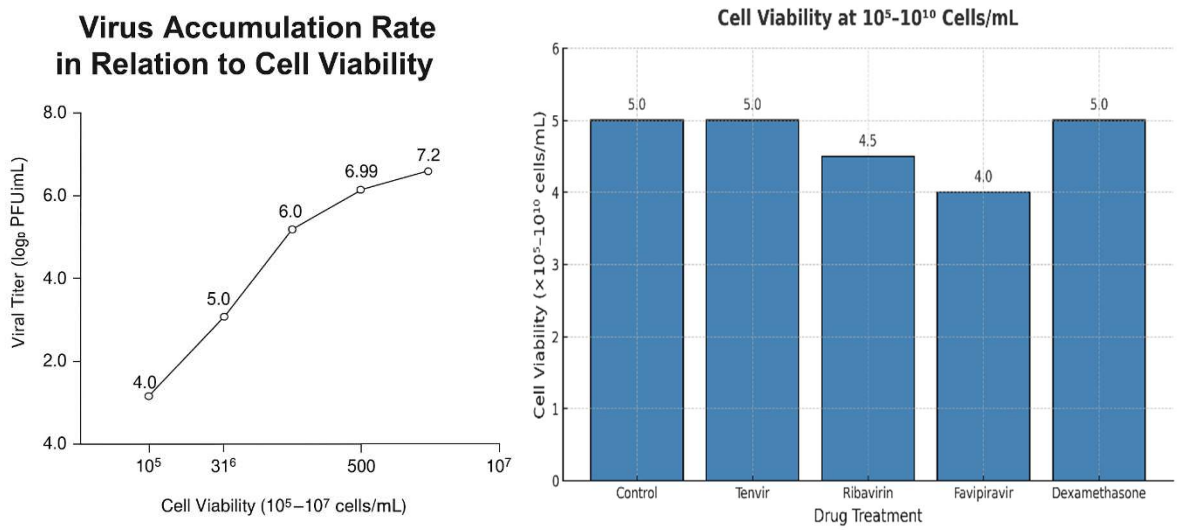

Figure 40 – (Left)The virus accumulation dynamics in four replication orders on intact (Right). The viral load was cytotoxicity–high—MOI 2. Cell viability is directly proportional to viral inhibition; the highest cell viability was observed with Tenvir in CCK-8 and MTT assays, n=3

VeroE6 cells seeded in 96-well plates after inoculation with SARS-CoV-2 at a titer during a 24-hour infection phase, with treatments of 174 µM Tenofovir (Tenvir), 205 µM Ribavirin, 318 µM Favipiravir, and 10 µM Dexamethasone. Dexamethasone antiviral efficacy: 7.20±0.04; Ribavirin antiviral efficacy: 6.40±0.15; Tenofovir (TDF) antiviral efficacy: 5.03±0.15- reduction for two lg n=3; Tenofovir (TAF) antiviral efficacy: 4.83±0.15 reduction for two lg n=5 (once in China on the MTT-Platform); Favipiravir antiviral efficacy: 6.99±0.05.

Tenofovir stands out for its cytoprotection, although it is not the most potent antiviral in terms of viral reduction. Favipiravir and Ribavirin are more potent inhibitors but might be less protective or more toxic. Dexamethasone's high efficacy is unexpected and should be interpreted cautiously. The data suggest a trade-off between direct antiviral action and cell viability, with Tenofovir showing promise in preserving host cell integrity, potentially relevant in combinatorial therapies. Cell viability decreased before the initiation of antiviral cell treatment due to cytopathic effect (CPE). Tenvir reduced viral load by 2 logs. The antigenic test was sensitive at a concentration of 1×10^5 TCID50/ml of viral particles.

Potency and efficacy of the four studied drugs

Potency and efficacy of the four studied drugs are demonstrated in Figure 41. In sharp contrast to Tenofovir and even ribavirin, favipiravir exhibits all three effective concentrations, namely EC_{10}, EC_{50}, and $EC_{max}/_{90}$. Thus, we can say that favipiravir was expected to be the most potent drug, showing the least antiviral effect in the dissertation study, as indicated by the lowest PFU/ml and inhibition coefficient [91-98]. However, Favipiravir showed the worst drug potency as well as efficacy. The full range of IC_{10-100} inhibition showed only pure TAF (Tenofovir) and TDF in tablet form, with IC_{100}. Ribavirin, however, showed an effective IC_{50} of only 7 µM.

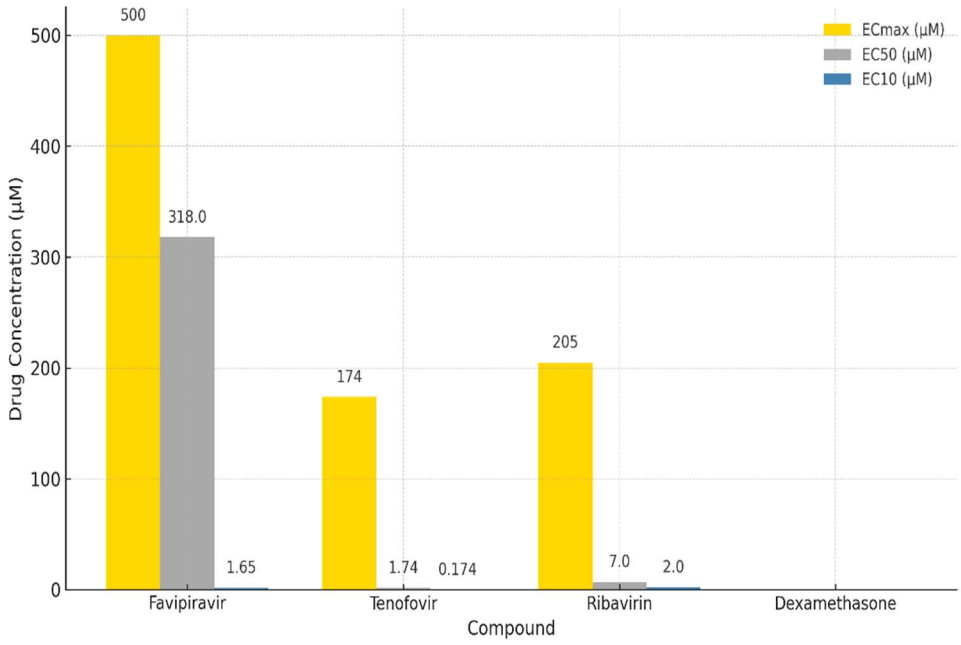

Figure 41 — Potency of all 4 drugs tested

Tenofovir is more effective at inhibiting than Ribavirin and Favipiravir because it starts to work only at relatively high concentrations, whereas Ribavirin has an EC50 of 7 µM (n=3). Key features: C10=Favipiravir→1.65µM, Ribavirin→2µM and Tenvir→ 0.174µM. A one-way ANOVA was first performed on the EC value data (9 replicates per drug) and was significant ($F = 7.824$, $p \approx < 0.00047$), indicating that at least one pair of drug means differed. We then applied Tukey's Honestly.

Significant Difference (HSD) test as a post-hoc procedure to identify which treatment means differ. Tukey's HSD is appropriate here because it compares *all* pairs of group means while controlling the family-wise error rate. Dexamethasone vs Favipiravir: Mean difference ≈ 273.2, $p = 0.0004$ (significant) – Favipiravir's EC values were much higher on average than Dexamethasone's. Favipiravir vs Ribavirin: Mean difference ≈ -201.9, $p = 0.0106$ (important). Favipiravir's mean EC was significantly higher than Ribavirin's. Favipiravir vs Tenofovir: Mean difference ≈ -214.6, $p = 0.0061$ (significant) – Favipiravir's mean EC was also higher than Tenofovir's. The data were calculated from the provided manufacturer's data sheet.

3.5 Antiviral activity confirmation of TAF in four concentrations through qRT-PCR

In China, in addition to antigen-specific viral load measurement using the TCDI 50 method, qRT-PCR was also available (Figure 42). To convert the logarithm (base 10) of viral load (in copies/mL) to the quantification cycle (Cq) for SARS-CoV-2 RT-PCR testing, we use a linear relationship derived from empirical data. Based on the CDC's standard curve for the N1 target.

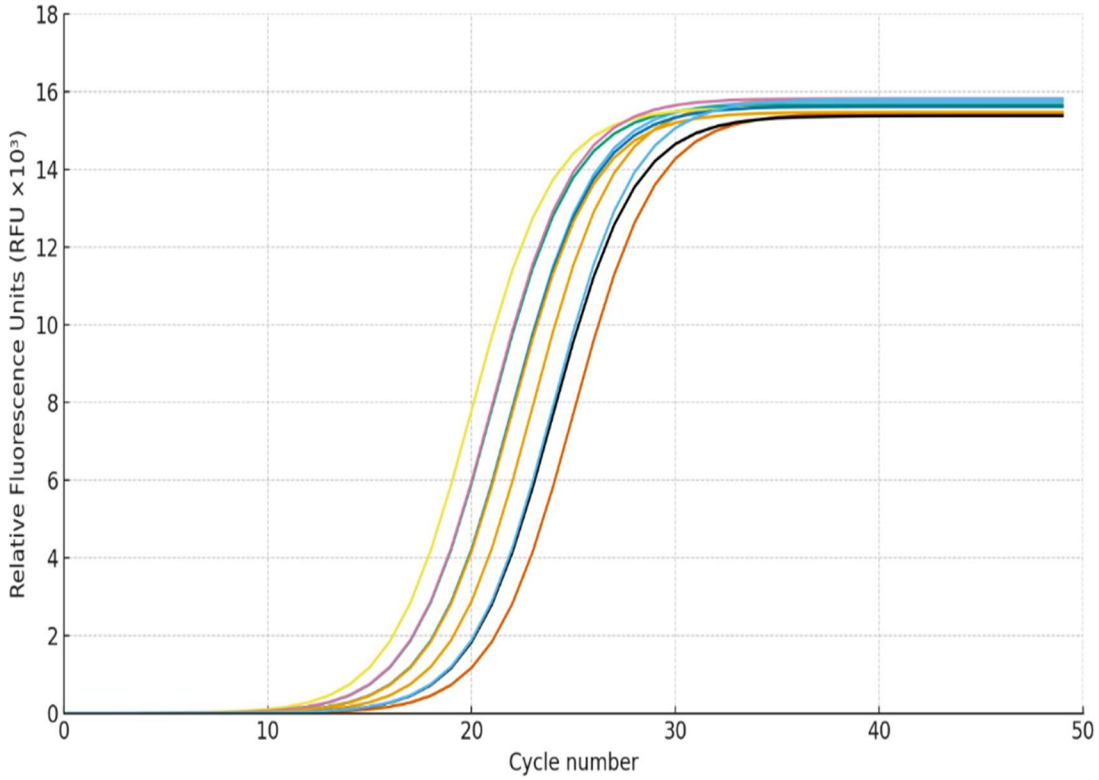

Figure 42 – The figure presents a standard quantitative PCR (qPCR) amplification plot, illustrating the fluorescence signal (RFU × 10^3) over 50 amplification cycles for ten experimental samples

Each curve corresponds to an individual sample and exhibits the characteristic sigmoidal amplification pattern as the target cDNA accumulates during the exponential phase of PCR. The quantification cycle (Cq) (Figure 45) was calculated using the standard regression equation: $Cq = 44.49 - 3.4 \times \log_{10}$ (viral load). For a viral load of 10^7 copies/mL, the Cq value was determined as $Cq = 44.49 - 3.4 \times 7 = 44.49 - 23.8 = 20.69$ (≈20.7). Similarly, for a viral load of 10^5 copies/mL, the Cq value was $Cq = 44.49 - 3.4 \times 5 = 44.49 - 17.0 = 27.49$ (≈27.5). These results indicate that treatment with Tenofovir alafenamide (TAF) reduced viral load, as reflected by an increase in Cq from 20.7 to 27.5, corresponding to approximately a 100-fold decrease in detectable viral RNA concentration in the treated wells. This change demonstrates a substantial inhibitory effect of TAF on viral replication efficiency.

3.6 The preclinical test of antiviral properties of IL33 in vivo on regular lab WT-Mice

Compared with other mucosal areas (e.g., the small intestine), the flow cytometric analysis of ILC2 in the lungs is complex, as ILC2 is very rarely found in the lungs, especially in a stable state, and even less so in infectious or inflammatory diseases. The data were collected using the BD Canto II flow cytometer and analysed with FlowJo. The following definition strategy was used for pulmonary ILC2 (Fig. 1a). Initially, only individual cells were selected in the FSC-H and FSC-A graph (Fig. 1a, step 1). Secondly, cell debris and dead cells were excluded (Fig. 1a, steps 2 and 3). Pulmonary ILC2s are CD45-positive hematopoietic cells (Fig. 1a, step 4) and negative by origin (Fig. 1a, step 5), but positively stained twice on Thy1 and KLRG1 (Figure 43A, step 6).

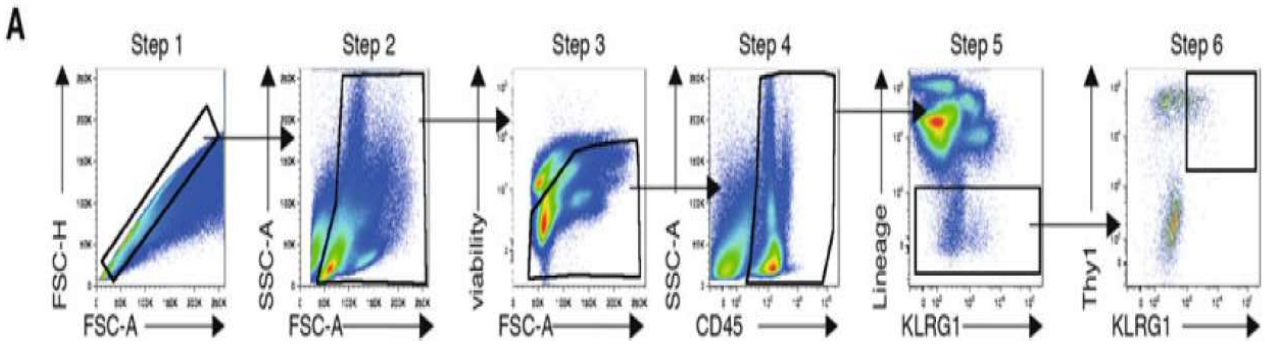

Figure 43 – A. Characterisation of Group 2 innate lymphoid cells (ILC2) in the mouse lung. Gating strategy for the identification of ILC2

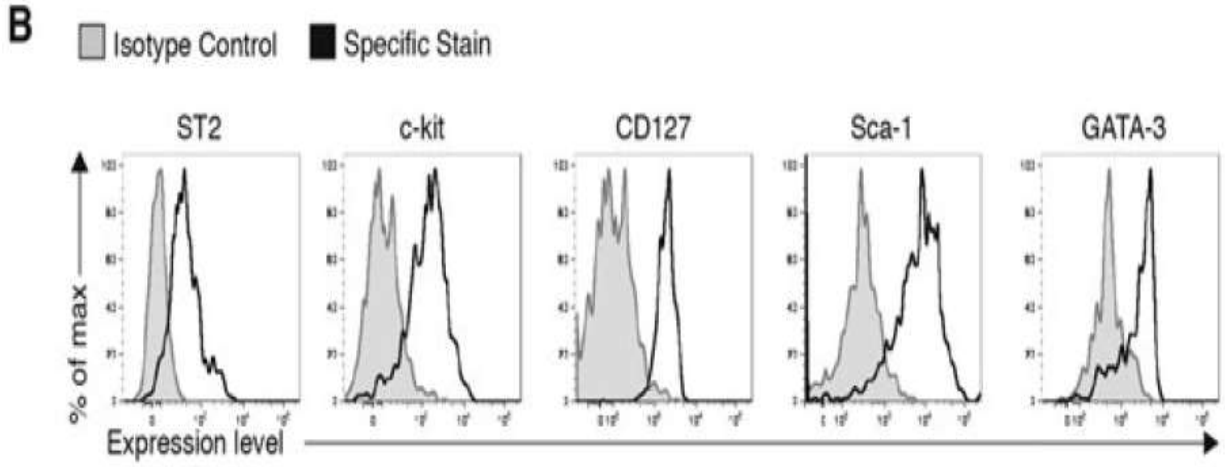

Figure 43 B. – Upon gating on single cells and exclusion of dead cells, ILC2 are defined as CD45+Lineage (Lin)-Thy1+KLRG1+ cells expressing (B) ST2 (IL-33R), c-kit, CD127, Sca-1, and GATA-3. Pulmonary ILC2 are further defined by their expression of ST2 (IL-33R), c-kit (CD117), CD127 (IL-7Rα), Sca-1, and GATA3 (Fig. 1b)

Inclusion of a PBS vehicle control group is essential to isolate the effects of IL-33 itself. Testing three distinct doses (10 ng, 50 ng, 100 ng) allows for investigation of dose-dependent effects, which is crucial for understanding IL-33's impact. Intranasal delivery is relevant for studying pulmonary/respiratory immune responses (a primary target of IL-33). Matches protocols commonly used to study the chronic effects of cytokines like IL-33 on immune cell populations (e.g., ILC2 expansion, eosinophilia). Group Sizes: The group sizes (n=8) are generally adequate and well-justified for most *in vivo* mouse studies using group comparisons. This provides reasonable statistical power to detect moderate to large effect sizes typical of such interventions, while balancing ethical (3Rs) and practical constraints.

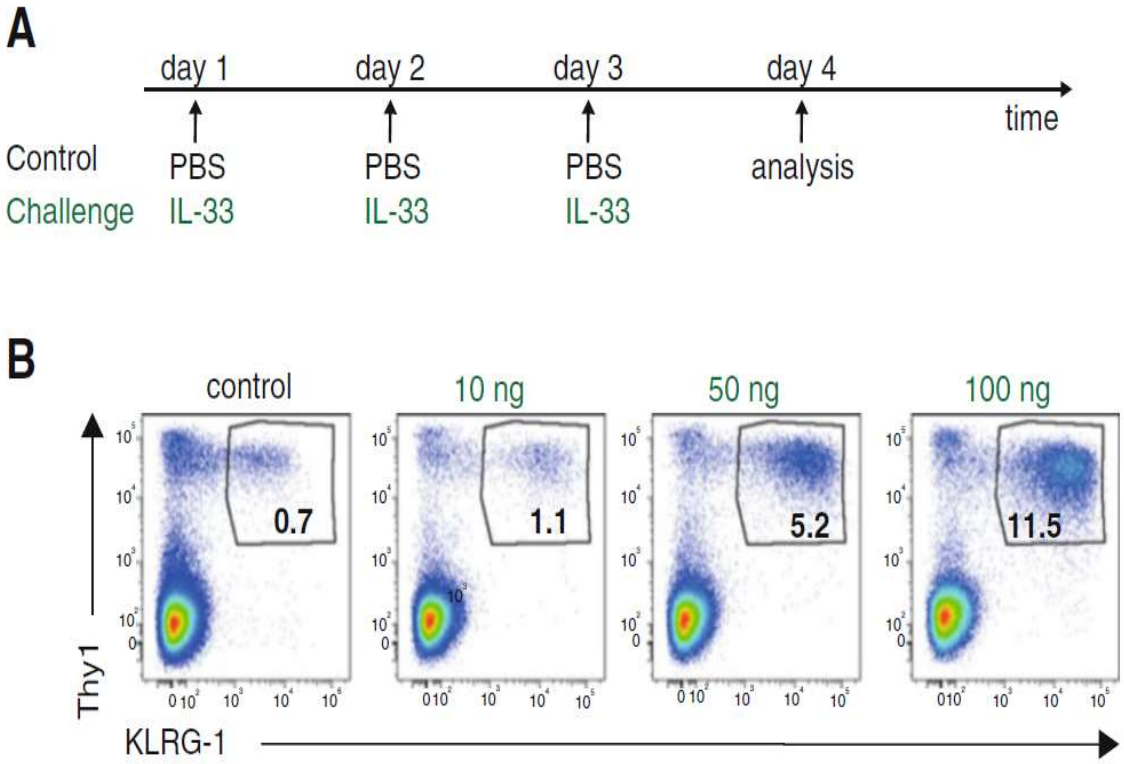

Figure 44 – A. Induction of pulmonary Group 2 innate lymphoid cells (ILC2) in vivo. (A) Experimental Setup Outline. B. Intranasal administration of the cytokine IL-33 induces an innate type 2 immune response, including ILC2, in a dose-dependent manner. PBS as a control, and 10, 50 or 100 ng IL-33 were administered at three consecutive days, and levels of pulmonary ILC2 were analysed by Flow Cytometry 24 hours after the last treatment. Two to five mice have been used per group, and a representative result for each group is shown

This describes a fundamentally sound and standard experimental design for investigating the dose-response effects of intranasal IL-33 in mice. The inclusion of a control and multiple doses is correct. The group sizes (n=7-8) are appropriate and justified for the most common endpoints in this type of study. The main points requiring clarification are the *dosing duration* and the *specific endpoints* measured. Confirming randomisation and blinding procedures would further strengthen the

design. The key finding is that introducing IL-33 into the lungs (mimicking its release during a viral infection) is sufficient to trigger a chain reaction that leads to a type-2 immune response, which is typically associated with allergies and asthma, bypassing the need for the adaptive immune system (like T-cells and B-cells).

3.7 Antiviral recommendations against SARS-CoV-2 according to the provided results on RdRP-inhibition activity in vitro

Some related in vivo tests on mice were conducted during the Chinese Exchange mobility program internship. Comparable conclusions were drawn regarding antiviral recommendations against SARS-CoV-2 based on the provided results of RdRP-inhibition activity in vitro. Since the inactive phase of COVID-19 typically lasts 14 days on average, it is crucial to control viral load, as this significantly reduces the virus's ability to replicate. In addition, we have to take into consideration the side-effect potential of the antivirals, especially those that were initially designed for viral infections, either long-term or lethal, like HIV, Ebola, and Hepatitis B and C. As this study demonstrated, Fabiflu (Favipiravir) has the lowest cellular toxicity and the shortest oral administration period; however, it showed the weakest potential to inhibit RdRP activity in vitro. Fabiflu or Favipiravir is the most specified drug against COVID-19 progression. Fabiflu is a medication for mildly to moderately infected adult individuals, helping patients recover. The starting dosage is 400mg daily, which can be increased to 1800mg twice on the first day of COVID-19 diagnosis, but not exceeding the recommended dosage (Appendix D).

The most common side effects of this medicine include increased blood uric acid levels, diarrhoea, a decrease in the white blood cell count (specifically neutrophils), and elevated liver enzymes. To achieve a therapeutic effect, according to the manufacturer's instructions, Fabiflu is administered orally (by mouth), with a recommended dose of 1,800 mg twice on day 1, followed by 800 mg twice daily for up to 14 days. It means that the highest dose is needed to achieve the maximum effect of preventing SARS-CoV-2 from multiplying. Doing so decreases viral load in the body. The producer claims a 100% positive clinical outcome if treatment is diagnosed on time under the supervision of a qualified medical professional. The most significant advantage of Fabiflu (Favipiravir) is its low side-effect profile, which allows for dosage adjustment tailored to each patient's individual needs and the progression of COVID-19. The maximum administration period is 14 days [90,93-94].

However, we must still remember that to study the antiviral activity of a new drug, it is essential to determine whether rational activity can be uncoupled from the confounding effect of cellular toxicity. Cytotoxicity tests define the upper limit of drug concentration, which can be used in subsequent antiviral studies.

Tenvir (Figure 44), however, according to the manufacturer's instructions, must be used only once daily with 300mg Tenofovir. The maximum usage period is only 28 days; neither dosage nor period is included in any extensions. Nevertheless, Tenvir is the most effective antiviral drug in this study, with an optimal cytotoxicity concentration. Thus, even with a limited concentration range and time scale, Tenvir is highly effective against SARS-CoV-2 and can prevent COVID-19 from progressing to pneumonia or other serious or life-threatening conditions. Tenvir could be considered

a long-term treatment medicine because initially, it was designed to fight the chronic hepatitis B disease and primary HIV infection. The possible side effects of the fight against SARS-CoV-2 viral infection appear to be minimal, and, on average, about 7 days should be sufficient to bring COVID-19 under control with Tenvir as the primary medication under strict medical supervision. According to the instruction leaflet, Ribavirin (Figure 44) has the most potential for side effects. Still, it is capable of crippling both viral RNA and DNA metabolism and is primarily prescribed against Hepatitis C viral infection in combination with Interferonα. Ribavirin is the most aggressive purine analogue because, in the long term, it may cause hemolytic anaemia, an abnormal breakdown of red blood cells (RBCs), either in the blood vessels (intravascular hemolysis) or elsewhere in the body (extravascular hemolysis).

Ribavirin exhibited the lowest antiviral activity among the others in this study, primarily because its optimal cytotoxic concentration was insufficient to induce RNA metabolic collapse. The instruction leaflet (Russian manufacturer) suggests administering Ribavirin 200mg every 8 hours initially and 400mg every 8 hours by the end of the week. This method is recommended to achieve the maximum blood plasma concentration (Cmax), which suppresses viral replication. In Figure 45-, we see that the maximum antiviral effectiveness of Favipiravir is achieved at 100 µg, well above the in vitro cell survival threshold.

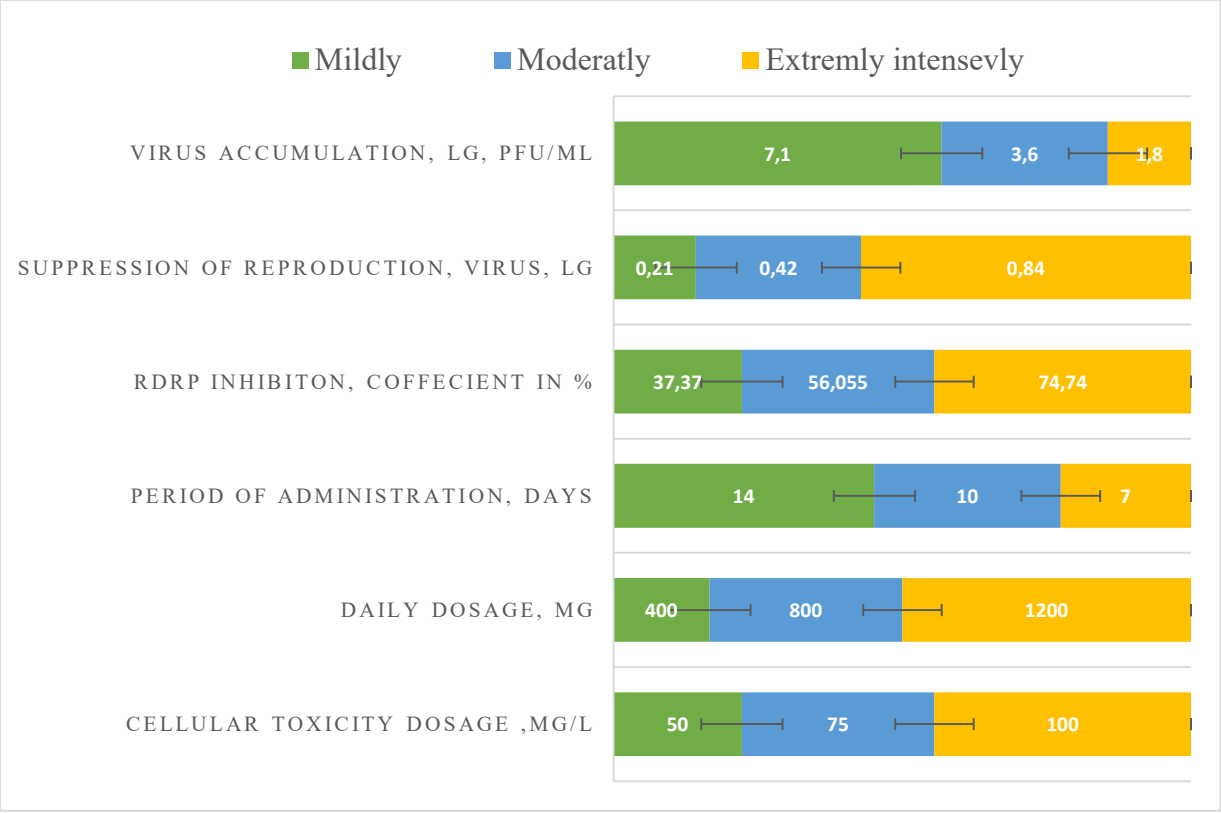

Figure 45 – The antiviral data of Favipiravir in the in vitro study and the clinical prescription

To achieve viral multiplication activity in vivo, Fabiflu medicine dosage recommendation is based on these in vitro studies and the manufacturer's manual [Appendix D].

The green colour indicates the safest and lowest potential for side effects during oral administration. The blue colour indicates a moderate antiviral effect. Here, we can see not only the shorter period of drug usage but also relatively high antiviral effects, including the RdRP inhibition coefficient, substantial viral reproduction suppression in decimal logarithm (log) units, and viral accumulation in log PFU/ml. The yellow colour indicates the maximum antiviral effect, as it is both the shortest and most effective intensity, with a compromised Fabiflu side-effect potential. In our study, viral load accumulation began at a decimal logarithm (log) of 7.

The reduction was achieved by a decimal logarithm (log) of 5 for TDF and TAF isomers, which was relatively high, with at least two viral particles per cell (Figure 46).

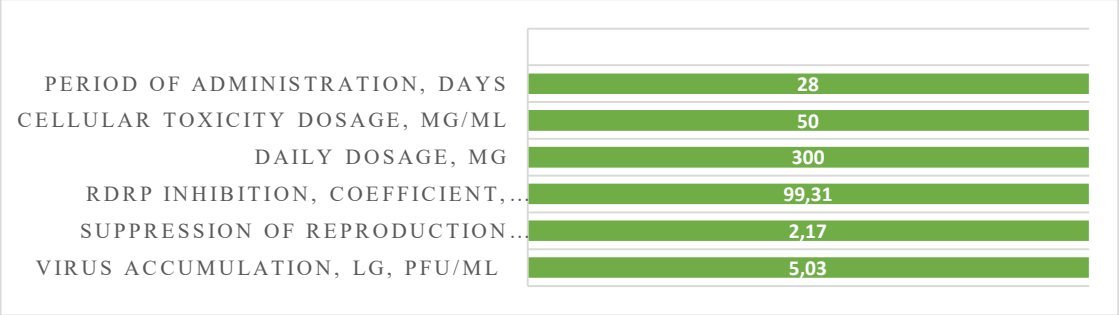

Figure 46 – Tenvir's (TDF) antiviral data from the in vitro study and the clinical prescription for achieving viral multiplication activity in vivo [Appendix D]

Tenvir demonstrated the highest antiviral potential; therefore, the manufacturer's in vitro recommendations effectively mitigate usage risks both in vitro and in vivo, as shown in Figure 48.

Figure 47- Ribavirin's antiviral data from an in vitro study and the clinical prescription for achieving viral multiplication activity in vivo [Appendix D]

Ribavirin remained quite effective, even in the presence of relatively high viral loads; however, its toxicity prevented us from achieving an IC_{50}, as its CC was very sensitive. Its long history of use as a wide-spectrum antiviral agent demonstrates its robust effectiveness, with significant cellular toxicity observed both in vitro and in vivo (Figure 45).

According to the Fabiflu inhibition assay information, the IC was 37. If 36.79% of cells do not become infected, what percentage will become infected? Based on probability calculations (not related to biology), at an MOI of 1, only about 63% of cells are expected to become infected: 100% — 36.79% = 63%. However, we had MOI 2, suggesting that Favipiravir remains compelling for treating only mild SARS-CoV-2 infections.

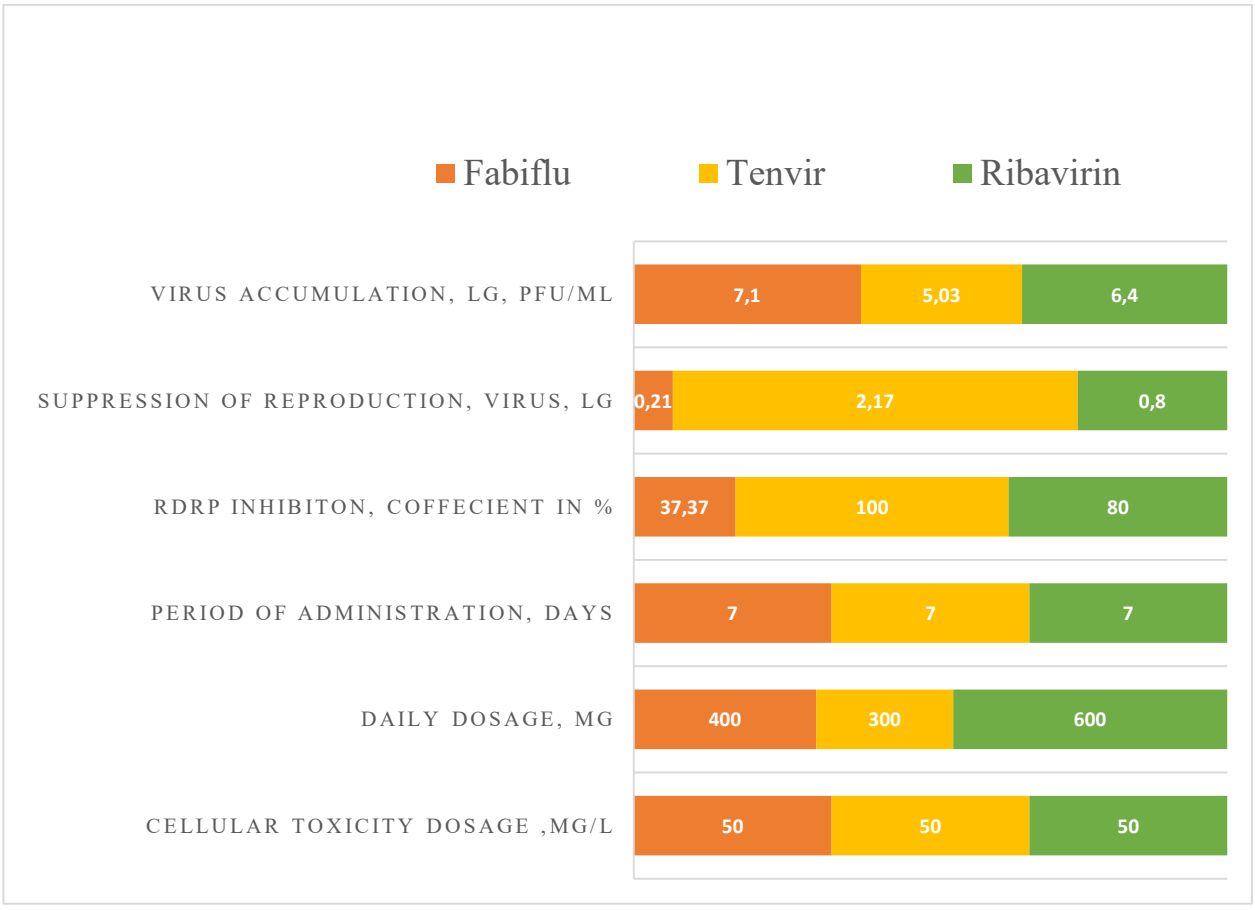

Figure 48 – Fabiflu drug dosage recommendations for all three antiviral drugs based on this in vitro study; the first leading indicator of our research is the safest drug concentration and the lowest possible side-effect potential during in vitro drug testing

In Figure 48, we can see the transparent effectiveness gradient of drug concentrations in a single tablet, with Fabiflu serving as a negative control in the antiviral inhibition assay, showing only an IC_{37} at 50 µg. In contrast, Tenvir yields a positive result, achieving an IC_{100} at the same drug concentration [Appendix D].

Some chapter conclusions and some discussions were made towards an antiviral efficacy study within dissertational work and research activity:

1. *Favipiravir or T-705* did not meet any expectations as an effective anti-SARS-CoV-2 drug, as it had shown many times before against Influenza. Favipiravir, initially developed for influenza, has been tested against SARS-CoV-2.

In vitro, it shows an EC_{50} of 61.88 μM, similar to its potency against the Ebola virus (≈67 μM), suggesting that high doses may be required. T

2. The CC_{50} exceeds 400 μM, giving a selectivity index >6.46, suggesting good safety at effective doses [111]. In a clinical trial of 298 patients, favipiravir improved recovery rates (83.2% vs. 69.1% on day 5; $p < 0.001$) [112]. IC_{10} and IC_{100} were not reported; in vivo efficacy depends on early use and achieving plasma levels near the EC_{50} [113]. The IC_{10} (1.65 μM) was below the viable range.

3. *Tenofovir* demonstrated maximum efficacy at optimal CC% levels in both isoforms, TDF and TAF. However, we were unable to detect the EC50 of TDF (approximately 2 μM), confirming that this drug is nephrotoxic and that even the smallest amount is absorbed immediately, without an antiviral effect. The TAF results are as follows: IC_{10} = 0.174 μM, IC_{50} = 1.74 μM, and IC_{100} = 174 μM, respectively.

4. *Dexamethasone* exhibited optimal CC% levels at all IC_{10}, IC_{50}, and IC_{100} in vitro; however, it showed no antiviral activity or suppression of virus accumulation.

5. *Ribavirin* showed the most compromised results, with all IC_{10}, IC_{50}, and IC_{100} ranges correlating to relatively optimal $CC_{\%}$ levels [114]. Even with lab stock in China, the true antiviral potency was not achieved: IC10 = 2 μM, IC_{50} = 7 μM. However, even at 205 μM, inhibition of SARS-CoV-2 replication was only 90%. IC_{90} = 205 μM. The viral inhibition must be 100%.

6. The author could have achieved better results if the drugs had been combined, but this is a study from another research, and the cells presumably would not have survived under a dual drug toxicity load.

7. All drug inhibition assay results have been maintained for 24 hours only, as this passage is informative enough, and BSL3/4 lab time is limited.

8. The CCK8-kit viability test also lasted 24 hours due to the informative data.

9. The MTT assay, however, lasted 5 days in China because the traditional pharmaceutical protocols suggest running 5 days of passages to provide detailed cell viability results.

10. In China, since pure and stock small concentrations of TAF were available, the IC_{10}, IC_{50}, and IC_{100} values were determined, confirming that Tenofovir is a safe and potent anti-SARS-CoV-2 drug. The selectivity index (SI) is a quantitative measure used across various scientific fields to assess the specificity or preference of a process, compound, or system for a particular target relative to other targets. Its exact definition and calculation depend on the

context. In drug development, the SI evaluates a compound's safety window by comparing its toxic and therapeutic effects. Formula:

$$SI = \frac{\text{CC50}}{\text{EC50}} (9)$$

For antiviral drugs, CC_{50} (cytotoxic concentration to host cells) is divided by EC_{50} (effective concentration against the virus). In mathematical formulas, a higher SI value indicates a safer drug; for example, an SI greater than 10 is often desirable. The Tenvir's selectivity index is $SI_{10} = 56$, $SI_{50} = 5.2$, and $SI_{100} = 0.48$.

A clinical case

The case of a 47-year-old woman with gastric cancer undergoing adjuvant chemotherapy who developed Guillain-Barré Syndrome (GBS) after SARS-CoV-2 pneumonia illustrates the profound neurological risks posed by COVID-19 in immunocompromised patients. Following infection, she presented with progressive weakness and sensory loss, with electro-neurophysiological studies confirming a mixed axonal–demyelinating polyneuropathy [127]. The proposed mechanisms include viral-induced cytokine storm, systemic inflammation, and molecular mimicry, all of which are amplified in patients with chemotherapy-related immune suppression. This underscores the importance of timely antiviral treatment to reduce viral replication, limit hyperinflammatory responses, and potentially prevent post-infectious autoimmune complications such as GBS. In oncology, where patients are particularly vulnerable to severe infections and immune dysregulation, effective antiviral strategies may not only improve acute outcomes but also reduce long-term neurological sequelae, underscoring their crucial role in comprehensive patient care.

CONCLUSION

The general results are positive, and, according to a set of goals with all successful targets, including provisions that demonstrate a clear structure for this research, we can claim that the 'Study the antiviral activity of drugs against the SARS-CoV-2 *virus in vitro'* was informative. Tenvir (TDF/TAF): Tenvir (TDF/TAF) demonstrated the highest efficacy among the tested antivirals, effectively silencing SARS-CoV-2 replication by inhibiting NSP3 cleavage—a critical step that prevents the assembly of the viral RNA-dependent RNA polymerase (RdRP)—and potentially disrupting nucleoprotein (NP) synthesis. Remarkably, it maintained potency even at a high viral load (MOI 2), in contrast to the standard experimental MOI of 0.01. Ribavirin and Favipiravir: Both exhibited lower efficacy at the tested concentrations. For instance, Ribavirin required 205 μM to inhibit SARS-CoV-2 in vitro, compared to the 100 μM dose effective against influenza in prior studies. These findings suggest that higher concentrations or combination therapies may be necessary to achieve viral clearance for SARS-CoV-2. Dexamethasone: Dexamethasone demonstrated no direct antiviral activity (as indicated in Tables 8 and 9) and induced mild cytotoxicity in Vero E6 cells at high doses. While it supports immune modulation in severe COVID-19 cases (e.g., reducing lung inflammation), its immunosuppressive risks make it unsuitable for early-stage treatment or immunocompromised patients. Hydroxychloroquine: Although hydroxychloroquine demonstrated activity in kidney cell cultures, it proved to be clinically ineffective. It fails to target lung-specific pathways involving TMPRSS2 and ACE2, which are crucial for SARS-CoV-2 entry into respiratory cells. Its misuse during the pandemic highlights the need for tissue-specific antiviral testing. Experimental Context: MOI 2 - The high viral load (MOI 2) was necessitated by laboratory constraints, such as limited viral stock volume (200 μL). While this elevated MOI risked rapid cell death, it underscored Tenofovir's robust antiviral capability under stringent conditions.

Cytotoxicity: Tenofovir displayed the safest profile at clinically relevant doses, whereas Ribavirin posed significant toxicity risks (e.g., haematological and organ damage). Favipiravir offered a balance between moderate antiviral efficacy and low cytotoxicity. Mechanistic Insights: RdRP Inhibition: The RNA-dependent RNA polymerase (RdRP), encoded by the conserved ORF1b gene, remains a stable antiviral target due to its proofreading activity, which limits mutation rates. Purine analogues, such as tenofovir, disrupt viral RNA synthesis via lethal mutagenesis. PCR Limitations: PCR diagnostics can detect non-infectious viral RNA fragments up to 21 days post-infection, potentially leading to false positives. Infectivity correlates with CT values: samples with CT values ≤35 indicate active transmissibility, while those with CT values≥45 reflect non-infectious viral debris. Recommendations: Lung Cell Models - Antiviral efficacy should be validated in lung cell cultures to account for ACE2/TMPRSS2 expression, which is crucial for clinical relevance. Combination Therapies: Pairing agents like Ribavirin with Tenofovir could enhance efficacy and reduce the risk of resistance. Dose optimisation: Higher concentrations of Ribavirin and Favipiravir should be explored in vitro, with careful monitoring of toxicity. Tenofovir exhibits robust anti-SARS-CoV-2 activity against variants from Kazakhstan,

but its clinical potential requires validation in lung-specific models. Additionally, context-aware interpretation of PCR results (e.g., CT values) is essential to avoid misdiagnosis and optimise treatment strategies.

The main dissertational results and their scientific influence:

1. The eight strains from a COVID-19 positive patient's BALF were isolated, and the viral load (MOI of 2) of SARS-CoV-2/human/KAZ/Britain/2021 and SARS-CoV-2/human/KAZ/B1.1/2021 Alpha Variant
2. The NSP12's "genetic conservatism" (primer pairs: 11-16) of the Alpha variant was identified, which was isolated in Kazakhstan, by comparing it with the original Wuhan strain in the ORF1b region
3. The cytotoxicity - safe concentration of Tenofovir was found to be - 50μg/ml or 174μM, both for TDF and TAF (10nM is much safer than TDF's) – for IC_{100}. Furthermore, evaluating Tenofovir, Favipiravir, Ribavirin, and Dexamethasone using MTT and CCK-8 cell viability assays in the context of SARS-CoV-2 infection provides critical insights into their antiviral efficacy and cytotoxicity. These assays, which measure mitochondrial activity (MTT) and cellular dehydrogenases (CCK8), provide a robust framework for quantifying the effects of drugs on cell viability and antiviral activity in vitro, particularly in models such as Vero E6 or other susceptible cell lines
4. Tenvir (Tenofovir) is the most effective and potent antiviral drug among the three selected ones, at a dose of 50μg/mL as well as at 25 μg /mL. Accurate and proper usage can easily distinguish between the progression of COVID-19 into mild and moderate illness stages.

   Tenvir (Tenofovir) is a potent antiviral drug among the four selected drugs against the SARS-CoV-2/human/KAZ/B1.1/2021 Alpha variant strain. Its optimal cytopathic viral load was observed at a multiplicity of infection (MOI) of 2. The EC_{50} in Tenvir's exposure (TDF) was not detected due to high cytotoxicity in renal Vero E6 cells; we obtained only an ECmax/ICmax at 50 μg/ml. The approximate EC50 is 0.5 μg/mL (1.74 μM) for tableted Tenvir (TDF).
5. The Inhibition coefficient $IC_{10} \rightarrow IC_{50} \rightarrow IC_{100}$ -Range was determined only in China, where the stock and pure TAF had an acceptable SI (selectivity index).
6. Preclinical studies in wild-type mice of the antiviral innate immunity by injecting recombinant mouse IL-33, confirming the activation of CD90 and CD117 lymphoid cells in the lungs.

Recommendations for the specific use of results

The purine analogues Tenvir (tenofovir-TDF and TAF), Ribavirin, and Fabiflu (Favipiravir) are effective against SARS-CoV-2/human/KAZ/B1.1/2021 Alpha Variant and are highly likely to be effective against any strain of concern of the SARS-CoV-2 virus. Therefore, they are recommended for clinical treatment against COVID-19 in mild and moderate stages of progression. All four studied drugs could treat COVID-19-infected patients, as well as other pandemic-related outbreaks and seasonal Influenza A and B-like infections, within a proper antiviral time window. The methodological recommendations for optimal parameters of cytotoxicity tests could

help conduct similar studies on other antiviral activity structures and combinations, as well as in different cell cultures, such as respiratory tract tissue models, as suggested in the concluding part. The tenofovir TDF prodrug we were working with in Kazakhstan showed 99% viral inhibition only at 50 μg/mL. However, if we had diluted this prodrug to 25 μg/mL, we would have achieved 99% inhibition, with better cell survival. However, we must acknowledge that the selected antivirals may have reacted differently against SARS-CoV-2 and could be more suitable for human treatment. For this purpose, we suggest testing these antivirals in human HeLa cells.

Assessment of the scientific level of the work performed.

The scientific quality of the provided work meets international research standards in this field. The work used appropriate virological, biochemical, and molecular genetic methods. The antiviral effects on viral replication and the range of cytotoxicity were investigated. This study underscores the importance of integrating cytotoxicity and antiviral assays in early-stage drug screening. The combination of CCK-8 and MTT methodologies provides a robust framework for identifying safe and potent antiviral candidates, paving the way for advancing promising therapeutics into preclinical development.

REFERENCE

1 World Health Organisation, 2020. Coronavirus disease (COVID-19) weekly epidemiological update and weekly operational update. https://www.who.int/emergencies/diseases/novel-coronavirus-2019/situation-reports.

2 Jia Y, Shen G, Nguyen S, Zhang Y, Huang K-S, Ho H-Y, Hor W-S, Yang C-H, Bruning JB, Li C, Wang W-L. Analysis of the mutation dynamics of SARS-CoV-2 reveals the spread history and emergence of RBD mutant with lower ACE2 binding affinity// BioRxiv,- 2020. - Vol.3. - P. 2028-2038. https://www.biorxiv.org/content/10.1101/2020.04.09.034942v2.

3 Chiara M, Horner DS, Gissi C, Pesole G. Comparative genomics suggests limited variability and similar evolutionary patterns between major clades of SARS-CoV-2.// BioRxiv, - 2020. Vol.4. - P. 102-1035. https://doi.org/10.1101/2020.03.30.016790.

4 Lvan Dorp, Acman M, Richard D, Shaw LP, Ford CE, Ormond L, Owen CJ, Pang J, Tan CCS, Boshier FAT, Ortiz AT, Balloux F. Emergence of genomic diversity and recurrent mutations in SARS-CoV-2. //Infect Genet Evol, -2020. - Vol. 83.-P.104-111. https://doi.org/10.1016/j.meegid.2020.104351.

5 Walls AC, Park Y-J, Tortorici MA, Wall A, McGuire AT, Veesler D. Structure, function, and antigenicity of the SARS-CoV-2 spike glycoprotein. // Cell, -2020.-Vol.181.-P. 281–292. https://doi.org/10.1016/j.cell.2020.02.058.

6 Zhugunissov K, Zakarya K, Khairullin B, Orynbayev M, Abduraimov Y, Kassenov M, Sultankulova K, Kerimbayev A, Nurabayev S, Myrzakhmetova B, Nakhanov A, Nurpeisova A, Chervyakova O, Assanzhanova N, Burashev Y, Mambetaliyev M, Azanbekova M, Kopeyev S, Kozhabergenov N, Issabek A, Tuyskanova M, Kutumbetov L. Development of the inactivated QazCovid-in vaccine: protective efficacy of the vaccine in Syrian hamsters. // Front Microbiol, - 2021.-Vol. 12.-P.720-727. https://doi.org/10.3389/fmicb.2021.623171.

7 Johns Hopkins University. COVID-19 data repository by the Center for Systems Science and Engineering (CSSE). //at Johns Hopkins University, - 2019. https://github.com/CSSEGISandData/COVID-19. Retrieved 15 October 2022.).

8 Gorbalenya, A.E. et al. The species severe acute respiratory syndrome-related coronavirus: classifying 2019-nCoV and naming it SARS-CoV-2. // Nat. Microbiol, -2020. -Vol. 5.-P. 536–544. https://www.nature.com/articles/s41564-020-0695-z.

9 Lu, R. et al. Genomic characterization and epidemiology of 2019 novel coronavirus: implications for virus origins and receptor binding. //Lancet, -2020.-Vol. 395. - P. 565–574. https://doi.org/10.1016/S0140-6736(20)30251-8.

10 Zhang YZ, Holmes EC. A Genomic Perspective on the Origin and Emergence of SARS-CoV-2. //Cell, -2020. -Vol. 16.- P. 223-227. https://doi.org/10.1016/j.cell.2020.03.035.

11 Zhang W, Cao S, Martin JL, Mueller JD, Mansky LM. Morphology and ultrastructure of retrovirus particles. // AIMS Biophys, - 2015. -Vol.2.-P. 343-369. https://doi.org/10.3934/biophy.2015.3.343.

12 Wyatt R, Sodroski J. The HIV-1 envelope glycoproteins: Fusogens, antigens, and immunogens. // Science, -1998. -Vol. 280.- P.1884-1888.
13 Wang, D. et al. Clinical characteristics of 138 hospitalized patients with 2019 novel coronavirus-infected pneumonia in Wuhan, China. // JAMA, - 2020.-Vol.323.- P. 1061–1069. https://doi.org/10.1001/jama.2020.1585.
14 Li, Q. et al. Early transmission dynamics in Wuhan, China, of novel coronavirus-infected pneumonia. // N. Engl. J. Med, -2020.-Vol. 382.- P. 1199–1207. https://www.nejm.org/doi/full/10.1056/nejmoa2001316.
15 Chan, J.F.W., et al. A familial cluster of pneumonia associated with the 2019 novel coronavirus indicating person-to-person transmission: a study of a family cluster. // Lancet, – 2020.-Vol. 395.- P. 514–523. https://doi.org/10.1016/S0140-6736(20)30154-9.
16 Clinical management of COVID-19. // WHO, – 2022. -P. 35- 62.
17 Burashev Y., Khaidarov S., et al. Coding Complete Genome Sequence of the SARS-CoV-2 Virus Strain, Variant B.1.1, Sampled from Kazakhstan. // Microbiology Resource Announcements, - 2022.-Vol.12.-№12. – online: https://journals.asm.org/doi/10.1128/mra.01114-22.
18 Wu, F. et al. A new coronavirus associated with human respiratory disease in China. // Nature, - 2020. Vol.579. P. 265–269. https://www.nature.com/articles/s41586-020-2008-3.
19 Hoffmann, M. et al. SARS-CoV-2 cell entry depends on ACE2 and TMPRSS2 and is blocked by a clinically proven protease inhibitor. // Cell, - 2020. -Vol.181.-P. 271–280. https://doi.org/10.1016%2Fj.cell.2020.02.052.
20 Perlman, S. and Netland, J. Coronaviruses post-SARS: update on replication and pathogenesis. // Nat. Rev. Microbiol, -2009.-Vol. 7. - P. 439–450. https://www.nature.com/articles/nrmicro2147.
21 Snijder, E.J. et al. Ultrastructure and origin of membrane vesicles associated with the severe acute respiratory syndrome coronavirus replication complex. // J. Virol, - 2006.-Vol. 80. - P.5927–5940.doi: 10.1128/JVI.02501-05.
22 Wu, H.-Y. and Brian, D.A. Subgenomic messenger RNA amplification in coronaviruses. // Proc. Natl. Acad. Sci. U. S. A, -2010.-Vol. 107.- P.12257–12262. https://doi.org/10.1073/pnas.1000378107.
23 Shailendra K. Saxena and Sai V. Chitti. Molecular Biology and Pathogenesis of Retroviruses. // Advances in Molecular Retrovirology, – 2016. - Vol. 12.- P. 9-24. doi: 10.5772/62885.
24 Varmus H. Retroviruses. // Science, -1988.- Vol.240.- P.1427-1435.
25 Coffin JM. Structure and classification of retroviruses. // In: Levy, JA. The Retroviridae (First edition). New York: Plenum, - 1992. -ISBN 0-306-44074-1.-Vol.3, №3.- P. 20.
26 Rabson AB, Graves BJ. Synthesis and processing of viral RNA. In: Coffin JM, Hughes SH, Varmus HE, editors. // Retroviruses. Cold Spring Harbor (NY): Cold Spring Harbor Laboratory Press. -1997. - Vol.1.- P.223-236.

27 Bharat TA, Davey NE, Ulbrich P, Riches JD, de Marco A, Rumlova M, Sachse C, Ruml T, Briggs JA. Structure of the immature retroviral capsid at 8 Å resolution by cryoelectron microscopy. // Nature, – 2012. Vol. 487.-P. 385-389.
28 Clinical management of COVID-19 15th September 2022, WHO, - P.110.
29 Clinical management of COVID-19 15th September 2022, WHO, - P.113-115.
30 Marilyn J. Roossinck, Viren. // Springer, -2020. Vol.1, №2 -P. 28-32. https://link.springer.com/book/10.1007/978-3-662-61684-0.
31 Lu, R. et al. Genomic characterization and epidemiology of 2019 novel coronavirus: implications for virus origins and receptor binding. // Lancet, - 2020. -Vol. 395. -P. 565–574.
32 Zhang, Y.Z. and Holmes, E.C. A genomic perspective on the origin and emergence of SARS-CoV-2. // Cell, - 2020.-Vol. 181.-P. 223–227.
33 Roe M.K. et al., Targeting novel structural and functional features of coronavirus protease nsp5 (3CL^{pro}, M^{pro}) in the age of COVID-19 // Journal of General Virology, – 2021. Vol.102. – P. 123-139. https://doi.org/10.1099/jgv.0.001558.
34 Joshi S, Parkar J, Ansari A, Vora A, Talwar D and Tiwaskar M. Role of favipiravir in treating COVID-19. // Int J Infect Dis. – 2021. -Vol.102. -P. 501-508.
35 Delang L, Abdelnabi R, and Neyts J. Favipiravir as a potential countermeasure against neglected and emerging RNA viruses. // Antiviral Res, – 2018.- Vol. 153.- P. 85-94.
36 Wang M, Cao R, Zhang L, Yang X, Liu J and Xu M: Remdesivir and chloroquine effectively inhibit the recently emerged novel coronavirus (2019-nCoV) in-vitro. // Cell Res, - 2020. – Vol.30. - P. 269-71.
37 Graci JD, Cameron CE. Mechanisms of action of ribavirin against distinct viruses. // Rev Med Virol, – 2006. – Vol. 16. – P. 37-48.
38 Myung J.1., Kye-Hyung Kim. In vitro antiviral activity of ribavirin against severe fever with thrombocytopenia syndrome virus. // Korean J Intern Med,- 2017.-Vol. 32. - P.731–737.
39 Lee N, Hui D, Wu A, et al. A major outbreak of severe acute respiratory syndrome in Hong Kong. // N Engl J Med, -2003. Vol. 348, №2. – P.1986-1994.
40 Falzarano D, de Wit E, Martellaro C, Callison J, Munster VJ, Feldmann H. Inhibition of novel beta coronavirus replication by a combination of interferon-alpha2b and ribavirin. // Sci Rep, – 2013.- Vol.3, №1. P. 1686.
41 Koren G, King S, Knowles S, Phillips E. Ribavirin in treating SARS: A new trick for an old drug? // CMAJ. – 2003.- Vol.168, №3. - P. 1289-1292.
42 Balzarini, J.; Holy, A.; Jindrich, J.; Naesens, L.; Snoeck, R.; Schols, D.; De Clercq, E. Differential antiherpesvirus and antiretrovirus effects of the (S) and (R) enantiomers of acyclic nucleoside phosphonates: Potent and selective in vitro and in vivo antiretrovirus activities of (R)-9 (2phosphonomethoxypropyl)-2,6-diaminopurine. // Antimicrob. Agents Chemother, - 1993. -Vol. 37, №1. - P. 332–338.
43 Edited Tsai, C.-C.; Follis, K.E.; Sabo, A.; Beck, T.W.; Grant, R.F.; Bischofberger, N.; Benveniste, R.E.; Black, R. Prevention of SIV Infection in Macaques by (R)-9-(2-Phosphonylmethoxypropyl) adenine. // Science, – 1995. - Vol. 270, №5. – P. 1197–1199.

44 Elfiky, A.A. Ribavirin, Remdesivir, Sofosbuvir, Galidesivir, and Tenofovir against SARS-CoV-2 RNA dependent RNA polymerase (RdRp): A molecular docking study. // Life Sci, - 2020.- Vol. 253. - P. 117-192.
45 Edited Li, G.; Yue, T.; Zhang, P.; Gu, W.; Gao, L.-J.; Tan, L. Drug Discovery of Nucleos(t)ide Antiviral Agents: Dedicated to Prof. Dr. Erik De Clercq on Occasion of His 80th Birthday. // Molecules, – 2021. - Vol. 26.-P. 923.
46 Choy, K.-T.;Wong, A.Y.-L.; Kaewpreedee, P.; Sia, S.F.; Chen, D.; Hui, K.P.Y.; Chu, D.K.W.; Chan,M.C.W.; Cheung, P.P.-H.; Huang, X.; et al. Remdesivir, lopinavir, emetine, and homoharringtonine inhibit SARS-CoV-2 replication in vitro. // Antivir. Res,- 2020. - Vol. 178. – P. 104-107.
47 Rob W. Brooker; Zaal Kikvidze. Importance: an overlooked concept in plant interaction research. // Journal of Ecology, – 2008.- Vol. 96, №7. - P. 703–708. https://doi.org/10.1111/j.1365-2745.2008.01373.
48 Neubig, Richard R. "International Union of Pharmacology Committee on Receptor Nomenclature and Drug Classification. XXXVIII. Update on Terms and Symbols in Quantitative Pharmacology". // Pharmacological Reviews, – 2003. - Vol. 55, №6. - P. 597–606. doi:10.1124/pr.55.
49 Yousuke. A., et.al. Favipiravir (T-705), a broad-spectrum inhibitor of viral RNA polymerase. // Proc. Jpn. Acad., Ser, -2009.- Vol.3, №8.- P.232-239.
50 Perales, C., Gallego, I., de Ávila, A. I., Soria, M. E., Gregori, J., Quer, J., & Domingo, E. The increasing impact of lethal mutagenesis of viruses. // Future Medicinal Chemistry, - 2019.- Vol. 11. – P. 123-133.
51 Perales, C., Martín, V., & Domingo, E. Lethal mutagenesis of viruses. // Current Opinion in Virology, - 2011.-Vol. 1, № 9. - P. 419–422. doi: 10.1016/j.coviro.2011.09.001.
52 Crotty, S., & Andino, R. Implications of high RNA virus mutation rates: lethal mutagenesis and the antiviral drug ribavirin. // Microbes and Infection, -2002.- Vol. 4, №11. - P. 1301–1307. doi:10.1016/s1286-4579(02)00008-4.
53 Espy, N., Nagle, E., Pfeffer, B., Garcia, K., Chitty, A. J., Wiley, M. Palacios, G. T-705 induces lethal mutagenesis in Ebola and Marburg populations in macaques. // Antiviral Research, -2019.-Vol.25.- P.123-152.
54 McDaniel, Y. Z., Patterson, S. E., & Mansky, L. M. Distinct dual antiviral mechanism that enhances hepatitis B virus mutagenesis and reduces viral DNA synthesis. // Antiviral Research. - 2019.-Vol. 25.-P.130-147.
55 Bull, J. J., Sanjuan, R., & Wilke, C. O. Theory of Lethal Mutagenesis for Viruses. // Journal of Virology, -2007.-Vol. 81, №2.- P. 2930–2939.
56 Xiaoying XuYuheng ChenXinyu LuWanlin ZhangWenxiu FangLuping YuanXiaoyan Wang. An update on inhibitors targeting RNA-dependent RNA polymerase for COVID-19 treatment: Promises and challenges. // Biochemical pharmacology. - 2022. -Vol. 205.- P.1236-1248.
57 Christian Powell, Christopher Chang, Stanley M. Naguwa, Gurtej Cheema, M. Eric Gershwin, Steroid-induced osteonecrosis: An analysis of steroid dosing risk. // Autoimmunity Reviews, - 2010. - Vol.33. - P.724-743.

58 Matthew K. SARS-associated coronavirus replication in cell lines. // Emerg Infect Dis. – 2006. - Vol. 12, №5. - P. 128-33. doi: 10.3201/eid1201.050496.
59 Arbeitskreis Blut, Untergruppe Bewertung Blutassoziierter Krankheitserreger. Influenza Virus. // Transfus Med Hemother, - 2009.-Vol.36.-P.32-39. doi: 10.1159/000197314.
60 Javanian, Mostafa Barary, Mohammad Ghebrehewet, Sam Koppolu, Veerendra Vasigala, Veneela Krishna Rekha Ebrahimpour, Soheil. A brief review of influenza virus infection //Journal of Medical Virology, – 2021. Vol.-93. P. 4638-4646. https://doi.org/10.1002/jmv.26990.
61 Peacock, Thomas P., Sheppard, Carol M., Staller, Ecco, Barclay, Wendy S., Host Determinants of Influenza RNA Synthesis// Annual Review of Virology,-2019.-Vol.6.-P. 215-233.https://doi.org/10.1146/annurev-virology-092917-043339.
62 N.M. Bouvier, P. Palese. The biology of influenza viruses // Vaccine, -2008.-Vol. 2, №7.- P. 49–53.
63 Palese P, Shaw ML. *Orthomyxoviridae*: the viruses and their replication. In: Knipe DM, Howley PM, editors. // Fields virology. Philadelphia: Lippincott Williams & Wilkins, - 2007.-Vol. 2, №3.-P.112-118.
64 Barbezange Cyril, Jones Louis, Blanc Hervé, Isakov Ofer, Celniker Gershon, Enouf Vincent, Shomron Noam, Vignuzzi Marco, van der Werf Sylvie. Seasonal Genetic Drift of Human Influenza A Virus Quasispecies Revealed by Deep Sequencing//Frontiers in Microbiology, -2018. -Vol. 9.-P. 1123-1137. doi: 10.3389/fmicb.2018.02596.www.frontiersin.org/journals/microbiology/articles/10.3389/fmicb.2018.02596.
65 Bedford, T., Riley, S., Barr, I. *et al.* Global circulation patterns of seasonal influenza viruses vary with antigenic drift. //Nature, -2015.-Vol. 523.-P.217–220 https://doi.org/10.1038/nature14460.
66 Bano I, Sharif M, Alam S. Genetic drift in the genome of SARS COV-2 and its global health concern. // J Med Virol. -2021.-Vol. 94.-P. 88 - 98. https://doi.org/10.1002/jmv.27337.
67 Walter Dörfer. Viren. // S. Fischer Verlag GmbH,- 2002.-Vol. 1, №3.-P. 70-72. ISBN 3-596-15369-7.
68 Wang, J., Wu, Y., Ma, C., Fiorin, G., Wang, J., Pinto, L. H., Lamb, R. A., Klein, M. L., & DeGrado, W. F. Structure and inhibition of the drug-resistant S31N mutant of the M2 ion channel of influenza A virus. //Proceedings of the National Academy of Sciences, - 2013.-Vol. 110.- P. 1315-1320. https://doi.org/10.1073/pnas.1216526110.
69 K. Martin, A. Helenius. Transport of incoming influenza virus nucleocapsids into the nucleus. // J. Virol. -1991.-Vol. 65.-P. 232–244.
70 Jiménez-Jiménez, F.J.; Alonso-Navarro, H.; García-Martín, E.; Agúndez, J.A.G. Anti-Inflammatory Effects of Amantadine and Memantine: Possible Therapeutics for the Treatment of Covid-19? // J. Pers. Med. – 2020.-Vol. 10. - P. 217-222. https://doi.org/10.3390/jpm10040217.
71 Richard Njunge. Rimantadine: A potential drug for COVID-19. // Authorea, -2020. Online: doi:10.22541/au.158506001.13968819. https://www.authorea.com/doi/full/10.22541/au.158506001.13968819.

72 Gautam Kumar., Kakade Aditi Sakharam. Tackling Influenza A virus by M2 ion channel blockers: Latest progress and limitations. // European Journal of Medicinal Chemistry, – 2024. - Vol. 267. - P. 116-172. https://doi.org/10.1016/j.ejmech.2024.116172.
73 Smieszek, S.P.; Przychodzen, B.P.; Polymeropoulos, M.H. Amantadine disrupts lysosomal gene expression: A hypothesis for COVID-19 treatment. // Int. J. Antimicrob. Agents, - 2020.- Vol. 20.- P.104-106. https://doi.org/10.1016/j.ijantimicag.2020.106004.
74 Abreu, G.E.A.; Aguilar, M.E.H.; Covarrubias, D.H.; Durán, F.R. Amantadine as a drug to mitigate the effects of COVID-19. // Med. Hypotheses, -2020.-Vol.140.- P.109-115. https://doi.org/10.1016/j.mehy.2020.109755.
75 Zhou, Y.; Gammeltoft, K.A.; Galli, A.; Offersgaard, A.; Fahnøe, U.; Ramirez, S.; Bukh, J.; Gottwein, J.M. Efficacy of Ion-Channel Inhibitors Amantadine, Memantine and Rimantadine for the Treatment of SARS-CoV-2 In Vitro. // Viruses**,** – 2021.- Vol.13.-P. 2082-2089. https://doi.org/10.3390/v13102082.
76 Jones JC, Marathe BM, Lerner C, Kreis L, Gasser R, Pascua PNQ, Najera I, Govorkova E A. A Novel Endonuclease Inhibitor Exhibits Broad-Spectrum Anti-Influenza Virus Activity In Vitro. // Antimicrob Agents Chemother, -2016.-Vol. 60.- P. 5504-5514. https://doi.org/10.1128/aac.00888-16.
77 Yang T. Baloxavir Marboxil: The First Cap-Dependent Endonuclease Inhibitor for the Treatment of Influenza. //*Annals of Pharmacotherapy*, -2019.- Vol.53.- P.754-759. doi:10.1177/1060028019826565.
78 Jiajie Feng, et al**.** Discovery of a Macrocyclic Influenza Cap-Dependent Endonuclease Inhibitor //J. Med. Chem, -2024. -Vol.67.-P.2570–2583. https://doi.org/10.1021/acs.jmedchem.3c01715.
79 Yan Lou, Lin Liu, Hangping Yao, Xingjiang Hu, Junwei Su, Kaijin Xu, Rui Luo, Xi Yang, Lingjuan He, Xiaoyang Lu, Qingwei Zhao, Tingbo Liang, Yunqing Qiu, Clinical Outcomes and Plasma Concentrations of Baloxavir Marboxil and Favipiravir in COVID-19 Patients: An Exploratory Randomized, Controlled Trial // European Journal of Pharmaceutical Sciences, – 2021.- Vol. 157.- P. 1-7. https://doi.org/10.1016/j.ejps.2020.105631.
80 Dufrasne F. Baloxavir Marboxil: An Original New Drug against Influenza. // Pharmaceuticals (Basel), – 2021. - Vol.24. - P.28-32. https://doi.org/10.3390/ph15010028.
81 Yuan S., Wen L., Zhou J. Inhibitors of Influenza A Virus Polymerase. // *ACS Infect. Dis,*- 2018.- Vol.4.-P.218–223. https://doi.org/10.1021/acsinfecdis.7b00265.
82 Ju H., Zhang J., Huang B., Kang D., Huang B., Liu X., Zhan P. Inhibitors of Influenza Virus Polymerase Acidic (PA) Endonuclease: Contemporary Developments and Perspectives. // *J. Med. Chem,* - 2017.- Vol.60.-P.3533–3551. https://doi.org/10.1021/acs.jmedchem.6b01227.
83 Hayden, F.G., Shindo, N., Influenza virus polymerase inhibitors in clinical development. // Curr Opin Infect Dis, - 2019. -Vol. 32.- P.176–186. https://doi.org/10.1097/.

84 Parra-Rojas, C.; Nguyen, V.K.; Hernandez-Mejia, G.; Hernandez-Vargas, E.A. Neuraminidase Inhibitors in Influenza Treatment and Prevention–Is It Time to Call It a Day? //*Viruses*, – 2018.- Vol. 10.- P.454-467. https://doi.org/10.3390/v10090454.
85 Havasi A, Visan S, Cainap C, Cainap SS, Mihaila AA and Pop LA. Influenza A, Influenza B, and SARS-CoV-2 Similarities and Differences – A Focus on Diagnosis. // *Front. Microbiol,* -2022.-Vol. 13. – P. 908-925. doi: 10.3389/fmicb.2022.908525.https://www.frontiersin.org/journals/microbiology/articles/10.3389/fmicb.2022.908525/full.
86 Dobson, J.; Whitley, R.J.; Pocock, S.; Monto, A.S. Oseltamivir treatment for influenza in adults: A meta-analysis of randomized controlled trials. // Lancet, -2015.- Vol. 385.-P. 1729–1737.
87 McClellan, K.; Perry, C.M. Oseltamivir. // Drugs, - 2001.-Vol. 61.-P. 263–283.
88 Zendehdel, Mohammad Bidkhori, Mohsen Ansari, Saeidreza Jamalimoghaddamsiyahkali, Azadeh Asoodeh. Efficacy of oseltamivir in the treatment of patients infected with Covid-19. // Annals of Medicine and Surgery, -2022.- Vol.77.- P. 103-110. https://doi.org/10.1016/j.amsu.2022.103679.
89 de Oliveira Formiga, R., et al. Neuraminidase is a host-directed approach to regulate neutrophil responses in sepsis and COVID-19. // *British Journal of* Pharmacology, - 2023.-Vol. 180.-P. 14-18. https://doi.org/10.1111/bph.16013.
90 Huang, J.; Song, W.; Huang, H.; Sun, Q. Pharmacological Therapeutics Targeting RNA-Dependent RNA Polymerase, Proteinase and Spike Protein: From Mechanistic Studies to Clinical Trials for COVID-19. // J. Clin. Med,- 2020.-Vol.9.- P.1131. https://doi.org/10.3390/jcm9041131.
91 Di Perri G. Tenofovir alafenamide (TAF) clinical pharmacology. // Infez Med, -2021.-Vol 10.-P.378-385. doi: 10.53854/liim-2904-4. PMID: 35146360; PMCID: PMC8805468.
92 Furuta Y, Takahashi K, Kuno-Maekawa M et al. Mechanism of action of T-705 against influenza virus. // Antimicrob Agents Chemother, - 2005.-Vol. 49, №4.-P. 981–986. DOI: 10.1128/AAC.49.3.981-986.2005.
93 R.B. MC Feedo, MPH, FACPM, FAAC COVID-19: Therapeutics and interventions currently under consideration. // Disease-a-Month, -2020/- Vol.66. -P.33-39.DOI: 10.1016/j.disamonth.2020.101058.
94 James M. Sanders, PhD, PharmD; Marguerite L. Monogue, PharmD; Tomasz Z. Jodlowski, PharmD; James B. Cutrell, MD. Pharmacologic Treatments for Coronavirus Disease 2019 (COVID-19)// Clinical Review & Education, -2020 – Vol. 3. -P.1824-1836. DOI: 10.1001/jama.2020.6019.
95 J. Grein, N. Ohmagari, D. Shin, G. Diaz, E. Asperges, A. Castagna, T. Feldt, G. Green, M.L. Green, F.-X. Lescure, E. Nicastri, R. Oda, K. Yo, E. Quiros-Roldan, A. Studemeister, J. Redinski, S. Ahmed, J. Bernett, D. Chelliah, D. Chen, S. Chihara, S.H. Cohen, J. Cunningham, A. D'Arminio Monforte, S. Ismail, H. Kato, G. Lapadula, E. L'Her, T. Maeno, S. Majumder, M. Massari, M. Mora-Rillo, Y. Mutoh, D. Nguyen, E. Verweij, A. Zoufaly, A.O. Osinusi, A. DeZure, Y. Zhao, L. Zhong, A. Compassionate Use of Remdesivir for Patients with Severe Covid-19. // The New England journal of medicine, -2021. - Vol. 2. -P. 2327-2336. DOI: 10.1056/NEJMoa2007016.

96 Warren TK, Jordan R, Lo MK, Ray AS, Mackman RL, Soloveva V, et al. Therapeutic efficacy of the small molecule GS-5734 against Ebola virus in rhesus monkeys. // Nature, - 2016.-Vol4. – P.531:381–5. doi:10.1038/nature17180.
97 Tchesnokov EP, Feng JY, Porter DP, Götte M. Mechanism of inhibition of Ebola virus RNA-dependent RNA polymerase by remdesivir. // Viruses, – 2019.-Vol.11.-P. 326-333. doi:10.3390/v1104032648.
98 Agostini ML, Andres E, Sims AC, Graham RL, Sheahan TP, Lu X, et al. Coronavirus susceptibility to the antiviral remdesivir (GS-5734) is mediated by the viral polymerase and the proofreading exoribonuclease. // mBio, - 2018.-Vol. 9-. P. 2018-2021. doi:10.1128/mBio.00221-18.
99 Хабриев Р.У. Руководство по экспериментальному (доклиническому) изучению новых фармакологических веществ/. Изд. -2-е.- М.: Медицина; 2005. – 127с.
100 Wu X., et al. Single-domain antibodies against SARS-CoV-2 and evaluation in a Vero E6 cytopathic effect–based neutralization assay // Cell Host & Microbe. – 2020. – Vol. 27. – P. 1–123. – doi: https://doi.org/10.1016/j.chom.2020.04.023. .
101 Barreto-Vieira D.F., da Silva M.A.N., Garcia C.C., Miranda M.D., Matos A.D.R., Caetano B.C., Resende P.C., Motta F.C., Siqueira M.M., Girard-Dias W., Archanjo B.S., Barth O.M. Morphology and morphogenesis of SARS-CoV-2 in Vero-E6 cells // Memórias do Instituto Oswaldo Cruz. – 2021. – Vol. 116. – Article e200443. – DOI: https://doi.org/10.1590/0074-02760200443.
102 Kinoshita H., Yamamoto T., Kuroda Y., et al. Improved efficacy of SARS-CoV-2 isolation from COVID-19 clinical specimens using VeroE6 cells overexpressing TMPRSS2 and human ACE2 // Scientific Reports. – 2024. – Vol. 14. – P. 24–28. – DOI: https://doi.org/10.1038/s41598-024-75038-4.
103 Aiewsakun P., Phumiphanjarphak W., Ludowyke N., Purwono P.B., Manopwisedjaroen S., Srisaowakarn C., Ekronarongchai S., Suksatu A., Yuvaniyama J., Thitithanyanont A. Systematic exploration of SARS-CoV-2 adaptation to Vero E6, Vero E6/TMPRSS2, and Calu-3 cells // Genome Biology and Evolution. – 2023. – Vol. 15. – Article evad035. – DOI: https://doi.org/10.1093/gbe/evad035.
104 Tschulena U., et al. Mutation of a diacidic motif in SIV-PBj Nef impairs T-cell activation and enteropathic disease. // Retrovirology. -2011. -Vol.14.-P. 213-22 DOI: 10.1186/1742-4690-8-14.
105 https://www.beckman.com/reagents/genomic/cleanup-and-size-selection/pcr/ampure-xp-protocol.
106 https://www.dojindo.com/EUROPE/products/CK04.
107 American Type Culture Collection P.O. Box 1549 Manassas, VA 20108 USA www.atcc.org.
108 Sun SH, Chen Q, Gu HJ, . A Mouse Model of SARS-CoV-2 Infection and Pathogenesis. // Cell Host Microbe. – 2020.-Vol.8. -P. 124-133. 10.1016/j.chom.2020.05.020.
109 Dinnon, K.H., Leist, S.R., Schäfer, A. *et al.* A mouse-adapted model of SARS-CoV-2 to test COVID-19 countermeasures. // Nature. -2020.-Vol. 586.- P. 560–566 https://doi.org/10.1038/s41586-020-2708-8.

110 Maria I. Zapata-Cardona, Lizdany Florez-Alvarez, Ariadna L. Guerra-Sandoval, Mateo Chvatal-Medina, Carlos M. Guerra-Almonacid, Jaime Hincapie-Garcia, Juan C. Hernandez, Maria T. Rugeles, Wildeman Zapata-Builes. In vitro and silico evaluation of antiretrovirals against SARS-CoV-2: A drug repurposing approach. // AIMS Microbiology. – 2023.-Vol. 9.- P. 20-40. doi: 10.3934/microbiol.2023002.
111 Joshi S, Parkar J, Ansari A, Vora A, Talwar D, Tiwaskar M, Patil S, Barkate H. Role of favipiravir in the treatment of COVID-19. // Int J Infect Dis.- 2021.- Vol. 102.- P. 501-508. doi: 10.1016/j.ijid.2020.10.069.
112 Siripongboonsitti, T., Muadchimkaew, M., Tawinprai, K. *et al.* Favipiravir treatment in non-severe COVID-19: promising results from multicenter propensity score-matched study (FAVICOV). // Sci Rep.- 2023.-Vol. 13.- P.148. https://doi.org/10.1038/s41598-023-42195-x.
113 Manuel Taboada. Effect of high versus low dose of dexamethasone on clinical worsening in patients hospitalised with moderate or severe COVID-19 pneumonia: an open-label, randomised clinical trial. // JF - European Respiratory Journal. -2022.- Vol.3-P.123-129. https://doi.org/10.1183/13993003.02518-2021.
114 Somovilla P,García-Crespo C,Martínez-González B,Soria ME,,de Ávila AI,Gallego I,Mínguez P,,Durán-Pastor A, Ferrer-Orta C, Salar-Vidal L,Esteban-Muñoz M, Zuñiga S, Sola I, Enjuanes L, Esteban J,Fernandez-Roblas R,Gadea I,Gómez J, Verdaguer N, Domingo E, Perales . Atypical Mutational Spectrum of SARS-CoV-2 Replicating in the Presence of Ribavirin. // Antimicrob Agents Chemother.-2023.-Vol. 67.-P.1315-22. https://doi.org/10.1128/aac.01315-22.
115 Khaidarov, S., Burashev , Y., Kozhabergenov , N., Usserbayev , B., Melisbek , A., Shirinbekov , M., Moldakaryzova, A., Beisenova , A., Mustafaeva , A., & Kydyrbaeva , A. Targeted in vitro- confirmation of the antiviral activity of Tenvir (Tenofovir) drug against the SARS-COV-2 virus variant B. in Kazakhstan and identifying NSP12 in the viral genome. // Eurasian Journal of Applied Biotechnology. - 2024.-Vol.2.-P. 49–60. https://doi.org/10.11134/btp.2.2024.6.
116 Artik Y, Cesur NP, Laçin NT. SARS-CoV-2 Mutations, Diagnosis and Their Concern. // Arch Mol Biol Genet.- 2022. -Vol.2 -P. 57-65. https://doi.org/10.33696/genetics.1.008.
117 Saken Khaidarov. Antiviral IL-33-stimulated group 2 innate lymphoid cells (CD-90 and CD-117) from mouse lungs. // Eurasian Journal of Applied Biotechnology. -2024.-Vol.4.-P. 84–90. https://doi.org/10.11134/btp.4.2024.8.
118 Leowattana W, Leowattana T, Leowattana P. SARS-CoV-2 viral load in the upper respiratory tract and disease severity in COVID-19 patients. // World J Meta-Anal. - 2022; -Vol. 10.-P. 195-205. http://dx.doi.org/10.13105/wjma.v10.i4.195.
119 Hansel TT, Johnston SL, Openshaw PJ Microbes and mucosal immune responses in asthma // Lancet. – 2013.- Vol. 381.-P. 861–873.
120 2. Wynn TA Type 2 cytokines: mechanisms and therapeutic strategies. // Nat Rev Immunol. -205.-Vol. 15. -P. 271–282.
121 Edwards MR, Bartlett NW, Hussell T, Openshaw P, Johnston SL the microbiology of asthma. // Nat Rev Microbiol. -2012.-Vol 10. -P. 459–471.

122 Diefenbach A, Colonna M, Koyasu S. Development, differentiation, and diversity of innate lymphoid cells. // Immunity. -2014.- Vol.41.-P. 354–365.
123 Bayan Nurgaliyeva, Saken Khaidarov, et.al. A Case of Autoimmune Complications Following Covid-19 Vaccination with Sinovac-CoronaVac (China) // Наука и здравоохранение. – 2024.-Vol.4.-P. 230-233. 10.34689/SH.2024.26.6.026
124 Saken Khaidarov, Yerbol Burashev. The SARS-CoV-2 epoch and proper managing strategies to face the challenges both in viral research and treatment// Казахский Национальный Университет Имени Аль-Фараби Вестник Серия биологическая. - 2023.-Vol. 3.-P. 4-25. https://doi.org/10.26577/eb.2023.v96.i3.01.
125 Saken Khaidarov, Edan Tulman. Perspectives of Biotechnological Development in Kazakhstan in Terms of Monoclonal and Other Recombinant Antibodies and Vaccines Against SARS-CoV-2 // Казахский Национальный Университет Имени Аль-Фараби Вестник Серия биологическая. - 2024.-Vol. 2.-P. 173-188. https://bb.kaznu.kz/index.php/biology/article/view/2389/168.
126 Khaidarov, S.; Hejran, A.B.; Moldakaryzova, A.; Izmailova, S.; Nurgaliyeva, B.; Beisenova, A.; Mustafaeva, A.; Nurzhanova, K.; Belova, Y.; Satbayeva, E.; et al. An Anti-HIV Drug Is Highly Effective Against SARS-CoV-2 In Vitro and Has Potential Benefit for Long COVID Treatment // Viruses. – 2025.-Vol.17.-P. 1170. https://doi.org/10.3390/v17091170
127 Nurgaliyeva B., Khaidarov S., Kan O., Moldakaryzova A., et al. Guillain-Barré syndrome following SARS-CoV-2 pneumonia in a patient receiving adjuvant chemotherapy for gastric cancer: a case report // Clinical Infectious Diseases. — 2025. — Vol. 9. — P. 344.
128 Polack F.P., Thomas S.J., Kitchin NClinical Trial Group Safety and Efficacy of the BNT162b2 mRNA Covid-19 Vaccine // N. Engl. J. Med. – 2020. – Vol. 383, No. 27. – P. 2603-2615. https://doi.org/10.1056/nejmoa2034577
129 Oster M.E., Shay D.K., Su J.R., Gee J., Creech C.B., Broder K.R., Edwards K., Soslow J.H., Dendy J.M., Schlaudecker E.P., et al. Myocarditis cases reported after mRNA-based COVID-19 vaccination in the US // JAMA. – 2022. – Vol. 327, No. 4. – P. 331-340.https://doi.org/10.1001/jama.2021.24110
130 Acevedo-Whitehouse K., Bruno R. Potential health risks of mRNA-based vaccine therapy: A hypothesis [Electronic resource] // Med. Hypotheses. – 2023. – Vol. 171. https://doi.org/10.1016/j.mehy.2023.111015
131 Gote V., Bolla P.K., Kommineni N., Butreddy A., Nukala P.K., Palakurthi S.S., Khan W. A Comprehensive Review of mRNA Vaccines // Int. J. Mol. Sci. – 2023. – Vol. 24, https://doi.org/10.3390/ijms24032700

APPENDIX A

The taxonomy of the SARS-CoV-2 strain human/KAZ/B 1.1/2021 the early SARS-COV2 linage

Hierarchical Classification

- Realm: Riboviria
- Kingdom: Orthornavirae
- Phylum: Pisuviricota
- Class: Pisoniviricetes
- Order: Nidovirales
- Family: Coronaviridae
- Subfamily: Orthocoronavirinae
- Genus: Betacoronavirus
- Subgenus: Sarbecovirus
- Species: *Severe acute respiratory syndrome-related coronavirus* (SARSr-CoV)
- Virus: SARS-CoV-2 (the causative agent of COVID-19)

Strain Designation Breakdown

The strain name human/KAZ/B 1.1/2021; alpha variant provides additional contextual information:

Host: Human (*Homo sapiens*).

Country: Kazakhstan (ISO alpha-3 code: KAZ). -Alpha Variant

Lineage: This likely refers to B.1.1 (per Pango nomenclature, a sublineage of the broader B.1 lineage). The space ("B 1.1") may reflect a formatting inconsistency; standard Pango lineages use dots (e.g., B.1.1).

Collection Year: 2021. -Data collected and submitted

- Lineage Context: B.1.1 is an early SARS-CoV-2 lineage that gave rise to notable sublineage (e.g., B.1.1.7, the Alpha variant). However, this specific strain (B 1.1) may represent a localized or less-documented sublineage in Kazakhstan.
- Taxonomic Clarification: While the hierarchical classification (Realm to Species) is universal for SARS-CoV-2, strain names like this one are isolate identifiers, not part of formal taxonomy. They often include host, geographic origin, lineage, and collection date.

Cross-referencing with databases like GISAID or Pango may clarify its phylogenetic relationships for global tracking.

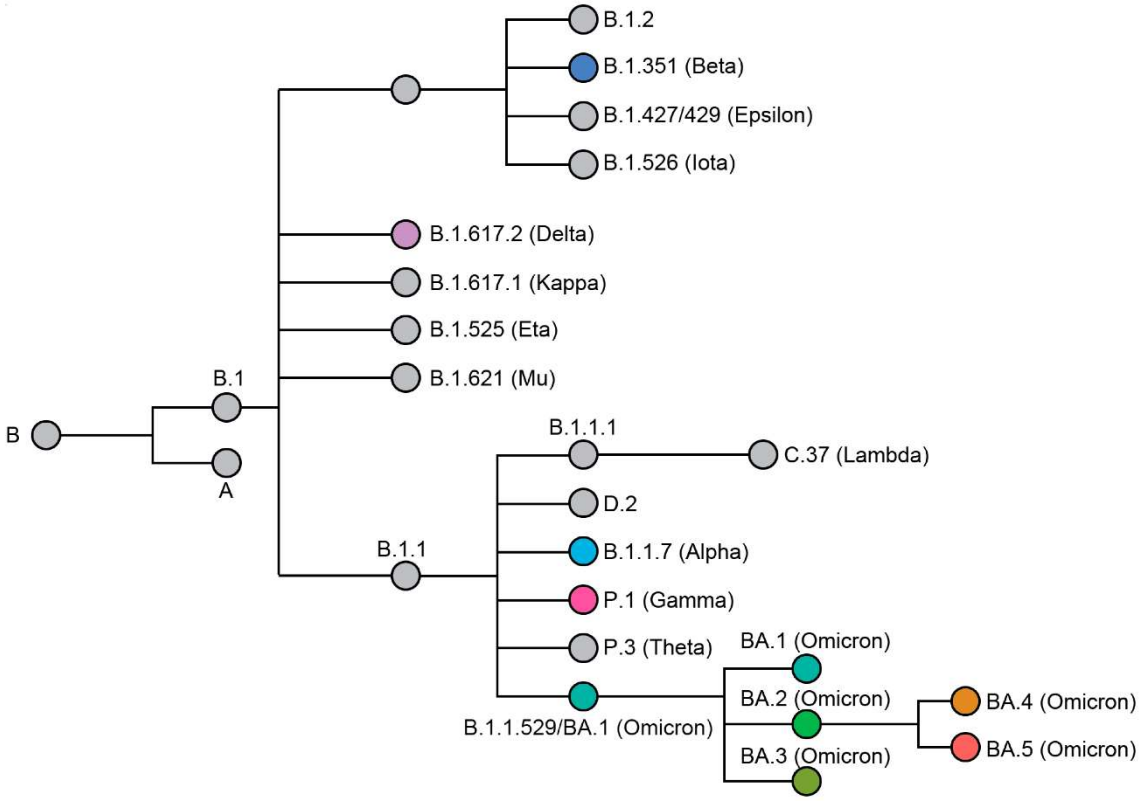

Figure 1– Phylogenetic relationship of named SARS-CoV-2 variants. A coloured node represents a variant of concern (VOC). The phylogenetic tree was adapted from data provided by NextStrain, CoVariants (i.e., covariants.org, http://covariants.org (accessed on 18 July 2022)), and Pangolin (i.e., cov-lineages.org, http://cov-lineages.org. Source: Wiegand, T.; Nemudryi, A.; Nemudraia, A.; McVey, A.; Little, A.; Taylor, D.N.; Walk, S.T.; Wiedenheft, B. The Rise and Fall of SARS-CoV-2 Variants and Ongoing Diversification of Omicron. Viruses. - 2022, -Vol.14.-P.20-29. https://doi.org/10.3390/v14092009

Lineage	Genomes	Date range	Comments
A	223	5 January–27 April 2020	The root of the pandemic lies in this lineage. Many Chinese sequences with global exports
A.1	1,116	20 February–25 March 2020	Primary outbreak in Washington State, USA
A.2	295	26 February–27 April 2020	European lineage
A.3	191	28 January–21 April 2020	USA lineage
A.5	118	23 February–26 April 2020	European lineage
B	1,713	24 December 2019–3 May 2020	The base of this lineage lies in China, with extensive global travel between multiple locations
B.1	7,438	24 January–10 May 2020	Comprises the large Italian outbreak; it now represents many European outbreaks, with travel within Europe and from Europe to the rest of the world
B.1.1	6,286	15 February–9 May 2020	Major European lineage; exports to the rest of the world from Europe
B.2	917	13 February–4 May 2020	With B.1, it comprises the large Italian outbreak
B.3	752	23 February–23 April 2020	UK lineage
B.4	258	18 January–14 April 2020	This is probably the primary Iranian outbreak

See https://cov-lineages.org/ for full details of each lineage.

Figure 2 – Proposed nomenclature of early major lineages of SARS-CoV-2. B1.1. The lineage was the closest to the SARS-CoV-2 strain/human/KAZ/B 1.1/2021, also known as the Alpha variant, due to European exports to the rest of the world. Source: Rambaut, A., Holmes, E.C., O'Toole, Á. *et al.* A dynamic nomenclature proposal for SARS-CoV-2 lineages to assist genomic epidemiology. *Nat* Microbiol. -2020.- Vol. 5.-P. 1403–1407. https://doi.org/10.1038/s41564-020-0770-5

APPENDIX B

The primary data of PCR tests (runs)

Table 1: The Quantitative Report, Test Information, and Quantitative Analysis Parameters.

The text name	Test 2021-03-29 (1)
Test begins	29.03.2021 10:24:30
Test ends	29.03.2021 12:10:50
Operator	Nurlan
Notes	none
Test run the version of	Rotor-Gene 1.8.17.5
Test signature	Test signature - correct.
Signal level Green	5,
Signal level Orange	5,
Signal level Red	5,
CT-value (Threshold)	0,05139
Exclude cycles till	1,000
Standard curve imported	None
Standard graph (1)	N/A
Standard graph (2)	N/A
Start normalization with a cycle (Cq)	11
Slope correction	None
Background Threshold (NTC)	0%
Response Efficiency Threshold	off
Normalization method	Dynamic background normalization

The samples were collected from patients with COVID-19 during the pandemic at the Scientific and Practical Centre for Sanitary and Epidemiological Expertise and Monitoring in Almaty. During Real-Time PCR identification, all samples showed a positive result, with a peak range of 17 to 30 cycles**.** Detection of SARS-COV-2 virus strains using real-time PCR and electron microscopy.

PCR identified the SARS-COV-2 virus from the samples received. The PCR conditions are presented in Tables 7 and 8.

Table 2 – Quantitative report, test information

The text name	Test 2021-03-29 (1)
Test begins	29.03.2021 **10:24:30**
Test ends	29.03.2021 **12:10:50**
Operator	Nurlan
Notes	None
The test was performed on the software version	Rotor-Gene 1.8.17.5
Test signature	Test signature -correct.
Signal level Green	5,
Signal level Orange	5,
Signal level Red	5,

Table 3– Quantitative analysis parameters

Ct-value (Threshold)	0,05139
Exclude cycles till	1,000
Standard curve imported	None
Standard graph (1)	N/A
Standard graph (2)	N/A
Start normalization with a cycle (Cq)	11
Slope correction	None
Background Threshold (NTC)	0%
Response Efficiency Threshold	off
Normalization method	Dynamic background normalization

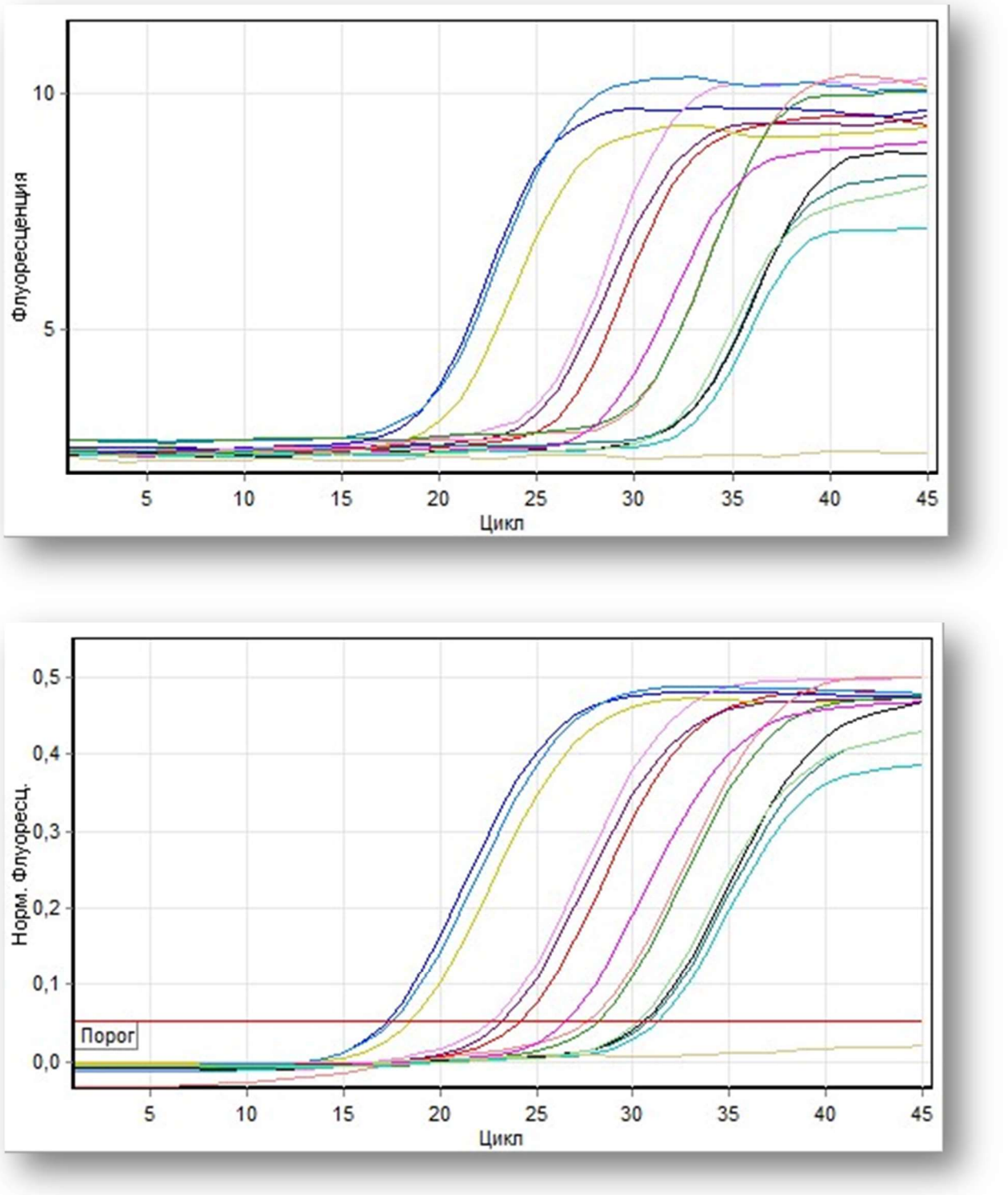

Figure 1 – The initial data are the fluorescent signals: cycling A—red and Quantitative data for Cycling A. Red. According to the peaks report, the following samples were taken for further processing with subsequent Ct (cycle threshold) values. Other samples with fewer than 20 cycles and more than 25 cycles were excluded [115]

*Note: Норм. Флюросенц. -Normal fluorescence. Порог -Threshold. Цикл – Cycle.

APPENDIX C

MONOGRAPH

VIRUSES (SARS-COV2, INFLUENZA A, D) MODERN SCIENTIFIC ASPECTS OF DIAGNOSIS AND TREATMENT

МІНІСТЕРСТВО ЗДРАВООХРАНЕНИЯ
РЕСПУБЛІКІ КАЗАХСТАН

КАЗАХСКІЙ НАЦИОНАЛЬНЫЙ МЕДИЦИНСКІЙ УНІВЕРСИТЕТ
ІІМ.С.Д.АСФЕНДИЯРОВА

С.Ж. Хайдаров, А.Ж. Молдакарызова Б. К. Нургалиева

ВИРУСЫ (SARS-COV2, INFLUENZA A, D) СОВРЕМЕННЫЕ НАУЧНЫЕ АСПЕКТЫ ДИАГНОСТИКИ И ЛЕЧЕНИЯ

МОНОГРАФИЯ

Алматы - 2025

УДК: УДК: 616.99-07-08:578.834
ББК: 55.1
Х– 12

Рецензенты:

1. Битанова Э.Ж. - к.м.н., ассоциированный профессор, заведующий кафедрой общей иммунологии имени А.А. Шортанбаева, КазНМУ им.С.Д.Асфендиярова
2. Бурашев Е.Д. – PhD, заведующий лаборатории «Мониторинг инфекционных заболеваний» Научно-исследовательский институт проблем биологической безопасности, Гвардеевск, Жамбылская область, Казахстан

Авторы:

Хайдаров С.Ж. - PhD, ассистент профессора кафедры молекулярной биологии и медицинской генетики КазНМУ им.С.Д.Асфендиярова

Молдакарызова А.Ж. - к.б.н., заведующий кафедрой молекулярной биологии и медицинской генетики КазНМУ им.С.Д.Асфендиярова

Нургалиева Б. К.- д.м.н., MSP, заведующий кафедрой пропедевтики внутренних болезней КазНМУ им.С.Д.Асфендиярова

Вирусы (SARS-CoV2, influenza A, D) современные научные аспекты диагностики и лечения

Монография / Авторы: Хайдаров С.Ж., Молдакарызова А.Ж., Нургалиева Б.К. 2025 //Алматы: ООО Print+, 2025. - 352с.

ISBN Представленная монография призвана расширить знания медицинских специалистов в области вирусологии. В работе проводится систематический анализ как традиционных, так и инновационных методов диагностики и лечения первичных вирусных инфекций. Ожидается, что данное исследование станет важным вкладом в развитие персонализированного подхода к ведению пациентов с первичными вирусными инфекцмами, способствуя улучшению исходов лечения и повышению качества их жизни.

УДК: УДК: 616.99-07-08:578.834
ББК: 55.1
Х– 12

Утверждено и разрешено к изданию типографским способом РГП на ПХВ «Национальный научный центр развития здравоохранения имени Салидат Кайрбековой» МЗ РК (№ от «___» ___ 2025 года).

APPENDIX D

DRUG BROCHURES

Favipiravir (pro-drug/active component)

Glenmark introduces higher strength (400 mg) of FabiFlu® to reduce pill burden of COVID-19 treatment

- *Glenmark is the first company in India to have received the regulator's approval for 400 mg dosage form*
- *Increased strength of FabiFlu® yet another milestone effort by Glenmark's in-house R&D*
- *Patients can now opt for a more relaxed dosage regimen when compared to 200 mg tablet and now need to take half the number of pills due to the introduction of 400 mg*
- *Glenmark remains the only company in India to successfully complete an* randomized, controlled, open-labelled, multi-center Phase 3 clinical trial on Indian patients with mild to moderate Covid-19

Mumbai, India; August 6, 2020: Glenmark Pharmaceuticals, a research-led, integrated global pharmaceutical company, today announced that it will introduce a 400 mg version of oral antiviral FabiFlu®, for the treatment of mild to moderate COVID-19 in India. The higher strength will improve patient compliance and experience, by effectively reducing the number of tablets that patients require per day.

A higher pill burden has been associated with lower adherence to therapy, the latter affecting viral suppression and overall treatment outcomes. Also reducing the pill burden has been a demand from doctors and patients to enable adherence. The 200 mg dosage of FabiFlu® required patients to take 18 tablets on Day 1 (nine in the morning and nine in the evening), followed by 8 tablets each day thereafter for a maximum of 14 days. With the new 400 mg version, patients will now have a more relaxed dosage regimen, with 9 tablets required on Day 1(4.5 in the morning and 4.5 in the evening), and thereafter 2 tablets twice a day from Day 2 till end of the course.

Figure 1 – Fabiflu brochure, source: https://glenmark.b-cdn.net/gpl_pdfs/media/Glenmark-introduces-higher-strength-400-mg-of-FabiFlu.pdf

Tenofovir -TDF (pro-drug/active component)

DOSAGE AND ADMINISTRATION

Adults

For the treatment of HIV or chronic hepatitis B: The dose of TENOFOVIR (TDF) is 300 mg once daily taken orally without regard to food.

In the treatment of chronic hepatitis B, the optimal duration of treatment is unknown. TENOFOVIR may be discontinued if there is HBsAg loss or HBsAg seroconversion.

Adolescent Patients with HIV-1 Infection (12 Years of Age and Over)

Body weight ≥35 kg (≥77 lb): Take one 300 mg TENOFOVIR tablet once daily orally, without regard to food.

Dose Adjustment for Renal Impairment

Significantly increased drug exposures occurred when tenofovir disoproxil fumarate was administered to patients with moderate to severe renal impairment (see **ACTION AND CLINICAL PHARMACOLOGY, Renal Insufficiency**). Therefore, the dosing interval of TENOFOVIR should be adjusted in patients with baseline creatinine clearance <50 mL/min using the recommendations in Table 15. These dosing interval recommendations are based on modeling of single-dose pharmacokinetic data in non-HIV and non-HBV infected subjects with varying degrees of renal impairment, including end-stage renal disease requiring hemodialysis. The safety and efficacy of these dosing interval adjustment recommendations have not been clinically evaluated in moderate to severe renal impairment, therefore, clinical response to treatment and renal function should be closely monitored in these patients.

No dose adjustment of TENOFOVIR tablets (300 mg) is necessary in patients with mild renal impairment (creatinine clearance 50–80 mL/min). Routine monitoring of calculated creatinine clearance, serum phosphorus, urine glucose and urine protein should be performed in patients with mild renal impairment **(see WARNINGS and PRECAUTIONS)**.

Figure 2 – Tenvir (TDF) brochure, source: https://pdf.hres.ca/dpd_pm/00059975.PDF

Ribavirin (pro-drug/active component)

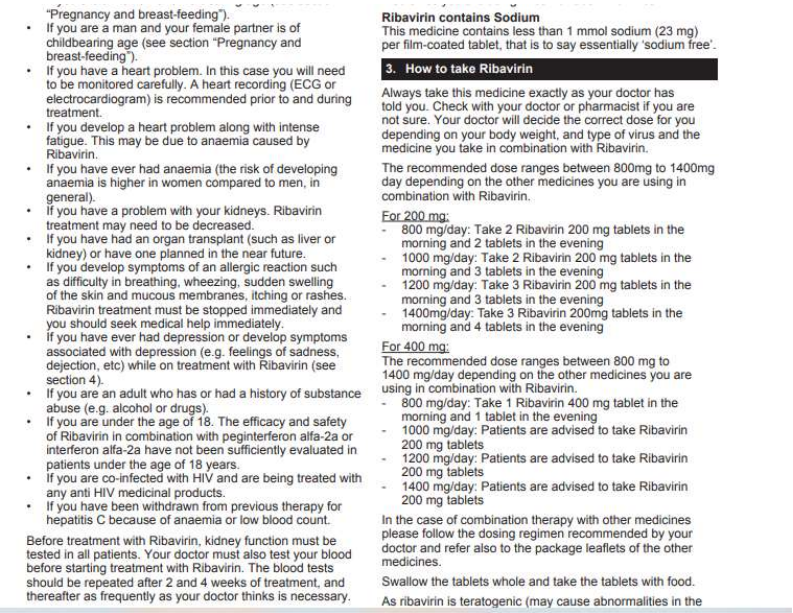

"Pregnancy and breast-feeding").
- If you are a man and your female partner is of childbearing age (see section "Pregnancy and breast-feeding").
- If you have a heart problem. In this case you will need to be monitored carefully. A heart recording (ECG or electrocardiogram) is recommended prior to and during treatment.
- If you develop a heart problem along with intense fatigue. This may be due to anaemia caused by Ribavirin.
- If you have ever had anaemia (the risk of developing anaemia is higher in women compared to men, in general).
- If you have a problem with your kidneys. Ribavirin treatment may need to be decreased.
- If you have had an organ transplant (such as liver or kidney) or have one planned in the near future.
- If you develop symptoms of an allergic reaction such as difficulty in breathing, wheezing, sudden swelling of the skin and mucous membranes, itching or rashes. Ribavirin treatment must be stopped immediately and you should seek medical help immediately.
- If you have ever had depression or develop symptoms associated with depression (e.g. feelings of sadness, dejection, etc) while on treatment with Ribavirin (see section 4).
- If you are an adult who has or had a history of substance abuse (e.g. alcohol or drugs).
- If you are under the age of 18. The efficacy and safety of Ribavirin in combination with peginterferon alfa-2a or interferon alfa-2a have not been sufficiently evaluated in patients under the age of 18 years.
- If you are co-infected with HIV and are being treated with any anti HIV medicinal products.
- If you have been withdrawn from previous therapy for hepatitis C because of anaemia or low blood count.

Before treatment with Ribavirin, kidney function must be tested in all patients. Your doctor must also test your blood before starting treatment with Ribavirin. The blood tests should be repeated after 2 and 4 weeks of treatment, and thereafter as frequently as your doctor thinks is necessary.

Ribavirin contains Sodium
This medicine contains less than 1 mmol sodium (23 mg) per film-coated tablet, that is to say essentially 'sodium free'.

3. How to take Ribavirin

Always take this medicine exactly as your doctor has told you. Check with your doctor or pharmacist if you are not sure. Your doctor will decide the correct dose for you depending on your body weight, and type of virus and the medicine you take in combination with Ribavirin.

The recommended dose ranges between 800mg to 1400mg day depending on the other medicines you are using in combination with Ribavirin.

For 200 mg:
- 800 mg/day: Take 2 Ribavirin 200 mg tablets in the morning and 2 tablets in the evening
- 1000 mg/day: Take 2 Ribavirin 200 mg tablets in the morning and 3 tablets in the evening
- 1200 mg/day: Take 3 Ribavirin 200 mg tablets in the morning and 3 tablets in the evening
- 1400mg/day: Take 3 Ribavirin 200mg tablets in the morning and 4 tablets in the evening

For 400 mg:
The recommended dose ranges between 800 mg to 1400 mg/day depending on the other medicines you are using in combination with Ribavirin.
- 800 mg/day: Take 1 Ribavirin 400 mg tablet in the morning and 1 tablet in the evening
- 1000 mg/day: Patients are advised to take Ribavirin 200 mg tablets
- 1200 mg/day: Patients are advised to take Ribavirin 200 mg tablets
- 1400 mg/day: Patients are advised to take Ribavirin 200 mg tablets

In the case of combination therapy with other medicines please follow the dosing regimen recommended by your doctor and refer also to the package leaflets of the other medicines.

Swallow the tablets whole and take the tablets with food.

As ribavirin is teratogenic (may cause abnormalities in the

Figure 3 –Ribavirin brochure, source: https://www.medicines.org.uk/emc/files/pil.7108.pdf

Dexamethasone (pro-drug/active component)

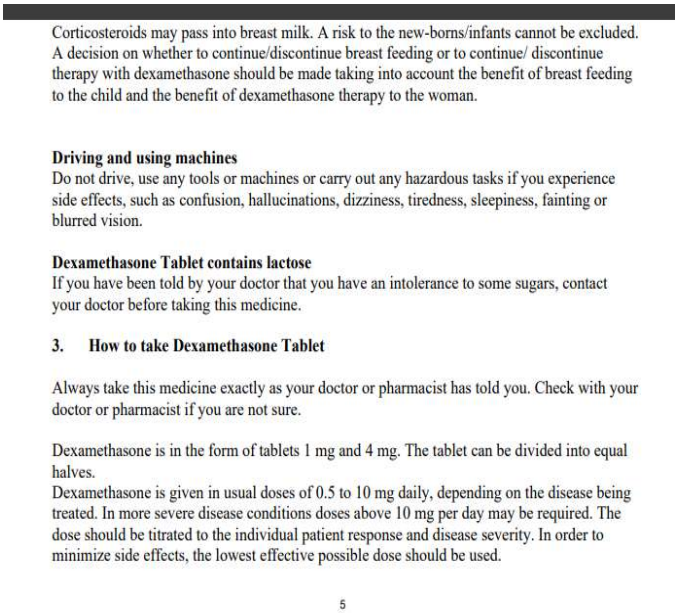

Corticosteroids may pass into breast milk. A risk to the new-borns/infants cannot be excluded. A decision on whether to continue/discontinue breast feeding or to continue/ discontinue therapy with dexamethasone should be made taking into account the benefit of breast feeding to the child and the benefit of dexamethasone therapy to the woman.

Driving and using machines
Do not drive, use any tools or machines or carry out any hazardous tasks if you experience side effects, such as confusion, hallucinations, dizziness, tiredness, sleepiness, fainting or blurred vision.

Dexamethasone Tablet contains lactose
If you have been told by your doctor that you have an intolerance to some sugars, contact your doctor before taking this medicine.

3. How to take Dexamethasone Tablet

Always take this medicine exactly as your doctor or pharmacist has told you. Check with your doctor or pharmacist if you are not sure.

Dexamethasone is in the form of tablets 1 mg and 4 mg. The tablet can be divided into equal halves.
Dexamethasone is given in usual doses of 0.5 to 10 mg daily, depending on the disease being treated. In more severe disease conditions doses above 10 mg per day may be required. The dose should be titrated to the individual patient response and disease severity. In order to minimize side effects, the lowest effective possible dose should be used.

5

Figure 4 –Dexamethasone brochure, source: https://www.medicines.org.uk/emc/files/pil.10720.pdf